ADSORPTIVE RECOVERY OF NANOPARTICULATE PROTEIN PRODUCTS: PHYSICAL AND BIOCHEMICAL CHARACTERISATION OF CANDIDATE SOLID PHASES

by

SHARON LOUISE WILLIAMS

A thesis submitted to

The University of Birmingham

for the degree of

DOCTOR OF PHILOSOPHY

Department of Chemical Engineering

The University of Birmingham

May 2002

Slowly, slowly, catchee monkey.

Terry Brooks – Time Gentlemen Please

I would like to dedicate this work to my partner KEVIN, and my parents PHIL and BRENDA, whose love and support has enabled me to achieve my goal

ACKNOWLEDGEMENTS

Firstly, I would like to thank Professor Andy Lyddiatt for his supervision, support and guidance and many wise words during my time with the Biochemical Recovery Group.

This studentship was funded by the Biotechnology and Biological Sciences Research Council (BBSRC). I gratefully acknowledge Dr Arvind Lali, Dr Igor Galaev and Professor Yan Sun for providing adsorbent materials.

I must also acknowledge the valuable discussions and friendships of everyone, past and present in the Biochemical Recovery Group and the life long friendships forged through happiness and a need to remain sane with Vicky, Sally, Rachel, Nyaradzo and Dave.

ABSTRACT

Adsorbent solid phases having suitable designs applicable to the generic recovery of nanoparticulate products have been demonstrated. Practical recovery of nanoparticulate mimics, of products such as plasmid DNA and viruses, as putative gene therapy vectors from both single component model systems and complex feedstocks has been studied.

The adsorbents employed in the study had one of four discrete designs (Type I-IV), including (I) microporous (pore size 0.02μm- 0.2μm), (II) macroporous (pore size > 0.6μm), (III) solid (non-porous) and (IV) pellicular (pore size 0.2μm-0.4μm). Commercially available adsorbents (STREAMLINE, Amersham Biosciences; Toyopearl HW-40, Tosohaas; POROS 50D, Applied Biosystems) and custom designed adsorbents (PVA composites supplied by Igor Galaev, Lund University; Celbead adsorbents supplied by Arvind Lali, Mumbai University; 2% ZsA and perfluorocarbon emulsions developed at the University of Birmingham) were included in the study.

The adsorbents were evaluated exploiting ligands appropriate for both anion exchange and pseudo-affinity chromatography employing both soluble and particulate forms of bovine and human serum albumin. Soluble protein was included in the study to represent cellular components of complex feedstocks and the separation of assemblies from components, whilst particulate protein, fabricated by coacervation and crosslinking procedures, served as surrogate size and charge mimics of less easily sourced viral and plasmid gene therapy vectors. Insect cell culture lysate was employed as an industrially relevant feedstock and experiments were completed exploiting representative nanoparticulate production systems.

Candidate adsorbents were physically characterised to assess their suitability for fluidised bed operation and biochemically characterised exploiting batch binding experimentation and laser scanning confocal microscopy. The adsorptive capacity and desorption efficiency of both nanoparticulate products and cellular component were strongly influenced by the physical design and geometry of the adsorbent solid phases together with the concentrations of interacting chemical ligands available for adsorption.

Microporous adsorbents (as defined above) developed for the purification of macromolecular products appeared to be less suited for the recovery of nanoparticulate products from complex feedstocks than macroporous or pellicular adsorbents.

CONTENTS

CHAPTER 6 – CONCLUSIONS AND FURTHER WORK

APPENDICES

LIST OF FIGURES

LIST OF TABLES

DEFINITIONS AND ABBREVIATIONS

ε	bed voidage
ρ_l	liquid density (g/ml)
ρ_p	particle density (g/ml)
2% ZsA	adsorbent comprised of zirconium silicate and 2% agarose
BSA	bovine serum albumin
BSAp	bovine serum albumin nanoparticles
BSAs	soluble bovine serum albumin
Buffer A	10mM Tris-HCl, pH 7.5 with 0.02% sodium azide and 0.01% Tween 20
Buffer B	conjugation buffer, 0.1M $NaHCO_3$, pH 8.3 with 0.5M NaCl
Buffer C	111mM sodium phosphate buffer, pH 6.4 with 0.02% sodium azide and 0.01% Tween 20
C*	equilibrium concentration of the adsorbate in the liquid phase
C_o	Initial adsorbate concentration in the liquid phase
D	diffusion coefficient
DEAE	diethyl aminoethyl, weak anion exchange ligand
δ	distance (m)
d_p	particle diameter (m)
DSP	downstream processing
F	measured fluorescence divided by the equilibrium fluorescence
FBAC	Fluidised Bed Adsorption Chromatography
FITC	fluorescein isothiocyanate
g	gravitational force
H	height of a fluidised bed (m)

H_o	settled bed height of an adsorbent bed (m)
HSA	human serum albumin
HSAp	human serum albumin nanoparticles
HSAs	soluble human serum albumin
I	integral fluorescence
i.d.	internal diameter (m)
IEC	ion exchange chromatography
k_1, k_2	rate constants
K_d	dissociation constant
K_d	dissociation constant (Langmuir adsorption isotherm)
KSCN	potassium isothiocyanate
LSCM	laser scanning confocal microscope
n	expansion index
N_A	Avogadro's number
PCS	photon correlation spectroscopy
pI	isoelectric point
PS-DVB	polystyrene divinylbenzene
PVA Mo	composite comprising PVA and molybdenum
PVA TiO_2	composite comprising PVA and titanium oxide
PVA Zr	composite comprising PVA and zirconium silicate
PVA	polyvinyl alcohol
q*	equilibrium concentration of the adsorbate on the adsorbent
q_m	maximum binding capacity (mg/ml adsorbent)
Q_{rel}	relative fluorescence capacity
$Q_{rel\equiv}$	relative fluorescence at equilibrium

R	gas constant
T_1	time (min)
T_2	absolute temperature
Tris	Tris (hydroxymethyl-)-aminomethane
Type I	microporous adsorbent structure
Type II	macroporous adsorbent structure
Type III	solid adsorbent structure
Type IV	pellicular adsorbent structure
U	linear velocity (cm/hr)
U_{mf}	minimum fluidisation velocity (m/s). The flow velocity at which a bed of adsorbent particles becomes suspended in an upward flow of liquid.
U_t	terminal velocity (m/s). The flow velocity at which a particle of a definite size and density is elutriated from a fluidised bed.
η	viscosity (kg/(m.s))

CHAPTER 1

INTRODUCTION

1.1 Downstream Processing in the Bioprocessing Industry

There has been much interest generated in the recovery of (i) nanoparticulate products such as plasmid DNA and viruses as putative gene therapy vectors, (ii) macromolecular assemblies as drug delivery vehicles and (iii) virus like particles as vaccine components (Prazeres *et al*, 1998; Andreadis *et al*, 1999). These nanoparticulate products have been recovered from complex feedstocks such as cell culture supernatants, fermentation broths and cell disruptates using techniques collectively described as downstream processing (DSP; Wheelwright, 1987). The objective of DSP is to determine a sequence of steps that will result in the generation of a desired product from the initial starting material. The individual steps tend to be designed based upon the biochemical and molecular behaviour of the desired product and the impurities within the system. This enables the establishment of an efficient and economic process that achieves the purity and specification of the end product required.

As a consequence of the sensitivity of nanoparticulate and protein products to temperature, pH, chemical reagents or processes that compromise the 3-dimensional structure and conformation of the product, a general approach to the downstream processing of such products has evolved (see Figure 1.1). However, individual steps during a purification process are product specific. Typical nanoparticulate products that require purification for gene therapy applications include viruses, such as adenoviruses, retroviruses and adeno-associated viruses and plasmid DNA (Lorens *et al*, 2001). For such products there are several criteria for the selection of appropriate techniques. The protocols selected must be capable of processing large volumes of viral/plasmid preparations having high yields and it is essential that the stability and activity of the product be preserved. As for any downstream processing procedure the operation must be easily scalable and have a relatively low cost. Finally the

Figure 1.1 Conventional downstream processing for nanoparticulate products

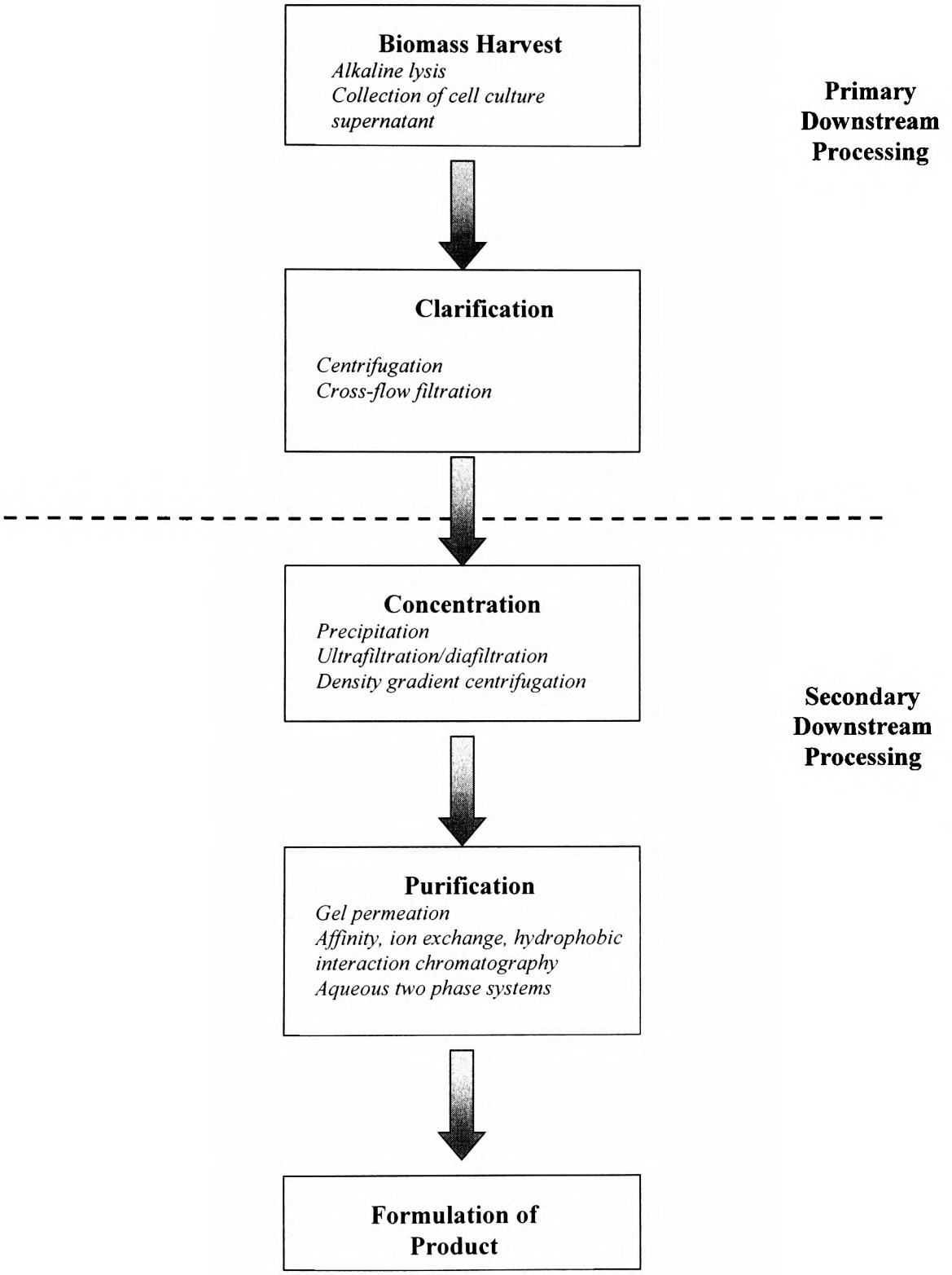

Figure 1.1 represents the conventional downstream processing steps required for the purification of nanoparticulate products such as plasmid DNA and viruses.

processing of the end product must meet the Food and Drug Administration (FDA) standards for biological therapeutics (Andreadis *et al*, 1999; Levy *et al*, 2000).

In the literature the downstream processing procedures employed for the purification of nanoparticulate products follow the same general procedures that have been developed for the purification of protein products. The initial DSP step is concerned with harvesting the product. In the case of viruses such as retrovirus, this involves the recovery from clarified cell culture supernatant, whilst plasmid DNA is harvested by alkaline cell lysis to release the DNA from within the host cell (Andreadis *et al*, 1999; Prazeres *et al*, 1999). As a consequence of the complex feedstocks associated with cell culture supernatants and cell lysates prior to purification there is the need for clarification and concentration of the product. Clarification is generally achieved using centrifugation methods that have been shown to be robust and operable procedures at process scale (Phillips *et al*, 1985), whilst concentration is achieved using precipitation, ultrafiltration/diafiltration or density gradient centrifugation techniques (Shabram *et al*, 1997; Andreadis *et al*, 1999; Ferreira *et al*, 2000). Subsequent purification is commonly achieved by chromatographic adsorption. Affinity, ion exchange and hydrophobic interaction chromatography have been described as effective tools for the primary purification of nanoparticulate products (Ferreira *et al*, 2000).

Fixed bed chromatography is generally exploited for the purification procedures, and consequently the preliminary clarification and concentration of the feedstock is an essential requirement. If this is not undertaken the particulate material within the feedstock will become trapped within the voids of the bed which leads to the formation of a plug that distorts or obstructs the flow of the liquid through the bed compromising the efficiency of the separation (Bierau *et al*, 2001).

1.2 General Problems Associated with Downstream Processing of Nanoparticulate Products

The number of downstream processing steps required to achieve the desired purity of a product considerably influences the cost of DSP. Datar *et al* (1993) and Lyddiatt and O'Sullivan (1998) have suggested that DSP can account for 70-80% of the total production costs due to the capital investment and amount of consumables required for each step and the time required for each individual operation. With each additional step there are also inherent handling losses affecting the recovery of the final product and the product activity.

The traditional techniques employed for the purification of nanoparticulates are not necessarily the ideal DSP operations for such products. The initial clarification step is often carried out using centrifugation or cross-flow filtration (Kahn *et al*, 2000). Their relative success in terms of the resolution of fractionation is dependent upon the differences in size and density between the product, product components and the cell debris and impurities. Also the potential for batch to batch variation of nucleic acid content influences the viscosity of the feedstock (Braas *et al*, 1996). If centrifugation is chosen as the desired operation for the clarification of the feedstock the hydrodynamic shear effects upon the nanoparticulates (viruses, plasmid DNA etc.) must be considered when using an industrial centrifuge (Brunner and Hemfort, 1988). Cross-flow filtration has also demonstrated process advantages, although Aimar *et al* (1989) and Walker (1998) highlighted that the pore size distribution of a clean membrane is constantly modified due to fouling. Consequently the resolution of the nanoparticle fraction will be compromised. This is also a factor influencing the use of ultra/diafiltration for the product concentration operational step. Other DSP operations employed for product concentration have also demonstrated practical limitations (Andreadis *et al*, 1999; Levy *et al*, 2000). Precipitation using reagents such as polyethylene glycol (PEG) or ammonium sulphate and density gradient centrifugation methods employing sucrose or

caesium chloride co-concentrate impurities such as inhibitors resulting in a loss of product activity and integrity.

1.3 Approaches to Optimising Downstream Processing Techniques for Nanoparticulate Products

The major problem associated with the downstream processing of nanoparticulate products is the loss of product integrity due to the number of operational steps required to clarify and concentrate the desired product. The ideal process is that whereby preliminary capture of the target product from the bulk feedstock is achieved by a process that combines clarification, concentration and product capture in a single unit operation.

There are four general approaches described in the literature that match the criteria required for the processing of biologically sensitive products. Aqueous two phase systems (ATPS) are liquid-liquid extraction systems formed by the mixing of aqueous solutions of polymers (e.g. poly-ethylene glycol, poly-vinyl alcohol) and second polymers or salt (dextran, modified starch, phosphate). Above critical concentrations there is a formation of two water rich phases (Huddleston *et al*, 1991). Complex feedstocks containing high biomass loads can be successfully processed in such systems (Huddleston *et al*, 1992) where the mechanical separation of the particulate material by centrifugation is circumvented by the thermodynamically controlled separation of the particulate materials and the desired product into two separate phases (Kula, 1990). In addition, nanoparticles such as inclusion bodies have been successfully recovered using this technique (Walker and Lyddiatt, 1996; 1999) as well as HIV-1 and HIV-2 viruses (Gilljam *et al*, 1994).

Another approach to simplify downstream processing operations is the inclusion of protein binding ligands to cross-flow filtration membranes thereby combining concentration, clarification and adsorption procedures. This technique has been exploited for the recovery of

proteins in solution (Tennikov *et al*, 1998), for the isolation of protein receptors from *Streptococci G* (Kasper *et al*, 1998) and for the recovery of lysozyme (Kacar and Arica, 2001). However, as indicated previously (see Section 1.2) fouling of the membrane will affect the integrity of the selected pore size and consequently yield of the recovered product.

Recent reports in the literature have suggested that affinity precipitation is a valuable technique for direct product capture from particulate containing feedstocks. Polymers such as N,N diethylacrylamide and poly-N-isopropylacrylamide can be affinity tagged with ligands such as iminobiotin, N-acetylglucosamine and *m*-aminophenyl boric acid. These are used to initially bind and co-precipitate the target product (Eggert *et al*, 1998). This is achieved by changing critical solution parameters such as temperature, pH or salt concentration resulting in the polymer-product complex precipitating out of the particulate containing feedstock. Affinity precipitation has been shown to successfully purify monoclonal antibodies from hybridoma cell culture supernatant (Taipa *et al*, 2000), separate lysozyme from hen egg white (Vaidya *et al*, 2001), and separate avidin from cell culture supernatant (Garret-Flaudy and Freitag, 2001).

The fourth approach to reducing the number of downstream processing steps is based upon the adsorption of the desired product to adsorbent particles in the presence of biomass. This can be achieved from different modes of operation including batch adsorption, suspended bed and fluidised bed adsorption operations (Lyddiatt, 2002). Batch adsorption is one of the simplest methods for separating a desired product from particulate containing feedstocks where the adsorbent particles are contacted with the feedstock in a stirred tank configuration (Robbins and Wang, 1986). After product capture the adsorbent particles are separated from the feedstock by decantation washing after which the product is eluted. Batch adsorption lacks high resolution in comparison to conventional frontal chromatography as the process is characterised by a single equilibrium stage. In addition, there are still problems

associated with recovery of the product loaded adsorbent from the feedstock. However, Hubbuch *et al* (2001) demonstrated the use of superparamagnetic supports for the rapid separation of product loaded adsorbent particles from fermentation broth after batch adsorption.

A recently reported approach has seen the development of a hybrid operation encompassing both stirred tank batch adsorption coupled with elution in an enclosed column system. This technique has been termed suspended bed chromatography (Levison *et al*, 2000; Quinones-Garcia *et al*, 2001). The mode of operation has been compared to both batch adsorption and column chromatography methods (Quinones-Garcia *et al*, 2001) and it was demonstrated that suspended bed chromatography performed well in comparison to batch adsorption, although column chromatography was highlighted as the most efficient separation technique. Whilst suspended bed chromatography is a viable process technique it is not necessarily suitable for the recovery of nanoparticulate products. The most common method of whole broth processing is the use of stable liquid fluidised beds whose fundamentals and characteristics are described in Section 1.4.

The washing and cleaning procedures are very important in fluidised bed operations as contacting the adsorbent particles with complex biological feedstocks significantly increases the physical challenge of the adsorbent. The removal of this material can require large washing volumes which increases both process times and cost. Hjorth *et al* (1995) demonstrated that to reduce the cell load by 10^5 when STREAMLINE particles were fluidised with an *Eschericia coli* homogenate containing 10^9 colony forming units per ml, 20 settled column volumes of washing buffer were required. Similar results were obtained by Hansson *et al* (1994) with whole *E.coli* cells. The presence of particulate containing feedstocks also influences other performance parameters in a fluidised bed adsorption operation. It has been demonstrated that the presence of cells and cell debris negatively

influences the achievable adsorption capacities of a desired product. Chase and Draeger (1992) showed that the presence of 3% dry mass of *Saccharomyces cerevisiae* cells reduced the equilibrium adsorption of BSA to Q Sepharose by 49%. In addition, Gilchrist *et al* (1994) were able to show that the presence of 2% dry mass of *S. cerevisiae* reduced the BSA capacity during adsorption in a single stage fluidised bed (serviced by recirculating feedstocks) by 20% for a titanium dioxide/ cellulose composite and 86% for the silica based DEAE Sepherosil LS. Therefore the physical design of adsorbent solid phases developed for fluidised bed adsorption demands consideration with respect to reducing the processing times by limiting the number of washing steps required after product adsorption whilst maximising the potential product capacities.

1.4 Fluidised Bed Adsorption Chromatography

Fluidised bed adsorption chromatography (FBAC) and the similar process of Expanded Bed Adsorption Chromatography (EBAC), has emerged as an efficient method for the recovery of products from complex feedstocks demonstrating advantages over the traditional methods of recovery, e.g. circumventing the need for clarification of feedstocks before application to a fixed bed chromatography column (Bierau, 2001).

The conventional chemical engineering view of a fluidised bed is one that is characterised by a significant degree of mixing as is exhibited by gas-fluidisation systems (Levenspiel, 1972) and it has been commonly assumed that a fluidised bed contactor generates a highly mixed system for the feedstock and adsorbent (Anspach *et al*, 1999), but this has been shown to not necessarily be the case (Lan *et al*, 1999). It has been demonstrated that the physical properties of the adsorbent particles can generate an inherently stable fluidised bed. If the adsorbent particles have an appropriate distribution of both size and density a classification occurs within the bed with large, dense particles located at the base of

the bed and light, less dense particles at the top of the bed. This segregation behaviour restricts the local mobility of the particles when fluidised (Chase, 1994; Thömmes *et al*, 1995; Barnfield Frej *et al*, 1997; Thömmes, 1997). In order to account for the difference in the mixing characteristics of the classified, stable fluidised bed and the conventional well mixed fluidised bed, the term Expanded Bed Adsorption has been adopted by several authors and a leading supplier of chromatography media and equipment (Amersham Biosciences; Chase, 1994; Hjorth, 1997). The work presented herein uses the term Fluidised Bed Adsorption Chromatography to refer to adsorbents fluidised under conditions seeking to minimize particle mixing.

Adsorbent particles within a bed are fluidised by the application of an upward liquid flow through the adsorbent particles that are not constrained by an upper flow adapter. Consequently the bed can expand upward resulting in spaces opening up between the adsorbent particles. Therefore, particulate containing feedstocks do not require clarification or concentration prior to the application of the material to the column. The spaces between the adsorbent particles allow the feedstock to pass freely through the bed without entrapment (refer to Figure 1.2). At the end of the adsorption phase the unbound or loosely bound material can be removed by washing the adsorbent particles whilst still in a fluidised mode. Subsequently, the adsorbed product can be eluted from the bed whilst the adsorbent particles are in a fluidised or fixed bed configuration. As a consequence of this mode of operation clarification, concentration and primary capture is achieved in a single unit operation, thus enabling the simplification of downstream processes alongside economic savings in both capital and operating costs.

Fluidised bed adsorption chromatography has previously been used for industrial applications including the industrial scale recovery of antibiotics such as novobiocin (Belter *et al*, 1973) and streptomycin (Barthels *et al*, 1958). In addition, at laboratory scale many

Figure 1.2 Diagrammatic representation of adsorbent particles in fixed and fluidised bed contactors

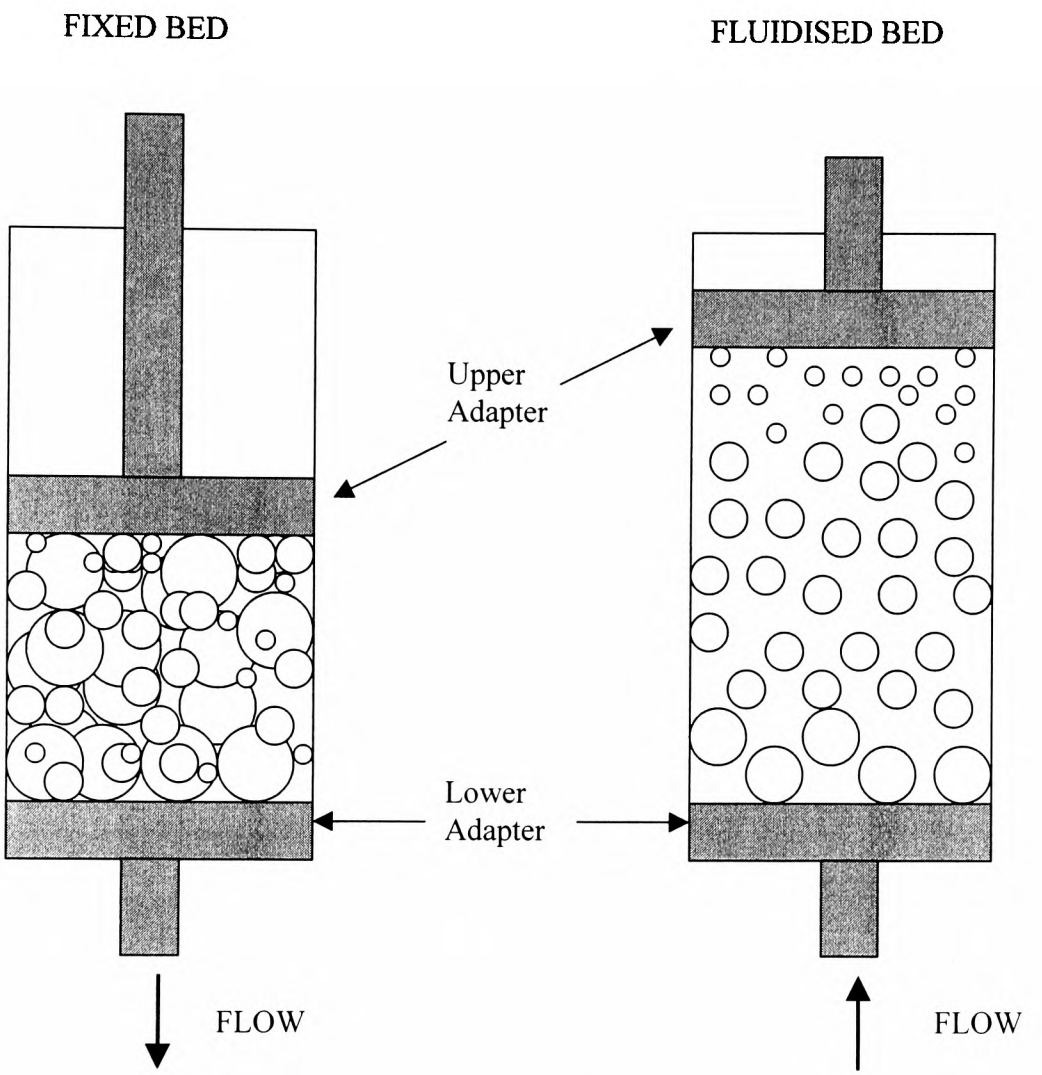

Figure 1.2 represents the configuration of a fixed bed and fluidised bed contactor. The adsorbent particles in a fixed bed are constrained by an upper and lower adapter. The intraparticle space (i.e. voidage) is minimal, therefore feedstock clarification is essential to avoid clogging of the bed. In a fluidised bed the adsorbent is fluidised by an upward liquid flow, not constrained by an upper flow adapter. The bed voidage is increased therefore particulate containing feedstocks can pass unhindered through the bed.

proteins have been purified using fluidised bed adsorption chromatography including proteins from *Eschericia coli* homogenates (Barnfield Frej *et al*, 1994; Zhang et al, 1999). Recombinant protein from animal cell culture supernatant (Erickson *et al*, 1994) and L-asparaginase from *Erwinia chrysanthemi* (Bierau *et al*, 1999) have also been purified. However, more recently interest has been shown in the fluidised bed recovery of larger products such as nanoparticulate mimics (Zhang *et al*, 2001), plasmid DNA (Varley *et al*, 1999) and whole cells (Ujam *et al*, 2000).

1.4.1 Principles of Fluidised Bed Adsorption Chromatography

Fluidisation is achieved by pumping liquid upwards through a settled bed of adsorbent particles. At low linear flow velocities the liquid passes through the voids in the bed. As the flow rate increases the adsorbent particles begin to move apart until they are suspended in the liquid phase. This is achieved when the velocity of the liquid phase exceeds a minimum value, termed the minimum fluidisation velocity (U_{mf}; see Figure 1.3). As the liquid flow increases the adsorbent particles move further apart resulting in a progressive bed expansion referred to as a steady state fluidisation (Kunii and Levenspiel, 1991). This steady state remains so long as the flow velocity does not exceed the terminal settling velocity (or the maximum fluidisation velocity) of the fluidised adsorbent particle (U_t). This is defined as the point when the adsorbent particles are elutriated from the column. The maximum fluidisation velocity depends upon the properties of the fluidising adsorbent particles and can be described by Stoke's law (see Equation 1.1). This indicates that U_t is dependent upon the particle diameter (d_p), particle density (ρ_p), the density of the liquid (ρ_l) and the viscosity of the liquid phase (η).

$$U_t = (\rho_p - \rho_l)\, d_p^2 g / 18\eta \qquad \text{Equation 1.1}$$

Figure 1.3 Operational window of fluidisation velocities

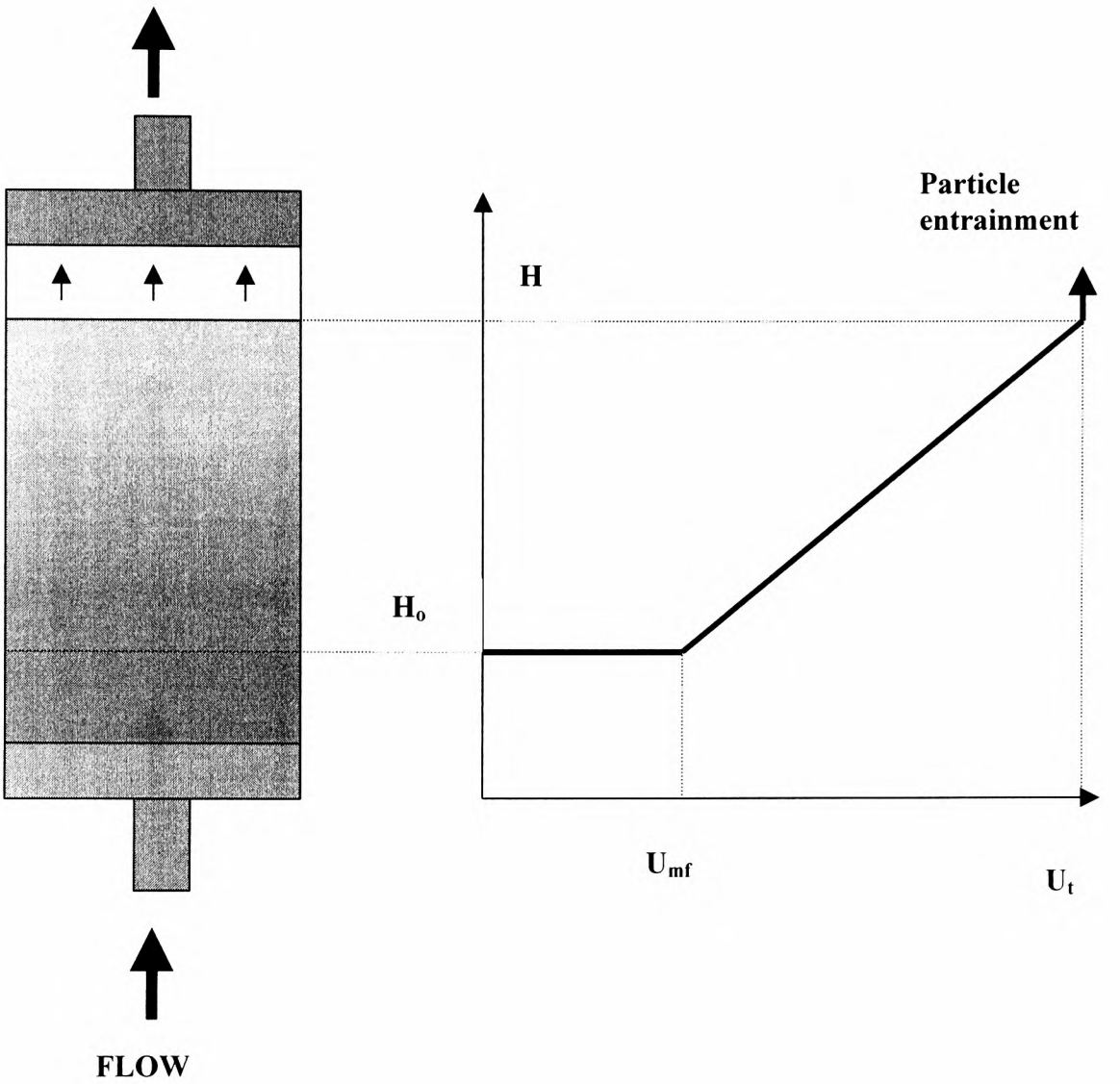

Figure 1.3 (reproduced from Bierau, 2001) represents the operational window of a fluidised bed process. This is defined by the minimum fluidisation velocity (U_{mf}), the velocity at which the adsorbent particles begin to fluidise and the terminal settling velocity (U_t) the velocity at which the particles are elutriated from the bed.

1.5 Design of Adsorbent Solid Phases Suitable for the Recovery of Nanoparticulate Products

As a consequence of the limitations associated with downstream processing of nanoparticulate products as outlined above, fluidised bed adsorption chromatography has been classified as a suitable DSP operation having the potential to circumvent current process bottlenecks. Therefore the next logical step is the establishment of design criteria for 'ideal' adsorbent solid phases suitable for the recovery of nanoparticulate products. These include (i) an enhanced density to make the adsorbent suitable for fluidised operation (see Equation 1.1), (ii) rapid adsorption/desorption rates to minimise the processing times to protect the integrity and activity of the desired product and to reduce costs associated with long processing times. (iii) Rapid washing procedures are required to minimise operational costs and (iv) adequate capacities and recoveries are required to optimise the purification of a desired product in a single step primary capture operation.

Conventional adsorbent solid phases designed for fixed bed adsorption processes are not suitable adsorbent solid phases for fluidised bed adsorption due to their limited density and size. For example, Sepharose FastFlow (Amersham Biosciences, Uppsala, Sweden) is a well characterised adsorbent for fixed bed chromatography (refer to Table 1.1). However, this adsorbent has been demonstrated to have a maximum fluidisation velocity of 3.7cm/min in water. Consequently, even in water the adsorbent particles are elutriated from the column at linear flow velocities greater then 3.8cm/min. In addition, if complex feedstocks such as fermentation broths or cell homogenates are considered (having viscosities of 0.003kg/m.s, for a 3% wet weight yeast homogenate; Thömmes, 1997) U_{mf} is reduced further. It is clear that enhanced densities and particle diameters are required for adsorbents suitable for fluidised bed adsorption chromatography (Chase and Draeger, 1992) to increase the fluid flow throughput, hence reduce processing times.

Table 1.1 Physical characteristics of Sepharose FastFlow

PHYSICAL PROPERTIES	DATA
Particle diameter (μm)	90
Particle density (g/ml)	1.13
U_t (cm/min)	3.7
U_{mf} (cm/min)	0.34

Table 1.1 represents the physical characteristics of Sepharose FastFlow (Affinity Chromatography: Principles and Practice; Amersham Biosciences, Uppsala, Sweden).

Denser adsorbent particles, such as silica were considered to be more appropriate materials for fluidised bed adsorption applications (Dasari *et al*, 1993; Finette *et al*, 1996). However, silica containing materials have limited stability at high pH values which makes them less suitable for pharmaceutical products where alkaline conditions are often used for sanitisation and clean in place procedures. There has been much work published concerned with the development of denser adsorbent solid phases employing higher flow rates for faster processing times and improvements in fluidised bed stability. Custom designed adsorbents were produced using hydrophilic natural polymers such as agarose, cellulose and trisacrylate base materials. These adsorbents were density enhanced by the addition of inert filler materials during the manufacturing process. Composite adsorbents have included cellulose-titanium dioxide (Gibson and Lyddiatt, 1990; 1993; Gilchrist *et al*, 1994) ceramic-hydrogel (Coffman *et al*, 1999) and dextran silica (Morton and Lyddiatt, 1992). In addition, other materials such as glass and zirconium have been modified to fabricate dense adsorbent solid phases suitable for fluidised bed operations. In 1995 Thömmes *et al* exploited controlled pore glass particles for the recovery of monoclonal antibodies. Fluoride modified zirconium (Mullick *et al*, 1999) has been used to successfully purify bovine serum albumin in a fluidised bed configuration.

More recently, pellicular adsorbents have been shown to be suitable adsorbents for the fluidised bed recovery of biological products (Zhang *et al*, 2001; Thwaites *et al*, 2002). These adsorbents are characterised by a dense core such as glass (Lihme *et al*, 1998), stainless steel (Palsson *et al*, 2000) or zirconium silicate (Sun *et al*, 2001) surrounded by a layer of porous material such as agarose. Commercial pellicular adsorbents such as Upfront Chromatography adsorbents are also available (Lihme *et al*, 1999). These adsorbents not only fulfil the fluidisable qualities desired but also the short diffusion distances of the thin porous layer promise rapid adsorption/desorption kinetics.

Conventional adsorption processes such as affinity, ion exchange and hydrophobic interaction chromatography have been employed as the purification operation for the recovery of nanoparticulate products such as viruses and plasmid DNA. However, current chromatographic technology has been developed primarily for the purification of macromolecular products such as proteins (1-5nm in diameter; Miyabe and Guiochon, 2000) and is not well suited to the recovery of nanoparticles that have a size range of 20-300nm in diameter and have complex surface characteristics (Zhang *et al*, 2001). Currently available adsorbent solid phases used for nanoparticulate recovery have characteristically small pore sizes that have been optimised for the purification of protein rather than nanoparticulate products (see Table 1.2). Small pore sizes (5-400nm in diameter) limits the diffusion of the nanoparticulates (20-300nm in diameter) into the adsorbent solid phase, thus only the external surface area is available for adsorption. In addition, low molecular weight contaminants (such as proteins, DNA and endotoxins) will enter the pores resulting in a process requirement for excessive washing steps to purge the internal volume of the adsorbent solid phases (Zhang *et al*, 2001; Thwaites *et al*, 2002). Therefore the adsorbent geometry should also be considered in addition to the density enhancement for the fluidised bed recovery of nanoparticulate products. Alternative adsorbent designs suitable, or custom designed for improved nanoparticulate recovery have been suggested (Lyddiatt and O'Sullivan, 1998; Braas *et al*, 2000; Zhang *et al*, 2001).

Adsorbent solid phases characterised by large pores (termed macropores in the present study; Type II) would facilitate an enhanced adsorption/desorption performance. The macropores would facilitate free diffusive or convective transport of nanoparticles into the internal volume of the adsorbent solid phase. In addition to commercial macroporous adsorbents such as POROS 50D (refer to Section 2.1.1) there are descriptions in the literature

Table 1.2 Adsorbent solid phases used for the purification of nanoparticulate products

ADSORBENT	MANUFACTURER	NANOPARTICULATE PRODUCT	REFERENCE
Sepharose FastFlow	Amersham Biosciences	Plasmid DNA	Levy *et al*, 2000
Cellufine Sulphate	Amicon	Feline herpes virus	O'Neil and Balkovic, 1993
Q Sepharose XL	Amersham Biosciences	AV_3 RSV GDNF adenovirus	Blanche *et al*, 2000
Resource Q	Amersham Biosciences	ACN 53 adenovirus	Shabram *et al*, 1997
Heparin-sepharose	Amersham Biosciences	Herpes simplex virus	O'Keeffe *et al*, 1999
Cellufine-heparin	Amicon	Herpes simplex virus	O'Keeffe *et al*, 1999
Toyopearl HW-75F	Tosohaas	ACN 53 adenovirus	Huyghe *et al*, 1995
Q Sepharose	Amersham Biosciences	Plasmid DNA	Prazeres *et al*, 1998

Table 1.2 lists some of the commercially available adsorbent solid phases currently exploited for the recovery of nanoparticulate products such as viruses and plasmid DNA.

of adsorbent solid phases custom fabricated with large macropores. Gustavsson *et al* (1998) described a superporous agarose bead prepared having an average pore diameter of 30μm by the emulsification of 6% agarose with the surfactant Span 85 in cyclohexane. This macroporous adsorbent was tested for comparison to Sepharose FastFlow in a fixed bed configuration (Palsson *et al*, 1999). Macroporous adsorbents suitable for operation in a fluidised bed have also been described in subsequently demonstrated to have a superior recovery of recombinant factor VIII SQ in the literature. Pai *et al* (1999; 2000) described macroporous cellulose adsorbent particles having a pore diameter of 3μm. The preparation method is currently under patent application. It was demonstrated that high flow rates could be used to fluidise the adsorbent particles shortening the contact time required for adsorbent saturation. However, as with all macroporous adsorbents the major process disadvantage is the loss of capacity due to the limited surface area available for adsorption.

As briefly mentioned earlier there are perceived process advantages to using pellicular adsorbent solid phases, which are comprised of a dense solid core surrounded by a porous layer, such as agarose. The enhanced densities achievable due to the dense core enables high flow rates to be employed to shorten processing times. In addition, the diffusion distances are reduced in proportion to the depth of the pellicle. In another approach solid adsorbents have been considered for their suitability as fluidised bed adsorbents. McCreath and colleagues developed perfluoropolymer particles consisting of either dense liquid or solid perfluorocarbons coated in a hydrophilic polymeric surfactant (McCreath *et al*, 1992; 1994; 1995). The advantage associated with solid adsorbents is rapid adsorption/desorption rates as there is exclusive surface binding. The washing procedures required to clean the adsorbent after contact with complex biological feedstocks are also perceived to be simpler since there is no internal volume that needs to be purged. However, as with macroporous adsorbents

there is a limited surface area available for binding resulting in lower bulk adsorption capacities.

1.6 Aim of the Study

The aim of the study presented here was to investigate adsorbent solid phases having different internal and external topographical designs for their suitability for the potential recovery of nanoparticulate products in fluidised bed adsorption operations, exploiting batch adsorption studies. It was envisaged that the study would highlight suitable adsorbent designs that demonstrated adequate capacities and recoveries of nanoparticulate products in addition to limiting the co-purification of impurities such as cells, cell debris and DNA.

1.6.1 Batch Adsorption Studies

It was highlighted in Section 1.4 that fluidised bed adsorption is the preferred method for the recovery of industrially relevant nanoparticulates from complex feedstocks; however this study was concerned with the screening of adsorbents suitable for the application to fluidised bed recovery. Consequently, batch adsorption studies were solely employed to investigate the adsorption of soluble and particulate protein to candidate adsorbent solid phases. As previously stated in Section 1.3, batch adsorption is a simple method where adsorbent particles are contacted with the desired product in a well mixed system and is a process characterised by a single equilibrium stage (Robbins and Wang, 1986). For the purpose of this study batch contacting processes were adopted as scouting procedures to identify adsorbent designs suited to larger scale fluidised bed adsorption of nanoparticulate products (see Section 1.4; Ferreira *et al*, 2000; Zhang *et al*, 2001).

1.6.2 The Relevance of the Need to Purify Nanoparticulate Products

The term nanoparticulate products encompasses all desirable products in the nanometer size range such as viruses, plasmid DNA and drug delivery vehicles for gene therapy that is a therapeutic modality with the potential of treating inherited and acquired diseases (Andreadis *et al*, 1999). There are two methods generally employed for introducing genes into cells; (i) physiochemical methods including DNA-liposome electroporation, poly (L) lysine-DNA aggregates and gene guns and (ii) biological methods utilising recombinant viruses, retroviruses, adenoviruses and adeno-associated viruses. Table 1.3 summarises the present number of ongoing gene therapy clinical trials.

As a consequence of the current gene therapy trials, it is becoming evident that large volumes of biologically active recombinant viruses are required for gene therapy. Typically *in vivo* gene transfer requires significantly large volumes of concentrated and pure viruses in the region of 10-1000ml per patient. Hence, large quantities of vector containing cell culture supernatant/lysate need to be processed. Cheaper and more efficient downstream processing steps need to be developed to meet the pharmaceutical demand for high quality, high yield virus and plasmid DNA products.

1.7 Thesis Outline

The study presented in Chapter 2 investigated the physical characterisation of adsorbent solid phases having different geometrical configurations and topographies. The aim was to establish if the adsorbents included in the study were potentially suitable for fluidised bed operations. Generally, nanoparticulate products, such as retroviruses or plasmid DNA are commonly recovered from complex feedstocks such as cell culture supernatants and cell lysates (Lorens *et al*, 2001; Thwaites *et al*, 2002). Consequently, fluidised bed adsorption chromatography was considered to be a suitable downstream processing application for nanoparticulate recovery, circumventing the requirement for prior clarification and

Table 1.3 The number of gene therapy trials currently in operation

GENE THERAPY VECTOR	PERCENTAGE OF CURRENT TRIALS (%)
Retrovirus	35.8
Adenovirus	27.7
Lipofection	13
Plasmid DNA	9.3
Pox virus	6.2
Adeno-associated virus	2.2
RNA transfer	0.8
Gene gun	0.8
Herpes simplex virus	0.5
Others	3.9

September 2001

Table 1.3 represents the present number of gene therapy trials currently running in addition to the vectors that are being used in the trials. This data was reproduced with permission from the Wiley Journal of Gene Medicine website, http://www.wiley.co.uk/genmed.

concentration of the feedstock (see Section 1.4). The adsorbents used were variously sourced from commercial suppliers (Amersham Biosciences; Applied Biosystems, Tosohaas) and custom fabricated prototype adsorbents produced in Birmingham, Mumbai University, India and Lund University, Sweden. The adsorbents studied herein were categorised with respect to the internal and external geometries. Microporous adsorbents having a pore size of less than 0.2μm were designated as Type I and macroporous adsorbents characterised by pores greater than 0.6μm were designated as Type II. Type III adsorbents were solid, or relatively solid assemblies and pellicular adsorbents were designated as Type IV. The quoted pore sizes of the adsorbent solid phases included in the study were based upon information supplied by the manufacturers. The pore sizes were not measured in the present study as the facilities required to determine pore size were not available within the group, hence it was too expensive to send samples to be sized elsewhere. The custom fabricated adsorbents were supplied with a minimal amount of information therefore physical characterisation studies were completed to assess the suitability of the adsorbent types for fluidised bed recovery of desirable products, in addition the adsorbent solid phases were derivatised with anion exchange chemistry.

Chapter 3 summarises the critical evaluation of adsorptive studies with nanoparticulate and protein products in batch binding experimentation. Adsorption and desorption studies with soluble and particulate BSA were compared for candidate adsorbents exploiting anion exchange chemistry. The aim of this study was to investigate the suitability of the selected adsorbent solid phases for fluidised bed recovery of nanoparticulate products such as viruses, plasmid DNA and drug delivery vehicles. For commercially realistic studies of virus or plasmid recovery, large quantities of product are required. Therefore to circumvent the practical problem of material supply synthetic protein nanoparticulates were exploited for the binding studies. In addition soluble protein components were included in the

study as a mimic for small molecular impurities that are expected to characterise cell culture supernatant, fermentation broths and cell disruptates and to illustrate problems associated with the separation of cellular assemblies from components. Suitable adsorbents were chosen for further experimentation as a consequence of the preliminary binding studies and the uptake kinetics of BSA nanoparticles were compared in batch binding studies.

Chapter 4 summarises the use of laser scanning confocal microscopy to provide a realistic picture of product distribution during the adsorption process within selected phases, and to validate the assumptions made as a consequence of the preliminary batch binding experiments. Both fluorescently labelled soluble and particulate BSA were used in the study to further investigate the impact of the pore structure of the adsorbent upon adsorption and desorption performance. As a consequence of the results of this study, adsorbent solid phases demonstrated as suitable for nanoparticulate recovery were chosen for further experimentation.

Chapter 5 summarises experiments that sought to demonstrate the affinity capture and recovery of nanoparticulate products exploiting a readily available model affinity system. Cibacron Blue 3GA and human serum albumin (HSA) have a reported affinity attributed to the specific interaction of the dye to the billirubin binding site on HSA due to the structural similarities of the dye and billirubin (refer forward to Section 5.1.2). The adsorbents that exhibited the best performance in the preliminary studies (Chapters 2-4) were further investigated herein exploiting HSAp manufactured in an equivalent manner to BSAp (refer to Section 3.2.3).

The aim of this study was to benchmark the affinity capture and recovery of nanoparticulate products exploiting realistic systems of equivalent viral particle loads in complex biological feedstocks. The capture and recovery of both the feedstock components and HSAp was determined using the Bradford assay and fluorescence assay respectively.

CHAPTER 2

PHYSICAL CHARACTERISATION OF ADSORBENT SOLID PHASES

2.1 General Introduction

Developments in the field of fluidised bed recovery of nanoparticulate products have been limited due to the lack of solid phases that have both suitable biochemical and physical characteristics. Adsorbents have been specifically designed for fluidised bed adsorptive recovery operations (McCormick, 1993), but current chromatographic technology has been developed primarily for the recovery of macromolecular products (1-5nm particle diameter). They are not necessarily suitable for the recovery of nanoparticulates that have a size range of 20-300nm, coupled with complex surface characteristics. As a consequence, nanoparticulate products tend to be recovered using a combination of ultracentrifugation and ultrafiltration protocols that are commonly scale limited (Kahn *et al*, 2000; see Figure 1.1). In addition, complex feedstocks such as cell lysates from animal and microbial cell cultures limit the efficiency of such processes.

Fluidised bed adsorption technology is an alternative process that can be employed for the direct recovery of nanoparticulates from complex particulate feedstocks (see Section 1.4). Fluidised bed adsorption chromatography is a single pass operation in which desired proteins are purified without the need for separate clarification, concentration and initial purification procedures. The adsorbent particles within the settled bed are fluidised by the application of an upward liquid flow from the base of the column contactor. The fluidisation of the adsorbent bed creates a distance between the adsorbent particles that allows for unhindered passage of cells, cell debris and other particulates during the application of a crude feedstock to the column (see Figures 1.2 and 1.3).

Work has been undertaken herein to investigate the 'ideal' adsorbent design for the recovery of nanoparticulate products in fluidised bed adsorption operations. The ideal particle for nanoparticulate recovery is defined in this study as an adsorbent that enables fluidised bed adsorptive recovery of nanoparticles with adequate separation of the product and the cellular impurities within the feedstock.

This chapter details the physical characterisation of adsorbent solid phases that were selected for study as candidate adsorbent particles. Currently available chromatographic adsorbents (designated Type I and depicted in Figure 2.1) are expected to reveal practical disadvantages. These include (i) the limited product accessibility to the internal surfaces within the adsorbent particle, due to restrictive pore dimensions (Type I adsorbents are characterised in this study as having a pore size of less than 200nm; refer to Figure 2.1), (ii) excessive washing times may be required to purge the internal particle volumes of feedstock contaminants and (iii) validating the adsorbent cleaning may be difficult as a consequence. Alternative adsorbent designs suitable or custom designed for improved nanoparticle recovery have been suggested (Lyddiatt and O'Sullivan, 1998; Braas *et al*, 2000; Zhang *et al*, 2001) and the adsorbent designs selected for this study are depicted in Figure 2.1. These adsorbents were variously sourced from commercial suppliers (Amersham Biosciences, Tosohaas, Applied Biosystems) and custom fabricated prototype adsorbents produced in Birmingham and other laboratories (Mumbai University, India; Lund University, Sweden; refer to Table 2.1).

2.1.1 Description of the Selected Adsorbent Solid Phases

For this study several adsorbents having different internal and external geometries were investigated to assess their suitability for the recovery of nanoparticulates exploiting fluidised bed adsorption chromatography (FBAC). The adsorbent designs used were (i) microporous Type I, Figure 2.1), (ii) macroporous (Type II, Figure 2.1), (iii) solid adsorbents

Figure 2.1 Internal and external configurations of the selected adsorbent solid phases

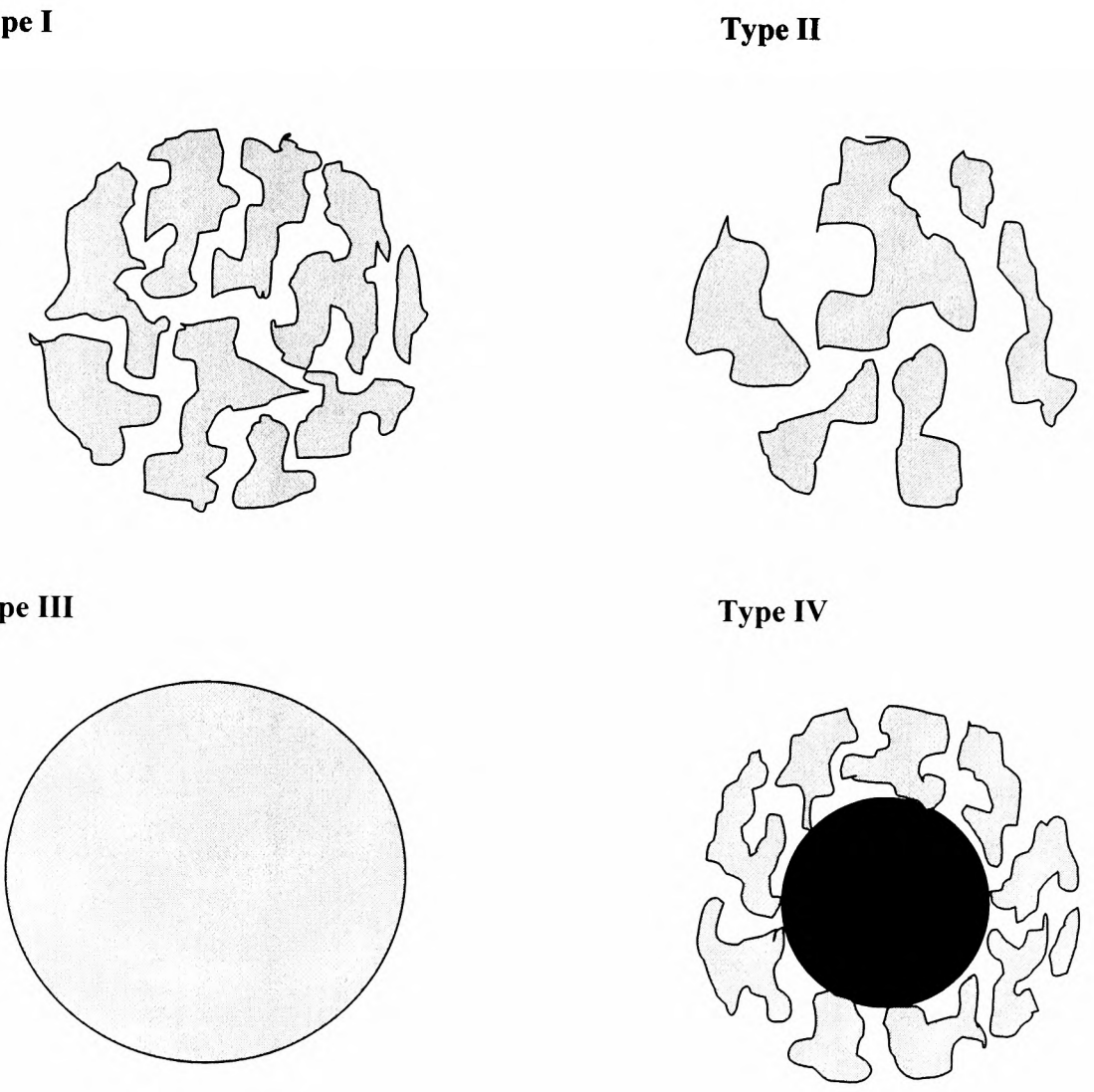

Figure 2.1 is a diagrammatic representation of the adsorbent configurations included in the present study. Microporous adsorbents are designated as Type I adsorbents and are characterised in this study by a pore size of less than 0.2μm. In addition, Type II adsorbents are classified as macroporous having a pore size of greater than 0.6μm in diameter and Type III adsorbents are designated as solid or relative solid adsorbents having either no pores or having a molecular size exclusion of 10,000 Daltons (refer to Table 2.1). Type IV adsorbents in this study are pellicular in nature, consisting of a dense, solid core surrounded by a layer of porous agarose material.

Table 2.1 Summary of the adsorbent solid phases included in the present study

ADSORBENT TYPE	ADSORBENT	PORE SIZE	ADSORBENT GEOMETRY	MANUFACTURER	REFERENCE
I	STREAMLINE (6%)	<0.2μm	Microporous	Amersham Biosciences	McCormick (1993)
II	Celbead (II)	3μm	Macroporous	Indian Construct	Pai *et al* (1999)
	Celbead Amino	3μm	Macroporous	Indian Construct	Pai *et al* (2000)
	POROS	0.6-0.8μm	Macroporous	Applied Biosystems	Rodrigues *et al* (1996)
	PVA	1μm	Macroporous	Swedish Construct	Personal Communication
	PVA Mo	1μm	Macroporous	Swedish Construct	Personal Communication
	PVA TiO_2	1μm	Macroporous	Swedish Construct	Personal Communication
	PVA Zr	1μm	Macroporous	Swedish Construct	Personal Communication
III	Perfluorocarbon Emulsion	0μm	Assumed Solid	Birmingham construct	McCreath *et al* (1996)
	Toyopearl	1000-10,000 MW	Virtual Solid	Tosohaas	Tosohaas Product Information
IV	2% ZsA	<0.4μm	Macroporous Pellicular	Birmingham Construct	Sun *et al* (2001)

Table 2.1 summarises the commercial and custom fabricated adsorbent solid phases that were included in the present study having different adsorbent configurations designated as Types I to IV. The aim of this study was to investigate candidate adsorbent solid phases suitable for fluidised bed recovery of nanoparticulate products. The respective manufacturers supplied the data for pore size of the PVA and Celbead composites and the commercial adsorbents.

(Type III, Figure 2.1) and (iv) pellicular adsorbents (Type IV, Figure 2.1, Zhang *et al*, 2001).

2.1.2 STREAMLINE

STREAMLINE is a commercial solid phase included in the study as the benchmark adsorbent classified as a Type I adsorbent (see Section 2.1; Figure 2.1). STREAMLINE was introduced in 1993 by Amersham Biosciences (Carlsson *et al*, 1993; McCormick, 1993), and was specifically designed for FBAC. The base material of the adsorbent was 6% crosslinked agarose (refer to Section 2.1.2.1) modified by the addition of inert crystalline quartz particles. This enhanced density composite adsorbent demonstrated superior fluidisation properties in comparison to the conventional fixed bed adsorbents available at that time. STREAMLINE is an established commercial adsorbent solid phase that has demonstrated a consistent hydrodynamic performance (Hjorth *et al*, 1995) and adsorption characteristics that are similar to standard fixed bed chromatography media. (Hjorth *et al*, 1995, Chang and Chase, 1996).

STREAMLINE has been proven to be a versatile adsorbent for fluidised bed recovery of a variety of biological materials. These include the recovery of recombinant proteins from *Eschericia coli* homogenates (Barnfield Frej *et al*, 1994; 1997; Lan *et al*, 1999), the recovery of proteins from unclarified yeast homogenates (Chang and Chase, 1996, Zurek *et al*, 1996) and fluidised bed adsorption of monoclonal antibodies from crude mammalian cell culture broths (Thömmes *et al*, 1995). STREAMLINE has been termed a microporous (Type I) adsorbent due to the limited size exclusion for globular proteins of 4×10^6 Daltons, that enabled only relatively small products (proteins, endotoxins such as lipopolysaccharides and molecules less than 0.2μm in diameter) to enter the porous structure.

2.1.2.1 Agarose

Agarose is a polysaccharide extracted from the natural polymer agar which is found in the cell wall of marine algae from the agarophyte group of genera including *Gelidium, Pterocladia, Acanthopeltis* and *Gracillaria* that are distributed world wide (Haug, 1975). One of the recognised structures of agar is neutral agarose that is comprised of two residues, 1,3,substituted β-D-galactopyranosyl and 1,4,substitued 3,6,anhydro-α-L-galactopyranosyl (Ergorov *et al*, 1970).

Agarose has been successfully exploited as the base material for several types of adsorbent solid phases because of its endogenous secondary and tertiary structure (see Section 2.1.2). The single fibres of agarose (assembled naturally from the primary linear structure), produce bundles of fibres that in turn become a fabric network containing 'large pores' (Amersham Biosciences, 1997). Figure 2.2 represents the open pore structure of agarose (Amersham Biosciences, 1997). In addition agarose contains primary and secondary hydroxyl groups, which allows for easy chemical derivatisation. In 1964, Hjerten proposed a method of adsorbent production using agarose that has been adapted and commonly used as the basis for adsorbent fabrication. Hjerten showed that due to the insolubility of agarose in water, it can be prepared by melting in an autoclave at 121°C under the pressure of one atmosphere. The beads are fabricated using an emulsification method with hot oil (85°C) under constant agitation whilst gelation of the agarose to form stable beads is achieved by controlled cooling. A distinctive feature of commercially available agarose is the low content of pyruvate and sulphate groups. This limits the non-specific binding of impurities to the agarose matrix during selective adsorption processes. For example a typical commercially available agarose such as Agarose VII from Sigma-Aldrich Ltd. (Poole, UK) has less than 1% sulphate and pyruvate groups compared to crude agar which can contain up to 10% sulphate groups and 2.5% pyruvate groups (Duckworth and Yaphe, 1971). There are

Figure 2.2 Secondary and tertiary structure of agarose

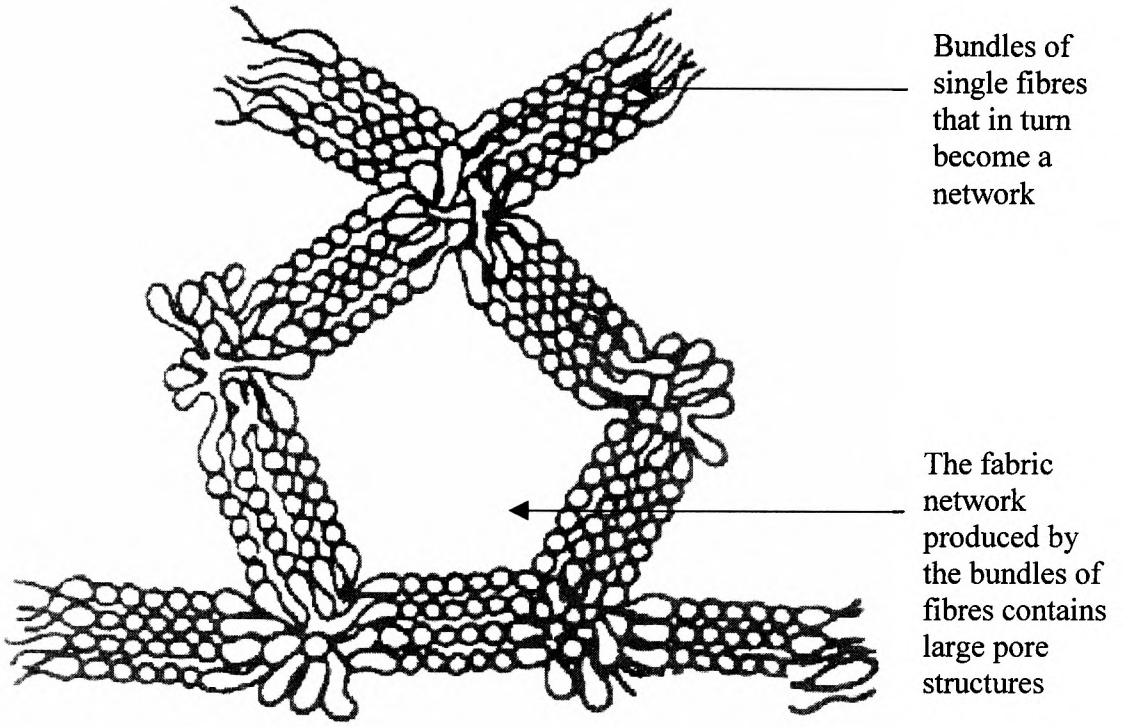

Figure 2.2 represents the secondary and tertiary structure of agarose formed due to hydrogen bonds reproduced from 'Affinity Chromatography: Principles and Methods' (Amersham Biosciences, Sweden).

commercially available adsorbent solid phases using agarose as the base material in addition to STREAMLINE, such as the Sepharose adsorbents (Amersham Biosciences, Uppsala, Sweden).

2.1.3 POROS 50D

POROS is a commercial macroporous adsorbent manufactured by Applied Biosystems and designated a Type II adsorbent in this study (see Figure 2.1). The POROS adsorbent used for this study was POROS 50D perfusion chromatography media, an adsorbent that has been specifically designed for perfusion chromatography (Afeyan et al, 1996; Rodrigues *et al*, 1996). In contrast to conventional chromatography materials, POROS adsorbents are engineered to contain two discrete pore types, (i) large 'throughpores' (or convective pores) and (ii) smaller diffusive pores. The convective pores (0.6μm-0.8μm in diameter) allow for convective flow to occur within the particles that carries the biological materials rapidly through the particle to the smaller diffusive pores (0.08μm-0.15μm in diameter; refer to Figure 2.3). This results in shorter distances over which diffusion must occur, thus reducing the time for the saturation capacity to be reached, which is economically desirable as the overall process time is reduced. POROS 50D consists of a crosslinked polymer, poly(styrene-divinylbenzene) (refer to Section 2.1.3.1) which is surface coated with a polyhydroxylated polymer functionalised with dimethylaminoalkyl groups. (Applied Biosystems Product Information).

2.1.3.1 Poly(styrene-divinylbenzene)

Poly(styrene-divinylbenzene) (PS-DVB) is formulated from a hydrocarbon compound comprised solely of carbon and hydrogen in the presence of benzene and is commonly termed an aromatic hydrocarbon. PS-DVB is generally recognised as having excellent

Figure 2.3 Internal structure of POROS 50D

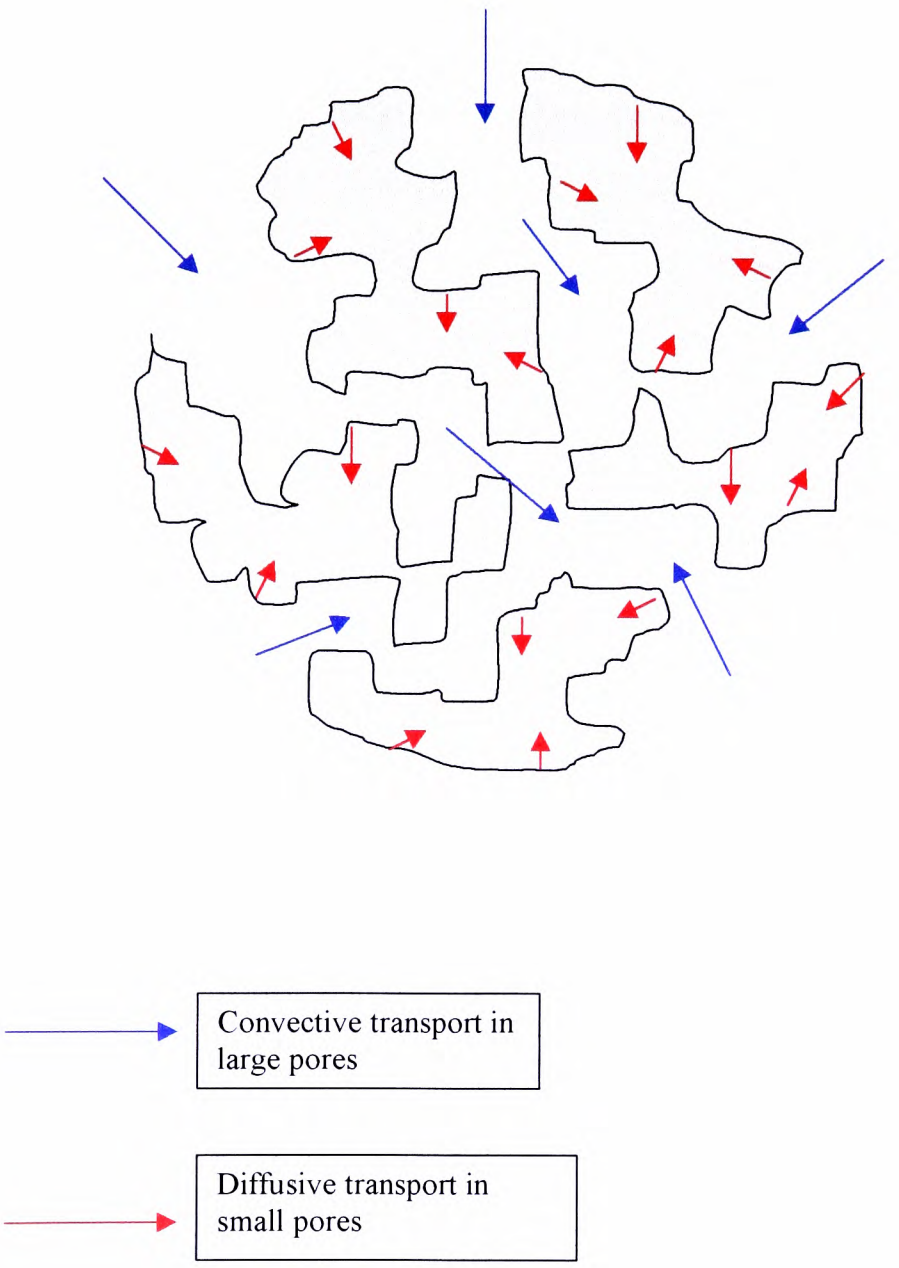

Figure 2.3 represents the flow through a macroporous particle of POROS. The large convective pores allows for liquid flow through the particle to the diffusive pores resulting in shorter diffusion distances for adsorption, thereby reducing the time taken to reach saturation capacity.

chemical and mechanical strength (the material does not compress under high pressures) in comparison to commonly used adsorbent materials such as agarose (Nash *et al*,1996). The chemical robustness of PS-DVB was investigated by Afeyan and Fulton (1991) who demonstrated that the material was stable in the presence of several types of harsh chemicals.

However, due to the nature of hydrocarbons the surface of PS-DVB adsorbents is extremely hydrophobic which promotes protein denaturation upon adsorption. Hence methods of surface modification of PS-DVB have been developed to exploit the chemical and mechanical strength of the material. These include (i) the adsorption of polyoxyethylene monomers onto the surface followed by polymerisation (Fulton *et al*, 1991) and (ii) the adsorption of polymers onto the surface followed by crosslinking, using polymers such as polyvinyl alcohol (PVA; Tuncel and Adil, 1993, Leonard *et al*, 1995).

2.1.4 Celbead Adsorbents

Celbeads were macroporous cellulose beads supplied by Dr Arvind Lali (Mumbai University, India) and prepared following a method for which a patent application has been filed. The adsorbents were classified Type II macroporous adsorbents in this study since they were claimed to have an average pore size of 3μm (Pai *et al*, 2000). No further information about the Celbead adsorbents was available prior to the initiation of the present study.

2.1.4.1 Cellulose

The only information made available to our laboratory concerning the Celbead adsorbents was that they were fabricated from cellulose. Cellulose is a linear polymer of glucose and is the most abundant polymer on earth. The repeating glucose units are linked in the β configuration allowing for the chains to crystallise. Cellulose is found in wood and natural fibres such as flax and cotton and tends to have a highly crystalline structure (90-

95%) which produces a high tensile strength material comprising plant cell walls. Cellulose is most commonly found to have polymer lengths equal to 1000 to 15000 glucose units and its crystalline form has been the subject of much study (Marchessault and Sarko, 1967; Krassig, 1984). X-ray crystallography studies have shown that there are at least four different crystalline forms of cellulose. Cellulose I is the naturally occurring form of cellulose showing a parallel arrangement of polymer chains. In comparison Cellulose II exhibits an antiparallel arrangement and is formed by the regeneration of Cellulose I from solution. Cellulose II is judged to be the more stable structure as the reaction to form Cellulose II from Cellulose I is irreversible (Gilchrist, 1996). Cellulose III and Cellulose IV are formed from Cellulose I and II by the addition of ammonia and hot glycerol respectively. These structures are less stable than Cellulose II as the original structure can be returned by simple treatment procedures with distilled water (Blackwell and Marchessault, 1971).

Cellulose has been successfully exploited as the base material for chromatography adsorbents (Peterson and Sober, 1956), although limitations were shown to be a lack in porosity and poor geometrical shape (Gibson, 1992).

2.1.5 PVA Adsorbents

The PVA adsorbents were supplied by Dr Igor Galaev (Lund University, Sweden) and prepared following an unreported and proprietary method. The limited information supplied indicated that the adsorbents were prepared using polyvinyl alcohol (PVA) as the base material together with various fillers added for density enhancement. The adsorbents were composites of PVA and (i) titanium oxide, (ii) molybdenum, (iii) zirconium silicate together with (iv) an adsorbent comprised solely of PVA. The adsorbents were described as crosslinked and macroporous, and designated herein as Type II adsorbents since they were claimed to have a pore size of 1μm (see Figure 2.1).

2.1.5.1 Polyvinyl Alcohol

Polyvinyl alcohol (PVA) is fabricated from polyvinyl esters, and is a synthetic colloid (Herrmann and Hoehnel, 1964). The polymer is now commercially available varying in degrees of polymerisation and states of hydrolysis. The starting material for the production of polyvinyl alcohol is a polymerised ester, vinyl acetate. PVA is produced from either acid or alkaline hydrolysis of this polymerised ester and the molecular weight of the final product depends on the degree of polymerisation and the molecular weight of the original polyvinyl acetate. The degree of polymerisation and hydrolysis affects the properties of PVA including solubility and viscosity.

PVA is not a commonly used base material for chromatographic adsorbents where conventional biocompatible assemblies include agarose (Davies *et al*, 1994), chitosan (Gallo and Hassan, 1988) and cellulose (Peterson and Sober, 1956). In recent years, PVA has been used as a polymeric surfactant for coating hydrophobic perfluorocarbon materials to fabricate dense solid adsorbents (McCreath *et al*, 1992; 1994, Zhang *et al*, 2001). The hydroxyls present on PVA allow for easy derivatisation making the material suitable for adsorption chromatography

2.1.6 Perfluorocarbon Emulsion Adsorbent Particles

Perfluorocarbon emulsion particles were included in this study as a representative solid, designated herein as a Type III adsorbent (see Figure 2.1). Perfluorocarbons are synthetic molecules comprised solely of carbon and fluorine atoms. They are characterised as being chemically and biologically inert and exhibit the properties of high density materials (1.6-2.1g/ml). Perfluorocarbons are insoluble in both aqueous and common organic solvents and demonstrate thermal stability (Fluorochem Product Information). There have been many applications for both solid and liquid perfluorocarbons including, (i) packings for reversed

phase chromatography (Williams *et al*, 1986), (ii) oxygen transport fluids (Lowe, 1987), (iii) liquid carriers for cell culture (Keese and Giaever, 1983), (iv) adsorbents for the extraction of organic pollutants (Josefson *et al*, 1984), (v) stationary phases in gas-liquid chromatography (Kirkland, 1963) and (vi) oxygen transport for bioreactors and microorganisms in culture (Aldercreutz and Mattiasson, 1982). They have also recently been used in both solid and liquid form as supports for chromatographic applications (Chang *et al,* 1993; Zhang *et al*, 2001).

The inherent hydrophobic nature of perfluorocarbons makes them unsuitable in the native state for chromatographic applications where hydrophilicity and ease of derivatisation are desirable features. Therefore a polymeric surfactant is added to the perfluorocarbon material to produce a hydrophilic layer around the hydrophobic core of perfluorocarbon. Perfluorocarbon materials have been used to produce perfluorocarbon emulsions, designed for chromatographic separation of biological materials including applications such as cell separations (McCreath and Chase, 1996a; McCreath and Chase, 1996b), immobilised enzymes in bioreactors (Yang and Chase, 1998) the recovery of nanoparticulate products (Zhang *et al*, 2001) and the recovery of proteins and enzymes from complex feedstocks (McCreath *et al*, 1994; 1995; Owen *et al*, 1997). The perfluorocarbon base material used in this study was perfluorodecalin as used by McCreath and Chase (1996b). Perfluorodecalin is a fully fluorinated, odourless, colourless oil that is chemically and thermally stable, non-toxic and non-flammable. The physical properties of perfluorodecalin are illustrated in Table 2.2a

2.1.7 Toyopearl HW-40

Toyopearl HW-40 is a commercial adsorbent solid phase 40μm in diameter classified as a Type III solid adsorbent in this study due to a molecular exclusion of 100-10,000 Daltons.

Table 2.2a Physical properties of perfluorodecalin

PROPERTY	DATA
Boiling Point (°C)	142
Molecular Weight	462
Density (g/ml)	1.917
Viscosity (mPas)	5.1

Table 2.2 represents the physical characteristics of perfluorodecalin, the base material of the solid perfluorocarbon emulsions (see Section 2.1.5). Perfluorodecalin is characterised as having a high density making the adsorbent suitable for fluidised bed adsorption recovery operation.

Table 2.2b A selection of commonly used ion exchangers.

ANION EXCHANGERS	FUNCTIONAL GROUP
Diethylaminoethyl (DEAE)	$-O-CH_2-CH_2-N^+H(CH_2CH_3)_2$
Quaternary aminoethyl (QAE)	$-O-CH_2-CH_2-N^+(C_2H_5)-CH_2-CHOH-CH_3$
Quaternary ammonium (Q)	$(-O-CH_2-CHOH-CH_2-)_2N^+(CH_3)_3$
CATION EXCHANGERS	**FUNCTIONAL GROUP**
Carboxymethyl (CM)	$-O-CH_2-COO^-$
Sulphopropyl (SP)	$-O-CH_2-CHOH-CH_2-O-CH_2-CH_2-CH_2SO_3^-$
Methyl Sulphonate (S)	$(-O-CH_2-CHOH-CH_2)_2SO_3^-$

Toyopearl is a semi rigid spherical resin produced from a hydrophilic vinyl copolymer composed exclusively of C, H and O atoms. Due to the presence of numerous free hydroxyl groups the total surface including the internal pore area is hydrophilic. This chemistry minimises non-specific adsorption and thus Toyopearl is an excellent resin for the separation of biomolecules. The material used in the present study was Toyopearl HW-40, which was mechanically stable (working pressures of 3 to 5 bar) and chemically stable at a working pH of pH 2-12.

2.1.8 2% Agarose Zirconium (2% ZsA)

2% agarose zirconium (2% ZsA) was an 'in house' fabricated prototype adsorbent produced by Professor Yan Sun, seconded to the Biochemical Recovery Group in 1999/2000 from Tianjin University, PR China (Sun *et al*, 2001). The adsorbent was a dense pellicular adsorbent (designated herein as a Type IV adsorbent, see to Figure 2.1) that consisted of a dense solid core of zirconium silicate (sourced from Glen Creston) surrounded by a 20μm pellicle of 2% agarose (see Section 2.1.2.1). This was an adsorbent specifically designed for fluidised bed adsorption chromatography with an enhanced density and an adsorption layer.

2.1.9 Ion Exchange Chromatography

Ion exchange chromatography (IEC) is one of the most frequently used chromatographic techniques (Bonnerjea *et al*, 1986). The technique is used for the separation and purification of many biological materials including proteins (Erickson *et al*, 1994; Hansson *et al*, 1994; Hjorth *et al*, 1995), plasmid DNA (Prazeres *et al*, 1998; Ferreria *et al*, 2000; Zhang *et al*, 2001) and viruses (Huyghe *et al*, 1995; Shabram *et al*, 1997; Blanche *et al*, 2000). Therefore it was selected as a suitable adsorption method in the present study.

IEC is a separation method that depends upon the principle of reversible adsorption of charged molecules to oppositely charged immobilised ion exchange groups. There are two types of ion exchangers, positively charged anion exchangers and negatively charged cation exchangers (see Table 2.2b). Separation is achieved due to the differences in charge between the molecules to be separated and the ion exchanger. This interaction can be controlled and influenced by varying conditions such as pH and ionic strength which alter the charge on the desired molecules but not the charge on the adsorbent solid phase.

Early types of ion exchanger were fabricated from synthetic resins, such as PS-DVB (Tooper and Wirth, 1956; refer to Section 2.1.3.1) and designed for procedures such as demineralisation, water treatment and the recovery of ions from waste products (Adams and Holmes, 1935). The hydrophobic nature of these materials made them unsuitable for use with biological molecules. In 1956, Peterson and Sober developed ion exchangers that exploited cellulose as the base material for use in biological separations. Subsequently there have been a variety of materials used for adsorbents employed for ion exchange chromatography. Including dextran (Molday and Mackenzie, 1982), chitosan (Gallo and Hassan, 1988) and agarose (Davies *et al*, 1994). As previously noted the interaction between an ion exchanger and a biological material is dependent on their relative charges. For anion exchangers the pH of the system must generally be above the isoelectric point (pI) of the biological molecule to make it negatively charged in order to adsorb to the positively charged adsorbent solid phases (see Figure 2.4). The type of ions present in the liquid phase determines whether the molecules are positively or negatively charged and the net charge changes from positive to negative as the concentration of OH^- ions increases. The isoelectric point is the pH at which the change occurs and the molecules carry no charge (see Figure 2.4). Therefore with cation exchangers the pH of the system must be below the pI to ensure that the molecule is positively

Figure 2.4 Diagrammatic representation of the modification of protein charge with changing pH

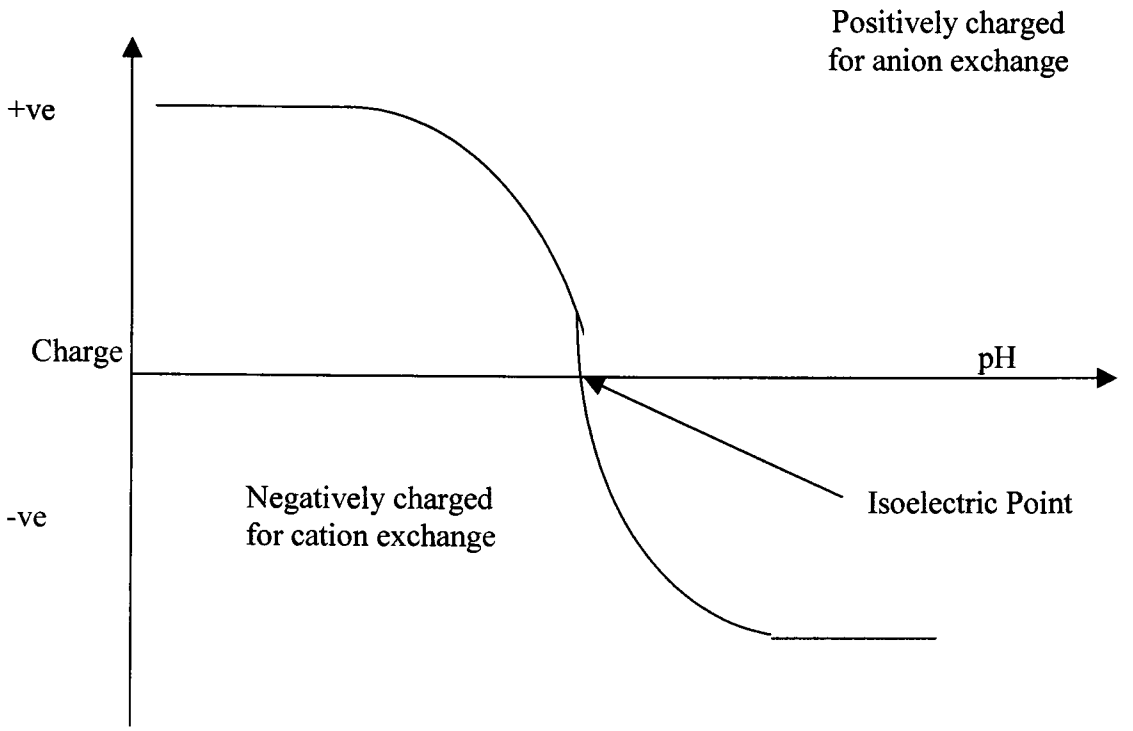

Figure 2.4 represents the change in the charge of a protein molecule as the pH increases. The isoelectric point (pI) indicated represents the pH at which the net charge of the protein molecule changes from positive to negative, where the molecule carries no net charge. When the pH of the protein molecule is below the pI, the protein is positively charged and can be recovered using anion exchange chromatography whilst when the pH is greater than the pI the protein can be recovered by cation exchange chromatography.

charged overall (see Figure 2.4). For example bovine serum albumin (BSA) has a pI of pH 5.1 (Righetti and Caravaggio, 1976) and thus at pH 7.5, BSA can be recovered using anion exchange chromatography and at pH 4.0 BSA can be recovered using cation exchange chromatography (Williams and Lyddiatt, unpublished data). Additionally, due to the dependence of the interaction on charge, the product adsorbed to the ion exchanger can be eluted using mild conditions such as changes in pH or by increases in the salt concentration of the system.

The ion exchange chemistry used in this study was the anion exchange diethylaminoethyl (DEAE) ligand selected as a commonly used chemistry with established preparative protocols (Peterson and Sober, 1956; Gilchrist, 1996). Furthermore, there are widely used commercial adsorbents exploiting DEAE chemistry, such as STREAMLINE DEAE, which were exploited as benchmark adsorbents in this study.

2.2 Materials and Methods

2.2.1 Chemicals

Agarose was supplied by Sigma-Aldrich (Poole, Dorset, UK) and zirconium silicate was sourced from Glen Creston (Middlesex, UK). All other chemicals used were reagent grade unless otherwise stated and supplied by Sigma-Aldrich (Poole, UK) or BDH (Poole, Dorset, UK).

2.2.2 Equipment

- Rotary mixing unit consisting of a speed adjustable rotary unit (Watson-Marlow Company Ltd, Cornwall, UK) and in house designed support fittings.
- pH meter, Hanna Instruments, H19321, Microprocessor Bench pH meter.
- Olympus BH-2 light microscope, Olympus Optical Company Ltd, London, UK.

- Peristaltic pump, model 101U (maximum output 15W), Watson-Marlow Company Ltd, Cornwall, UK.
- Malvern Mastersizer, version 2.18, Malvern Instruments Ltd, Malvern, UK.
- Polytron PT3000 Homogeniser, Philip Harris Scientific, (Formerly of Kinematica, Germany).
- Pharmacia LKB Ultrospec III spectrophotometer, Amersham Biosciences, Uppsala, Sweden.
- Magnetic stirrer/ hotplate, Stuart Scientific Company Ltd, UK.
- Fluid FL200L Power Unit, Labortechnik, Germany
- General laboratory glassware

2.2.3 Fabrication of Perfluorocarbon Emulsion Particles

A method established by McCreath and Chase (1996a) was adopted for the fabrication of perfluorocarbon emulsion particles. The principle of perfluorocarbon emulsion production was based on the interaction between the hydrophilic polymeric surfactant, polyvinyl alcohol (PVA) and the hydrophobic perfluorodecalin oil.

A solution of PVA (9,000-10,000MW, 80% hydrolysed) was prepared in 200ml of distilled water at a concentration of 10mg/ml. The PVA solution was added to a baffled glass vessel that contained 50ml of perfluorodecalin oil. The contents were then homogenised using a Polytron PT3000 homogeniser (Philip Harris Scientific, UK) at 17500rpm for 45 seconds. The emulsion was allowed to settle and then 100ml of the supernatant was removed to eliminate a proportion of the excess uncoupled PVA from the system. This was replaced with 50ml of distilled water. The suspension was mixed using a magnetic stirrer/ hotplate and heated to 40°C in a water bath for 30 minutes. Glutaraldehyde (200µl of 25% w/v) was added to the suspension as the crosslinking reagent. Mixing was continued for 10 minutes after

which crosslinking was catalysed by the addition of hydrochloric acid to the suspension to a final concentration of 0.25M. This suspension was mixed for 1 hour before 4g of NaOH (in 20ml of distilled water) was added to stop the crosslinking reaction. The mixture was stirred for a further 10 minutes. The emulsion was repeatedly washed in distilled water until all the unbound PVA had been removed (refer to Section 2.2.3.1) then the emulsion was stored at 4°C in distilled water containing 0.02% sodium azide. Before experimental use, the emulsion was degassed thoroughly.

2.2.3.1 Iodometric Assay

This was the method used to determine the amount of PVA bound to the perfluorodecalin oil to form the perfluorocarbon emulsion. The method was adapted from a protocol reported by Garvey *et al* (1974) based upon difference analysis. The PVA concentration was measured spectrophotometrically using an iodine reagent to visualise the PVA in solution, which contained 0.45% (w/v) potassium iodide, 0.225% (w/v) iodine and 3.6% (w/v) boric acid in deionised water. PVA solutions were analysed by diluting the sample to an appropriate amount in a 2ml volume followed by the addition of 1ml of iodine reagent. This produced a green coloured complex that was measured at 670nm using a spectrophotometer against a blank sample. The PVA-iodine complex is thought to form due to the random coil structure of PVA in solution. In the presence of iodine atoms, a helical structure is induced followed by intramolecular helix association. Iodine complexes with groups of 12 PVA residues that when supported by one boric acid molecule, form a single helical turn that entwines one iodine atom. This complex resulted in a colour change that was measured spectrophotometrically between 580 and 700nm. In order to determine the PVA concentration of the samples a calibration curve was determined using known concentrations of PVA measured at 670nm (refer to Appendix I).

2.2.4 Fabrication of 2% Agarose Zirconium

The 2% ZsA adsorbent solid phase was a dense, pellicular Type IV adsorbent fabricated by Professor Yan Sun (Tianjin University, PR China) using an oil in water emulsification method (Sun *et al*, 2001) first reported by Hjerten (1964). The vessel used was a 2 litre-glass tank with an internal diameter of 12cm and a removable baffle frame (4 baffles). The impeller was 83mm in diameter and the vessel was water jacketed to ensure temperature control. Sunflower oil (1.5 litres) containing 12.8g/litre Span 80 was added to the vessel and heated to 80°C using the temperature controlled water jacket. Mixing was employed by the use of an impeller driven by a power unit (Fluid FL200L, Labortechnik, Germany) at 1160rpm. In a separate glass vessel agarose was dissolved in distilled water at 4% (w/v) under heating with magnetic stirring. Washed zirconium silicate particles (sourced from Glen Creston) were added to this agarose in a volume ratio of 1:7. After the temperature of the slurry was increased to 85-90°C it was pumped into the oil phase at a flow rate of 20ml/min. After mixing the oil emulsion slurry for 30 minutes, cold water was added to the water jacket to cool the suspension to 20-24°C and the agitation was stopped. The agarose coated zirconium particles were allowed to settle for 30 minutes. The particles were then separated from the oil phase and washed in acetone in order to remove all the oil phase whilst the final polishing was done with excess volumes of distilled water.

2.2.4.1 Composite Crosslinking

Crosslinking of the polymer content of the adsorbent enhances the structural and mechanical strength. The method of crosslinking used with the agarose composites was chemically based using epichlorohydrin, which using a three-carbon propane 2-ol spacer arm reacts with a primary amine group to form a secondary amine linkage that is very stable. The protocol was adapted from a method proposed by Porath *et al* (1971). The adsorbent particles

were suspended in an equal volume of 0.1M NaOH containing 5g/litre of sodium borohydride that effectively removes the sulphate groups present in native agarose (see Section 2.1.2.1). After mixing for 30 minutes epichlorohydrin was added to a final concentration of 2% (v/v) and the reaction was allowed to continue for 4 hours at 25°C. Once the reaction was assumed to be completed the adsorbent solid phase was washed in excess volumes of distilled water.

2.2.5 Fabrication of PVA Adsorbents

The PVA adsorbents were manufactured by a proprietary method and supplied by Dr Igor Galaev, (Lund University, Sweden), no method of fabrication was provided. Four different PVA adsorbents were supplied having different fillers of molybdenum, zirconium silicate (sourced from Glen Creston), titanium oxide and an adsorbent composed solely of PVA. All of the adsorbents were supplied crosslinked using an undisclosed method.

2.2.6 Fabrication of Celbead Adsorbents

The Celbead adsorbents were manufactured using a proprietary method and supplied by Dr Arvind Lali (Mumbai University, India). The fabrication method is under patent application. Three different Celbead adsorbents were supplied, and two were employed in this study and referred to as Celbead (II) and Celbead Amino. The Celbead Amino adsorbent was claimed to be crosslinked cellulose beads with surface amino and hydroxyl groups. The adsorbent had a density of 1.67g/ml (Pai *et al*, 2000) that was considered to be high in comparison to the density of STREAMLINE (1.2g/ml; see Section 2.1.2). The adsorbent was claimed to be 60% pore volume, therefore it was assumed that a high density filler was added to the cellulose base material to achieve the enhanced density that was experimentally measured.

2.2.7 Physical Characteristics

2.2.7.1 Adsorbent Shape

The appearance and shape of the adsorbents was recorded using a light microscope Olympus BH-2 (with the support of photography) with a magnification of x40, x100 or x200. As a comparison, the shape of the commercial benchmark, STREAMLINE was recorded.

2.2.7.2 Size Distribution Determination

The size distribution of the adsorbent solid phases was determined using a Malvern Mastersizer (version 2.18, Malvern Instruments Ltd, UK). The principle of the Mastersizer is based upon light scattering, which delivers a fast, non-intrusive method of particle sizing. The optical configuration employed for the measurement of adsorbent size was conventional Fourier optics. Fourier optics is based on the principle of Fraunhofer diffraction. This is the diffraction of a parallel beam observed at a distance from the diffracting aperture. A lens produces the parallel beam prior to diffraction whilst the adsorbent particle within the beam causes the laser to diffract and a subsequent lens focuses the generated pattern (Figure 2.5; Malvern Instruments Manual). The analyser laser beam used in the device was a Helium-Neon laser that formed the parallel, monochromatic beam of light. The adsorbent particles were introduced to the system via the flow cell (Figure 2.5). The light scattered by the adsorbent particles was reflected through a focusing lens that focuses the diffraction pattern of the scattered light onto a custom designed detector. The unscattered light was brought to a focus on the detector and passed out of the system. The results generated by the Malvern Mastersizer were expressed in terms of equivalent spheres and are volume based. Thus, within a specific size range, x% of the distribution means that the total volume of all adsorbent particles of the diameter within this range, represent x% of the total volume of the

Figure 2.5 Particle sizer system

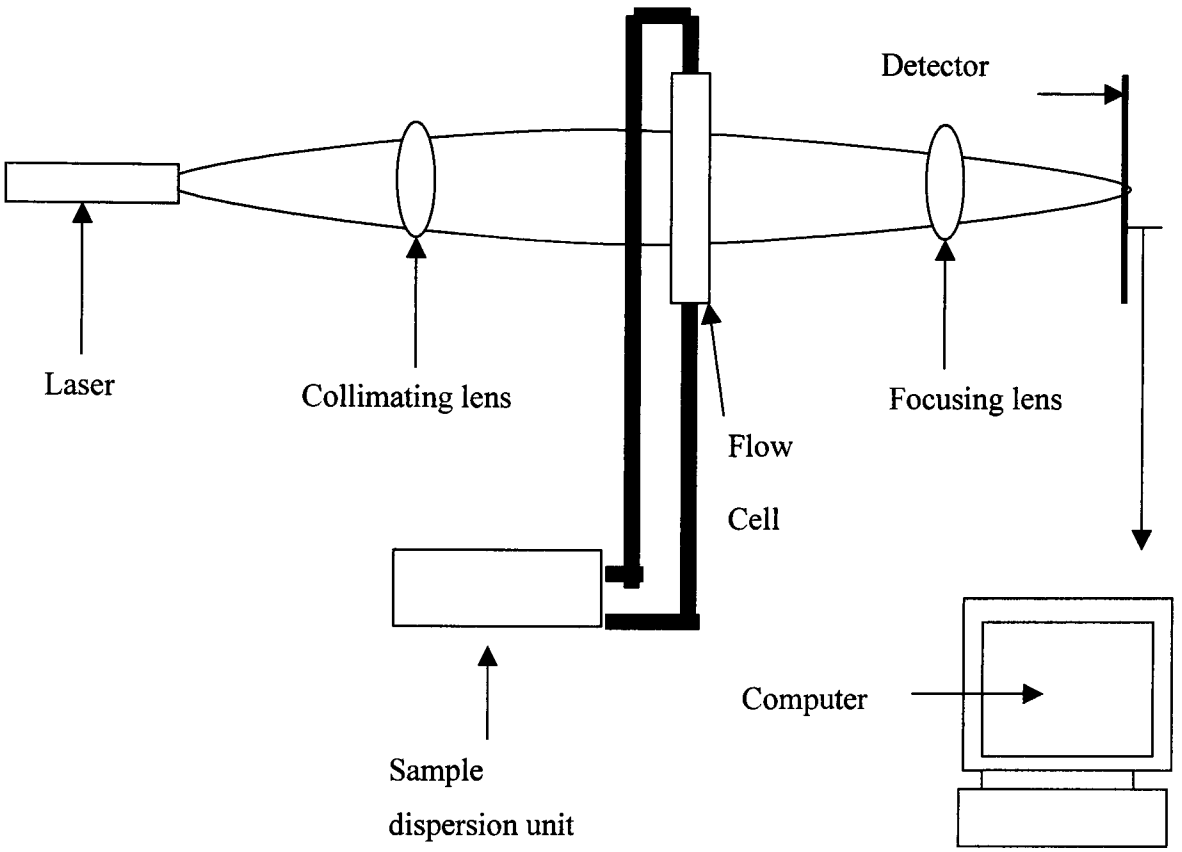

Figure 2.5 represents the particle sizer system used in the Malvern Mastersizer (Malvern Instruments, UK). The sample to be analysed was added to the sample dispersion unit which moved the adsorbent through the flow cell. The parallel laser beam passing through the flow cell was diffracted by the presence of the adsorbent particles. This diffracted beam was focused onto a detector which sends the information to a computer where the particle size is analysed based upon the relationship between the laser diffraction and the particle size assuming that the particles are spherical (see Section 2.2.7.2).

adsorbent particles (Mastersizer Reference Manual). Using the Malvern Mastersizer the particle size range and average particle size was determined for all the adsorbents used in this study.

2.2.7.3 Density Determination

The density of the adsorbents was determined using a simple method of water displacement to yield a value for the wet weight density. A volumetric flask (50ml) was filled with distilled water to the calibrated mark. This weight was taken as weight Xg. An amount of vacuum filtered adsorbent (filtered using a Buchner filter until liquid flow ceased) was added to the flask and the new weight recorded as Yg. The excess water above the calibrated mark was removed and the weight noted as Zg. It was assumed that at ambient temperature the density of the distilled water was 1.0g/ml hence the adsorbent density was determined using the following equation

$$\text{Density (g/ml)} = Y\text{-}X \,/\, Y\text{-}Z$$

Equation 2.1

2.2.8 Measurement of Bed Expansion Characteristics

A volume of pre-equilibrated adsorbent (equilibrated in 10mM Tris-HCl, pH 7.5, 0.02% sodium azide with 0.01% Tween 20, Buffer A) was added to a 1cm (i.d) Omnifit column to a settled bed height (H_o) of 15cm. The settled bed was fluidised by applying an upward liquid flow to the base of the column contactor using a peristaltic pump (refer to Figure 2.6). The bed was expanded in stepwise increases by increasing the linear flow

Figure 2.6 Diagrammatic representation of the mode of bed expansion

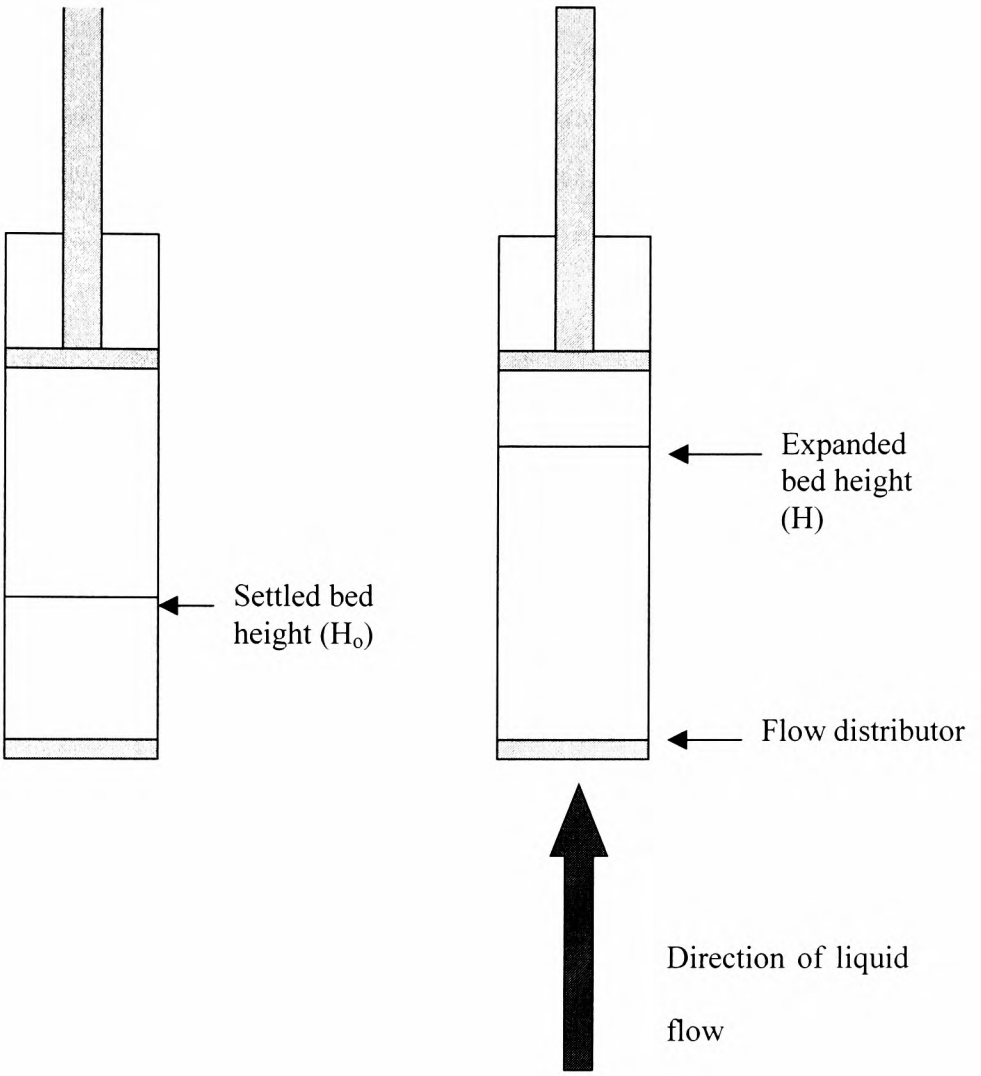

Figure 2.6 represents the expansion of adsorbent within a column contactor when liquid is passed through the column in an upward flow from the base of the column through a flow distributor. The flow is increased and decreased stepwise and the bed height measured with respect to the flow rate entering the column. The bed expansion was determined as H/Ho.

velocity. Between each step the bed was allowed to stabilise for approximately 15 minutes, then the bed height and flow rate was measured up to a maximum expansion. The flow velocity applied to the bed was then decreased stepwise and the bed expansion measured after stable bed expansion was achieved. The settled bed height was recorded as H_o and the stabilised bed expansion was recorded as H, whilst the degree of expansion was expressed as follows:

$$\% \text{ Bed Expansion} = H\text{-}H_o/H_o \times 100$$

Equation 2.2

2.2.9 Ion Exchange Derivatisation

The method used for anion exchange derivatisation was first proposed by Peterson and Sober (1956) and further developed by Gilchrist (1996) and Zhang *et al* (2001). NaOH (16ml at 5.88M) was added to 20g of vacuum filtered adsorbent in small aliquots. The volume of liquid added to the adsorbent was limited to increase the efficiency of the reaction. In order to ensure a thorough coating of all the adsorbent particles only small aliquots of alkali were added and were mixed thoroughly between each addition. The mixture was then allowed to stand in an ice bath for 30 minutes with occasional stirring, which ensured the full penetration of the alkali into the adsorbent particles. Diethylaminoethyl chloride hydrochloride (2.4g in 16ml of distilled water) was added to the mixture in small aliquots to ensure that the system was well mixed. The reactants were then transferred to a round-bottomed flask and attached to a rotary mixing unit that was submerged into a water bath at 80-85°C and the flask rotated for 2 hours. The reaction products were cooled on ice until the mixture was at ambient temperature, whereupon 84ml of 2M NaCl was added in several aliquots. The strong alkaline conditions used in the procedure promoted the production of

reaction side products that are difficult to remove. The presence of salt facilitated the filtration of the impurities from the adsorbent solid phase in addition to controlling the swelling of the adsorbent. The adsorbent was vacuum washed with 1M NaOH using a glass sinter, until the filtrate was clear. The adsorbent cake was subsequently washed with 200ml of 1M HCl and 200ml of 1M NaOH. The adsorbent was suspended in 150ml of 1M NaOH diluted to 1litre with distilled water and left to stand overnight at room temperature. The adsorbent slurry was finally washed with deionised water and stored in 0.02% sodium azide at 4°C.

2.2.9.1 Small Ion Capacity Determination

Small ion capacity estimation was undertaken following a method described by Helfferich (1962) and based upon the establishment of a pH titration curve. Ion exchange capacity was defined as the number of ionic groups per specified amount of ion exchanger and measured in milliequivalents of chloride ions per gram of adsorbent. Vacuum filtered adsorbent was washed in 1M NaOH to completely convert the DEAE anion exchanger to the OH^- form, and then washed with deionised water to remove the excess base. Anion exchangers in their hydroxyl form are insoluble bases that can be considered to act like soluble bases, and hence be titrated with acid. Recording the pH to form a pH titration curve can monitor the neutralisation of the insoluble base. Vacuum filtered adsorbent (1g) was suspended in 50ml of 0.5M NaCl and titrated with 0.01M HCl. Aliquots of 20µl of 0.01M HCl were added and the equilibrium pH of the adsorbent slurry was recorded. A considerable time period (greater than 30 minutes) was required between additions of acid in order to ensure that equilibrium conditions had been established. The titration end point was taken as the point of greatest change of pH per fixed aliquot of acid.

For correct interpretation of the pH titration curve, the mechanism of the titration must be fully explained. Once the adsorbent was completely converted to the OH^- form the solid phase was placed in a salt solution followed by the addition of the titrant. Upon the addition of the HCl the ion exchange took place. The OH^- ions that were released from the solid phases immediately combined with the added H^+ ions:

$$H^+ + OH^- \longrightarrow H_2O$$

According to the Le Chatelier principle the neutralisation of the OH^- ion in solution drives the ion exchange to completion. Cl^- ions are almost completely taken up as long as there are OH^- ions still present on the adsorbent. Therefore the amount of OH^- ions released from the adsorbent was stoichometrically equivalent to the amount of HCl added. Theoretically the pH of the supernatant remains unchanged. Once all the OH^- ions had been replaced by Cl^- ions further additions of the HCl caused a sharp decrease in pH. As seen in Figure 2.7 there was a noticeable pH drop in the initial stages of the titration that was due to the weak nature of DEAE. The hydroxyl groups on the anion exchanger are weakly dissociated which resulted in the adsorbent being reluctant to exchange OH^- groups for the Cl^- ions. Due to this the ion exchange was incomplete after HCl addition resulting in a pH drop. As more HCl was added to the system the ion exchange was driven further to completion, shown by a small plateau in the central region of the titration, and a sharp decrease in pH at the titration end point.

2.3 Results and Discussion

2.3.1 Physical Characteristics of Adsorbent Solid Phases

The main characteristics of the adsorbent solid phases investigated herein include size distribution, shape, density and bed expansion characteristics. All of these properties were recognised to have an influence upon the physical and biochemical performance of the adsorbents for product recovery (refer to Equation 2.3; Section 2.3.2).

Figure 2.7 Small Ion Capacity Determination of STREAMLINE DEAE

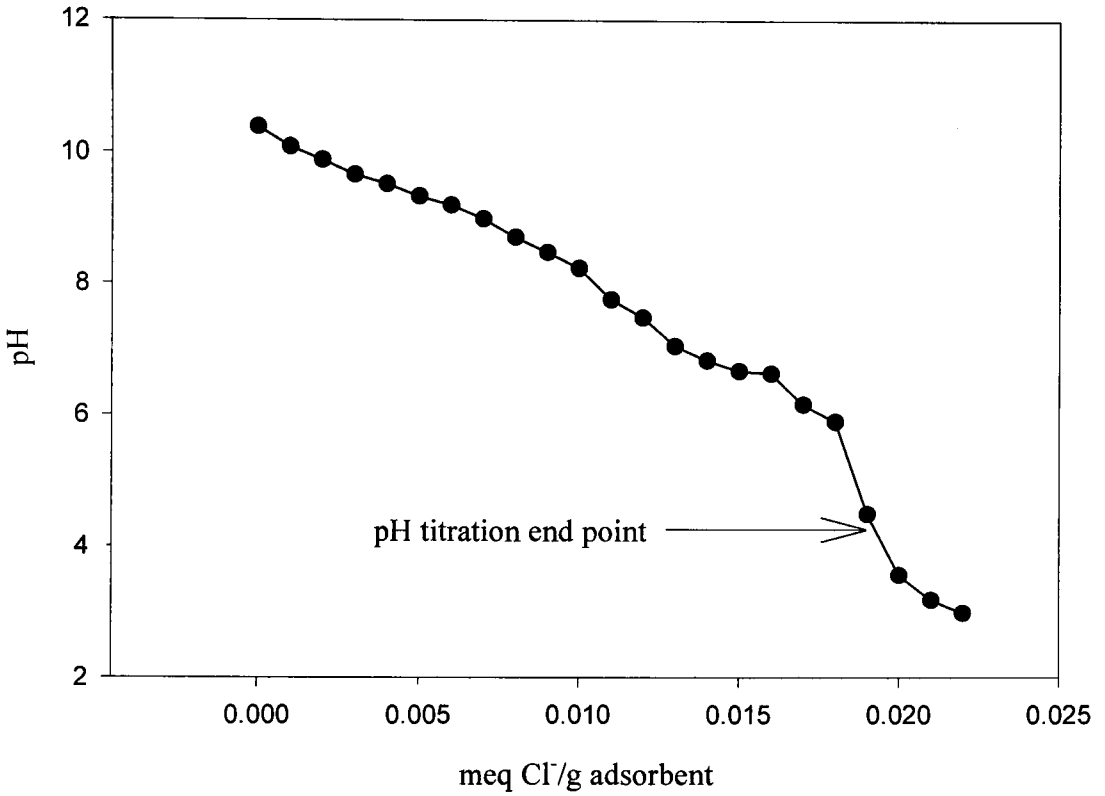

Figure 2.7 represents the pH titration of STREAMLINE DEAE, showing the drop in pH with the addition of aliquots of 0.01M HCl. Adsorbent (1g) was added to 50ml of 0.5M NaCl. Between each addition of acid the pH was allowed to equilibrate for at least 30 minutes. The titration end point was determined as the point at which there was the greatest drop in pH per fixed aliquot of acid.

2.3.1.1 Adsorbent Shape

The commercial adsorbent solid phases STREAMLINE (Type I; Figure 2.1), POROS (Type II; Figure 2.1) and Toyopearl (Type III; Figure 2.1) were characterised by microscopic analysis to reveal apparently spherical shapes (Figures 2.8-2.10). The custom fabricated perfluorocarbon emulsion particles (Type III, Figure 2.1; Figure 2.11) were also characterised by a spherical adsorbent shape for the droplet particles, in contrast to the irregularly shaped 2% ZsA adsorbent (Type IV, Figure 2.1). The light micrograph enabled the zirconium filler material to be visualised showing that the agarose pellicle surrounding the zirconium filler is irregular, as is the number of zirconium particles per adsorbent particle (Figure 2.12). This is also seen with the PVA Zr adsorbent particles (Type II, Figure 2.1; Figure 2.16). The shape of the PVA adsorbents (Type II, Figure 2.1) is generally near spherical and the fillers can clearly be seen in PVA (Figure 2.13), PVA TiO_2 (Figure 2.14), PVA Mo (Figure 2.15) and PVA Zr (Figure 2.16). Both Celbead materials (Type II, Figure 2.1) appeared to be the least spherical of the experimental adsorbents and exhibited a very irregular shape (Figures 2.17 and 2.18).

2.3.1.2 Size Distribution of Adsorbent Solid Phases

The adsorbent solid phases sourced for this study exhibited a wide distribution of sizes. The adsorbents were sized using a Malvern Mastersizer (see in Section 2.2.7.2) which generated data recording the apparent size distribution of the adsorbent populations. Figure 2.19a represents the narrow size distribution of the commercial benchmark adsorbent, STREAMLINE, in comparison to Figure 2.19b that illustrates the wide size distribution of PVA Mo. Such a characteristic is representative of all the custom fabricated prototype adsorbents. STREAMLINE had a more discrete size range as a specific range of adsorbent

Figure 2.8 Optical light micrograph of STREAMLINE

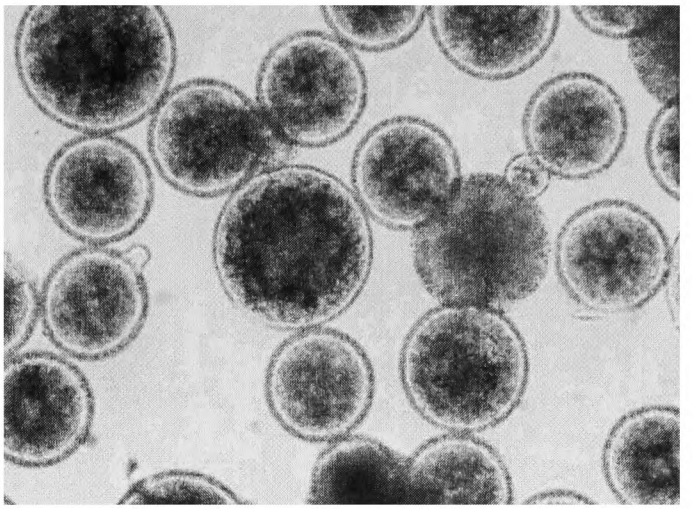

|-------| = 100μm

The optical light micrograph represents the commercial adsorbent STREAMLINE which has an average size of 200μm (refer to Table 2.3). The image was recovered at times 100 magnification (1cm = 100μm).

Figure 2.9 Optical light micrograph of POROS 50D

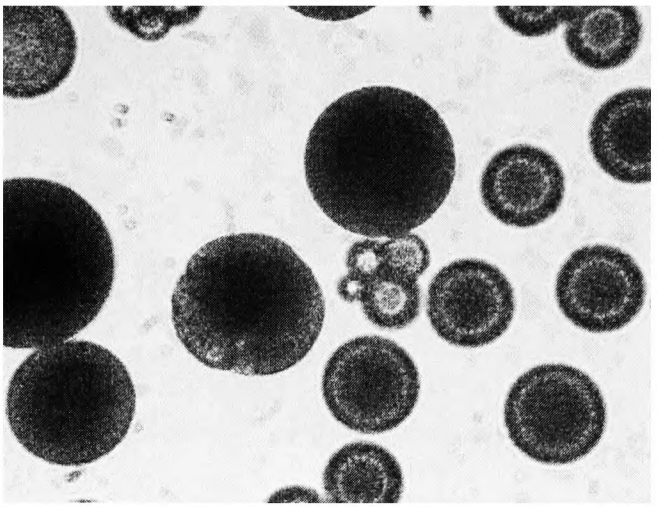

|-------| = 25μm

Figure 2.10 Optical light micrograph of Toyopearl

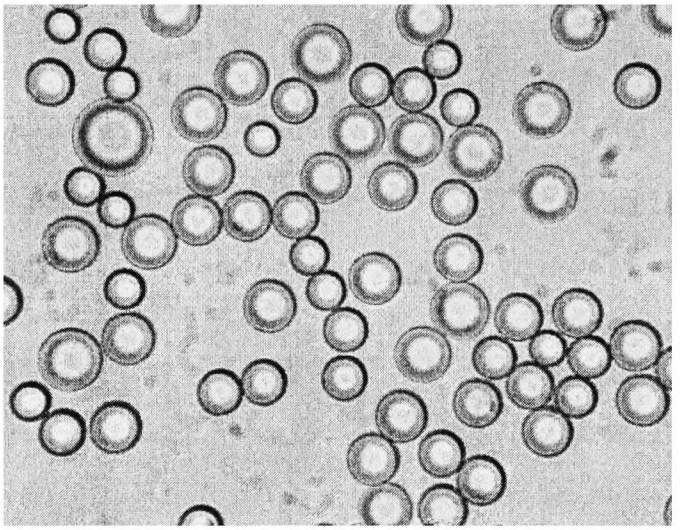

|-------| = 50μm

Both of these adsorbents are commercial adsorbents that had an average size of 50μm and 40μm respectively (refer to Table 2.3). The image of POROS was recovered at 400 times magnification (1cm = 25μm) and Toyopearl at 200 times magnification (1cm = 50μm).

Figure 2.11 Optical light micrograph of perfluorocarbon emulsion

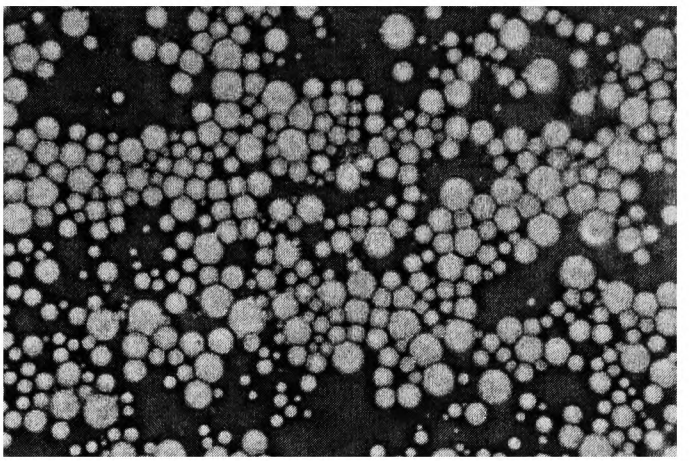

|-------| = 25μm

Figure 2.12 Optical light micrograph of 2% ZsA

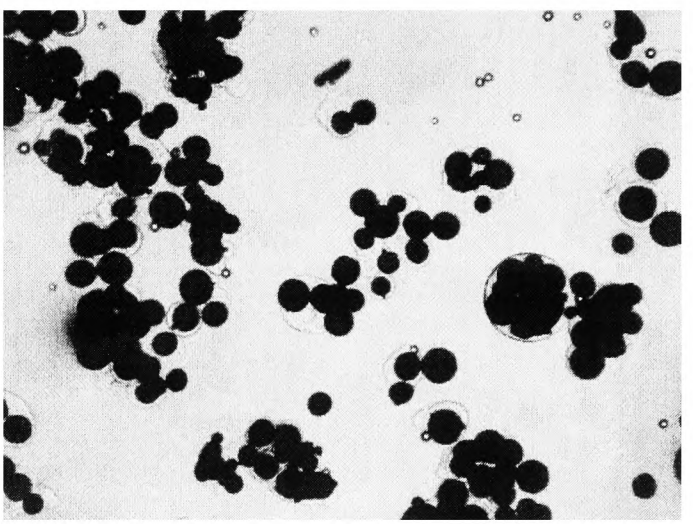

|-------| = 250μm

These are both adsorbents that were assembled in the Biochemical Recovery Group at Birmingham University. Perfluorocarbon emulsions were fabricated using a method proposed by McCreath and Chase (1996a) and the 2% ZsA was assembled by Professor Yan Sun (Sun et al, 2001; Tianjin University, PR China). The image of perfluorocarbon emulsion was recovered at 400 times magnification (1cm = 25μm) and 2% ZsA image was recovered at 40 times magnification (1cm = 250μm).

Figure 2.13 Optical light micrograph of PVA

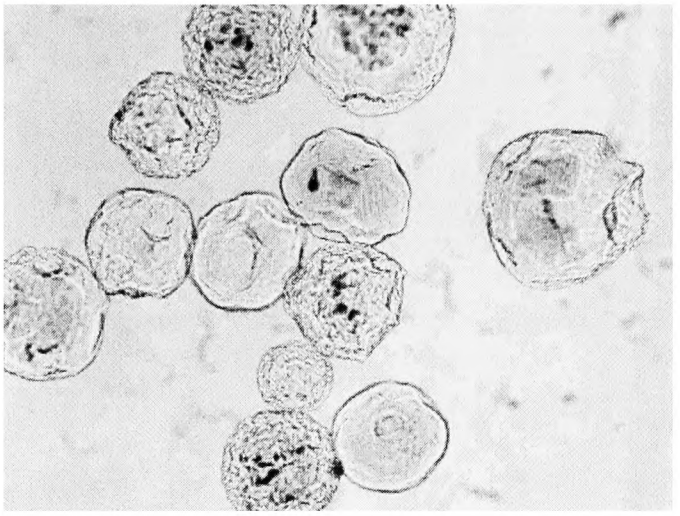

|-------| = 100μm

Figure 2.14 Optical light micrograph of PVA TiO_2

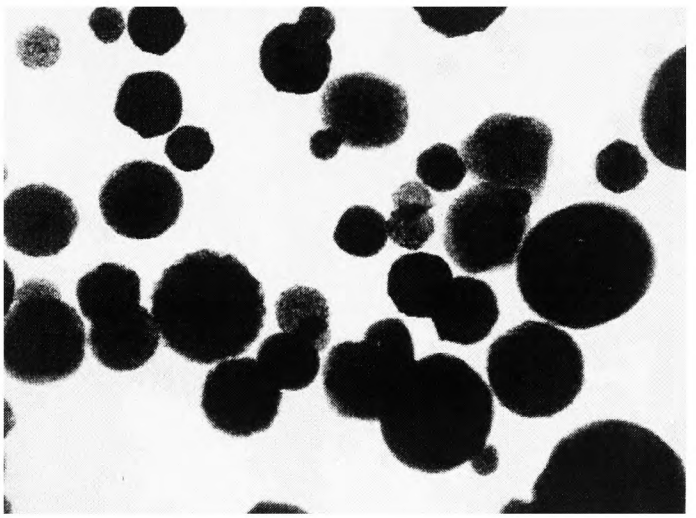

|-------| = 250μm

The optical light micrographs above represent PVA and PVA TiO_2 adsorbents that were manufactured and supplied by Igor Galaev (Lund University, Sweden). The image of PVA was recovered at 100 times magnification (1cm = 100μm) and PVA TiO_2 at 40 times magnification (1cm = 250μm).

Figure 2.15 Optical light micrograph of PVA Mo

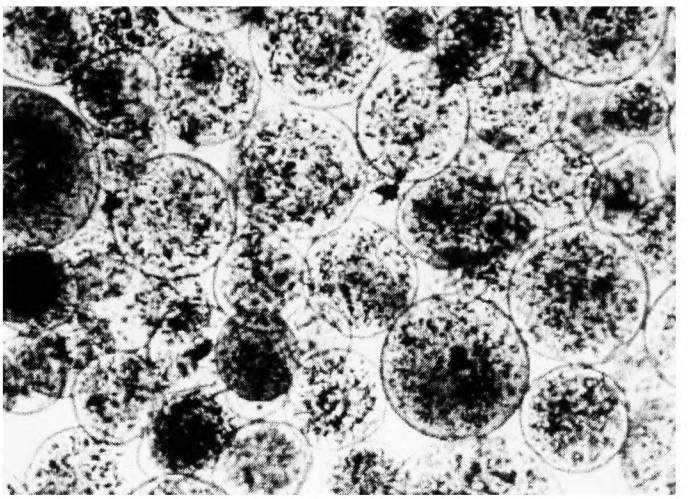

|-------| = 250μm

Figure 2.16 Optical light micrograph of PVA Zr

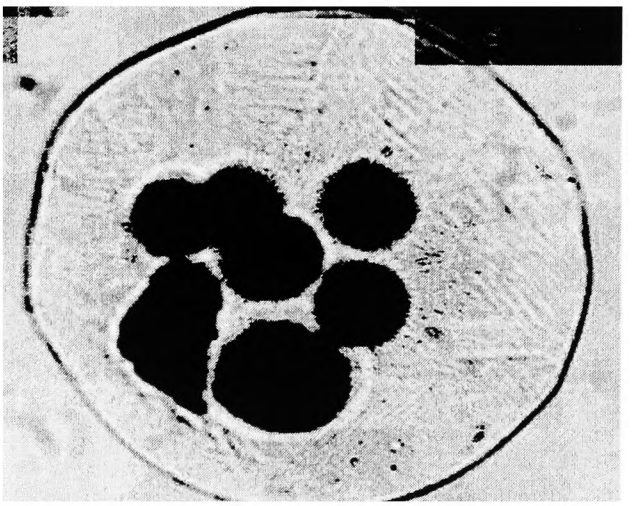

|-------| = 100μm

The optical light micrographs represent PVA Mo and PVA Zr adsorbents that were manufactured and supplied by Igor Galaev (Lund University, Sweden. The image of PVA Mo was recovered at 40 times magnification (1cm = 250μm) and PVA Zr was recovered at 100 times magnification (1cm = 100μm).

Figure 2.17 Optical micrograph of Celbead (II)

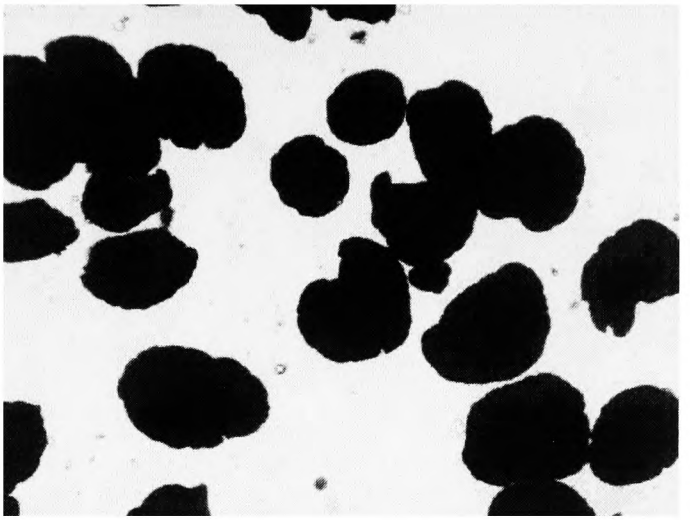

|-------| = 250μm

Figure 2.18 Optical light micrograph of Celbead Amino

|-------| = 250μm

The optical light micrographs above represent the Celbead adsorbents fabricated by Arvind Lali (Mumbai University, India). The Celbead (II) and Celbead Amino images were recovered at 40 times magnification (1cm = 250μm).

Figure 2.19 Size distribution graphs a) STREAMLINE and b) PVA Mo

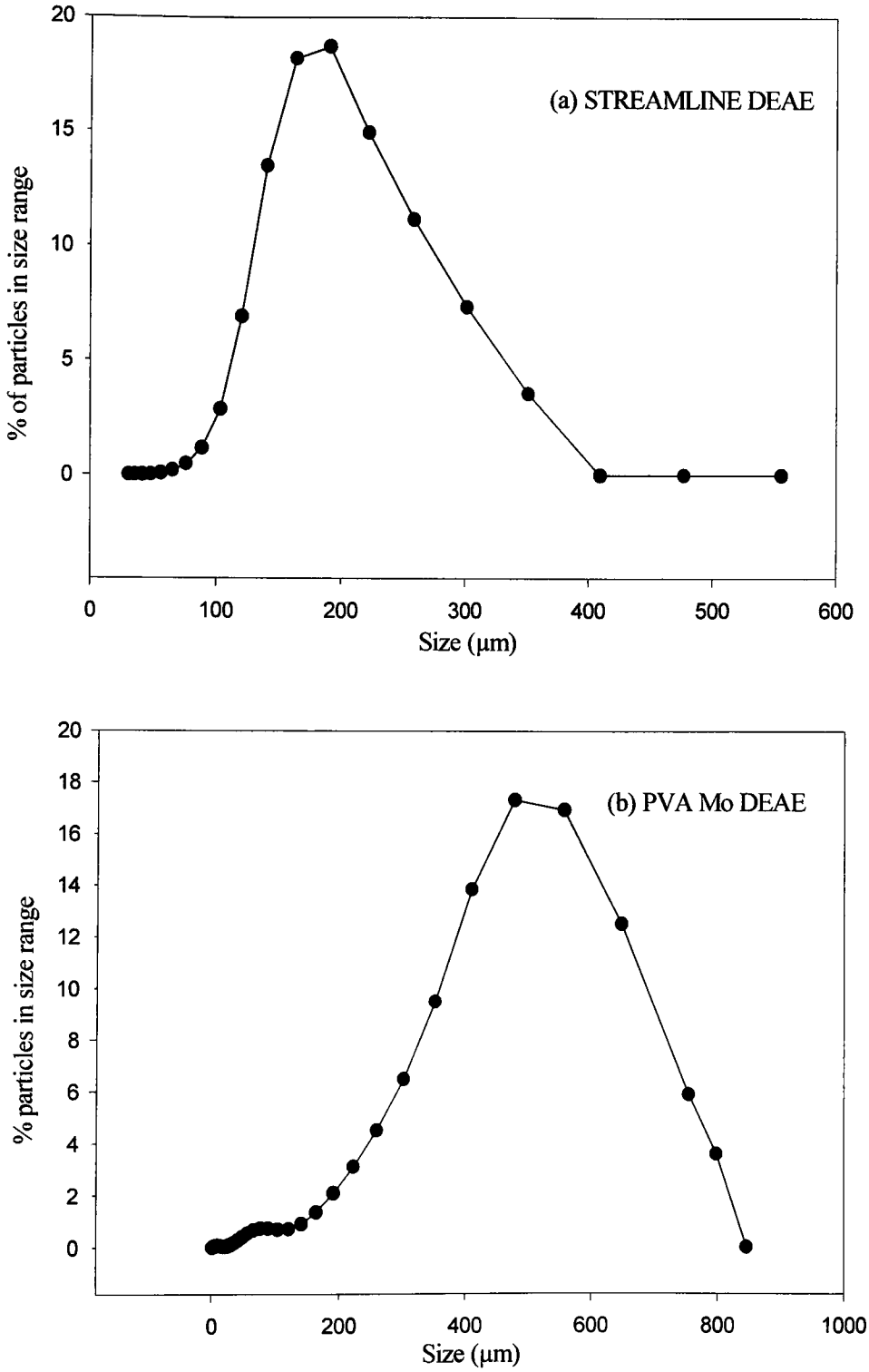

These graphs represent the size distribution profiles of the commercial adsorbent STREAMLINE (Figure 2.19a) in comparison to the 'in house' fabricated adsorbent PVA Mo (Figure 2.19b). The traces were generated from the Malvern Mastersizer (Malvern Instruments, Malvern, UK). The adsorbent particles were suspended in water.

size is selected for the commercial market. The size distribution analysis enabled the average particle size of each adsorbent to be determined. This illustrated a marked difference in particle size of the selected adsorbents from the perfluorocarbon emulsions at 10μm in diameter (Type III, see Figure 2.1) to PVA Zr with a diameter of 515μm (Type II, see Figure 2.1; refer to Table 2.3). Adsorbent particle size is an important factor to be considered in terms of the bed expansion performance of the adsorbents (refer to Equation 2.3, Section 2.3.2).

2.3.1.3 Density Determination

The measurement of density for each of the adsorbent solid phases was carried out since density is recognised to be an influencing factor upon the bed expansion properties of adsorbents (refer to Equation 2.3; Section 2.3.2). The density of the adsorbents under study varied depending on both the base material and also the filler that was contained within the adsorbent structure. The highest density adsorbent used in this study was the perfluorocarbon emulsion (Table 2.3) where the density was due to the perfluorodecalin base material (density = 1.917g/ml; see Table 2.2a). All of the custom designed adsorbents showed higher densities than the Type I benchmark adsorbent, STREAMLINE (see Figure 2.1), except the adsorbent that consisted solely of PVA (see Table 2.3). Since STREAMLINE was a commercial adsorbent specifically designed for fluidised bed adsorption chromatography and the selected adsorbents had superior densities the data suggested that these adsorbents would also show a superior bed expansion performance.

2.3.2 Bed Expansion Characterisation

It was important to characterise the bed expansion properties of the adsorbent solid phases in order to assess the suitability of the adsorbents for fluidised bed recovery of

Table 2.3 Average adsorbent particle sizes and density

ADSORBENT TYPE	ADSORBENT	DENSITY (g/ml)	SIZE (μm)
I	STREAMLINE	1.2	209
II	Celbead (II)	1.38	395
	Celbead Amino	1.45	398
	POROS	1.01	50
	PVA	1.01	390
	PVA Mo	1.39	423
	PVA TiO_2	1.13	428
	PVA Zr	1.37	515
III	Perfluorocarbon emulsion	2.1	10
	Toyopearl	1.46	30
IV	2% ZsA	1.67	209

Particle sizes of both the commercial and custom fabricated prototype adsorbents were determined using a Malvern Mastersizer (Malvern Instruments Ltd, UK). This technique is based upon the principle of light scattering therefore it is a fast and non-intrusive technique for particle sizing. The pattern of light scattering is converted into equivalent spheres which is then expressed as a volume percentage (see Section 2.2.7.2). In addition, the densities were based on wet weight adsorbent densities and were determined using a simple method of water displacement (see Section 2.2.7.3). Both the size and density of the adsorbent solid phases are important characteristics since both affect the sedimentation of adsorbent particles according to Stokes law (refer to Section 3.2.3). Each figure represents an average determined from triplicate measurements.

biological materials. For experimental characterisation a single buffer system was applied to determine the degree of bed expansion of the selected adsorbent solid phases. Figure 2.20 illustrates the bed expansion characteristics of the adsorbents in 10mM Tris-HCl, pH 7.5 with 0.02% sodium azide and 0.01% Tween 20 (Buffer A). The bed expansion at a specific linear flow velocity increased with the decreasing density of the adsorbent solid phases, with the exception of the perfluorocarbon emulsion (Type III, see Figure 2.1). This adsorbent had a density of 2.1g/ml (refer to Table 2.3), the highest density overall, but the expansion was poor which was attributed to the small size (10μm) of the adsorbent (see Figure 2.3). According to Stoke's Law (see Equation 2.3) the particle diameter (p) has a greater effect on sedimentation velocity than the particle density (ρ).

$$U_t = (\rho_p - \rho_l)dp^2g/18\eta \qquad \text{Equation 2.3}$$

Two adsorbents (POROS, Type II; see Figure 2.1 and Toyopearl, Type III; see Figure 2.1) were not subjected to the bed expansion tests, since the limited size and density of both materials compromised controlled bed expansion (see Table 2.3).

There are numerous theories and correlations describing the liquid fluidisation of particles (Di Felice, 1995) including bed expansion characterisation. One of the most commonly used methods is the simple correlation of Richardson and Zaki (1954) where the expansion of particles in liquid is characterised by the following equation

$$U = U_t \times \varepsilon^n \qquad \text{Equation 2.4}$$

which correlates the voidage of the bed (ε) with the linear velocity (U) using the terminal settling velocity of a single particle (U_t) and the expansion index (n). The terminal settling velocity and bed expansion index is determined from measurements of the bed void volume

Figure 2.20 Bed expansion profiles of adsorbent solid phases

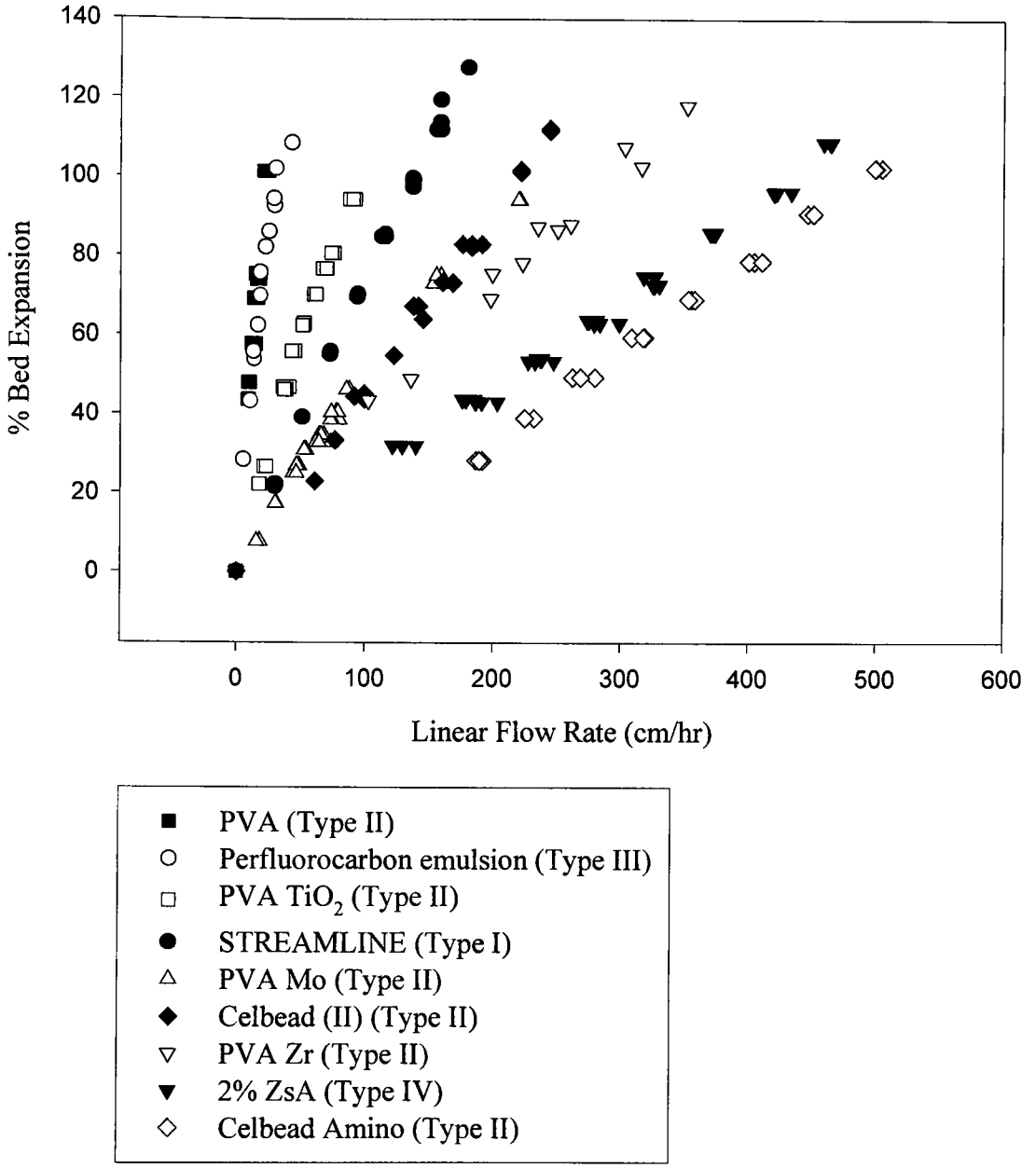

The liquid phase used for the bed expansion was 10mM Tris-HCl, pH 7.5, 0.02% sodium azide and 0.01% Tween 20. The settled bed height used was 15cm in a 1cm (i.d) Omnifit column. The flow was applied to the base of the column using a peristaltic pump. The bed was allowed to settle for 15 minutes until stable and the bed height was measured against the flow rate entering the column. Triple determinations were completed for each bed expansion test.

at different linear velocities. A double –log plot of ε vs U enables n and U_t to be determined from the slope and intercept respectively using linear regression analysis.

The Richardson and Zaki analysis was not the method chosen for bed expansion characterisation in this study because this equation assumes that the particles are monodisperse, spherical particles. As a consequence of the physical characterisation studies some of the selected adsorbent solid phases were shown to be non-spherical (see Figures 2.17 and 2.18) and all the adsorbent solid phases were characterised with a wide particle size distribution (see Figure 2.19).

2.3.3 Anion Exchange Derivatisation

The adsorbents used were derivatised with diethylaminoethyl (DEAE) chemistry that is defined as a weak anion exchanger in the face of the limited degree of ionisation of the group over a wide pH range. The DEAE chemistry was introduced using a method from Peterson and Sober (1956) adapted by Gilchrist (1996). The protocol adopted herein followed the original method except for the use of an 'in house' built rotary mixing unit to accommodate batch reactions of 50ml which limited any mechanical destruction of the adsorbents during the mixing process. The success of the reaction was indicated by a minimal generation of fines and was quantified in terms of the small ion capacity using the method reported in Sections 2.2.9.1 and 2.3.3.1.

2.3.3.1 Small Ion Capacity Determination

The amount of DEAE groups immobilised covalently upon the adsorbent solid phase was quantified using pH titration following the method reported by Helfferich (1962) and developed by Griessbach (1939). An anion exchanger in the hydroxyl (OH^-) form was considered to be an insoluble base, which could be neutralised by the addition of acid. This

neutralisation was measured by monitoring the pH of the system and a pH titration curve could be produced relating the molarity of acid added to the changing pH. Figure 2.7 illustrates a representative pH titration curve determined for the commercial adsorbent, STREAMLINE DEAE. The titration end point of the neutralisation was determined as the greatest change of pH per fixed aliquot of acid added (see Section 2.2.9.1). Small ion capacity was measured in terms of milliequivalents of Cl^- ions per milliliter of adsorbent. The shape of the pH titration curve was typical of that for a 'weak' DEAE anion exchanger (Peterson and Sober, 1956; see Section 2.2.9.1).

Table 2.4 represents the small ion capacities for all the adsorbent solid phases used (Types I-IV) which demonstrates there was a variation in capacity for the different adsorbent types. The PVA adsorbents (Type II, see Figure 2.1) and the perfluorocarbon emulsion (Type III, see Figure 2.1) exhibited the lowest small ion capacities. This was attributed to the hydroxyls on the PVA being less reactive than those found on agarose and cellulose thus diminishing the coupling reaction. The Celbead materials also demonstrated low capacities in comparison to the other adsorbent solid phases investigated in the study. However the pore volume of this adsorbent was reported to be 60% of the total adsorbent volume (Pai *et al*, 2000), which indicated that there was a limited surface area available for ligand attachment. In addition, it was unknown whether the Celbead materials were crosslinked, which would have had further impact upon adsorbent derivatisation (Gilchrist, 1996). The data expressed in Table 2.4 may be over estimations due to the extended times required for equilibration and it could not be guaranteed that equilibrium had been reached. However the small ion capacity determined for STREAMLINE DEAE by pH titration (170μmol) compared favourably with the data supplied by the manufacturers (120-180μmol).

Table 2.4 A summary of the small ion capacities determined for the selected adsorbent solid phases.

ADSORBENT TYPE	ADSORBENT	SMALL ION CAPACITY (μmol Cl^-/ml adsorbent)
I	STREAMLINE	170
II	Celbead (II)	41
	Celbead Amino	300*
	POROS 50D	100
	PVA	1.6
	PVA Mo	2.78
	PVA TiO_2	3.3
	PVA Zr	54.4
III	Perfluorocarbon emulsion	8
	Toyopearl	490
IV	2% ZsA	89

*For Celbead Amino the small ion capacity equivalent is μmol amine groups/ml adsorbent as determined at Mumbai University, India.

The small ion capacities of the adsorbent solid phases were determined by the generation of a pH titration curve (see Figure 2.7). The titration end point was determined as the point at which there was the largest drop in pH per fixed aliquot of HCl added and the small ion capacity was determined as the Cl- molar equivalent added at the titration end point (see Section 2.3.3.1)

2.3.4 General Conclusions

The aim of this chapter was to investigate the physical characteristics of a variety of adsorbent solid phases having different internal and external geometries. The adsorbent used were either commercial or custom fabricated prototype adsorbents produced in Birmingham, or in other laboratories (Mumbai University, India; Lund University, Sweden; see Table 2.1). The physical characteristics investigated were size, shape, density and bed expansion. The adsorbents exhibited a variety of sizes from 10μm (perfluorocarbon emulsion) to 515μm (PVA Zr; see Table 2.3). The density of these adsorbents also varied from 1.12g/ml to 2.1g/ml, however the increase in density did not necessarily correspond to a decrease in bed expansion (see Figure 2.20). This was attributed to the relative sizes of the adsorbent, as the adsorbent that had the highest density (perfluorocarbon emulsion) had the smallest adsorbent size (see Table 2.3). All of the fluidisable adsorbents demonstrated superior expansion characteristics in comparison to the commercial benchmark, STREAMLINE. Toyopearl (Type III, see Figure 2.1) and POROS (Type II, see Figure 2.1) were not included in the bed expansion tests due to their limited density (see Table 2.3). During bed expansion the top of the bed was indiscernible due to the adsorbent particles being entrained out of the column contactor as a result of the upward liquid flow velocity applied to the bed to fluidise the adsorbent particles.

The commercial adsorbents all exhibited a spherical geometry (see Figures 2.8-2.10) and the custom fabricated adsorbents were generally spherical (see Figures 2.11-2.16), except for the Celbead materials (Type II, see Figure 2.1; Mumbai University, India) which were very irregular in shape, particularly Celbead Amino (see Figure 2.17-2.18). The difference in shape between the Celbead materials suggested that the adsorbents were fabricated using different unknown manufacturing methods. However, due to the enhanced densities they demonstrated adequate bed expansion behaviour in comparison to STREAMLINE (Type I,

see Figure 2.1; see Figure 2.20). The selected adsorbent solid phases were derivatised with DEAE or amino anion exchange chemistries and showed a variety of small ion capacities (see Table 2.4), as a consequence of both the surface area available for ligand attachment and the reactivity of the hydroxyls on the adsorbent base material. The measurement of small ion capacity represents the number of anion exchange groups immobilised to the adsorbent solid phase. However, all of these groups will not be available for adsorption due to the groups being inaccessible to both soluble and particulate products. A realistic measurement of the number of groups available for adsorption can be determined from batch binding experiments with soluble and particulate protein.

As stated (see Section 2.1) the aim of this study was to investigate candidate adsorbent solid phases as ideal adsorbents for fluidised bed adsorptive recovery of economically desirable nanoparticulate products such as viruses, plasmid DNA and drug delivery vehicles. Chapter 2 investigated the physical characterisation of the selected adsorbent solid phases. The results demonstrated that the adsorbent solid phases (Types I-IV) exhibited a variety of sizes, densities, shapes and small ion capacities. The physical characterisation studies suggested that Celbead Amino (Type II, see Figure 2.1) exhibited superior bed expansion characteristics in comparison to the adsorbent solid phases included in the study.

CHAPTER 3

BIOCHEMICAL CHARACTERISATION OF ADSORBENT SOLID PHASES

3.1 General Introduction

There has been a growing interest in the manufacture of nanoparticulate products (see Section 2.1) that has not been matched by the development of chromatographic adsorbents suitable for the fluidised bed recovery of such products. Currently available chromatographic adsorbents are expected to show process disadvantages as noted in Section 2.1, and thus alternative adsorbent configurations have been investigated as candidate adsorbents for nanoparticulate recovery (designated Type I to IV, see Figure 2.1). Chapter 2 detailed the physical performance of the adsorbents selected for this study (see Table 2.1) and the data generated suggested that Celbead Amino (Type II, see Figure 2.1) demonstrated the best performance in terms of the fluidisable quality of the adsorbent (see Figure 2.20).

Chapter 3 describes the study of commercial and custom designed adsorbent solid phases, classified as Types I to IV (see Figure 2.1), that have been critically evaluated in adsorptive studies with nanoparticulate and protein products in batch binding experimentation. This is justified as follows. A major problem associated with commercially realistic studies of virus or plasmid recovery, is the quantity of nanoparticulates required for representative binding studies. Effective working capacities of ion exchangers and other adsorbents are not widely reported in the literature, however they appear to be between 10^9 and 10^{12} particles per milliliter of settled adsorbent (O'Neil and Balkovic, 1993; Hughye *et al*, 1995). Lyddiatt and O'Sullivan (1998) described naïve calculations with respect to the number of 50nm spheres (i.e. an average virus particle) that could be packed as a single layer upon the surface of a 100μm spherical, solid adsorbent particle. The yielded values

approximated to 10^{12} particles per milliliter of settled adsorbent. Typical virus harvest titres have been claimed to be in the range of 10^{6} to 10^{11} virus particles per milliliter of cell culture supernatant. Therefore for one milliliter of settled adsorbent 1-1000 litres of supernatant will be required for saturation to be achieved.

The practical problem of material supply for the primary scouting experiments was circumvented by exploiting synthetic nanoparticulates, such as particulate BSA formed by coacervation and crosslinking to form protein nanoparticles (see Section 3.1.1). Preliminary batch binding experiments were completed using both soluble bovine serum albumin (BSA, refer to Section 3.1.3) and particulate BSA. The separation of soluble BSA from particulate BSA is a model for all nanoparticulate recovery with respect to the separation of product assemblies from product components. In addition, the recovery of soluble BSA can be representative of the separation of products from components of complex feedstocks.

3.1.1 Fabrication of Synthetic Protein Nanoparticulates

Protein nanoparticles were employed as representative nanoparticulate products in the present study and were fabricated as size and charge mimics. The nanoparticles can be fabricated having different sizes representative of a variety of nanoparticular products such as plasmid DNA, viruses and drug delivery vehicles (see below). Protein nanoparticles are an example of macromolecular assemblies that have been produced as putative drug delivery vehicles for the delivery of intravenous drugs to specific organs or target sites within the body (Lin *et al*, 1994). Such protein nanoparticles have been modified for both drug delivery functions and gene therapy applications (Coester *et al*, 2000; Langer *et al*, 2000).

The protein nanoparticles used in this study were fabricated following a method proposed by Lin *et al* (1993) based upon the principle of coacervation which is the reversible aggregation of particles of an emulsion into liquid droplets preceding flocculation. The

protein used for this study was bovine serum albumin (refer to Section 3.1.3) which is characterised as having a high content of charged amino acids such that the protein is insoluble in organic solvents (refer to Section 3.1.3). BSA nanoparticles (BSAp) can be prepared by adding water miscible organic solvents, such as ethanol or acetone to the BSA solution, to encourage the protein to aggregate into small particles which can be subsequently stabilised by the addition of crosslinking reagents. The nanoparticle size is dependent on several factors including the amount of coacervation agent added, the mixing conditions, temperature and the viscosity of the solution (Lin *et al*, 1994).

3.1.2 Nanoparticle Sizing using Photon Correlation Spectroscopy

The size distribution of the fabricated BSAp was analysed by photon correlation spectroscopy (PCS) using a Malvern Zetasizer 1000HS/IHPL (Malvern Instruments, UK) made available by Dr L. Seymour, (Cancer Research Centre, University of Birmingham).

PCS is the industrially preferred method of sub-micron particle size analysis. The PCS equipment comprises a 5mW helium neon laser and 90° scattering optics linked to a computer for real time analysis of the results. The samples analysed in the PCS device should consist of well dispersed particles in a liquid medium. In such conditions the particles are in constant random motion, referred to as Brownian motion and PCS measures the speed of this motion by passing a laser (at a wavelength of 532nm) through the sample at 90°. PCS relates the diffusion speed of the particles to the speed of Brownian motion using the Einstein-diffusion equation.

$$D = \delta^2/2T = RT/6\pi\eta rN_A \qquad \text{Equation 3.1}$$

As a result of Brownian motion, particles migrate an average distance (δ) in each small time interval (T). The diameter of the particles can be determined from the Einstein-diffusion equation where D is the diffusion coefficient, N_A is Avogadro's number, and R is the gas

constant and T absolute temperature. The measurements determined by PCS include the average particle size and the Polydispersity Index (PI) which is a measure of the range of particle sizes within the measured sample. The measurement must be below 0.7 (70%) for the average particle size to be determined accurately, a higher PI indicates that the particle size range is too large for the device to accurately measure the speed of the Brownian motion. The data generated expresses the particle size as a percentage of the total number of particles in any one size range.

3.1.3 Bovine Serum Albumin

Bovine serum albumin (Fraction V powder, 96% purity) was the protein chosen for this study on the basis of its availability and relatively low cost. Serum albumin is a nonglycoprotein, i.e. the protein does not contain covalently linked sugar residues (Cohn *et al*, 1947) and has been shown to have a molecular weight of 66.7kD with an isoelectric point of pH 5.1 (see Section 2.2.9). Albumins are characterised by a low content of tryptophan and methionine residues together with a high content of cysteine residues and charged amino acids. These include aspartate, glutamate, lysine and arginine (Peters, 1985) with glycine and isoleucine also present in lower numbers than in an average protein (see Table 3.1). Aspartate and glutamate residues are negatively charged amino acids and are the residues that will primarily interact with the positively charged DEAE anion exchange chemistry immobilised to the adsorbent solid phases (see Section 2.2.9; 2.2.9.1). Serum albumin is a soluble protein that exhibits a good stability due to the high total charge of the protein in addition to the many disulphide bonds present in the protein.

Table 3.1 Amino acid composition of bovine and human serum albumin

AMINO ACID RESIDUE	NUMBER OF AMINO ACIDS	
	BSA	HSA
Aspartate (-ve)	41	36
Glutamate (-ve)	59	62
Lysine (+ve)	59	59
Histidine (+ve)	17	16
Arginine (+ve)	23	24

Table 3.1 summarises the number of charged amino acids present in both bovine and human serum albumin (Peters, 1995).

3.1.4 Estimation of the Maximum Binding Capacity for the Selected Adsorbent Solid Phases

Subsequent to the adsorption/desorption batch binding experiments, the maximum binding capacity of the selected adsorbent solid phases was estimated using Langmuir assumptions. The Langmuir isotherm permits an estimate of how much product an adsorbent is capable of adsorbing (q_m) and how tightly the product binds to the immobilised ligand (k_d). Consequently the estimates made from the Langmuir isotherm can be applied to the scale up of a chromatographic separation and the approximation of the desorption behaviour of the product for a particular immobilised ligand.

The principle of separation by ion exchange chromatography is dependent upon the reversible adsorption of charged molecules to oppositely charged immobilised ion exchange groups (see Section 2.1.9). This interaction can be described by an equilibrium relationship

$$A + B \underset{k_2}{\overset{k_1}{\rightleftharpoons}} AB \qquad \text{Equation 3.2}$$

The rate constants, k_1 and k_2 govern the forward and backward direction of the reaction whilst the equilibrium relationship is described by the dissociation constant (K_d) which is equal to the ratio of k_2/k_1. Several isotherm models have been proposed for determining both the dissociation constant (K_d) and maximum binding capacity (q_m) including linear, Freundlich, bi-Langmuir, Langmuir and Freundlich-Langmuir isotherm models. In 1984 Chase proposed the Langmuir isotherm model to describe affinity chromatography and it is recognised as the most popular model due to its simplicity and good agreement with experimental data (Lan *et al*, 2001). The Langmuir model is based on the following equation

$$q^* = q_m C^*/(K_d + C^*) \qquad \text{Equation 3.3}$$

(Chase, 1984)

The constants q* and C* represent the equilibrium concentration of the biomolecules for the adsorbent solid phase and liquid phase respectively. The maximum binding capacity is represented by q_m whilst K_d is the dissociation constant of the solute-adsorbent complex, that represents a measure of the affinity between the biomolecules and the adsorbent solid phase.

The Langmuir isotherm (Langmuir, 1916) was proposed to describe the adsorption of gases onto surfaces and several assumptions are made when applying the model to protein adsorption,

i) the biomolecule can bind to the ligand via independent binding sites,

ii) the kinetics of the interaction follows first order approximations (i.e. the rate of reaction is proportional to the concentration of a single reactant),

iii) the stoichiometry of the protein-ligand interaction remains 1:1 throughout the isotherm range,

iv) all binding sites are of equal energy,

v) a molecule adsorbed onto one binding site does not influence the adsorption of another molecule on a neighbouring binding site (Chase, 1984),

The Langmuir isotherm has been widely accepted as a method for describing protein adsorption to ion exchange and affinity adsorbents. However, Langmuir assumptions may be unrealistic due to a number of effects, such as the heterogeneity of the protein and adsorbent surface and the tendency of the protein molecules or adsorbent particles to aggregate. As a result this model is considered to be more an empirical model rather than a theoretical model (Lan *et al*, 2001).

3.2 Materials and Methods

3.2.1 Chemicals

The Bradford Assay reagent was supplied by PERBIO (formerly Pierce Warriner Ltd, Cheshire, UK) and Bovine Serum Albumin (Fraction V powder, 96% purity) was supplied by Sigma-Aldrich (Poole, Dorset, UK). All other chemicals used were reagent grade unless otherwise stated and supplied by Sigma-Aldrich (Poole, Dorset, UK) or BDH (Poole, Dorset, UK).

3.2.2 Equipment

- Malvern Zetasizer 1000HS/IHPL, Malvern instruments Ltd, Malvern, UK.
- Rotary blood mixer, Stuart Scientific Company Ltd, UK.
- Pharmacia LKB Ultrospec III spectrophotometer, Amersham Biosciences, Uppsala, Sweden.
- pH meter, Hanna Instruments, H19321, Microprocessor Bench pH meter.
- Millipore ultrafiltration unit, Millipore, Bedford MA, USA
- Beckman Centrifuge, Model J2-21, Beckman Coulter Research
- Peristaltic pump, model 101U (maximum output 15W), Watson-Marlow Company Ltd, Cornwall, UK.
- General laboratory glassware

3.2.3 Preparation of BSA Nanoparticles

BSA nanoparticles were prepared following a method proposed by Lin *et al* (1993) adapted by Zhang *et al* (2001). A BSA solution (300ml) at a concentration of 5mg/ml was prepared in 10mM Tris-HCl buffer, pH 7.5 containing 0.02% sodium azide and 0.01% Tween 20 (Buffer A). A volume of absolute ethanol was added to the BSA solution, under

constant magnetic agitation, using a peristaltic pump until the solution became turbid indicating the formation of protein nanoparticles. Glutaraldehyde (150µl of 50% w/v) was subsequently added to crosslink the protein nanoparticles formed by coacervation. The reaction was continued for 1 hour at room temperature under magnetic agitation. To block any unreacted aldehyde groups 75µl of 1M ethanolamine was added and the reaction continued for one hour. To stabilise the so-formed nanoparticles, Tween 20 was added to a final concentration of 0.01% (v/v). Larger particles (greater than 200nm in diameter) were sedimented from the mixture by centrifuging for 30 minutes at 48,400g at a temperature of 10°C. Ethanol was removed from the mixture by dialysis with distilled water overnight (100ml of supernatant to 500ml of distilled water). Soluble BSA was separated from the BSA nanoparticles by ultra/diafiltration using a polyacrylonitrile/polyvinylchloride copolymer membrane with a molecular weight exclusion of 300,000 Daltons (supplied by Millipore, Bedford, MA, USA). In accordance with the manufacturers guidelines, before use the membrane was washed in distilled water whilst in between uses the membrane was washed in a 0.5% solution of Tergazyme for 30 minutes followed by washing in distilled water to remove any debris from the membrane surface. Soluble BSA was determined to be fully removed when the BSA concentration of the permeate was less than 1% of the concentration of the nanoparticle solution. The protein concentration was determined using the Bradford assay (see Section 3.2.6) and finally to remove any remaining large nanoparticles the supernatant was filtered through a 0.2µm cellulose nitrate membrane (Millipore, Bedford, MA, USA). The final nanoparticle yield, after dia/ultrafiltration, was approximately 220µg of nanoparticles (soluble BSA equivalents) per milliliter of supernatant in a final volume of 200ml (equivalent to a yield of approximately 2.5%). The final nanoparticle yield was very low, and could be attributed in part to the degree of aggregation observed on the addition of the coacervation agent (ethanol) and the centrifugation (at 48,400g) selected for a narrow

range of particle sizes (100-500nm, see Section 3.3.3). The nanoparticle size was determined using photon correlation spectroscopy (see Section 3.1.2).

3.2.4 Nanoparticle Sizing by Photon Correlation Spectroscopy

The BSA nanoparticles were sized using the Malvern Zetasizer HS1000, whilst suspended in Buffer A (10mM Tris-HCl, pH 7.5, 0.02% sodium azide with 0.01% Tween 20) at a protein concentration of 220μg/ml. A sample of nanoparticles (0.6ml) was added to a 1.5ml disposable cuvette and placed into the device. The nanoparticle size was determined by computer analysis using the Einstein-diffusion equation (see Section 3.1.2).

3.2.5 Primary Scouting Experiments with the selected Adsorbent Solid Phases and Soluble and Particulate BSA

The selected adsorbent solid phases were assessed in primary scouting experiments with both BSAs and BSAp exploiting batch binding experimentation. Before use the adsorbents were exhaustively washed in Buffer A to equilibrate the system. Adsorbent (0.1ml) was added to 1.5ml of protein solution (either soluble or nanoparticulate) and rigorously mixed at room temperature using a rotary mixer. Samples of the supernatant (0.1ml) were taken at regular time intervals over 2 hours resulting in the removal of approximately 40% of the supernatant. The soluble BSA solution had an initial concentration of 5mg/ml whilst the initial BSA nanoparticle concentration was 220μg/ml. The binding profiles were plotted as C/Co values (equilibrium concentration divided by the initial concentration) against time. After 2 hours the remaining protein solution was removed and the adsorbent washed in Buffer A (5 x 1ml) to remove any unbound or loosely bound protein. The elution solution was Buffer A containing 1.0M NaCl. Protein loaded adsorbent (0.1ml) was added to 1.5ml of elution buffer and rigorously mixed for 2 hours at room temperature

using a rotary mixer and samples of the supernatant (0.1ml) were taken at regular time intervals and the protein concentration determined using the Bradford assay (refer to Section 3.2.6). The protein capacity was determined by difference analysis of the initial and intermediate protein concentrations, whilst the percentage recovery was determined as the concentration of protein eluted as a percentage of the total protein bound.

3.2.6 Total Protein Determination – The Bradford Assay

The total protein concentration was determined using a commercially available assay reagent supplied by PERBIO (formerly Pierce and Warriner Ltd, Cheshire, UK). The assay is based upon a method proposed by Bradford (1976) where the assay reagent is comprised of the dye Coomassie G-250 suspended in phosphoric acid and solubilising agents (Coomassie Protein Assay Reagent Kit Instructions). Coomassie G-250 primarily binds to arginine residues in proteins and to other aromatic and basic residues. In an acidic environment, when Coomassie G-250 binds to the protein, an absorbance shift occurs from 465nm to 595nm with a simultaneous colour change from brown/red to blue. This reaction can detect protein concentrations as low as 1μg/ml. The Bradford assay reagent has been shown to be compatible with commonly used buffers and reagents.

As previously stated the assay depends on the binding of Coomassie G-250 to arginine, basic and aromatic amino acid residues, consequently the efficacy will vary depending on the amino acid composition of the protein. As a result the protein concentration determined using the Bradford assay is expressed as an equivalent to the standard protein used. For this study the standard was generated using BSA at concentrations between 0-30μg/ml in Buffer A. The standards were incubated in an equal volume of assay reagent for 5 minutes at room temperature (e.g. 0.5ml of sample + 0.5ml of assay reagent). The absorbance of the standards was determined at 595nm against a buffer blank and assay reagent (see

Appendix II). Experimental samples diluted to a suitable concentration were prepared using the same method as the standards and the total protein determined from the standard curve. All the samples were analysed in duplicate.

3.2.7 Determination of Maximum Binding Capacity

Subsequent to the adsorption/desorption batch binding experiments the maximum binding capacity of the adsorbent solid phases was estimated in addition to estimates of how tightly the BSAp were bound. Information on the binding kinetics of the system is an important factor to be considered when scaling up chromatographic adsorption processes. Before use the adsorbents were washed exhaustively with Buffer A to ensure that the system was equilibrated. Adsorbent (50μl) was added to 1.5ml of BSA nanoparticle solutions of increasing concentration from 0μg/ml to 220μg/ml, and mixed for five hours at room temperature using a rotary mixer. The protein concentration was determined using the Bradford assay (refer to Section 3.2.6). The equilibrium binding concentrations were used to estimate the maximum binding capacity (q_m) and the dissociation constant (K_d) for BSA nanoparticles binding based upon Langmuir assumptions.

A Langmuir isotherm was produced by plotting the concentration of protein per unit volume of adsorbent (q*) against the equilibrium protein concentration (C*) where q* was determined from the following equation

$$q^* = \text{volume of supernatant} \times (Co - C^*/\text{volume of adsorbent}) \qquad \text{Equation 3.4}$$

where Co was the initial protein concentration and C* represented the protein concentration at equilibrium. The values of K_d and q_m were determined from straight line plots of C*/q*

against C*. The x-axis (C*) intercept was $-K_d$ and the gradient was equal to $1/q_m$ (see Figure 3.1).

3.2.8 The Effect of Small Ion Capacity on the Adsorptive/Desorptive Behaviour of BSAp

Subsequent to BSAp batch binding experiments the impact of the ion exchange ligand concentration (referred to as small ion capacity; see Section 2.2.9.1) upon BSAp recovery was investigated as an important process parameter to be considered when designing adsorbent solid phases suitable for fluidised bed recovery of nanoparticulate products. The adsorbent particles within the perfluorocarbon emulsion were judged to be inherently solid in nature, and consequently all the ion exchange chemistries immobilised onto the adsorbent were expected to reside at the surface and be available for protein adsorption. It was therefore expected that if modifying the immobilisation procedure reduced the small ion capacity, the number of ion exchange groups directly involved in protein binding would also be reduced. Five perfluorocarbon emulsion solid phases were produced having different small ion capacities by modifying the proposed derivatisation method (see Section 2.2.9).

Perfluorocarbon 1 was produced using the method stated in Section 2.2.9 whereas perfluorocarbon 2 and 3 were produced by reducing the initial concentration of diethylaminoethyl chloride hydrochloride by $1/50^{th}$ and $1/100^{th}$ respectively with a reaction time of 120 minutes at 85°C. Perfluorocarbons 4 and 5 were produced using diethylaminoethyl chloride hydrochloride at the same concentration as perfluorocarbon 3, but the DEAE was immobilised at room temperature for 120 minutes and 10 minutes respectively. The small ion capacity of these adsorbents was determined using the pH titration method proposed by Helfferich (1962; see Section 2.2.9.1).

Figure 3.1 Example Langmuir and linear isotherm plots

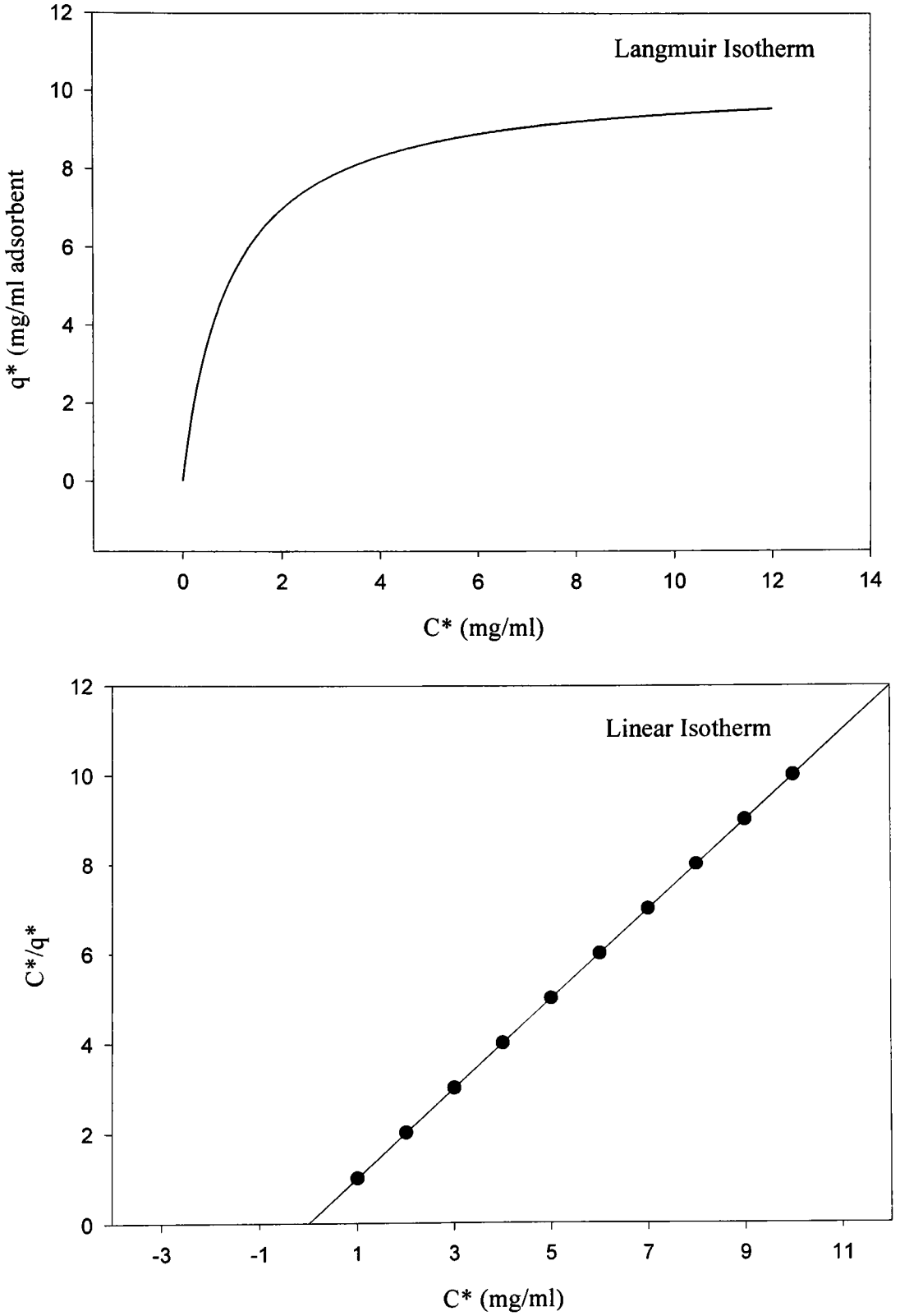

Figure 3.1 represents example plots for the Langmuir isotherm and linear isotherm from which the dissociation constant and the maximum binding capacity can be determined and described in Section 3.2.7. Using the Linear Isotherm -Kd is equal to the X-axis intercept whilst the gradient is equal to 1/qm.

3.3 Results and Discussion

The performance of four configurations of adsorbent solid phases (designated Types I to IV, Figure 2.1) has been critically evaluated in the anion exchange recovery of BSAs and BSAp.

3.3.1 Preliminary Study of Adsorptive Capture of Soluble BSA

BSAs was included in the present study as a mimic for the adsorptive behaviour of small molecular impurities that are present in complex feedstocks such as virus containing cell culture supernatants. In addition, the separation of soluble and particulate BSA is a model system representative of the problems associated with the separation of products from product components. It is interesting to note that during the preparation of the synthetic BSA nanoparticles the soluble and particulate BSA was sepaated exploiting dia/ultrafiltration, a conventional technique employed for the purification of nanoparticulates such as viruses (Lyddiatt and O'Sullivan, 1998). The adsorptive capture of BSAs is summarised in Figure 3.2, which indicates that all the adsorbent solid phases designated Type II to IV (see Figure 2.1) reached an adsorption equilibrium within 30 minutes, with the exception of STREAMLINE DEAE (Type I, see Figure 2.1). This was attributed to the internal and external geometry of the adsorbent solid phases in the study. Type I adsorbents are characterised by pore dimensions of less than 0.2μm in this study, established for macromolecular, rather than nanoparticulate products (see Table 2.1). The tortuous, porous network thought to characterise STREAMLINE DEAE, is expected to result in diffusion limited BSAs adsorption hence, longer times will be required for equilibrium to be reached. Solid phases characterised by large macropores (Type II, see Figure 2.1) are thought to facilitate transport of the protein into the internal volume of the adsorbent reducing the diffusion distances for adsorption. This would result in a rapid adsorptive performance that

Figure 3.2 Adsorption of soluble BSA to the selected adsorbent solid phases

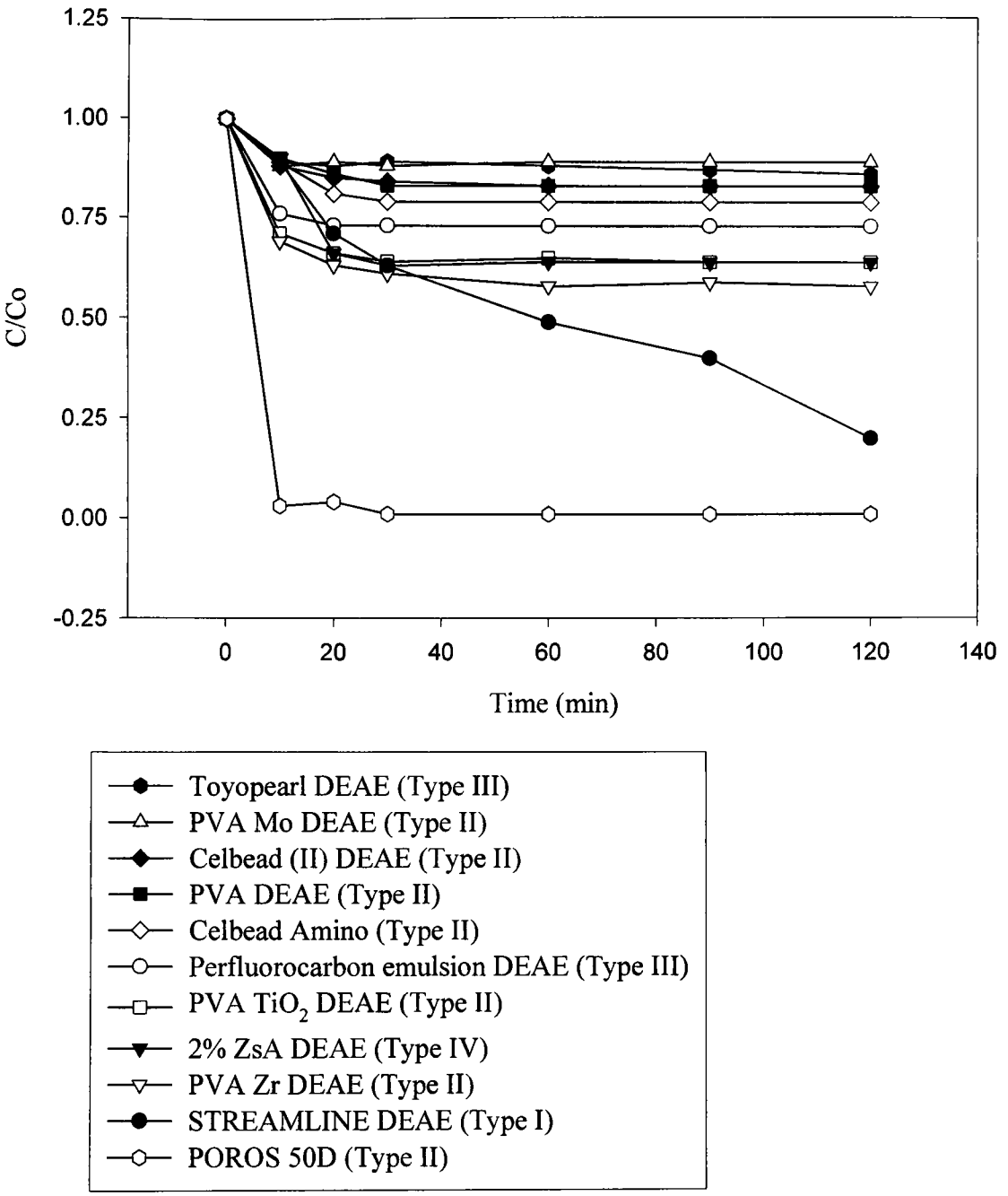

Figure 3.2 represents the adsorption of BSAs for adsorbents derivatised with anion exchange chemistry. Adsorbent (0.1ml settled volume) was added to 1.5ml of BSAs (5mg/ml dissolved in Buffer A) and mixed for 2 hours at room temperature using a rotary mixer. Samples were taken at regular time intervals and analysed using the Bradford assay (see Section 3.2.6). C/Co represents the protein concentration with respect to the initial protein concentration.

(Buffer A = 10mM Tris-HCl, pH 7.4 with 0.01% Tween 20 and 0.02% sodium azide).

was characteristic of all the Type II adsorbents included in the study (POROS 50D, Celbead (II), Celbead Amino, PVA, PVA TiO_2, PVA Mo and PVA Zr). Perfluorocarbon emulsion DEAE and Toyopearl DEAE (Type III, see Figure 2.1) and the Type IV adsorbent, 2% ZsA, were also characterised by a rapid adsorptive performance in comparison to STREAMLINE DEAE. Type III adsorbents were expected to demonstrate rapid adsorption characteristics, as BSAs should adsorb exclusively to the surface of the adsorbent solid phase. A pellicular adsorbent was included in this study having the potential to reduce adsorption processing times. The adsorbent was comprised of a solid, dense core of zirconium silicate surrounded by a 20μm pellicle of porous agarose (see Figure 2.1 and 2.12) that results in shorter diffusion distances over which adsorption occurs in comparison to STREAMLINE DEAE that is characterised by an agarose continuum. This was illustrated in the preliminary batch binding experiments (see Figure 3.2).

Table 3.2 represents a summary of BSAs capacities for the selected adsorbent solid phases determined from the batch binding studies (see Section 3.2.5). It was observed that POROS 50D exhibited the highest BSAs capacity whilst Celbead (II) DEAE exhibited the lowest binding capacity under the same experimental conditions. Both were Type II, macroporous adsorbents, however the adsorbent designs were claimed to be different. POROS 50D was comprised of both convective pores (0.6-0.8μm in diameter) and diffusive pores (0.08-0.15μm in diameter) that resulted in a large surface area over which protein adsorption could occur. In contrast, Celbead (II) DEAE was claimed to have a pore volume of 60% of the total adsorbent volume (Pai *et al*, 2000) which would dramatically reduce the surface area available for adsorption.

3.3.2 The Recovery of Soluble BSA from the Selected Adsorbent Solid Phases

The impact of the external and internal adsorbent geometry upon the recovery of BSAs from the selected adsorbent solid phases was investigated to predict the recovery

Table 3.2 Summary of soluble BSA binding capacities and recoveries from the preliminary binding studies

ADSORBENT TYPE	ADSORBENT	SMALL ION CAPACITY (μmol Cl-/ml adsorbent)	BSA CAPACITY (mg/ml adsorbent)	% BSA RECOVERY
I	STREAMLINE DEAE	170	60.0	77.2
II	Celbead (II) DEAE	41	0.4	113.1
	Celbead Amino	300*	0.45	30.0
	POROS 50D	100	74.25	77.0
	PVA DEAE	1.6	0.9	100.0
	PVA Mo DEAE	2.78	9.6	65.6
	PVA TiO_2 DEAE	3.3	10.2	102.9
	PVA Zr DEAE	54.4	5.44	57.9
III	Perfluorocarbon emulsion DEAE	20	5.4	93.3
	Toyopearl DEAE	490	11.25	36.8
IV	2% ZsA	89	39.0	80.1

Table 3.2 summarises the adsorptive capacities and percentage recovery of BSAs for the selected adsorbent solid phases having four different configurations (designated Types I to IV, see Figure 2.1). The adsorption capacities were determined from 120 minute batch binding experiments (see Section 3.2.5 and Figure 3.2) with an initial common BSAs concentration of 5mg/ml. BSAs was recovered in 1M NaCl after 5 x 1ml washes with Buffer A, and the recovery is expressed as a percentage of the estimated adsorption capacity. (Buffer A = 10mM Tris-HCl, pH 7.4 with 0.01% Tween 20 and 0.02% sodium azide).

behaviour of macromolecular impurities expected to be contained in nanoparticulate containing feedstocks (e.g. cell debris and product components). The desorptive recovery of BSAs in 1M NaCl is summarised in Figure 3.3 and indicates that BSAs was desorbed from the majority of the selected adsorbent solid phases to reach a constant recovery within 30 minutes. In contrast, a slower release of BSAs was observed for Toyopearl DEAE (Type III, see Figure 2.1) which suggested that there was BSAs penetration into this assumed solid adsorbent. Toyopearl DEAE is characterised by the manufacturers (Tosohaas) as having a molecular weight exclusion of 100-10,000 Daltons (see Table 2.1); hence any penetration of BSAs, having a molecular weight of 67,000 Daltons (see Section 3.1.3), was unexpected. Consequently, two conclusions were possible; (i) the initial classification of the adsorbent as a Type III solid adsorbent (see Figure 2.1) was incorrect, or (ii) the high concentration of anion exchange groups at the surface of the adsorbent (refer to Table 3.2) inhibited the rapid release of BSAs (refer forward to Figure 3.7). In contrast, perfluorocarbon emulsion DEAE had a constant level of desorption within 10 minutes that confirmed the classification of the adsorbent as a Type III, solid particle. Near quantitative recovery of BSAs (93.3%; refer to Table 3.2) was an encouraging observation for the Type III adsorbent. The desorption profiles of the remaining adsorbent configurations (Type I, II and IV, see Figure 2.1) suggested that BSAs recovery was diffusion limited, indicating there was BSAs penetration during adsorptive capture, as was concluded in Section 3.3.1.

Table 3.2 also represents a summary of the BSAs recoveries for the selected adsorbent solid phases determined from batch recovery experimentation (see Figures 3.2 and 3.3). It was observed that 2% ZsA (Type IV), Celbead (II) DEAE (Type II), PVA DEAE (Type II) and perfluorocarbon emulsion DEAE (Type III) exhibited good recoveries in comparison to STREAMLINE DEAE (Type I, see Figure 2.1) whilst Celbead Amino (Type

Figure 3.3 Recovery of soluble BSA from the selected adsorbent solid phases

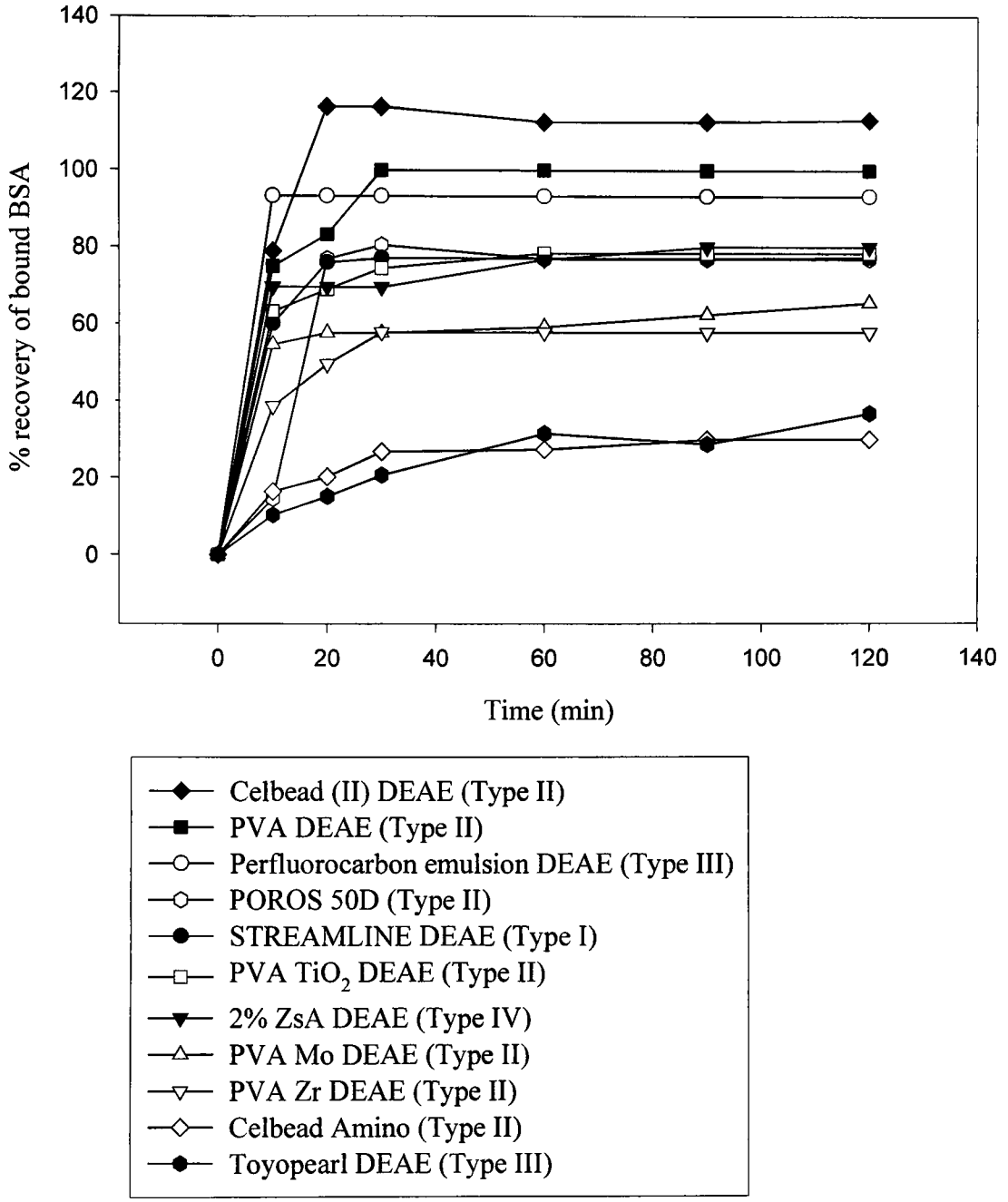

Figure 3.3 represents the recovery of BSAs from adsorbents derivatised with anion exchange chemistry. After BSAs was adsorbed to the adsorbent (see Figure 3.2) was washed in Buffer A to remove unbound protein from the system (5 x 1ml). Adsorbent (0.1ml) was added to 1.5ml of 1.0M NaCl (in Buffer A) and mixed at room temperature for 2 hours using a rotary mixer. Samples were taken at regular time intervals and analysed using the Bradford assay (refer to Section 3.2.6).

The percentage recovery of BSAs was expressed as a percentage of the BSAs adsorbed.

(Buffer A = 10mM Tris-HCl, pH 7.4 with 0.01% Tween 20 and 0.02% sodium azide).

II) and Toyopearl DEAE (Type III) exhibited the poorest recoveries that was attributed to both the small ion capacity and adsorbent design.

3.3.3 BSA Nanoparticle Sizing

Figure 3.4 represents the size distribution profile of the fabricated BSA nanoparticles. The nanoparticles have a size distribution between 100 and 500nm, with an average nanoparticle diameter of 154nm. 82% of the nanoparticles were 100-200nm in diameter.

3.3.4 The Adsorptive Capture of BSA Nanoparticles to Selected Adsorbent Solid Phases

BSA nanoparticles (BSAp) were employed as representatives of less easily sourced nanoparticulate products, such as viruses, having a particle size of approximately 150nm (see Section 3.3.3; see Figure 3.4). The adsorptive capture of BSAp to the selected adsorbent solid phases (Types I to IV) is summarised in Figure 3.5 that indicates two distinct adsorption profiles. The adsorbents having pore dimensions that were expected to exclude nanoparticles, Type III (solid, see Figure 2.1) reached an adsorption equilibrium within 20 minutes, an observation explained by assuming that there was dedicated external surface binding of BSAp. In contrast, the adsorbents believed to possess larger pores (Type II macroporous adsorbents, see Figure 2.1) reached an equilibrium after an experimental time of 60 minutes, which suggested nanoparticle penetration. This was not however characteristic of all the Type II adsorbents. POROS 50D, PVA DEAE and Celbead Amino demonstrated rapid adsorptive capture of BSAp to reach adsorption equilibrium within 20 minutes. It was concluded that the adsorptive behaviour of POROS 50D was a consequence of the challenge sample being totally depleted, suggesting that the adsorption capacity could be greater if the initial load (1.5ml at 220μg/ml in this study) concentration was greater. In addition, the 60 minutes after the experiment was initiated. This suggested nanoparticle penetration as

Figure 3.4 Size distribution of BSA nanoparticles

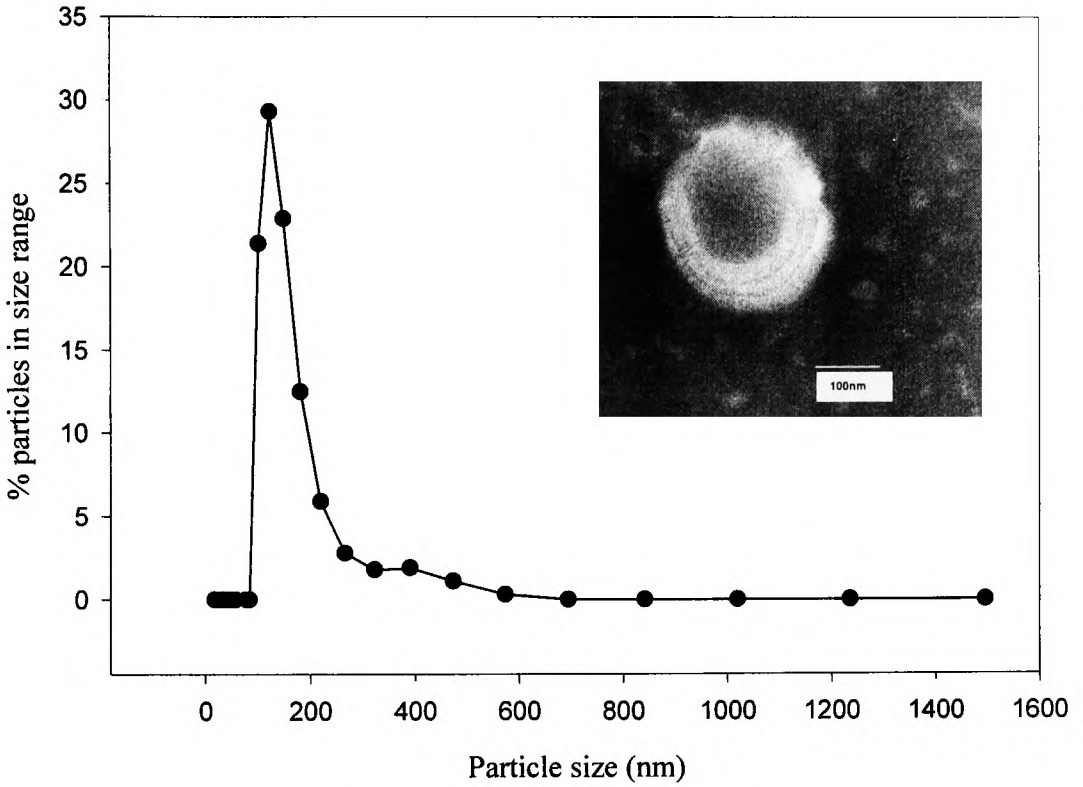

Figure 3.4 represents the size distribution of the fabricated BSA nanoparticles measured by photon correlation spectroscopy. The average particle size was determined as 154nm based on the Einstein-Diffusion Equation (see Section 3.1.2). In addition the nanoparticles were shown to be spherical in nature by electron microscopy (inset), and the size of the nanoparticle was also confirmed by this analysis.

Figure 3.5 Adsorption of BSA nanoparticles to the selected adsorbent solid phases

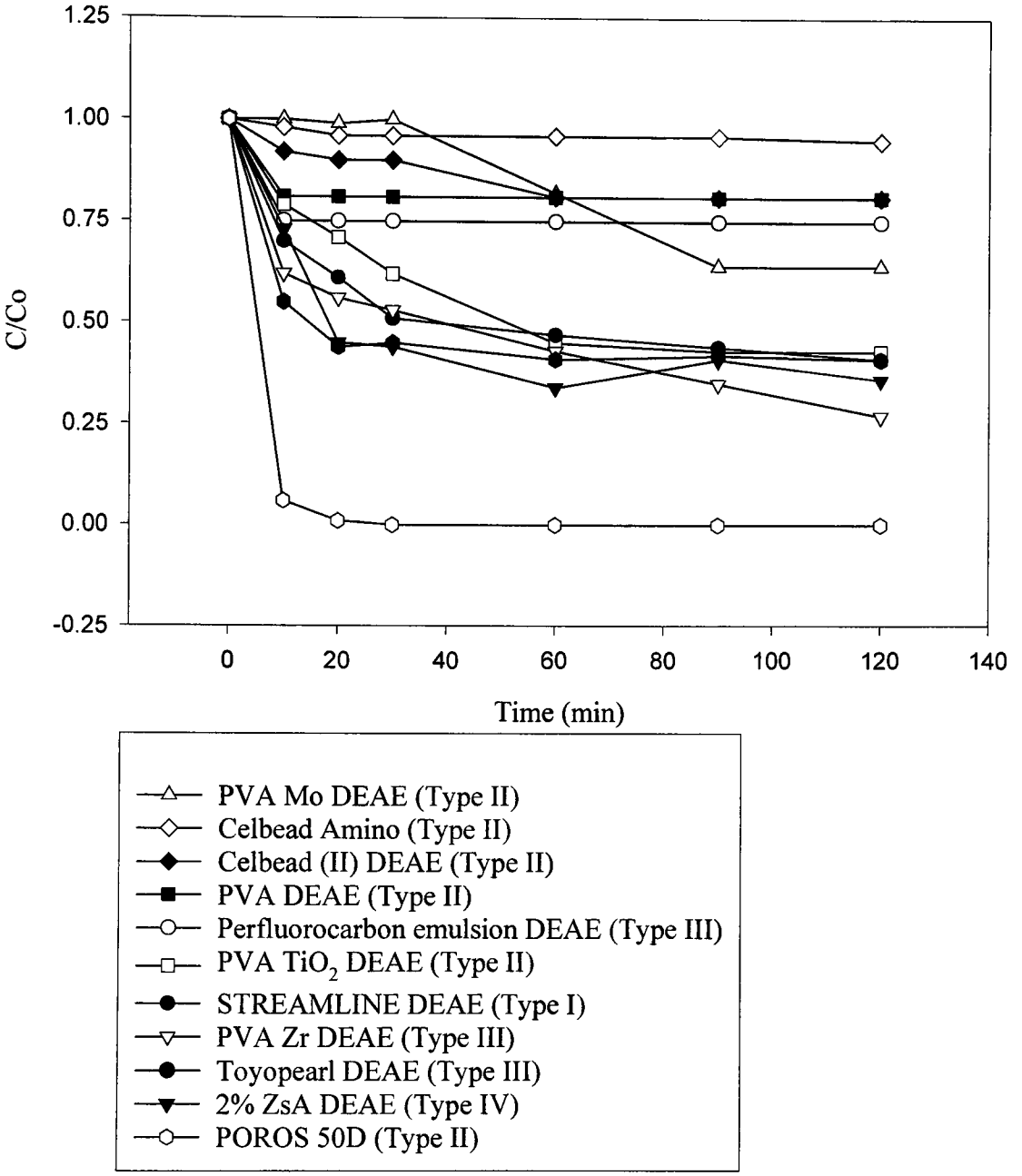

Figure 3.5 represents the binding of BSAp (150nm in diameter) to adsorbents derivatised with anion exchange chemistry. Before use the adsorbents were washed in Buffer A to equilibrate the system followed by the addition of 0.1ml of adsorbent to 1.5ml of BSAp (220µg/ml). The adsorbent samples were mixed at room temperature for 2 hours with samples taken at regular time intervals. The samples were analysed using the Bradford assay (refer to Section 3.2.6). C/Co represents the protein concentration with respect to the initial load (Buffer A = 10mM Tris-HCl, pH 7.4 with 0.01% Tween 20 and 0.02% sodium azide).

results suggested that PVA DEAE and Celbead Amino were not macroporous adsorbents. The Type IV adsorbent included in the study (2% ZsA), reached an adsorption equilibrium indicated for Type II adsorbents, which was attributed to the less than 0.4μm pore dimensions of the 2% agarose layer of the pellicular adsorbent. The commercial benchmark STREAMLINE DEAE (Type I, see Figure 2.1) also appeared to allow BSAp to penetrate the agarose structure. It was concluded that the penetration might be due to smaller BSAp penetrating the 0.2μm pores that were assumed to characterise agarose (see Section 2.1.2.1).

Table 3.3 represents the summary of the calculation of BSAp capacities for the selected adsorbent solid phases as estimated particle numbers and Table 3.4 summarises the protein and particle capacities for the adsorbent solid phases. It was observed that POROS 50D (Type II macroporous adsorbent) exhibited the highest binding capacity that was attributed to the large surface area available as a consequence of the pore structure (see Sections 2.1.3 and 3.3.1; and Figure 2.3). In contrast Celbead Amino (Type II, see Figure 2.1) had the poorest BSAp capacity which, in addition to the rapid adsorption profile suggested that the adsorbent structure was not macroporous. It was interesting to note that the estimated BSAp numbers per milliliter of settled adsorbent for all the adsorbent solid phases were similar and of the same order of magnitude as the reported values for virus purification protocols (Hughye *et al*, 1995; O'Neil and Balkovic, 1993).

3.3.5 Batch Recovery of BSA Nanoparticles

BSAp were included in the present study as representative nanoparticulate products. Consequently, the recovery efficiency of BSAp from the adsorbent solid phases was a critical parameter to be considered in the design of adsorbent solid phases for the recovery of economically desirable nanoparticulate products.

Table 3.3 Calculation for the estimation of BSAp numbers as a function of the measured protein concentration

PARAMETER	VALUE
Diameter of one nanoparticle	0.000015cm
Volume of a sphere	$\pi d^3/6$
Volume of one nanoparticle	1.77×10^{-15} cm^3
Number of particles per ml of supernatant	5.65×10^{14}
Number of particles per g of protein (based upon density assumptions)	5.65×10^{14}
Number of particles per mg of protein	5.65×10^{11}

The number of 150nm particles bound to the adsorbent solid phases was estimated from the protein concentrations measured by the Bradford assay (see Section 3.2.6). The estimated particle number was based upon the assumption that the BSAp were spherical (refer to Figure 3.4) and had a density of 1.0g/ml (the BSAp did not sediment in solution, data not shown). To estimate particle numbers from protein concentrations the number of BSAp per ml was determined by dividing 1ml by the volume of one nanoparticle (see above) to calculate that 5.65 x 10^{14} particles would be present in 1ml of BSA solution. Assuming that particle density was 1.0g/ml, there are 5.65 x 10^{14} particles per gram of protein that can be expressed as 5.65 x 10^{11} particles per milligram of protein.

Table 3.4 Summary of BSA nanoparticle capacities and recoveries from preliminary batch binding experiments

ADSORBENT TYPE	ADSORBENT	SMALL ION CAPACITY (µmol Cl-/ml adsorbent)	BSAp CAPACITY (mg/ml adsorbent)	BSAp CAPACITY (particles/ml adsorbent)	% RECOVERY
I	STREAMLINE DEAE	170	1.95	1.1×10^{12}	53.8
II	Celbead (II) DEAE	41	0.63	0.36×10^{12}	64.3
	Celbead Amino	300*	0.15	0.08×10^{12}	57.5
	POROS 50D	100	3.3	1.86×10^{12}	34.1
	PVA DEAE	1.6	0.6	0.34×10^{12}	85.9
	PVA Mo DEAE	2.78	1.13	0.64×10^{12}	92.9
	PVA TiO_2 DEAE	3.3	1.8	1.0×10^{12}	34.7
	PVA Zr DEAE	54.4	1.67	0.94×10^{12}	71.9
III	Perfluorocarbon emulsion DEAE	20	0.83	0.47×10^{12}	38.2
	Toyopearl DEAE	490	1.95	1.1×10^{12}	47.7
IV	2% ZsA	89	1.95	1.1×10^{12}	73.0

* For Celbead Amino the small ion capacity equivalent is µmol amine groups/ml adsorbent as determined at Mumbai University, India.

Table 3.4 summarises the adsorptive capacities and recoveries of BSAp calculated from batch adsorption and desorption studies (see Sections 3.3.4 and 3.3.5 respectively; Figures 3.5; 3.6). The adsorption studies were completed using 0.1ml of settled volume adsorbent added to 1.5ml of BSAp at a concentration of 220µg/ml and desorption was achieved in 1M NaCl. The estimated particle numbers were calculated as noted in Table 3.3. The capacity was determined by difference analysis of the initial load and the concentration after 120 minutes, whilst the recovery is the protein recovered as percentage of the protein adsorbed. (Buffer A = 10mM Tris-HCl, pH 7.4 with 0.01% Tween 20 and 0.02% sodium azide).

Following binding under standardised conditions to adsorbent solid phases having different configurations (see Section 3.2.5; Types I-IV, see Figure 2.1), BSAp were effectively desorbed by 1M NaCl (refer to Figure 3.6). The commercial benchmark, STREAMLINE DEAE (Type I) reached an apparent equilibrium concentration of desorbed product within the shortest time, at 20 minutes which was attributed to a limited degree of nanoparticle binding or entrapment (i.e. limited penetration at adsorption). In contrast, the adsorbents characterised by large pores (Type II, see Figure 2.1) reached a constant recovery after 60 minutes contact time, suggesting that BSAp were characterised by diffusion limited desorption. This observation confirmed the classification of the adsorbents (POROS 50D, PVA DEAE, PVA TiO_2 DEAE, PVA Mo DEAE, PVA Zr DEAE and Celbead (II) DEAE) as Type II adsorbent solid phases. The desorption behaviour of BSAp from the Type III adsorbents was unexpected, as Toyopearl DEAE reached a desorption equilibrium later than the microporous benchmark STREAMLINE DEAE, despite being classified as a virtual solid adsorbent expected to adsorb BSAp exclusively at the external particle surface. However, it was subsequently assumed that the slow release was attributable to the high small ion capacity as concluded for BSAs and *not* due to significant nanoparticulate penetration (see Section 3.3.2). BSAp also desorbed slowly from perfluorocarbon emulsion DEAE (Type III) which initially suggested that the BSAp had penetrated the internal volume of the solid adsorbent. However, the rapid desorption of BSAs indicated that the Type III classification for perfluorocarbon emulsion DEAE was correct (see Section 3.3.2). It was concluded that as with Toyopearl DEAE, the number of anion exchange groups available for binding strongly influenced the desorption efficiency of BSAp from the adsorbent solid phase (refer to Section 3.3.6). The slow desorptive behaviour of 2% ZsA (Type IV, see Figure 2.1) confirmed that

Figure 3.6 Recovery of BSA nanoparticles from the selected adsorbent solid phases

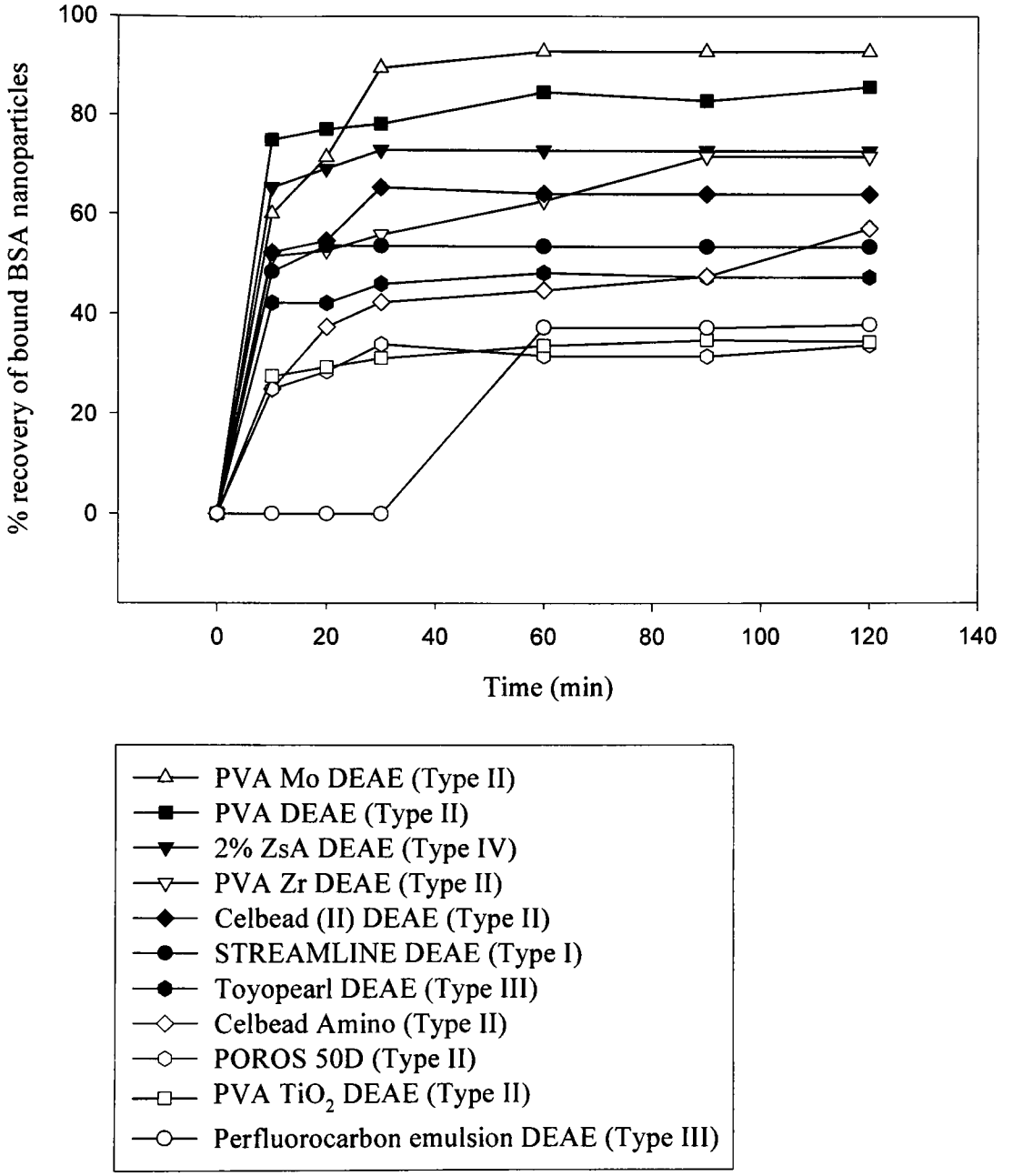

Figure 3.6 represents the recovery of BSAp (150nm in diameter) from adsorbents derivatised with anion exchange chemistry. After the adsorbent was loaded with BSAp and washed (5 x 1ml) 0.1ml of adsorbent was added to 1.5ml of 1.0M NaCl (in Buffer A). The adsorbent was mixed for 2 hours at room temperature using a rotary mixer. Samples were taken at regular time intervals and analysed using the Bradford assay (refer to Section 3.2.6).

(Buffer A = 10mM Tris-HCl, pH 7.4 with 0.01% Tween 20 and 0.02% sodium azide).

there was a degree of nanoparticle penetration that was suggested by the adsorptive capture profiles (see Section 3.3.1).

Table 3.4 is a summary of the recovery of BSAp from the selected adsorbent solid phases expressed as a percentage of the experimentally determined adsorption capacities. In comparison to the commercial benchmark, STREAMLINE DEAE (Type I, see Figure 2.1) the Type II adsorbents showed good recoveries, with the exception of POROS 50D and PVA TiO_2 which might be a consequence of the internal structure of the adsorbents. POROS 50D was characterised by two discrete pore sizes (see Section 2.1.3, see Figure 2.2) that could promote particle entrapment resulting in a low recovery. In addition, the poor recovery of BSAp from PVA TiO_2 DEAE could also be attributed to particle entrapment. However, both the method of manufacture and the internal structure of this adsorbent was unknown and thus conclusions regarding the adsorbent performance could not be made. The Type III adsorbents (Toyopearl DEAE and perfluorocarbon emulsion DEAE) both exhibited poor performances which again indicated that the number of anion exchange groups available at the adsorbent surface was too high (refer to Section 3.3.6).

3.3.6 Effect of Small Ion Capacity on the Recovery of BSA Nanoparticles

The adsorption/desorption batch binding experiments exploited in the present study indicated that the accessible anion exchange ligand concentration (related to the small ion capacity; SIC) influenced the recovery of BSAp (see Section 3.3.2 and 3.3.5). It was thought that a higher number of anion exchange groups available for each individual BSAp assembly promoted a stronger interaction that was more difficult to chemically disrupt than weaker interactions to allow for product release (refer to Figure 3.7). To investigate this theory the adsorption/desorption performance of BSAp with custom fabricated perfluorocarbon

Figure 3.7 Effect of small ion capacity on BSA nanoparticle recovery

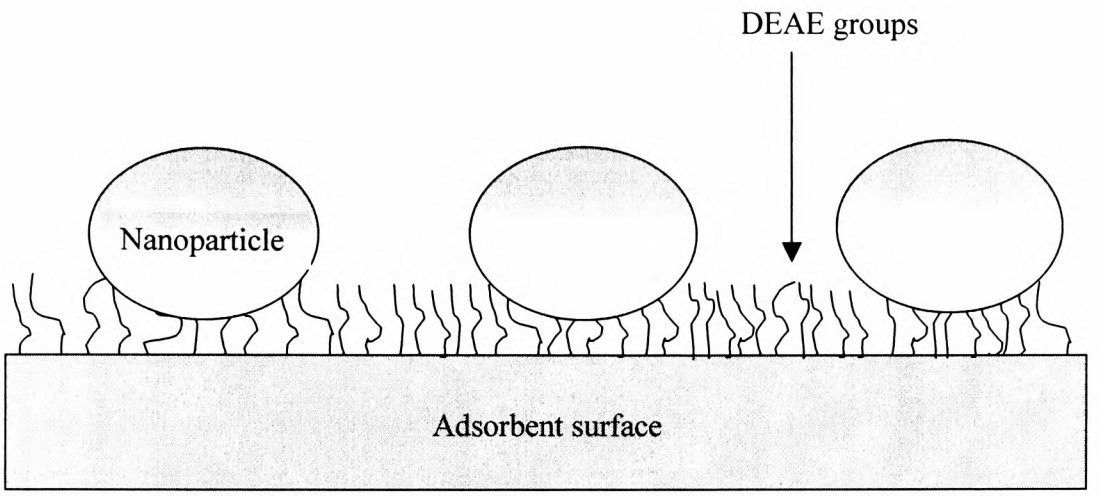

Figure 3.7a represents the binding of nanoparticles to DEAE upon an adsorbent surface. Many DEAE groups are attached per nanoparticle resulting in a tighter binding of the product to the adsorbent solid phase.

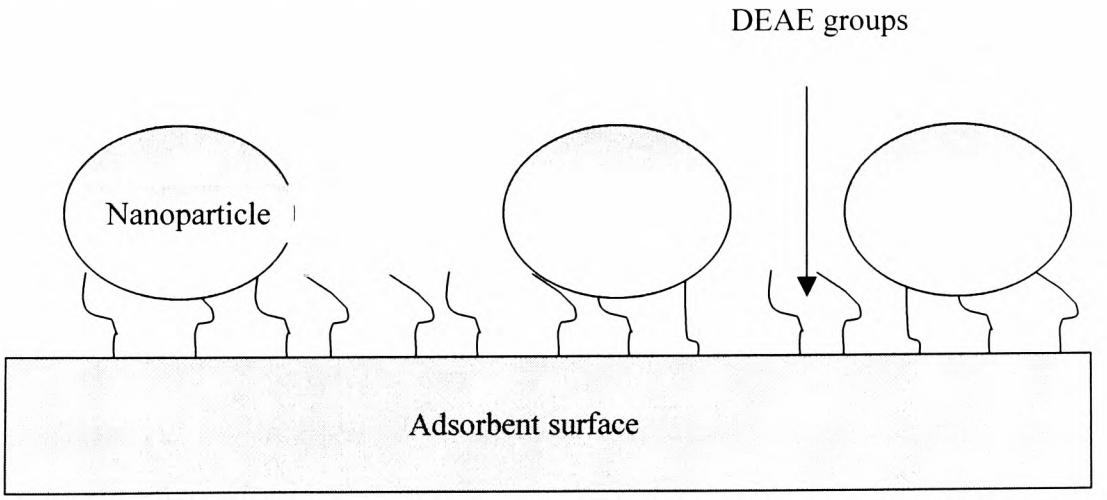

Figure 3.7b represents the binding of nanoparticles to DEAE immobilised onto an adsorbent solid phase. In comparison to Figure 3.7a the number of DEAE groups per nanoparticle is much lower, hence the recovery should be easier as the nanoparticles are less tightly bound to the adsorbent.

emulsion DEAE having different SIC was compared in batch adsorption and desorption experiments (see Section 3.2.5).

Perfluorocarbon emulsion adsorbent particles were designated as a Type III solid adsorbent (see Figure 2.1), and thus identified as suited to the investigation of the effect of small ion capacity on the recovery of BSAp (see Section 3.2.8). The adsorptive capture of BSAp is summarised in Figure 3.8 which indicates that all the perfluorocarbon emulsion adsorbents reached equilibrium within 10 minutes of common contacting. In addition the adsorptive capacity decreased with decreasing small ion capacity that was attributed to fewer anion exchange groups being available for BSAp adsorption. The desorption experiments performed in 1M NaCl indicated that the recovery of bound BSAp was also influenced by the small ion capacity. Perfluorocarbon 1 and 2 were characterised by poor recoveries in comparison to the commercial benchmark STREAMLINE DEAE (see Table 3.4), however when the small ion capacity was reduced to below 6μmol Cl-/ml adsorbent, good BSAp recoveries were achieved. As noted previously (see Section 3.3.5) the desorption profile of BSAp from perfluorocarbon 1 (20μmol Cl-/ml adsorbent; see Figure 3.9) is characterised by no apparent release of BSAp until 30 minutes after the desorption was initiated. This was attributed to the high concentration of ion exchange groups available at the surface of the solid, Type III adsorbents. This brief study highlighted that the concentration of ligand involved in the adsorption process is a critical factor to be considered when designing adsorbent solid phases for a specific purification procedure.

3.3.7 Maximum Binding Capacity Determination

The selected adsorbent solid phases were characterised using batch binding studies with

Figure 3.8 Effect of small ion capacity on the binding of BSA nanoparticles

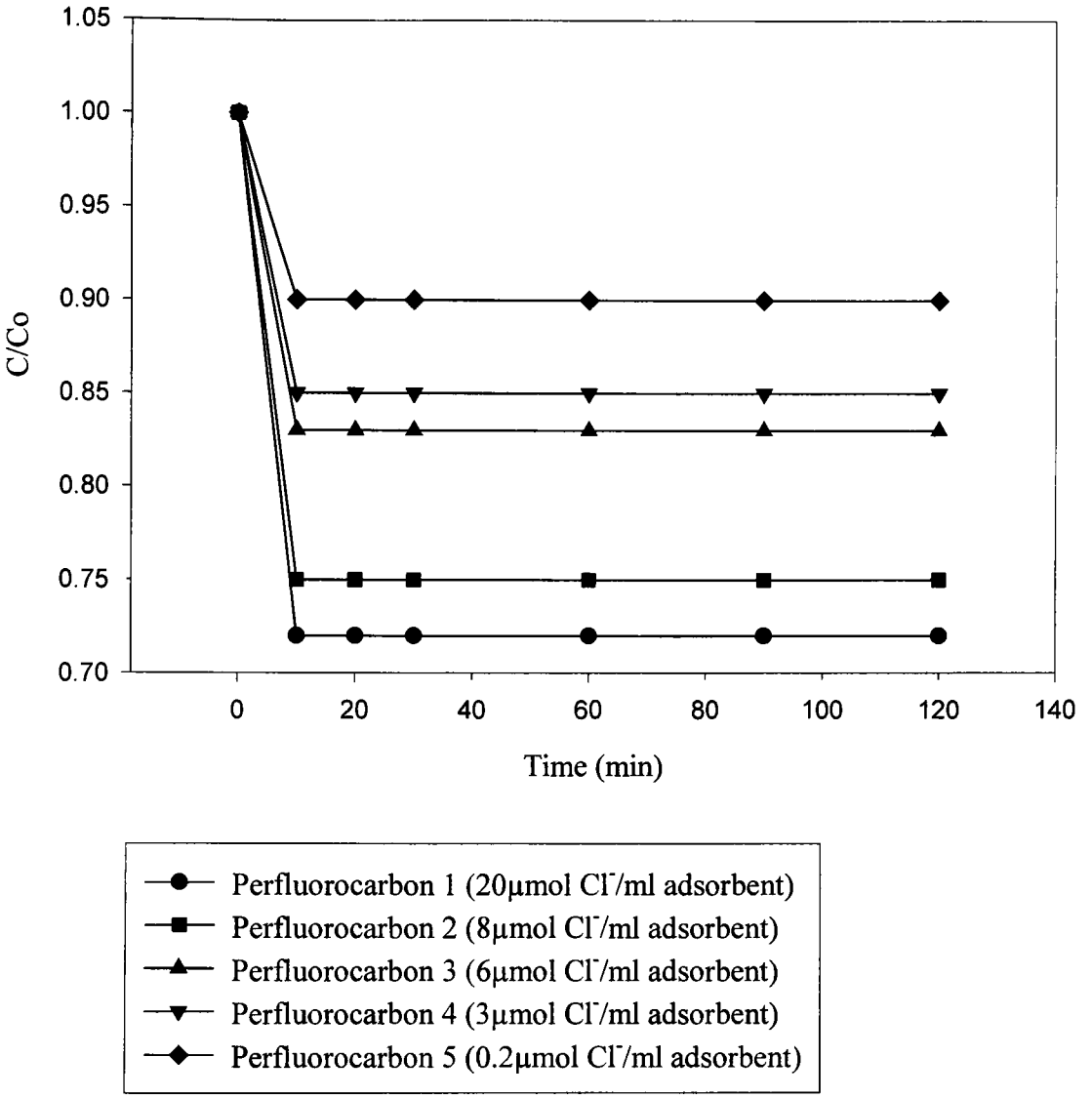

Figure 3.8 represents the binding of BSAp to perfluorocarbon emulsion with different small ion capacities. Before use the adsorbents were washed in Buffer A to equilibrate the system. Adsorbent (0.1ml) was added to 1.5ml of BSAp at 220µg/ml (suspended in Buffer A). The adsorbents were mixed for 2 hours at room temperature using a rotary mixer. Samples (0.1ml) were taken at regular time intervals and analysed using the Bradford assay (refer to Section 3.2.6).

C/Co represents the protein concentration with respect to the initial load (Buffer A = 10mM Tris-HCl, pH 7.4 with 0.01% Tween 20 and 0.02% sodium azide).

Figure 3.9 Effect of small ion capacity on the recovery of BSA nanoparticles

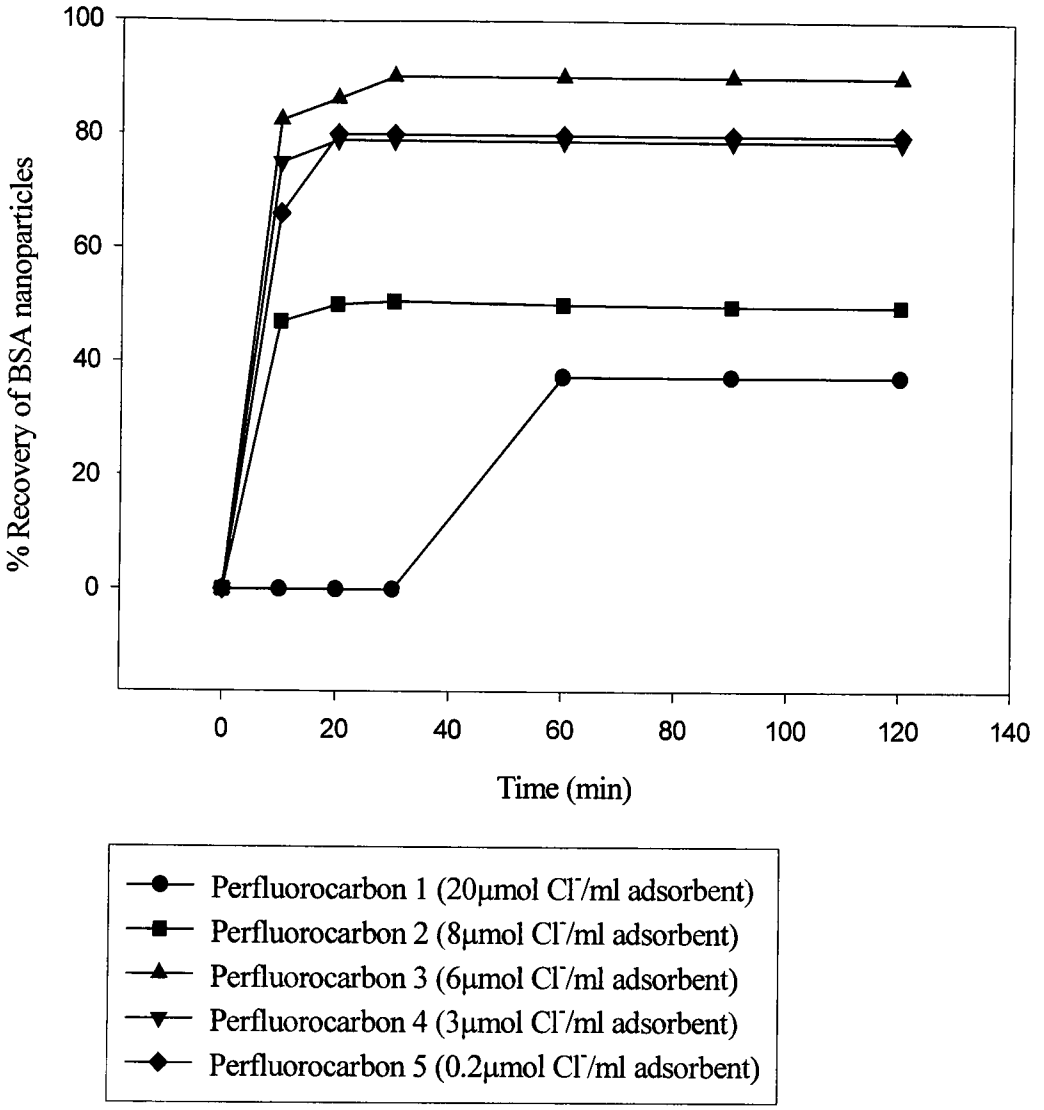

Figure 3.9 represents the recovery of BSAp from perfluorocarbon emulsion adsorbents with different small ion capacities. Subsequent to the BSAp binding the adsorbent was washed in Buffer A to remove unbound BSAp (5 x 1ml). Adsorbent (0.1ml) was added to 1.5ml of 1.0M NaCl (in Buffer A). The adsorbents were mixed for 2 hours at room temperature using a rotary mixer. Samples (0.1ml) were taken at regular time intervals and analysed using the Bradford assay (refer to Section 3.2.6).

The percentage recovery is the protein recovered expressed as a percentage of the protein adsorbed (Buffer A = 10mM Tris-HCl, pH 7.4 with 0.01% Tween 20 and 0.02% sodium azide).

BSAp to estimate the maximum binding capacities using Langmuir assumptions (Chase, 1984). The preliminary batch binding studies (see Section 3.2.5) were conducted as one-off binding experiments that could only indicate whether the adsorbents worked, as the capacities calculated only indicated the amount of BSAp bound under the specified conditions (see Section 3.2.5). As noted in Section 3.1.4, the Langmuir isotherm can be used to estimate how much product the adsorbent is capable of adsorbing (q_m) in addition to the affinity of the product for the immobilised anion exchange ligand (k_d). This data is important when considering design of the scale up of a chromatographic separation and the information also allows clear comparisons to be made between the adsorbent solid phases included in the study.

As a consequence of the adopted experimental methods (see Section 3.2.7) significant quantities of BSAp and adsorbent were required for the study. As a consequence adsorbent solid phases that demonstrated a poor performance in the physical characterisation studies and the adsorption/desorption studies were eliminated from further study at this stage. The adsorbents carried forward for further investigation were:

(i) STREAMLINE DEAE (Type I, see Figure 2.1),

(ii) Celbead (II) DEAE (Type II),

(iii) Celbead Amino (Type II),

(iv) PVA Mo DEAE (Type II),

(v) PVA TiO_2 DEAE (Type II),

(vi) PVA Zr DEAE (Type II),

(vii) 2% ZsA DEAE (Type IV).

Figure 3.10 represents a comparison of the experimental data with the Langmuir isotherm. Firm conclusions cannot be drawn from the isotherms due to the limited maximum concentration of BSAp (220μg/ml) available for this study as an equilibrium level representative of saturation binding was not reached. Consequently linear isotherms were constructed to determine values for q_m and k_d (see Section 3.2.7; refer to Figure 3.11). Table 3.5 summarizes the values for q_m and k_d for each of the adsorbent solid phases remaining in the study. The predicted q_m data suggests that the adsorptive capacities calculated by batch binding experiments (see Table 3.4) are close to the experimentally estimated q_m values, and thus the assumption made about the adsorbent classifications (Types I to IV) based upon the adsorption data are valid. In addition, the close comparison of the experimental data to the linear isotherm (a reciprocal plot of the Langmuir isotherm) suggested that the binding of BSAp to the adsorbents followed Langmuir assumptions (see Section 3.1.4). K_d is the ratio of the desorption rate constant to the adsorption rate constant and all of the adsorbent solid phases were characterised by a low k_d (refer to Table 3.5), that indicated that the desorption is slow compared to the adsorption. The low k_d values suggest that there is a strong interaction between the BSAp and the anion exchange ligand, which will have process implications when scaling up the desorption process for effective, efficient recovery.

3.3.8 General Conclusions

The aim of this chapter was to critically evaluate commercial and custom designed adsorbent solid phases (designated Types I to IV) in adsorptive studies with nanoparticulate and protein products in batch binding experimentation. To circumvent problems associated with achieving representative binding studies with commercially realistic products such as viruses, plasmid DNA or drug delivery vehicles, BSAp and BSAs were included as

Figure 3.10 Langmuir isotherms for BSA nanoparticle binding to the selected adsorbent solid phases

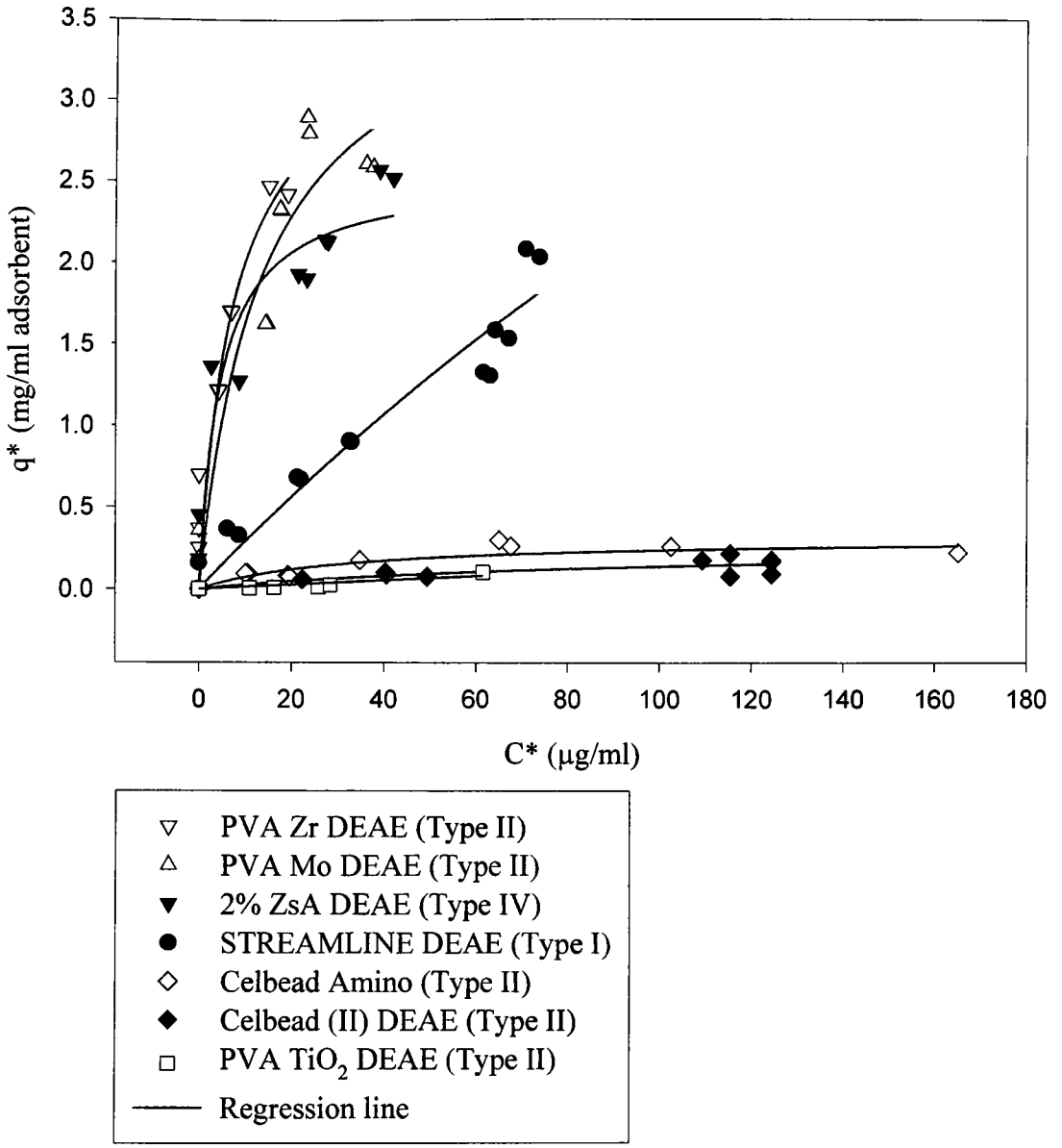

Figure 3.10 represents the linear isotherms for BSAp adsorbing to adsorbents derivatised with anion exchange chemistry. Before use the adsorbent was washed in Buffer A to equilibrate the system. Adsorbent (50µl) was added to 1.5ml of BSAp at increasing concentrations (0-220µg/ml). The samples were mixed for 5 hours at room temperature using a rotary mixer. The protein concentration after binding was determined using the Bradford assay (refer to Section 3.2.6).

The regression lines were generated using non-linear regression using the SigmaPlot graphics package.

(Buffer A = 10mM Tris-HCl, pH 7.4 with 0.01% Tween 20 and 0.02% sodium azide

Figure 3.11 Linear isotherm for BSA nanoparticles binding to the selected adsorbent solid phases

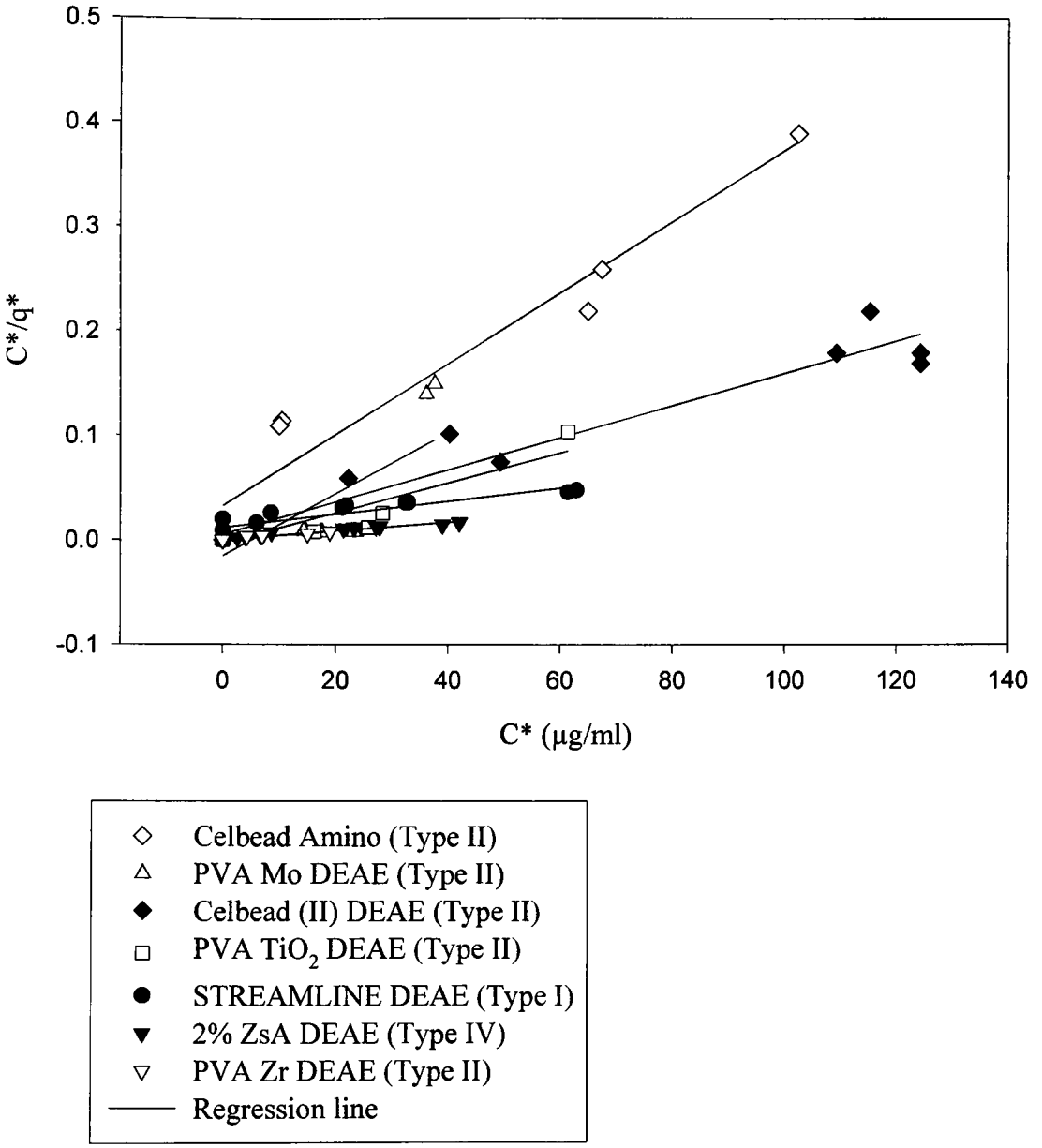

Figure 3.11 represents the linear isotherms for BSAp adsorbing to adsorbents derivatised with anion exchange chemistry. Before use the adsorbent was washed in Buffer A to equilibrate the system. Adsorbent (50µl) was added to 1.5ml of BSAp at increasing concentrations (0-220µg/ml). The samples were mixed for 5 hours at room temperature using a rotary mixer. The protein concentration after binding was determined using the Bradford assay (refer to Section 3.2.6)
(Buffer A = 10mM Tris-HCl, pH 7.4 with 0.01% Tween 20 and 0.02% sodium azide).

Table 3.5 Maximum binding capacity and dissociation constant predictions

ADSORBENT TYPE	ADSORBENT	MAXIMUM CAPACITY (q_m, mg/ml adsorbent)	DISSOCIATION CONSTANT (K_d, M)
I	STREAMLINE DEAE	1.67	1.7×10^{-11}
II	Celbead (II) DEAE	0.63	8.2×10^{-10}
	Celbead Amino	0.24	1.73×10^{-11}
	PVA Mo DEAE	0.33	2.19×10^{-11}
	PVA TiO_2 DEAE	0.71	4.3×10^{-10}
	PVA Zr DEAE	2.5	5.97×10^{-9}
IV	2% ZsA	2.5	1.04×10^{-11}

Table 3.5 represents the maximum binding capacities (q_m) and dissociation constants (K_d) estimated from linear isotherm analysis (see Section 3.2.7). Batch binding experiments over a broad range of BSAp concentrations were conducted to construct the linear isotherm. Q_m is a measure of the maximum concentration of BSAp that adsorbs to each adsorbent solid phase, and k_d is a measure of the affinity of BSAp to the anion exchange groups.

representative nanoparticulate products and molecular impurities. It is noteworthy that the experimental program reported here was entirely achieved with a single batch of BSAp prepared from a stock protein concentration of 220μg/ml. For the purpose of this study the commercial benchmark adsorbent was STREAMLINE DEAE designated as a Type I, microporous adsorbent. The remaining adsorbents included in the present study, designated Types II to IV were characterised by a wide range of BSAs capacities and in general the batch desorption analyses recorded good recoveries. In addition, the adsorbent solid phases were further investigated with BSAp that indicated that the number of BSAp bound per milliliter of adsorbent was similar for each adsorbent configuration and again in general the recoveries were good. Subsequent to the completion of the physical characterisation studies and the batch adsorption/desorption studies POROS 50D, PVA DEAE, perfluorocarbon emulsion DEAE and Toyopearl DEAE were eliminated from the study due to their judged poor performance under a number of categories. The adsorption/desorption studies for the selected adsorbent solid phases suggested that the internal and external structure of the adsorbents influences the adsorption and desorption of both soluble and particulate products. In addition, the ligand concentration appears to be a critical factor to be considered for efficient recovery of the desired product.

CHAPTER 4

LASER SCANNING CONFOCAL MICROSCOPY AS A TOOL FOR INVESTIGATING ADSORPTIVE CAPTURE OF SOLUBLE AND PARTICULATE PROTEIN

4.1 General Introduction

The adsorption of both soluble and particulate protein has been studied for a variety of adsorbents having different internal and external geometries designated Types I to IV (see Figure 2.1). Batch binding and finite batch experiments have been used to measure the adsorption of BSAs and BSAp in addition to measuring protein uptake kinetics to investigate the suitability of the adsorbents for nanoparticulate recovery. These methods are indirect measurements that only yield information regarding the rates of adsorption and not the manner of protein adsorption or the location of the protein product within the adsorbent solid phase. Therefore to obtain a realistic picture of adsorptive separations, laser scanning confocal microscopy (LSCM) was employed as a technique to directly visualise fluorescent derivatives of the protein (both soluble and particulate) within the adsorbent structure. Overall in the present study, selected adsorbent solid phases were investigated for their suitability as fluidised bed adsorbents for the recovery of nanoparticulate products such as viruses, plasmid DNA and drug delivery vehicles. In this chapter LSCM was employed to investigate the adsorptive behaviour of BSAp (representative of nanoparticulate products) and BSAs (representative of molecular component impurities), to adsorbent solid phases having different internal and external geometries. The adsorbents retained in the study are represented in Table 4.1. Adsorbent solid phases that demonstrated a poor performance in

Table 4.1 Summary of the adsorbent solid phases remaining in the study

ADSORBENT TYPE	ADSORBENT	PORE SIZE	ADSORBENT GEOMETRY	MANUFACTURER
I	STREAMLINE (6%)	<0.2μm	Microporous	Amersham Biosciences
II	Celbead (II)	3μm	Macroporous	Indian Construct
	Celbead Amino	3μm	Macroporous	Indian Construct
	PVA Mo	1μm	Macroporous	Swedish Construct
	PVA TiO_2	1μm	Macroporous	Swedish Construct
	PVA Zr	1μm	Macroporous	Swedish Construct
IV	2% ZsA	>0.4μm	Pellicular Macroporous	Birmingham Construct

Table 4.1 represents the commercial and custom fabricated adsorbent solid phases that were remaining in the study subsequent to the physical and biochemical characterisation studies described in Chapters 2 and 3. STREAMLINE DEAE was a commercial adsorbent supplied by Amersham Biosciences (see Section 2.1.2), the PVA adsorbents were supplied by Igor Galaev (Lund University, Sweden; see Section 2.1.5), the Celbead adsorbents were supplied by Arvind Lali (Mumbai University, India; see Section 2.1.4) and the 2% ZsA was fabricated at Birmingham University by Yan Sun (see Section 2.2.1). The pore size data was supplied by the respective manufacturers.

terms of the recovery of BSAs and BSAp (see Chapter 3) were eliminated from the study as unsuitable candidate solid phases for fluidised bed recovery of particulate products.

4.1.1 Laser Scanning Confocal Microscopy

Laser Scanning Confocal Microscopy (LSCM) has recently been identified as a useful tool for studying the adsorption of proteins to chromatographic matrices, and has been established as a valuable instrument for obtaining high resolution images and three dimensional reconstruction of a variety of biological materials. LSCM offers several advantages over conventional light microscopy since the depth discriminating property of LSCM is harnessed to produce virtual optical sections of the specimen. Optical sectioning is a scientifically accepted description of acquiring images using a confocal microscope (Ljunglöf and Hjorth, 1996), as an alternative method to microtome sectioning which is both destructive and time consuming (Subramanian *et al*, 1994). Figure 4.1 represents the simplified optics of a LSCM. The argon-krypton laser beam is emitted from the light source and the beam is deflected onto an objective lens via a dichroic mirror (a colour selective mirror that reflects a particular band of spectral energy). The objective lens focuses the laser beam onto a focal plane within the fluorescent specimen being imaged, which is termed a scanning beam that scans the image in an X-Y plane (refer to Figure 4.2). The mixture of reflected and fluorescent light from the imaged specimen is captured by the same objective lens which focuses the beam back through the dichroic mirror, which deflects the reflected light but allows the fluorescent light to pass through to a photodetector via a pinhole aperture (Pawley, 1995). In addition the fluorescent light not within the focal plane is deflected by the pinhole aperture that results in the out of focus information both above and below the focal plane being greatly reduced (Pawley, 1985). A two dimensional optical section is generated by performing a laser sweep across a specimen centered on the focal plane. As the laser

Figure 4.1 Simplified diagrammatic representation of the optics of a laser scanning confocal microscope

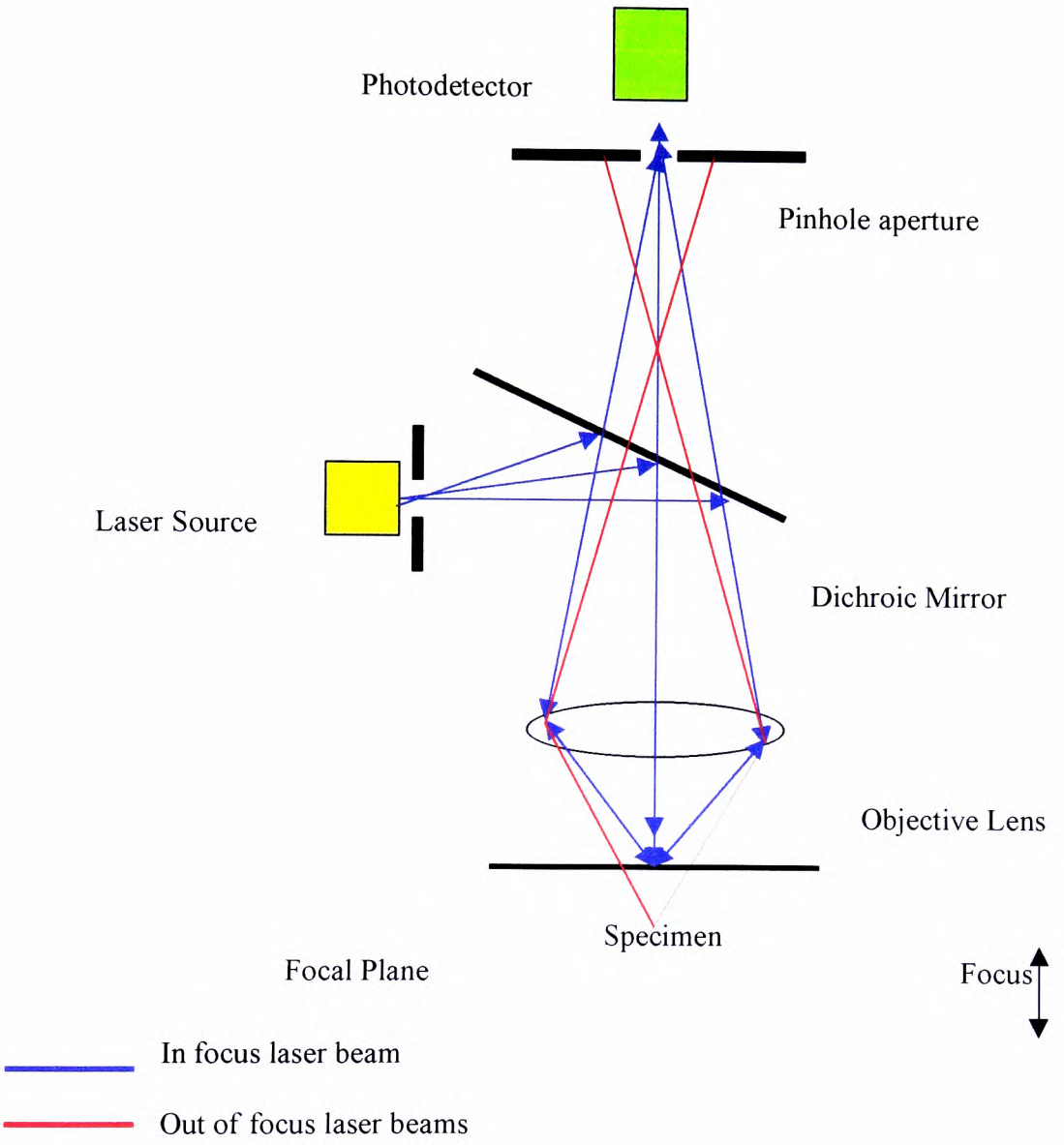

Figure 4.1 represents a simplification of the critical optics of a laser scanning confocal microscope in addition to the track of the fluorescent and transmitted light from the specimen to the photodetector. The focal plane of the image can be altered by moving the platform to image the adsorbent samples at varying depths (see Section 4.1.1).

Figure 4.2 Diagrammatic representation of the focal planes used in laser scanning confocal microscopy

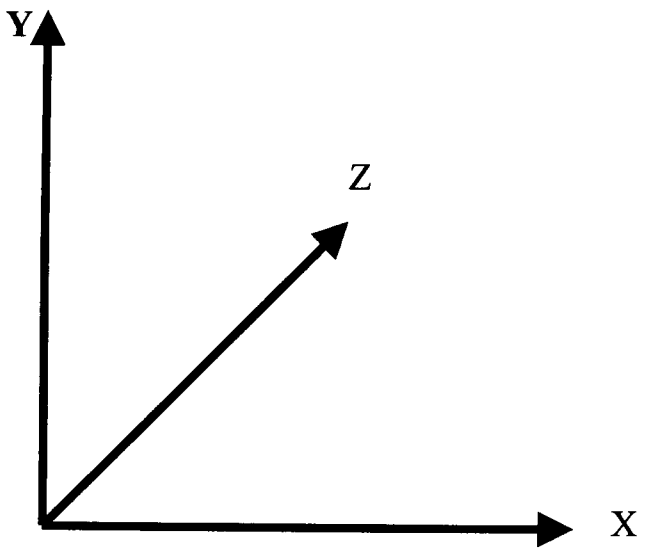

Figure 4.2 represents the focal planes used in laser scanning confocal microscopy, X, Y and Z. An image scanned in the XY plane produces a 2 dimensional representation of the sample. If X-Y scans are generated at equal increments through the Z plane a three-dimensional image is generated by stacking the 2 dimensional images.

scans across the specimen, the analogue light signal detected by the photodetector is converted into a digital signal contributing to a pixel-based image displayed on the computer attached to the LSCM. The relative intensity of the fluorescent light emitted from the specimen corresponds to the resulting pixel image. The plane of focus (termed the Z plane; refer to Figure 4.2) is selected by a computer controlled fine stepping motor that moves the microscope stage up and down to facilitate specimen imaging at varying depths. Stacks of optical sections taken at successive focal planes (known as a Z stack) can be reconstructed to generate a three dimensional view of the specimen.

As previously stated LSCM has become a valuable tool for analysing protein adsorption within chromatographic adsorbents e.g. (i) direct imaging of protein after binding procedures (Ahmed and Pyle, 1999; Linden *et al*, 1999), (ii) visualisation of protein transport in porous adsorbents (Ljunglöf and Thömmes, 1998) (iii) visualisation of ligand distribution within the adsorbents (Ljunglöf *et al*, 2000) and (iv) investigation of the binding of plasmid DNA to individual chromatographic adsorbent particles (Ljunglöf *et al*, 1999; Thwaites *et al*, 2002). LSCM was included in the present study to further investigate the influence of the adsorbent configuration (designated Types I to IV, see Figure 2.1) on the adsorptive/desorptive performance of BSAs and BSAp. The soluble and particulate proteins were fluorescently labelled and visualised after contacting with the adsorbent solid phases.

4.1.2 Fluorescent Probes used in Laser Scanning Confocal Microscopy

Biological specimens to be imaged by LSCM must necessarily be labelled with a fluorescent probe. The essential requirements for a such probe used in LSCM are that they (i) conjugate easily and irreversibly with the protein, (ii) do not affect the biological characteristics of the protein, (iii) have a high fluorescence emission, (iv) be stable and (v) display a strong contrast to the background fluorescence of the material (Shepperd and

Shotton, 1997). Commonly used fluorescent probes for LSCM are represented in Table 4.2. Several factors must be considered when selecting LSCM probes including the excitation/emission wavelength of the probe to be used, the lasers and the filters available and the decay of the fluorescent signal due to photobleaching, induced by exposure to UV light.

4.1.2.1 Fluorescein Isothiocyanate

Fluorescein isothiocyanate (FITC) is one of the most commonly used fluorescent probes for protein conjugation. In addition to an excellent fluorescence yield and good water solubility, FITC has an excitation maximum that closely matches the 488nm spectral line of the argon-krypton laser used in LSCM (Pawley, 1995; refer to Section 4.1.1). FITC was introduced by Riggs *et al* (1958) and is characterised by a molecular weight of 389 Daltons and exhibits a characteristic wavelength of maximum absorption and emission of 495nm and 525nm respectively (refer to Figure 4.3). However, fluorescein based probes and their conjugates have several practical disadvantages including (i) a relatively high rate of photobleaching (Song *et al*, 1995), (ii) pH sensitive fluorescence (Sjoback *et al*, 1995) where FITC has a pKa of approximately pH 6.4 thus reducing the signal below pH 7.0, and (iii) natural quenching by 50% upon analyte conjugation.

4.2 Materials and Methods

4.2.1 Chemicals

Fluorescein isothiocyanate was supplied by Sigma-Aldrich, (Poole, Dorset, UK). All other chemicals were reagent grade, unless otherwise stated and supplied by Sigma-Aldrich (Poole, Dorset, UK) or BDH (Poole, Dorset, UK).

Table 4.2 Commonly used fluorescent probes used in laser scanning confocal microscopy

FLUORESCENT PROBE	EXCITATION (nm)	EMISSION (nm)	APPLICATION	REFERENCE
BODIPY	503	512	Labelling of living neurons	Durand *et al* (2000)
Picogreen	490	525	DNA staining	Thwaites *et al* (2002)
Propidium Iodide	536	617	Quantitation of apoptosis	Zhang *et al* (1999)
Rhodamine 123	511	534	Protein labeling	Ahmed and Pyle (1999)
Snarf 1	563	639	Intracellular pH monitoring	Ondarza and Hootman (1997)
Texas Red	596	615	Cell nuclei labeling	Lundell and Hirsh (1994)

Table 4.2 represents a summary of the commonly used fluorescent probes used in laser scanning confocal microscopy including the excitation and emission wavelengths.

Figure 4.3 Absorption and emission spectra for fluorescein isothiocyanate

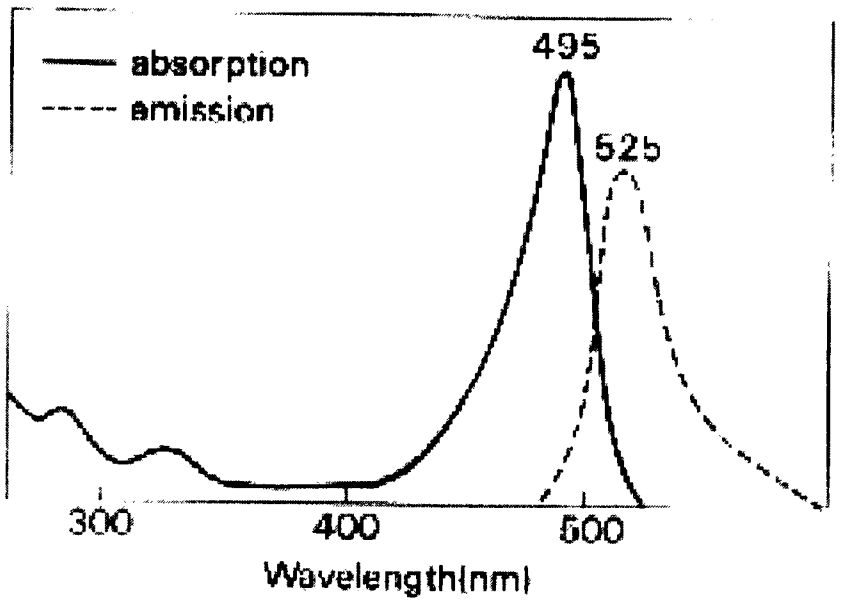

Figure 4.3 represents the absorption and emission spectra for fluorescein isothiocyanate (FITC) showing the maximum absorption wavelength to be 490nm and the emission wavelength to be 525nm. FITC is a commonly used fluorescent probe for laser scanning confocal microscopy that was used in this study to visualise the penetration of soluble and particulate BSA within the internal structure of selected adsorbent solid phases. (Reproduced from Pawley, 1985).

4.2.2 Equipment

- Leiss 510 Laser Scanning Confocal Microscope, Zeiss Ltd, Stockport, UK
- Rotary blood mixer, Stuart Scientific, UK
- Pharmacia LKB Ultrospec III spectrophotometer, Amersham Biosciences, Uppsala, Sweden
- pH meter, Hanna Instruments, H19321, Microprocessor Bench pH meter
- General laboratory glassware

4.2.3 Conjugation of Fluorescein Isothiocyanate to Soluble and Particulate BSA

Fluorescein isothiocyanate was selected as a suitable covalent probe for the visualisation of protein adsorption exploiting LSCM. The conjugation method employed was proposed by Kawamura (1977) and adapted by Zhanren Zhang (personal communication). BSAp were initially suspended in Buffer A (10mM Tris-HCl, pH 7.5 with 0.01% Tween 20 and 0.02% sodium azide) subsequent to the diafiltration operational step of the manufacturing process. For the probe to be successfully conjugated the protein nanoparticles were buffer exchanged into conjugation buffer (0.1M $NaHCO_3$, pH 8.3 with 0.5M NaCl; Buffer B). Due to the sample volumes being processed, PD-10 desalting columns (Amersham Biosciences, Uppsala, Sweden) were selected as a suitable method for buffer exchange. These columns contained 9.1ml of Sephadex G-25 medium gel filtration media consisting of beaded dextran particles (50-150μm in diameter) crosslinked using epichlorohydrin with a molecular weight exclusion of 5 x 10^3 Daltons (for globular proteins). The PD-10 column, having a void volume of 2.5ml, was initially equilibrated with 25ml of Buffer B followed by the addition of 2.5ml of BSAp suspended in Buffer A. The initial bed effluent was discarded, 3.5ml of Buffer B was added and the void volume of effluent containing BSAp suspended in Buffer B was collected. FITC was added to 2.5ml of BSAp (in Buffer B) in a volume of

0.16μl of a stock solution of FITC (1mg/ml), per microgram of protein (either soluble or particulate). The nanoparticle/FITC mixture was rigorously mixed at room temperature for 1 hour using a rotary mixer and subsequently added to a fresh PD-10 column pre-equilibrated with Buffer A to separate the FITC conjugated BSAp from the unbound fluorescent dye. After 2.5ml of FITC conjugated BSAp were added the effluent was discarded and 3.5ml of Buffer A was added and the effluent containing the FITC conjugated BSAp was collected. BSAp-FITC were stored at 4°C in the absence of ultraviolet light to ensure that there was no degradation of the FITC due to photobleaching. The procedure used for conjugating FITC to BSAs was the same as the proposed method for BSAp, except the initial BSA was mixed in Buffer B circumventing the initial buffer exchange step.

4.2.4 Adsorption of Fluorescently Labelled Soluble and Particulate BSA for Visualisation in LSCM

All of the adsorbent solid phases imaged using LSCM were loaded with fluorescently labelled BSAs and BSAp exploiting batch binding experimentation. Adsorbed BSAs and BSAp were imaged at regular time intervals during a 30 minute experiment and after 24 hours. The equilibrium experiments were completed by adding 0.1ml of adsorbent (extensively washed in Buffer A to equilibrate the system) to 1.5ml of fluorescently labelled BSA (either soluble or particulate) and mixed for 24 hours at room temperature using a rotary mixer. After 24 hours the remaining protein solution was removed and the adsorbent extensively washed in Buffer A to remove unbound or loosely bound labelled protein. The adsorbent samples were then immediately imaged by LSCM. In addition the adsorption of BSAs and BSAp to the selected adsorbent solid phases was investigated over 30 minutes. Before use the adsorbent was extensively washed in Buffer A to equilibrate the system, after which 0.1ml was added to 1.5ml of fluorescently labelled protein (either soluble or

particulate) and mixed at room temperature. Samples of the supernatant (0.1ml) and the adsorbent (10µl) were taken at 1, 10, 20 and 30 minutes. The adsorbent was washed in Buffer A (5 x 1ml) to remove unbound or loosely bound protein and imaged by LSCM (refer to Section 4.2.5), whilst the protein concentration of the supernatant was determined using the Bradford assay (see Section 3.2.6). Both experiments were conducted with BSAs at a concentration of 5mg/ml and BSAp at 220µg/ml as in previous batch binding studies (see Section 3.2.5).

4.2.5 Laser Scanning Confocal Microscopy Analysis

The Laser Scanning Confocal Microscope (Leiss 510 supplied by Zeiss Ltd) was made available by D.Hardie (Department of Immunology, University of Birmingham). Subsequent to the protein binding procedure (see Section 4.2.4), the adsorbents were all washed in Buffer A to remove unbound protein from the system. A sample of the washed adsorbent was then suspended in a drop of distilled water on a petri dish and the adsorbent was imaged through a x10 magnification lens (in addition to a x10 eyepiece lens) using water immersion. The samples were analysed using a 488nm and 534nm laser to detect the FITC fluorescence and the transmission image respectively. The initial image was captured at 128 pixels/mm to ascertain the settings of the confocal microscope for a blank image to minimise background fluorescence. The size of the pinhole aperture (see Section 4.1.1) was minimised to reduce the amount of out of focus light included in the final image. Once the settings had been adopted for a single adsorbent the same settings were used for the fluorescently labelled adsorbent samples. To produce a clear, sharp picture the image was captured at 512 pixels/mm. A complete scan of each adsorbent sample was made using the Z stack function, which enabled a series of X-Y scans to be generated throughout the entire depth of the adsorbent particles.

4.3 Results and Discussion

The adsorption and desorption behaviour of BSAs and BSAp to the selected adsorbent solid phases (designated Type I, II and IV; see Figure 2.1) was investigated further by laser scanning confocal microscopy (LSCM), to assess the product distribution within the adsorbent structure and to determine a method for direct measurement of protein and particulate adsorption.

4.3.1 Visualising Intraparticle Soluble and Particulate Protein Transport in the Selected Adsorbent Solid Phases by Laser Scanning Confocal Microscopy

Subsequent to the adsorption/desorption studies summarised in Chapter 3, several conclusions about the performance of the selected adsorbent solid phases were made (Types I to IV; see Figure 2.1) that were attributed to known characteristics of the internal and external design of the adsorbents. This chapter describes the use of LSCM to visualise the distribution of the protein products (BSAs and BSAp) within the adsorbent solid phases in an attempt to validate the conclusions made in Chapter 3. The scanning technique employed by the laser scanning confocal microscope imaged the fluorescent protein molecules or particles in an X-Y plane (see Figure 4.2) and detected the fluorescence response of the FITC-conjugated proteins by a simultaneous excitation and emission of the probe.

After the adsorbent was challenged with fluorescently labelled BSAs or BSAp the adsorbent particles were scanned for a fluorescence response. Figure 4.4A represents the adsorption of fluorescently labelled BSAs to STREAMLINE DEAE after a 24 hour contact time (Type I; see Figure 2.1). The profile indicates that BSAs has adsorbed in a thin 33μm outer layer upon the adsorbent (equivalent to 31.6% of the adsorbent radius) whilst the inner volume of the adsorbent appeared to be unused. This behaviour was also noted in Figure

Figure 4.4 Confocal microscopy images of STREAMLINE DEAE (Type I adsorbent) contacted with soluble and particulate BSA imaged after 24 hours

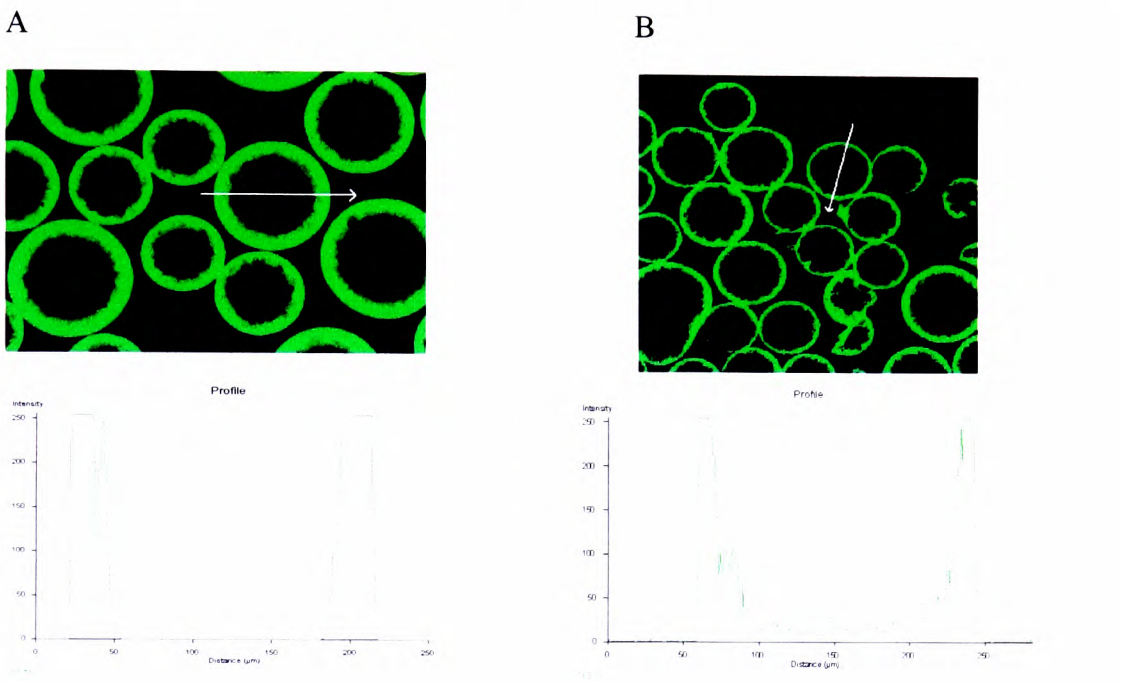

Figure 4.4 represents the fluorescence profiles generated by confocal microscopy after a contact time of 24 hours with both (A) fluorescently labelled BSAs and (B) BSAp. The proteins were adsorbed to STREAMLINE DEAE (Type I adsorbent, see Figure 2.1) using batch binding methods where 0.1ml of adsorbent was added to 1.5ml of fluorescently labelled BSA (either soluble or particulate) and mixed for 24 hours at room temperature using a rotary mixer. After adsorption the unbound protein was removed from the system and the adsorbent excessively washed using Buffer A. The adsorbent was then imaged using a laser scanning confocal microscope, from which the central optical slice of the adsorbent was selected and the fluorescence profiles were generated.

(Buffer A = 10mM Tris-HCl, pH 7.4 with 0.01% Tween 20 and 0.02% sodium azide).

4.4B that illustrates the fluorescence profile of BSAp after a contact time of 24 hours, where BSAp penetrated to a depth of 22.5μm (21.5%) of the adsorbent particle radius. This limited penetration observation was expected for BSAp due to the estimated diameter of the nanoparticles (150nm; see Section 3.3.3). It was expected that penetration into the 6% (w/v) agarose material of STREAMLINE DEAE would be limited and that the adsorption would predominate at the external surface of the adsorbent. In reality, BSAp appeared to penetrate the adsorbent structure to a degree as suggested by the adsorption/desorption profiles in Section 3.3.4. This was attributed to the size distribution of BSAp where nanoparticles smaller than 150nm are present (see Figure 3.4). In contrast, the limited penetration of BSAs into the STREAMLINE DEAE structure was unexpected as it was assumed that at apparent equilibrium in the batch binding experiment the protein would be evenly distributed throughout the adsorbent. The reasons for this observation were unknown but might be attributed to:

(i) the optical properties of the dense crystalline quartz particles within the STREAMLINE structure masking the fluorescence signal from FITC labelled BSAs adsorbed within the inner volume of the adsorbent

(ii) or, a complete BSAs adsorption equilibrium had not been attained within the 24 hour contact period.

To investigate this observation further, binding studies were completed as illustrated in Figure 4.5. STREAMLINE DEAE was incubated with fluorescently labelled BSAs for 48 hours after which the fluorescence image was scanned. The resulting profile demonstrated that the penetration of BSAs into the adsorbent particle increased with increase in contact time. The profile in Figure 4.5B indicated that BSAs had penetrated 48μm into the adsorbent radius after 48 hours (equivalent to 45.9%) in comparison to 33μm (31.6%) after a 24 hour contact time (see Figure 4.5A). This implied that significant fluorescence masking was not

Figure 4.5 The adsorption of soluble BSA to STREAMLINE DEAE after contact times of 24 and 48 hours

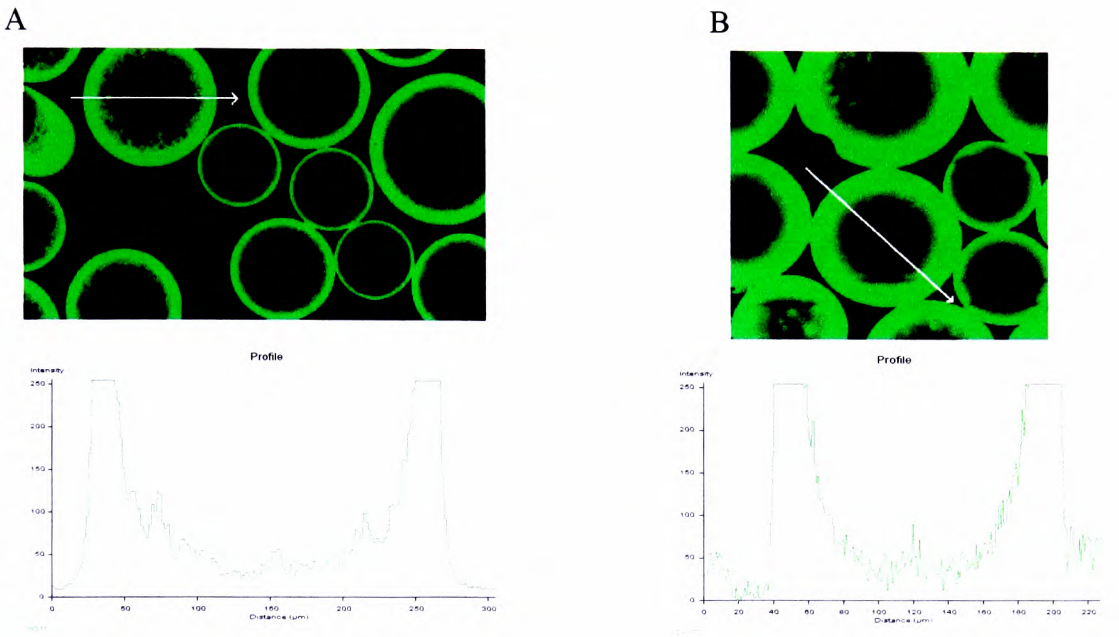

Figure 4.5 represents the fluorescence profiles generated by confocal microscopy after a contact time of (A) 24 hours and (B) 48 hours for fluorescently labelled BSAs. The protein was adsorbed to STREAMLINE DEAE (Type I adsorbent, see Figure 2.1) using batch binding methods where 0.1ml of adsorbent was added to 1.5ml of fluorescently labelled BSAs and mixed for 24 hours or 48 hours at room temperature using a rotary mixer. After adsorption the unbound protein was removed from the system and the adsorbent excessively washed using Buffer A. The adsorbent was then imaged using a laser scanning confocal microscope, from which the central optical slice was selected and the fluorescence profiles were generated.

(Buffer A = 10mM Tris-HCl, pH 7.4 with 0.01% Tween 20 and 0.02% sodium azide).

occurring, but that the adsorbent had not reached equilibrium. Several binding experiments were completed using STREAMLINE DEAE and the same binding pattern was observed in each, therefore it was concluded that to achieve equilibrium with soluble protein an extended contact time was required

In addition to the equilibrium binding studies, the adsorption of BSAs and BSAp to STREAMLINE DEAE was investigated over a shorter period of 30 minutes to measure the progression of adsorption with time. Figures 4.6 and 4.7 represent the adsorption of fluorescently labelled BSAs and BSAp to STREAMLINE DEAE respectively at time intervals of 1, 10, 20 and 30 minutes (see Section 4.2.4). The fluorescence profiles indicated that with elapsed time BSAs and BSAp penetrated into the adsorbent structure and Figure 4.8 represents the degree of penetration expressed as percentage of the radius of the adsorbent particle in which fluorescence was detected. The degree of penetration of both BSAs and BSAp agree with the results generated from the adsorption studies completed in Chapter 3. BSAs adsorption progressed slowly suggesting diffusion limited adsorption as was indicated in Figure 3.2. Additionally, BSAp also appeared to penetrate the adsorbent as time elapsed as implied in Figure 3.5.

The results indicated that the degree of penetration of BSAs after a 30 minute contact time (25.1μm or 23.9%) was very similar to that after a 24 hour contacting period (2.5μm or 21.5%; see Figure 4.4 and Figure 4.8). This suggested that once penetration had reached a depth of approximately 30μm (28.7%) the rate of adsorption appeared to decrease but within 48 hours it was observed that the penetration had reached 47.8% (50μm). The protein adsorption was also measured indirectly using the Bradford protein assay. The data obtained demonstrated that the concentration of adsorbed protein was greater at 24 hours than at 30 minutes (data not shown). The transmission photomicrograph of STREAMLINE DEAE, illustrated in Figure 2.8 suggests that the quartz particles contained within the adsorbent are

Figure 4.6 Confocal microscopy images of STREAMLINE DEAE contacted with fluorescently labelled soluble BSA

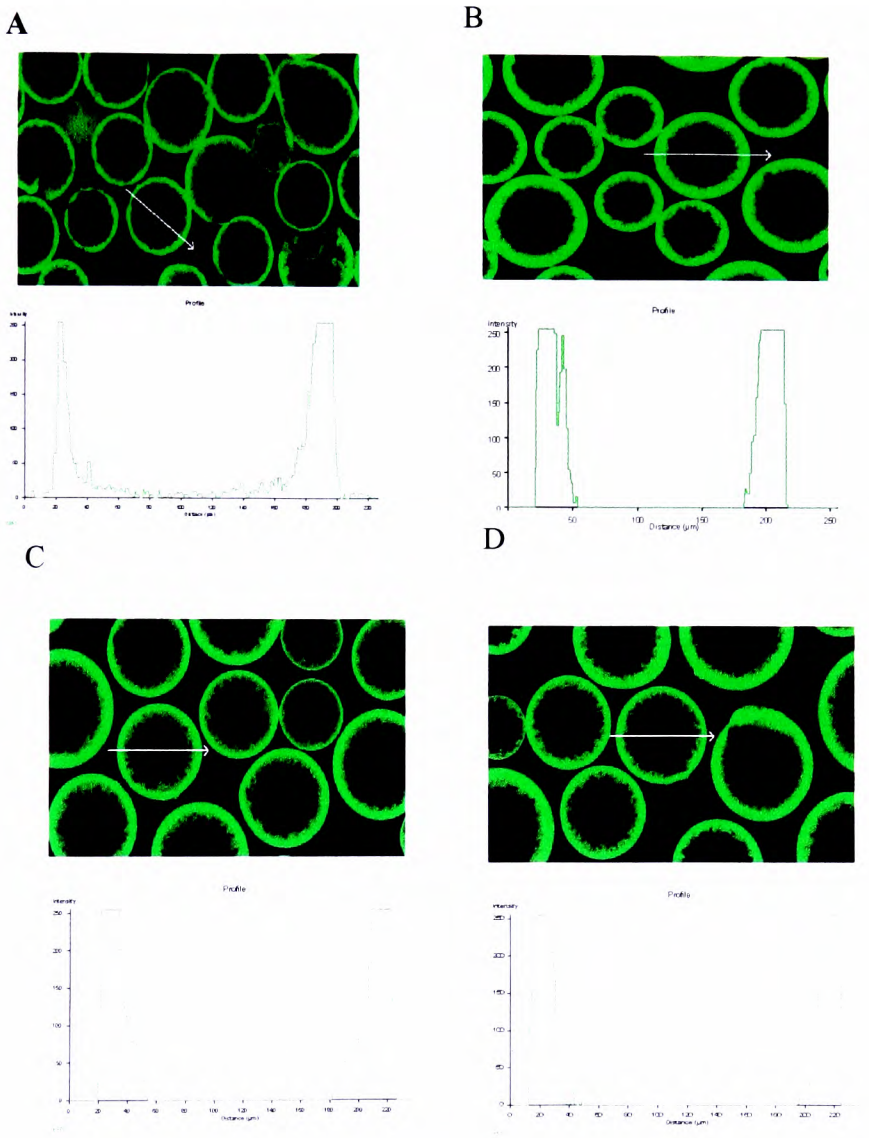

Figure 4.6 represents the fluorescence profiles generated by confocal microscopy after a contact time of 30 minutes with fluorescently labelled BSAs. The nanoparticles were adsorbed to STREAMLINE DEAE using batch binding methods where 0.1ml of adsorbent was added to 1.5ml of fluorescently labelled BSAs. At regular time intervals of 1, 10, 20 and 30 minutes (A-D) 10µl of adsorbent was removed and washed in Buffer A to remove unbound protein, and imaged using confocal microscopy. For each time interval adsorbent sample the central optical slice was selected and the fluorescence profile generated.
(Buffer A = 10mM Tris-HCl, pH 7.4 with 0.01% Tween 20 and 0.02% sodium azide).

Figure 4.7 Confocal microscopy images of STREAMLINE DEAE contacted with fluorescently labelled BSA nanoparticles

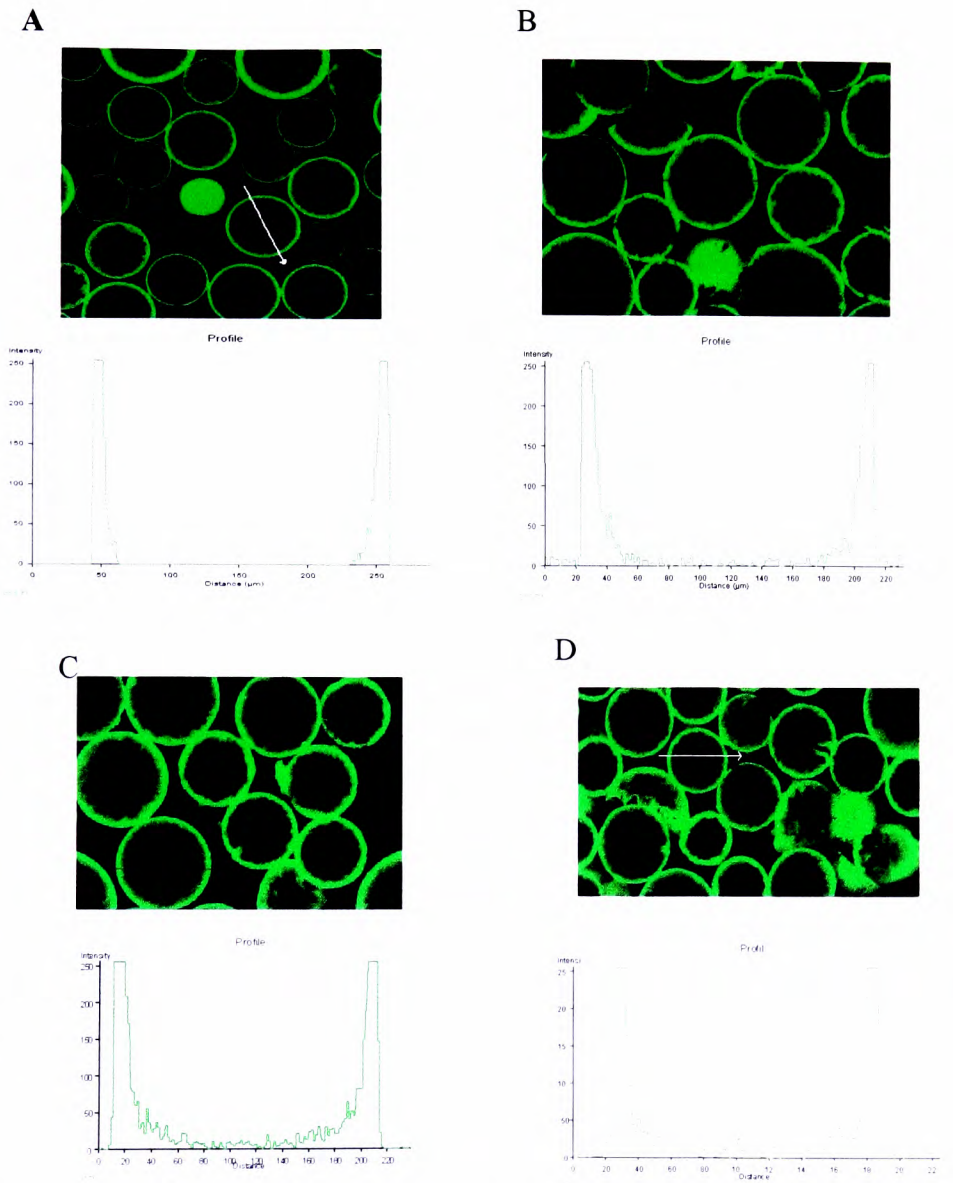

Figure 4.7 represents the fluorescence profiles generated by confocal microscopy after a contact time of 30 minutes with fluorescently labelled BSAp. The nanoparticles were adsorbed to STREAMLINE DEAE using batch binding methods where 0.1ml of adsorbent was added to 1.5ml of fluorescently labelled nanoparticles. At regular time intervals of 1, 10, 20 and 30 minutes (A-D) 10µl of adsorbent was removed and washed in Buffer A (10mM Tris-HCl, pH 7.4 with 0.01% Tween 20 and 0.02% sodium azide) to remove unbound nanoparticles, and imaged using confocal microscopy. For each time interval adsorbent sample the central optical slice was selected and the fluorescence profile generated.

Figure 4.8 Bar chart representing the percentage of the radius of a STREAMLINE DEAE adsorbent particle utilised for soluble and particulate BSA adsorption

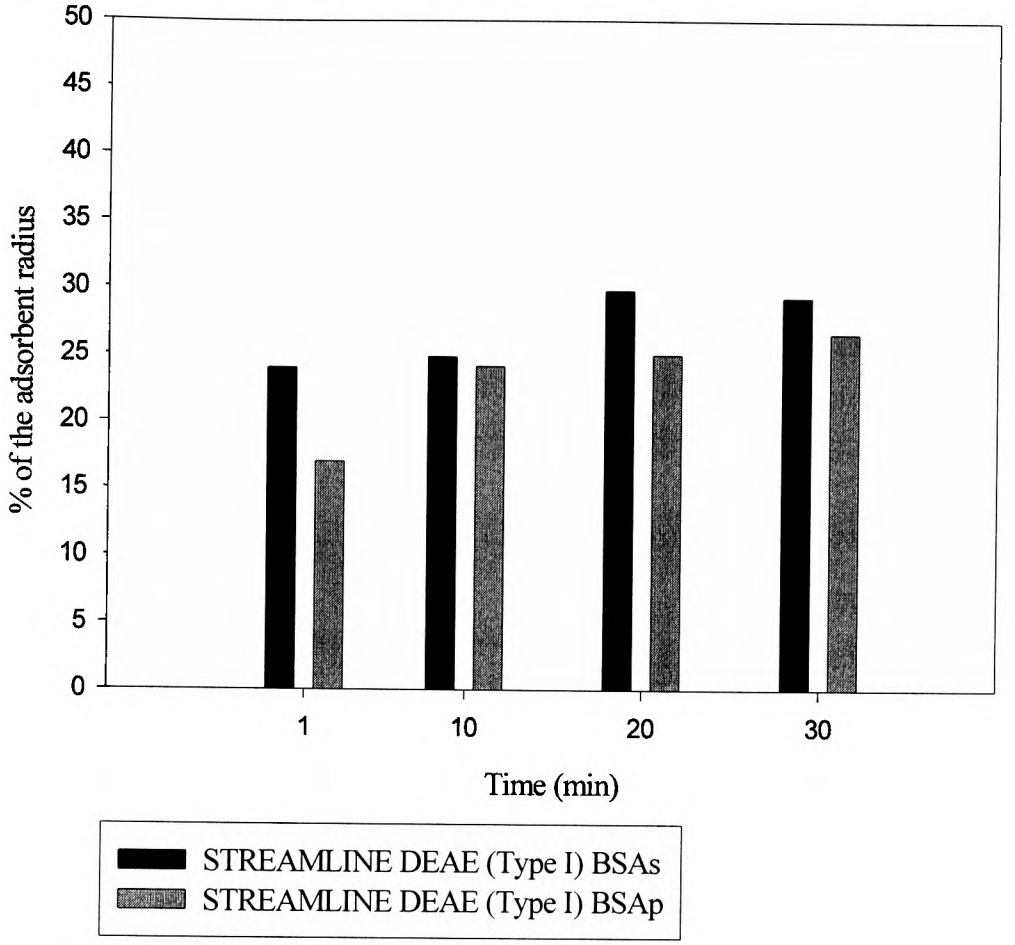

Figure 4.8 represents the penetration of both fluorescently labelled BSAs and BSAp into the adsorbent particles of STREAMLINE DEAE expressed as a percentage of the adsobent radius in which adsorption was observed. The penetration was calculated from fluorescence profiles generated by confocal microscopy (see Figure 4.6). A sample of adsorbent (0.1ml) added to 1.5ml of fluorescently labelled BSAs and BSAp and mixed at room temperature using a rotary mixer. Samples were taken at regular time intervals and analysed using confocal microscopy and the Bradford assay.

(Buffer A = 10mM Tris-HCl, pH 7.4 with 0.01% Tween 20 and 0.02% sodium azide).

not distributed within the outer 30μm of the adsorbent radius. Consequently it may be surmised that the degree of penetration of BSAs is increasing with time, but within the particle structure the distribution of the fluorescently labelled protein could be too disperse to be detected using LSCM. Alternatively the presence of the inert quartz particles could have inhibited the efficient diffusion on BSAs within the structure or the quartz could have a quenching effect of the fluorescence. This would result is less fluorescence being detected by the confocal microscope.

Equilibrium binding studies (24 hours) and short time course experiments (30 minutes) were completed for each adsorbent solid phase remaining in the study (see Section 3.3.6). The Type II adsorbents included in the study (refer to Table 4.1) were characterised by the manufacturing process to possess large pores (greater than 0.6μm in diameter; see Figure 2.1; Table 2.1) and the adsorption/desorption profiles produced in Chapter 3 suggested that these pores would facilitate the transport of nanoparticles into the adsorbent structure. The results from time-based batch binding experiments indicated that the adsorption of BSAs was rapid suggesting that it was not diffusion limited (see Figure 3.2) whereas the adsorption of BSAp (150nm in diameter; see Figure 3.4) was less rapid. This suggested that the nanoparticles penetrated the adsorbent structure, but that the transport was diffusion limited.

Figure 4.9 illustrates the equilibrium fluorescence profiles of PVA TiO_2 DEAE and PVA Mo DEAE (both Type II) with both BSAs and BSAp in experiments completed in an equivalent manner to tests with STREAMLINE DEAE. The adsorption behaviour of BSAs and BSAp within both PVA TiO_2 and PVA Mo appears to predominate in an outer layer of the adsorbent structure. Figure 4.9A and 4.9B represent PVA TiO_2 contacted with fluorescently labelled BSAs and BSAp respectively and both appeared to exhibit the same degree of penetration at 23.4% and 26.7% of the radius of randomly selected adsorbent

Figure 4.9 Confocal microscopy images of PVA TiO_2 DEAE and PVA Mo DEAE (Type II adsorbents) contacted with soluble and particle BSA after 24 hours

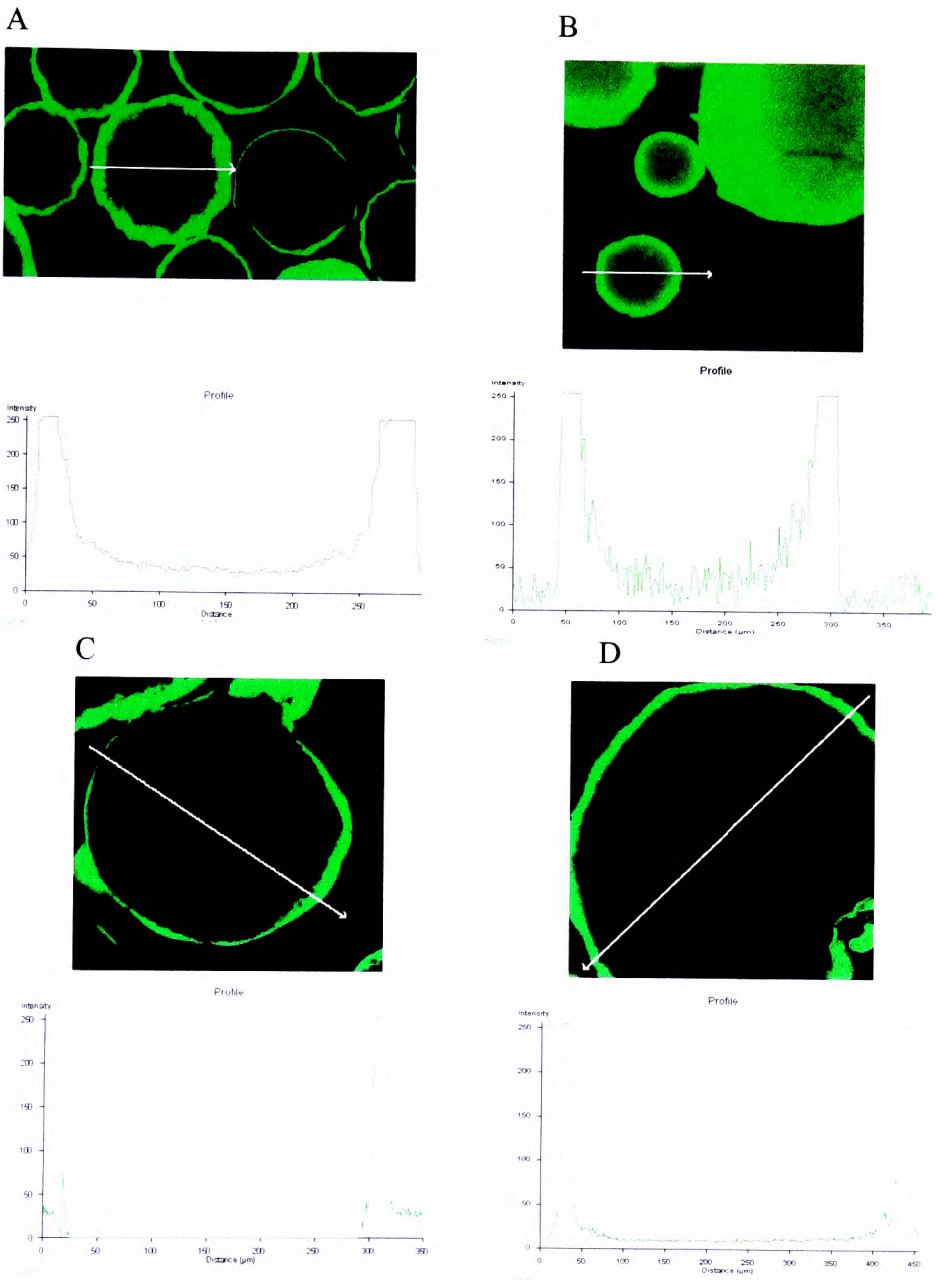

Figure 4.9 represents the fluorescence profiles of PVA TiO_2 DEAE and PVA Mo DEAE generated from confocal microscopy after a contact time of 24 hours with both fluorescently labelled (A) and (C) BSAs and (B) and (D) BSAp. Adsorbent (0.1ml) was added to 1.5ml of protein (soluble or particulate) and mixed at room temperature for 24 hours using a rotary mixer. After adsorption the adsorbents were washed excessively in Buffer A (10mM Tris-HCl, pH 7.4 with 0.01% Tween 20 and 0.02% sodium azide) to remove unbound protein, the adsorbenst were then imaged using confocal microscopy. The central optical slice of the adsorbents was selected and the fluorescence profiles generated.

particles. It is interesting to note that this similarity is also observed for PVA Mo where the penetration of BSAs and BSAp are 11.2% and 13.9% of the radius respectively. It was assumed that there would be a greater degree of penetration into these Type II macroporous adsorbents in comparison to STREAMLINE DEAE a Type I microporous adsorbent (see Figure 2.1) due to the large pore diameter (claimed to be 1μm; see Table 2.1). However the penetration appears to be limited, but both BSAs and BSAp penetrate approximately to the same degree into the radius of the adsorbent that suggests that there is unrestricted diffusion of BSAp and BSAs into the adsorbent structure up to a point.

A higher degree of penetration may not have been observed due to the operation of the experiments in batch mode, as the penetration was solely diffusion mediated. Large macropores are expected to encourage convective flow through the adsorbent structure, but a pressure drop is required to induce this type of flow (i.e. POROS; Afeyan and Fulton, 1991). It would be interesting to investigate the adsorption of BSAp to these adsorbents in a fixed bed operation. Figures 4.10 and 4.11 represent the adsorption of BSAs and BSAp to PVA TiO_2 and PVA Mo respectively expressed as the percentage radius in which fluorescence was detected over time for randomly selected particles. The results validate the conclusions made in Chapter 3 based upon the adsorption/desorption studies. Figure 4.10 indicates that there was a decline in the penetration of BSAp from 10 minutes to 30 minutes that may be attributed to further penetration of the FITC conjugated nanoparticles into the adsorbent structure. This would have resulted in lower concentrations of FITC BSAp that could not be detected by laser scanning confocal microscopy.

The final PVA adsorbent included in this study, PVA Zr DEAE (Type II; see Figure 2.1 and Table 2.1), was incubated with BSAs and BSAp in an equivalent manner to the previous experiments but an unusual effect was observed as indicated in Figure 4.12. All of

Figure 4.10 Bar chart representing the percentage of the radius of a PVA TiO_2 DEAE adsorbent particle utilised for soluble and particulate BSA adsorption

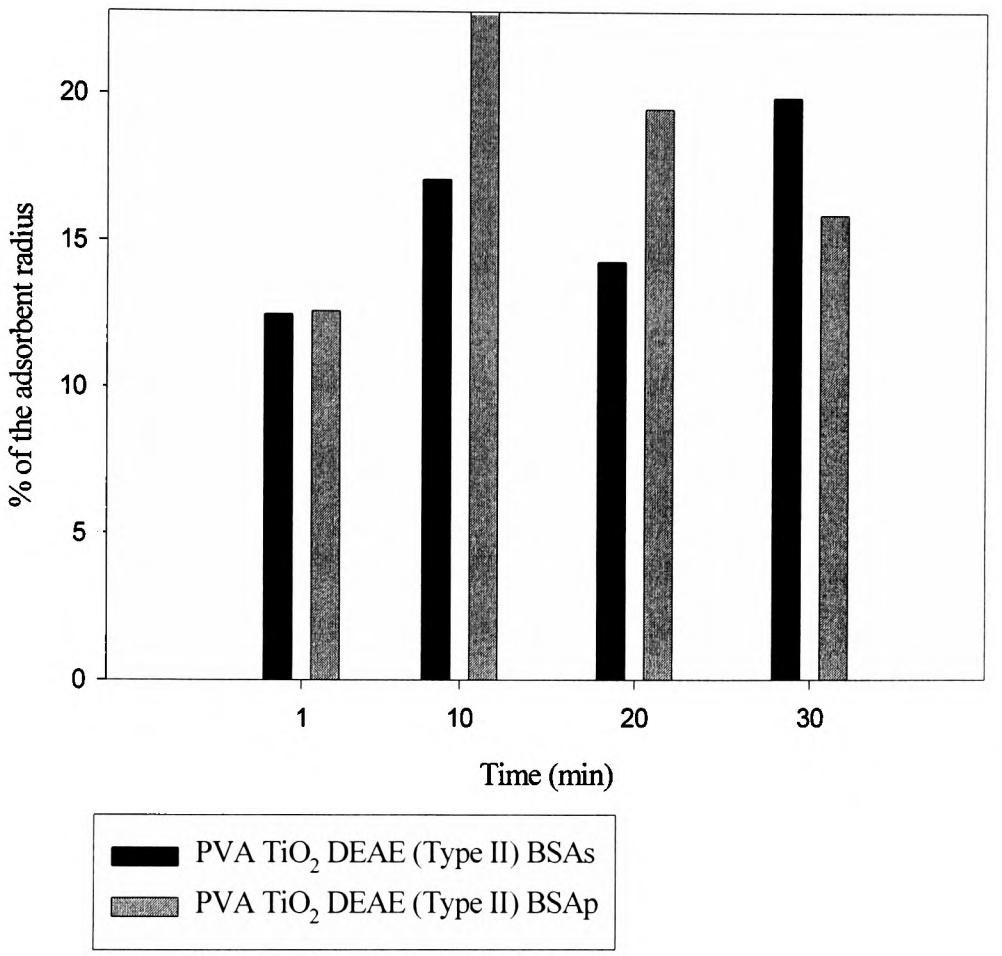

Figure 4.10 represents the penetration of both fluorescently labelled BSAs and BSAp into the adsorbent particles of PVA TiO_2 DEAE expressed as the percentage of the radius in which adsorption occurred. The radius was calculated from fluorescence profiles generated by confocal microscopy (see Figure 4.6). A sample of adsorbent (0.1ml) was added to 1.5ml of fluorescently labelled BSAs and BSAp and mixed at room temperature using a rotary mixer. Samples were taken at regular time intervals and analysed using confocal microscopy and the Bradford assay.

Buffer A = 10mM Tris-HCl, pH 7.4 with 0.01% Tween 20 and 0.02% sodium azide)

Figure 4.11 Bar chart representing the percentage of the radius of a PVA Mo DEAE adsorbent particle utilised for soluble and particulate BSA adsorption

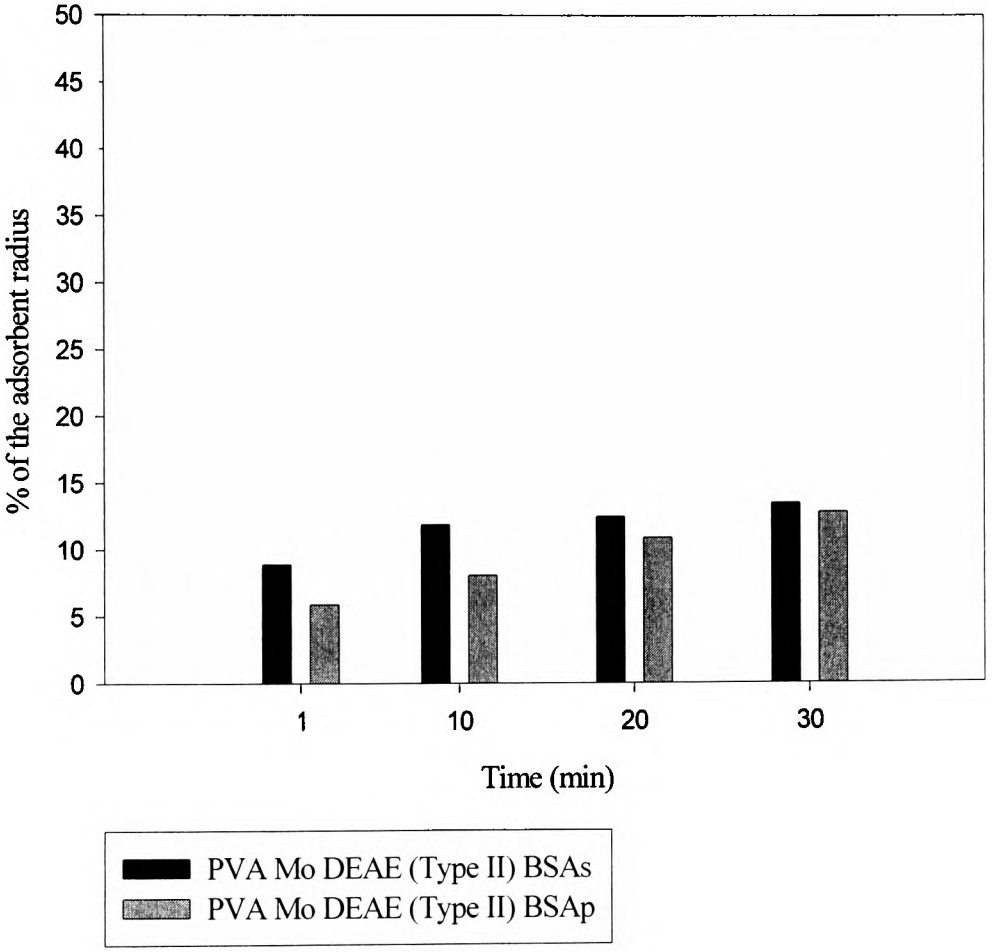

Figure 4.11 represents the penetration of both fluorescently labelled BSAs and BSAp into the adsorbent particles of PVA Mo DEAE expressed as a percentage of the radius in which adsorption occurred. The radius was calculated from fluorescence profiles generated by confocal microscopy (see Figure 4.6). A sample of adsorbent was added to 1.5ml of fluorescently labelled BSAs and BSAp and mixed at room temperature using a rotary mixer. Samples were taken at regular time intervals and analysed using confocal microscopy and the Bradford assay.

(Buffer A = 10mM Tris-HCl, pH 7.4 with 0.01% Tween 20 and 0.02% sodium azide).

Figure 4.12 Confocal microscopy images of PVA Zr DEAE (Type II adsorbent) contacted with soluble and particulate BSA and imaged after 24 hours

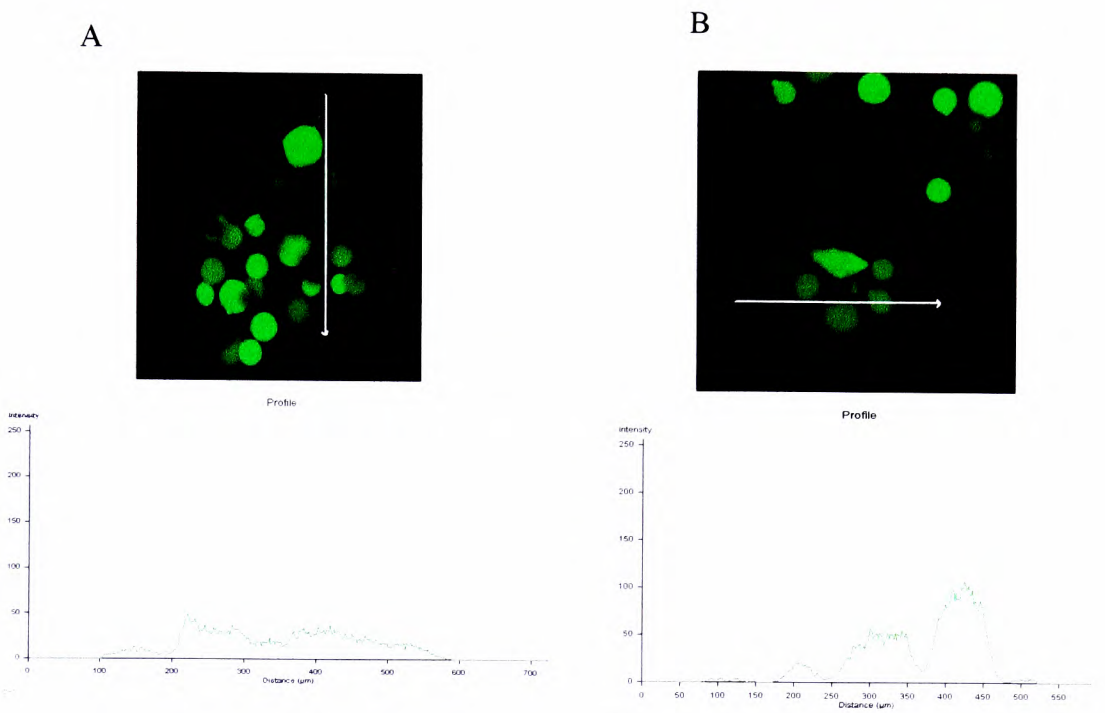

Figure 4.12 represents the fluorescence profiles generated by confocal microscopy after a contact time of 24 hours with both (A) fluorescently labelled BSAs and (B) BSAp. The proteins were adsorbed to PVA Zr DEAE (Type II adsorbent) using batch binding methods where 0.1ml of adsorbent was added to 1.5ml of fluorescently labelled BSA (either soluble or particulate) and mixed for 24 hours at room temperature using a rotary mixer. After adsorption the adsorbent was excessively washed in Buffer A to remove any unbound protein. The adsorbent was then imaged using confocal microscopy, from which the central optical slice was selected and the fluorescence profile generated.

(Buffer A = 10mM Tris-HCl, pH 7.4 with 0.01% Tween 20 and 0.02% sodium azide).

the protein (both BSAs and BSAp) appeared to adsorb to the surface of the zirconium silicate core and not the PVA coating. As noted previously (see Section 2.1.5) the method of production for the PVA adsorbent (supplied by Igor Galaev) was unknown and therefore critical information concerning the preparation of the zirconium silicate prior to being added to the PVA as a high density filler was not available. The zirconium silicate encapsulated in this adsorbent was sourced from the same batch used in the fabrication of the pellicular adsorbent 2% ZsA (see Section 2.2.4) which did not exhibit the same effect for either BSAs or BSAp (refer forward to Figure 4.14). During the manufacturing process for 2% ZsA, the zirconium silicate was extensively washed in water (see Section 2.2.4). It is possible that in the fabrication procedure for PVA Zr, the silicate was either not exhaustively washed or chemically treated in a manner sufficient to reduce protein adsorption to the filler. Additionally it can be concluded that the adsorbent contains large 1μm pores as claimed (see Section 2.1.5) that enabled both BSAs and BSAp to fully penetrate the PVA base material of the adsorbent.

Figure 4.13 represents a similar analysis of the Celbead adsorbents, the final Type II macroporous adsorbents included in the study (see Section 2.1.4) and the images indicate that Celbead (II) DEAE and Celbead Amino are structurally different. Celbead (II) DEAE allowed BSAs and BSAp to penetrate into the adsorbent structure in a manner that suggested the presence of large pores. However, the fluorescence profiles also demonstrated that a large percentage of the internal adsorbent area was unavailable for adsorption which accounted for the low adsorption capacities measured and expressed in Tables 3.2 and 3.3. In contrast Celbead Amino exhibited exclusive surface binding and no BSAs or BSAp penetration (see Figure 4.13C; Section 3.3.4). The confocal microscopy images confirm the Celbead Amino adsorbent to be non-porous and thus the original assumption of classification of the adsorbent

Figure 4.13 Confocal microscopy images of Celbead (II) DEAE and Celbead Amino (Type II adsorbents) contacted with soluble and particulate BSA imaged after 24 hours

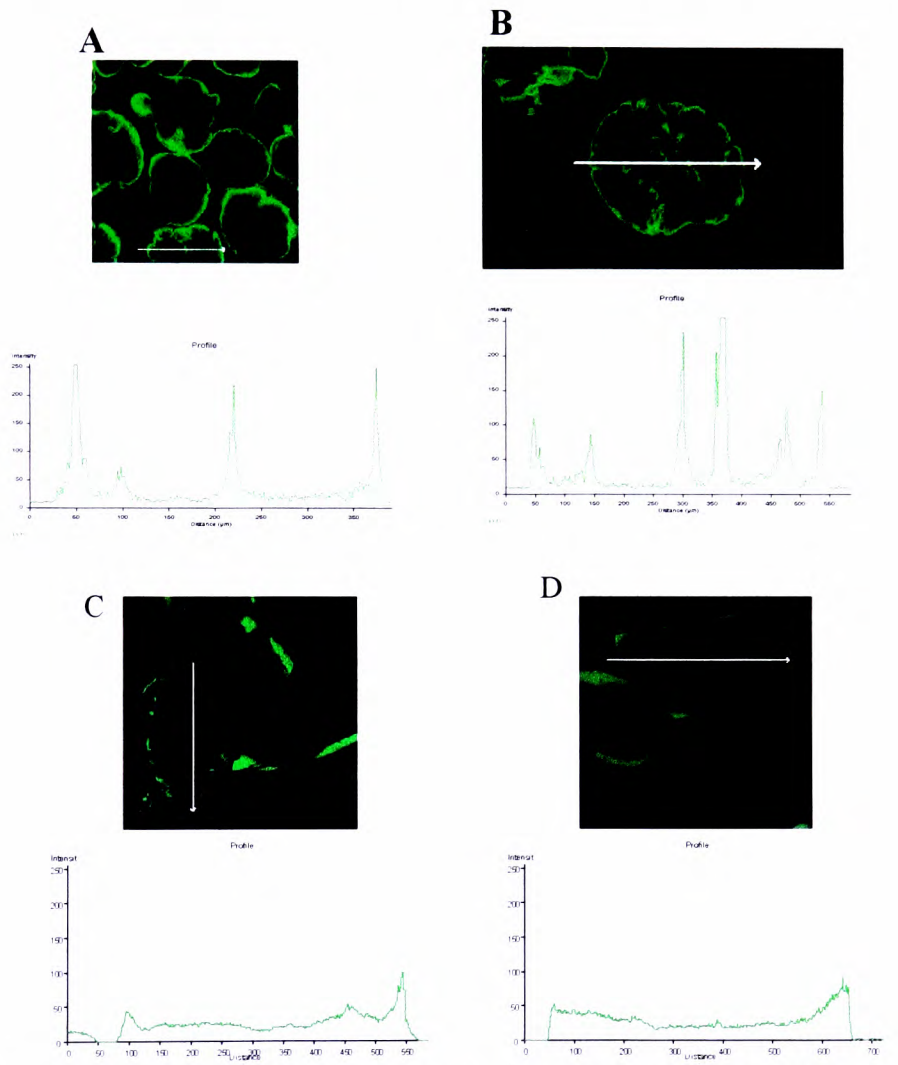

Figure 4.13 represents the fluorescent profiles generated by confocal microscopy after a contact time of 24 hours with both (A) and (C) fluorescently labelled BSAs and (B) and (D) BSAp. The proteins were adsorbed to Celbead (II) DEAE and Celbead Amino using batch binding methods where 0.1ml of adsorbent was added to 1.5ml of fluorescently labelled BSA (either soluble or particulate) and mixed at room temperature for 24 hours using a rotary mixer. After adsorption the adsorbents were excessively washed with Buffer A to remove unbound protein. The adsorbents were then imaged using confocal microscopy from which the central optical slice was selected and the fluorescence profiles were generated.
(Buffer A = 10mM Tris-HCl, pH 7.4 with 0.01% Tween 20 and 0.02% sodium azide).

as a Type II macroporous adsorbent (see Figure 2.1) appears to be incorrect. In addition, due to the nature of the adsorption profiles and the irregular shape of the Celbead adsorbents (see Figures 2.17 and 2.18) it was not possible to calculate the percentage radius of individual adsorbent particles.

The final adsorbent included in the study was a Type IV pellicular adsorbent designated as 2% ZsA (see Figure 2.1 and Table 2.1) and confocal microscopy images illustrating the adsorption of BSAs and BSAp are represented in Figure 4.14. The initial observation from the fluorescence images is that BSAs completely penetrated the agarose layer of the pellicular adsorbent up to the zirconium silicate core (Figure 4.14A). In contrast, BSAp adsorbed exclusively to the adsorbent surface with approximately 10% of the adsorbent radius being used for adsorption that is equal to 10.5μm penetration (see Figure 4.15). This suggested that there was a degree of penetration into the 2% agarose layer. However it has been demonstrated by Thwaites *et al* (2002) that apparent penetration of plasmid DNA into 6% agarose structures was attributed to surface roughness as opposed to actual penetration. Consequently, the small degree of BSAp penetration observed in 2% ZsA could be attributed to such surface characteristics.

It is noteworthy that a significant BSAp penetration was observed for 6% STREAMLINE DEAE of 22.5μm after a 24 hour contact time, whereas for 2% ZsA there is virtually no apparent penetration. This observation was unexpected as a 6% agarose gel would be expected to allow the penetration of globular proteins having a molecular weight of 10,000 to 5,000,000 Daltons and a 2% agarose gel allows the penetration of proteins having molecular weights of 250,000 to 450,000,000 Daltons (BioRad Product Information). It was therefore expected that BSAp would penetrate further into 2% ZsA adsorbent particles in comparison to 6% STREAMLINE particles.

Figure 4.14 Confocal microscopy images of 2% ZsA (Type IV adsorbent) contacted with soluble and particulate BSA and imaged after 24 hours

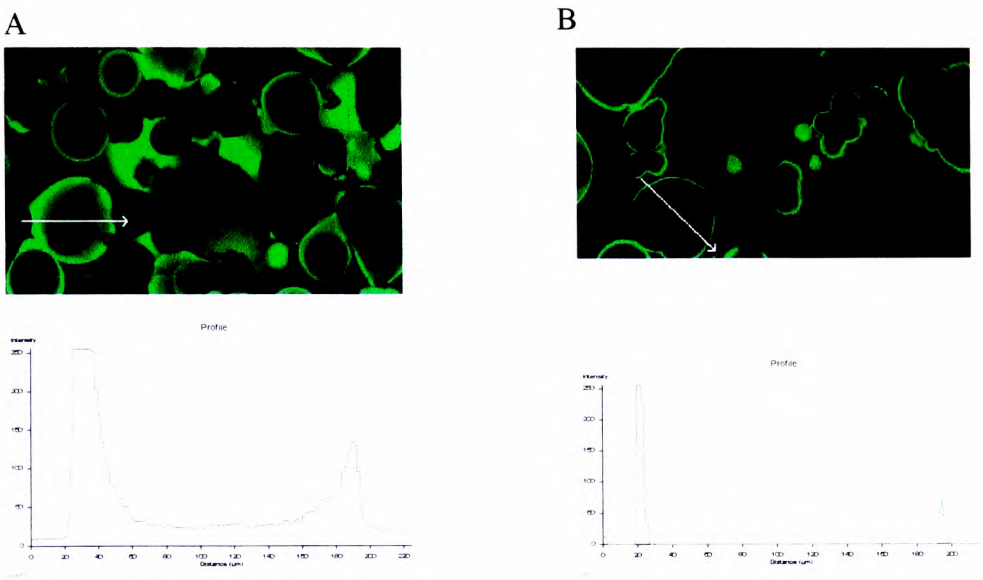

Figure 4.14 represents the fluorescence profiles generated by confocal microscopy after a contact time of 24 hours with both (A) fluorescently labelled BSAs and (B) BSAp. The proteins were adsorbed to 2% ZsA (Type IV adsorbent) using batch binding methods where 0.1ml of adsorbent was added to 1.5ml of fluorescently labelled BSA (either soluble or particulate) and mixed at room temperature for 24 hours using a rotary mixer. After adsorption the adsorbent was excessively washed in Buffer A to remove unbound protein. The adsorbent was the imaged using confocal microscopy from which the central optical slice of the adsorbent was selected and the fluorescence profiles were generated.

(Buffer A = 10mM Tris-HCl, pH 7.4 with 0.01% Tween 20 and 0.02% sodium azide).

Figure 4.15 Bar chart representing the percentage of the radius of a 2% ZsA DEAE adsorbent particle utilised for soluble and particulate BSA adsorption

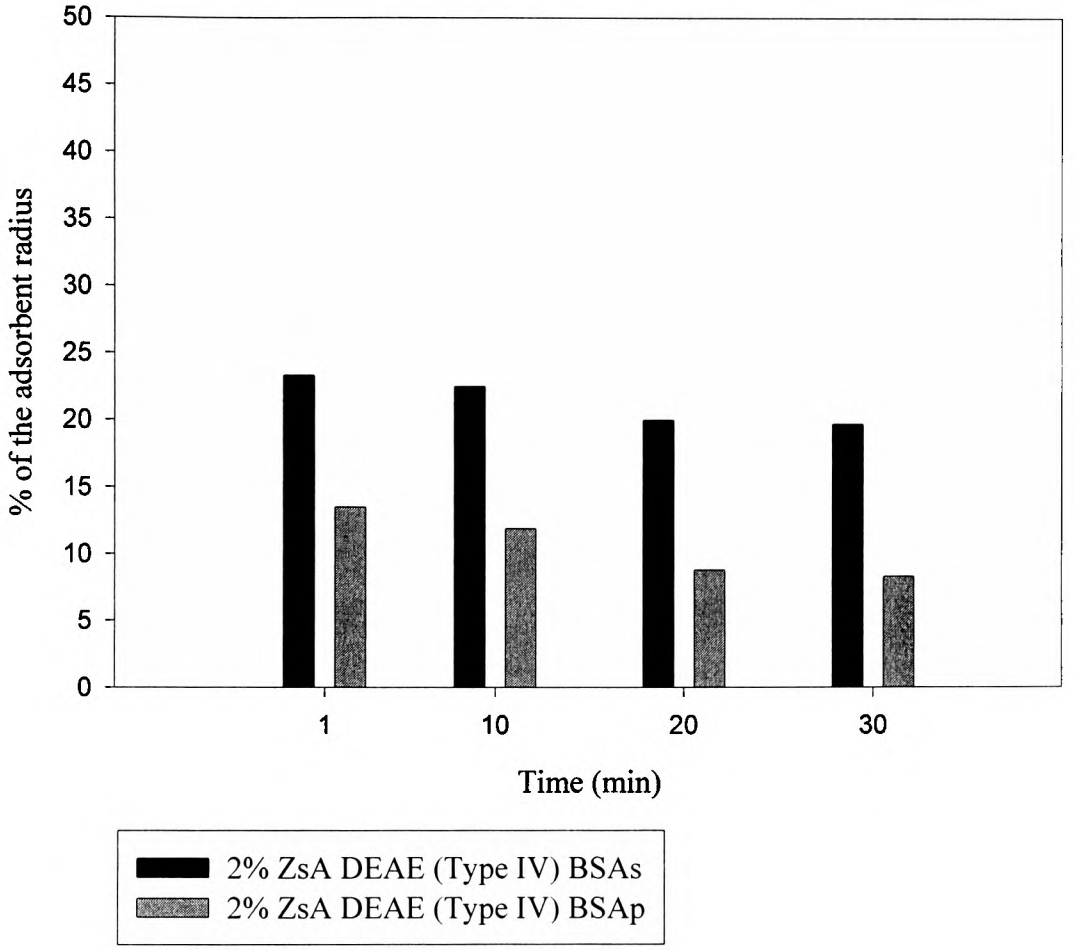

Figure 4.15 represents the penetration of both fluorescently labelled BSAs and BSAp into the adsorbent particles of 2% ZsA expressed as a percentage of the particle radius in which adsorption occurred. The radius was calculated from fluorescence profiles generated by confocal microscopy (see Figure 4.6).

(Buffer A = 10mM Tris-HCl, pH 7.4 with 0.01% Tween 20 and 0.02% sodium azide).

4.3.2 Direct Evaluation of the Fluorescence Profiles

The relative intensity of the fluorescent light emitted from the adsorbent sample corresponds to the resulting pixel image generated by the computer. Therefore from the individual profile for each adsorbent sample loaded with fluorescently labelled BSAs or BSAp a calculation of the relative concentration of the adsorbate within the adsorbent particles is possible. Linden *et al* (1999) described a simple calculation for determining the relative capacity of the adsorbents that has been modified and applied to the work described herein. The integral fluorescence (I) within the volume of the adsorbent particle where adsorption has occurred is calculated using Equation 4.1, which takes into consideration the volume of the adsorbent particle used for adsorption. By relating this value to the adsorbent particle volume (Equation 4.2) the relative capacity (Q_{rel}) is obtained in arbitrary units per cm^3 of adsorbent.

$$I = \text{area under the curve } [(r_a^3 - r_i^3)\ {}^4/_3\ \pi] \qquad \text{Equation 4.1}$$

For equation 4.1 the area under the curve was calculated using a Sigma Plot graphics package transformation that integrates the area under curves using the trapezoidal rule.

$$Q_{rel} = I \,/\, \text{volume of 1 particle} \qquad \text{Equation 4.2}$$

The data calculated using these equations allows the confocal microscope images to be quantified in terms of the fractional approach to equilibrium ($F = Q_{rel}/ Q_{rel\equiv}$ verses time) from direct measurements within the adsorbent particles, in addition to the observation of the product transport within the adsorbent solid phases.

Figures 4.16 and 4.17 represent the batch uptake curves for all the adsorbents constructed after the integration and normalisation of the fluorescence profiles for both BSAs

Figure 4.16 Batch uptake curves representing the normalised and integrated fluorescence from the laser scanning confocal microscopy images for BSAs

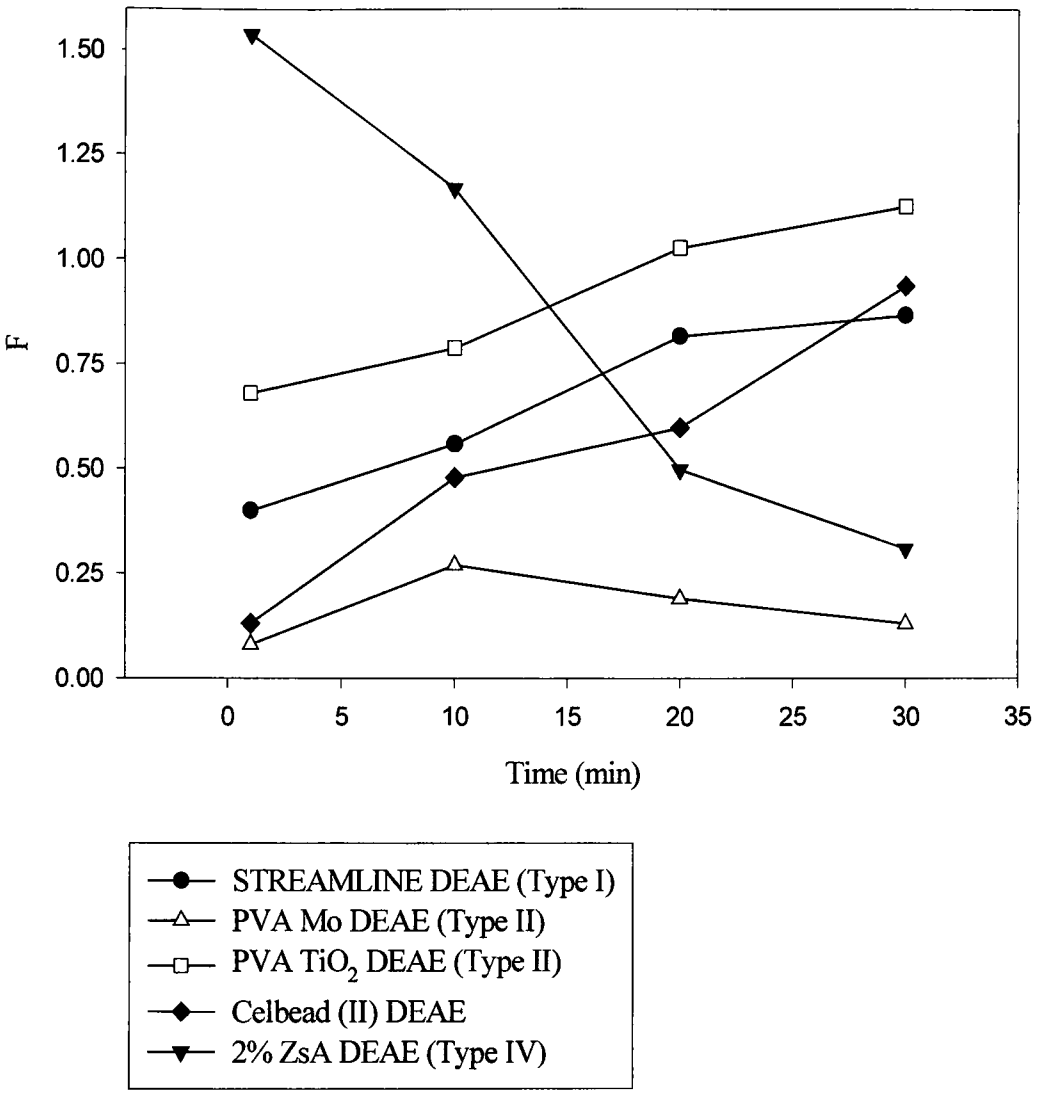

Figure 4.16 represents the fractional approach to equilibrium after the integration and normalisation of the fluorescence profiles within a 30 minute adsorption experiment (see Figure 4.6). A sample of adsorbent (0.1ml) was added to 1.5ml of fluorescently labelled BSAs and mixed at room temperature using a rotary mixer. Samples of both the adsorbent and supernatant were taken at regular time intervals and the adsorbent samples imaged by confocal microscopy. The resulting fluorescence profiles were used to calculate the relative fluorescence (F; see Equations 4.1 and 4.2). The relative fluorescence for Celbead Amino and PVA Zr DEAE could not be calculated as neither were characterised by a spherical adsorption profile.

(Buffer A = 10mM Tris-HCl, pH 7.4 with 0.01% Tween 20 and 0.02% sodium azide).

Figure 4.17 Batch uptake curves representing the normalised and integrated fluorescence from the laser scanning confocal microscopy images for BSAp

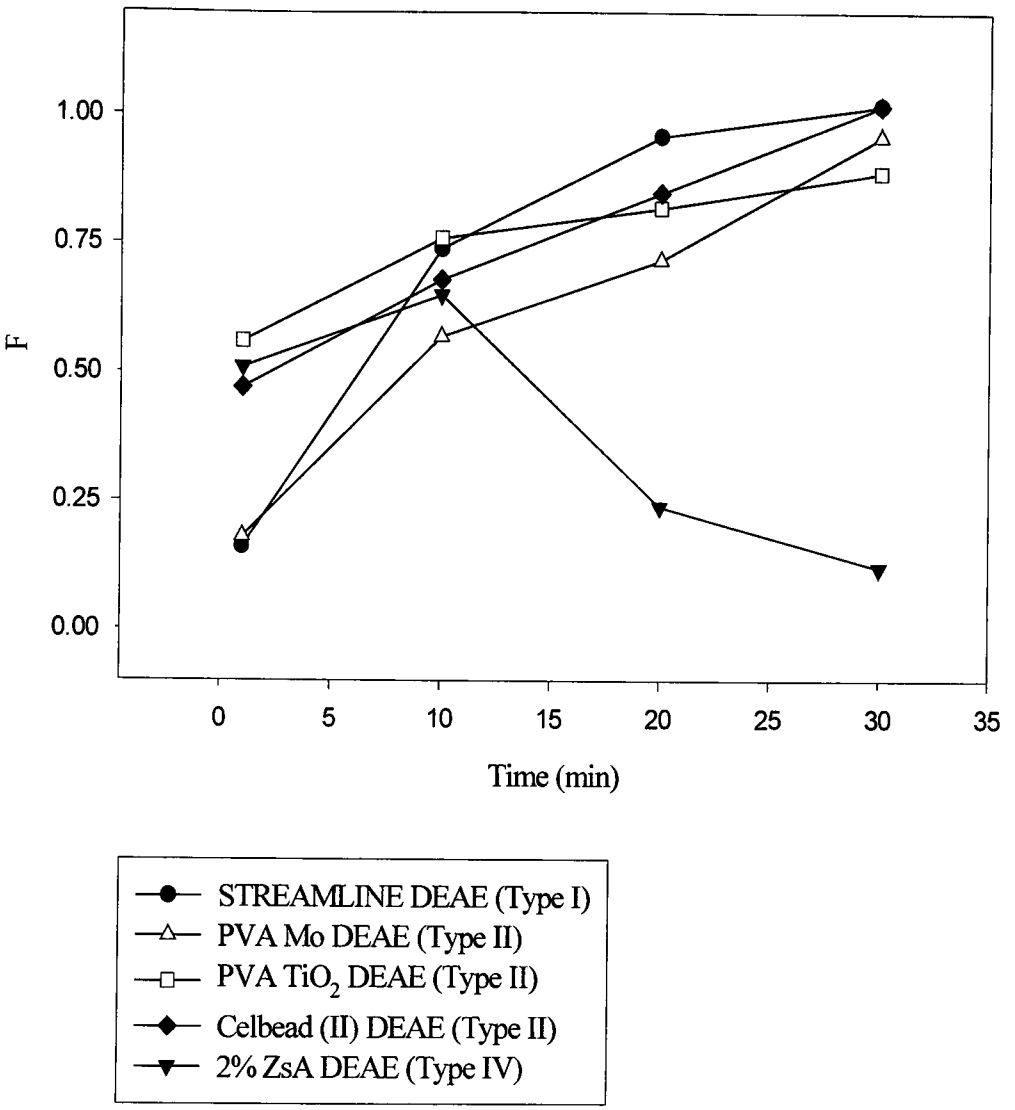

Figure 4.17 represents the fractional approach to equilibrium after the integration and normalisation of the fluorescence profiles within a 30 minute adsorption experiment (see Figure 4.6). A sample of adsorbent (0.1ml) was added to 1.5ml of fluorescently labelled BSAp and mixed at room temperature using a rotary mixer. Samples of both the adsorbent and supernatant were taken at regular time intervals and the adsorbent samples imaged by confocal microscopy. The resulting fluorescence profiles were used to calculate the relative fluorescence (F; see Equations 4.1 and 4.2). The relative fluorescence of Celbead Amino and PVA Zr DEAE could not be calculated as neither were characterised by a spherical adsorption profile.

and BSAp respectively. The curves illustrate that as the experiment progressed the fluorescence generally increased in line with the concentration of adsorbed protein. The exception was the pellicular Type IV adsorbent, 2% ZsA where the recorded fluorescence actually decreased as the experiment progressed. This was attributed in part to the zirconium silicate particles contained within the agarose material of the adsorbent whose dense nature could potentially compromise the optical properties and mask the full fluorescence of the labelled BSAs and BSAp (see Figure 4.15).

It was important to validate the quantitative interpretation of the confocal images with an independent method (for example the Bradford protein assay) to indirectly measure the decrease in the fluid phase protein concentration overtime (see Section 4.2.4). Figures 4.18 and 4.19 represent a comparison of the direct measurement of adsorption using LSCM and the indirect measurement using the Bradford assay for the commercial benchmark STREAMLINE DEAE. The fractional approach to equilibrium for fluorescence (F) is expressed as the relative capacity (Q_{rel}) divided by the relative capacity at equilibrium ($Q_{rel\equiv}$; see Equation 4.2). In addition, the fractional approach to equilibrium for the protein concentration is expressed as the concentration of adsorbed protein (C) divided by the equilibrium adsorption capacity (C_o).

It was observed that the adsorption profiles did not correlate for either BSAs (see Figure 4.18) or BSAp (see Figure 4.19). This indicated that the measured maximum fluorescence capacity was much lower than the equivalent protein capacity suggesting that the maximum fluorescence determined was much lower than would have been expected. This observation could be attributed to the presence of composite materials in the adsorbent structure affecting the optical properties of the adsorbent. This adsorption pattern was observed for the other adsorbents included in the study. Similar experiments have been

Figure 4.18 The fractional approach to equilibrium for the adsorption of BSAs to STREAMLINE DEAE comparing both fluorescence analysis and protein analysis

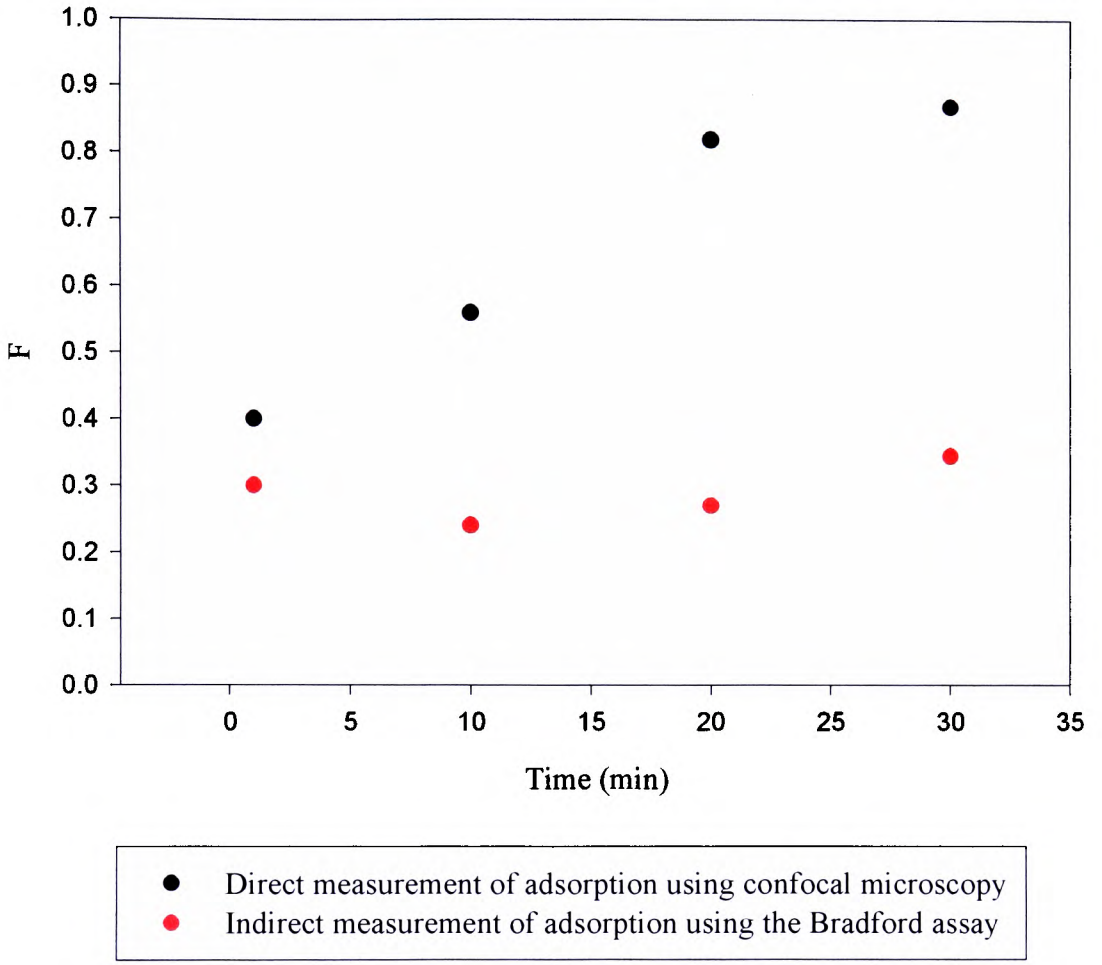

Figure 4.18 represents the comparison of the adsorption profiles for STREAMLINE DEAE calculated from confocal microscopy and protein analysis using the Bradford assay. A sample of adsorbent (0.1ml) was added to 1.5ml of fluorescently labelled BSAs and mixed at room temperature using a rotary mixer. Samples of both the adsorbent and supernatant were taken at regular time intervals and the adsorbent analysed using confocal microscopy (see Equations 4.1 and 4.2) and the supernatant was analysed using the Bradford assay and expressed as a fractional approach to equilbrium over time (F; see Section 4.3.2)..

Figure 4.19 The fractional approach to equilibrium for the adsorption of BSAp to STREAMLINE DEAE comparing both fluorescence analysis and protein analysis

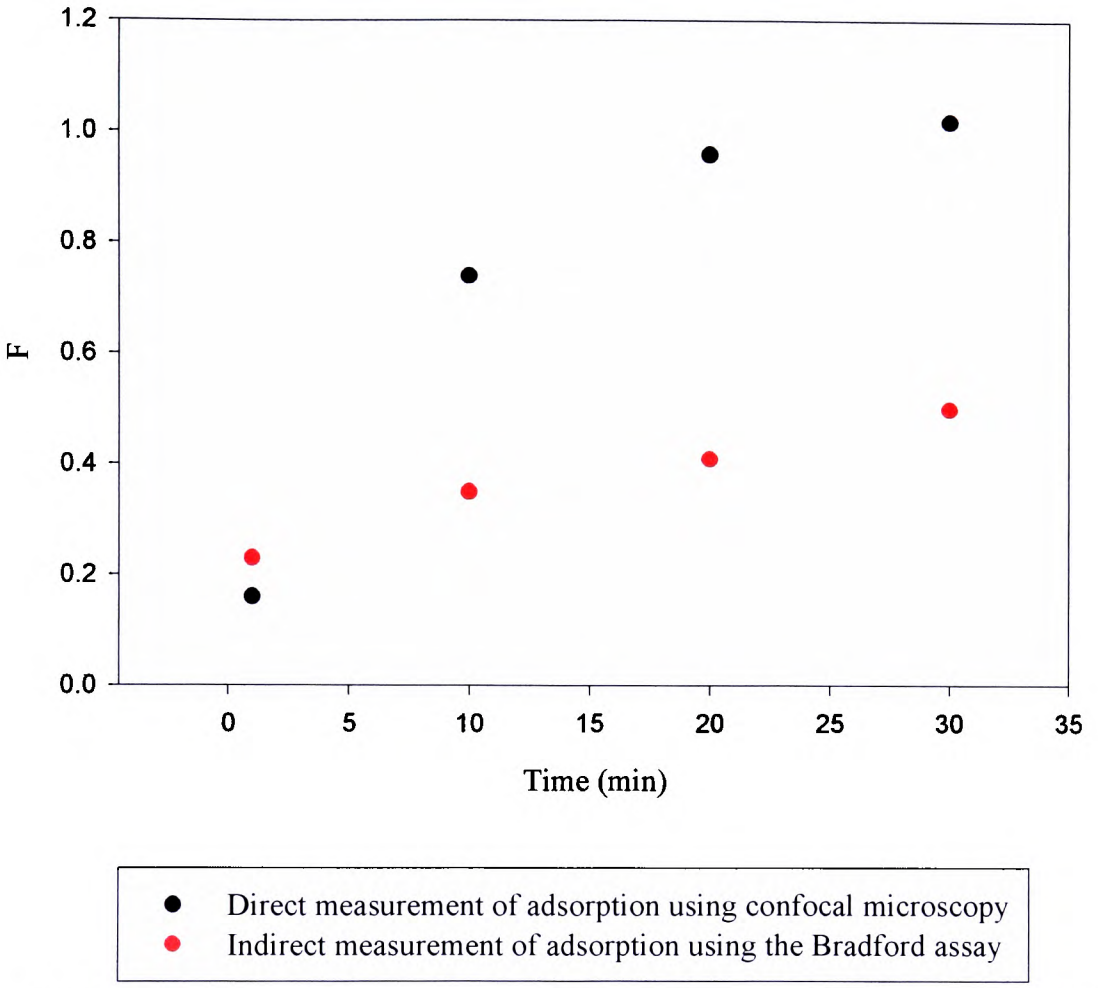

Figure 4.19 represents the comparison of the adsorption profiles for STREAMLINE DEAE calculated from confocal microscopy and protein analysis using the Bradford assay. A sample of adsorbent (0.1ml) was added to 1.5ml of fluorescently labelled BSAs and mixed at room temperature using a rotary mixer. Samples of both the adsorbent and supernatant were taken at regular time intervals and the adsorbent analysed using confocal microscopy (F, see Equations 4.1 and 4.2) and the supernatant was analysed using the Bradford assay and expressed as a fractional approach to equilibrium over time.

reported in the literature (Ljunglöf and Hjorth, 1996; Ljunglöf and Thömmes, 1998; Linden *et al*, 1999) where this method has been successfully employed as a technique for directly measuring protein uptake. It was concluded from this study that the success of the method is dependent upon the adsorbent solid phases in which the fluorescently labelled protein is imaged. In the literature the adsorbent solid phases employed were Sepharose adsorbents that consist solely of agarose (see Section 2.1.2.1). Therefore there are no density enhancing materials that will interfere with the detection of the fluorescence from the probe. Each adsorbent used in the present study contained a high-density filler, either quartz, molybdenum, titanium oxide or zirconium silicate, all of which have different optical properties to the base material of the adsorbent solid phases.

4.3.4 General Conclusions

The technique of LSCM was employed in the present study to directly visualise the protein (both soluble and particulate) within the structure of the adsorbent solid phases, to validate the conclusions made about the adsorbents subsequent to the adsorption/desorption studies (see Sections 3.3.1 and 3.3.4). In addition, the technique was investigated as a method for the direct measurement of the adsorption of BSAs and BSAp. The results suggested that quantitative interpretation of the technique was not reliable for adsorbents that contained materials having poor optical qualities (see Section 4.3.3). However, the technique was seen to be a useful tool to qualitatively visualise the distribution of the protein products within the adsorbent solid phases. As with any technique, there are associated limitations where the adsorption is observed at the single particle level however for the purpose of this study particles were randomly selected from the adsorbent sample. The fluorescence profiles were analysed in triplicate, to ensure that the data generated represented an average adsorption distribution. This technique can also be used to predict the performance of adsorbent solid

phases used for chromatographic separations, and to determine experimental conditions such as the concentration of protein and the contact time required for an adsorbent to reach equilibrium and also assess the efficiency of a chromatographic adsorbent for capture of a specific product.

The study indicated that Celbead (II) DEAE and Celbead Amino adsorbents had a limited surface area available for adsorption and were considered to be unsuitable for the fluidised bed recovery of nanoparticulate products. The adsorptive and desorptive performance of the PVA TiO_2 DEAE adsorbent was generally good, but no better than other Type II adsorbents. The disappointing bed expansion performance (see Figure 2.20), was the criterion exploited to reject PVA TiO_2 DEAE from the study.

The remaining adsorbents, PVA Zr DEAE, PVA Mo DEAE, STREAMLINE DEAE and 2% ZsA, were considered to be the most suitable adsorbents for the fluidised bed recovery of nanoparticulate products from the range of the adsorbent initially selected for study. The initial scouting experiments exploited 'clean' systems containing only soluble or particulate BSA in buffer. Further experiments exploiting complex feedstocks such as cell culture supernatants and yeast homogenates were required to investigate the performance of the adsorbent solid phases in realistic systems from which nanoparticulates could be sourced and recovered.

It is noteworthy that FITC conjugated proteins and protein nanoparticles are expected to behave differently in comparison to native products (refer Forward to Section 5.2.6). FITC binds primarily to the positively charged lysine residues of BSA (see Table 3.1) therefore this interaction would not be likely to interfere with the adsorption of BSAs and BSAp to the anion exchange adsorbents. The negatively charged aspartate and glutamate residues are assumed to be the amino acids involved in the adsorption of the protein to the positively charged anion exchange adsorbents. However, the presence of FITC bound to the protein

may interfere with this interaction and so it is important to be aware that the images produced of protein adsorption using LSCM may not be identical with the adsorption of native proteins to the same adsorbent solid phases.

CHAPTER 5

THE AFFINITY CAPTURE OF NANOPARTICULATE PRODUCTS FROM CELL CONTAINING INSECT CELL CULTURE LYSATE

5.1 General Introduction

Preliminary studies described in Chapters 2 to 4 have critically evaluated adsorbent solid phases characterised by different internal and external geometries for their suitability as adsorbents for the fluidised bed recovery of nanoparticulate products. Table 5.1 summarises the qualities of the adsorbents that demonstrated a promising performance for such an application. The important criteria for an ideal adsorbent are (i) adequate fluidisable characteristics, (ii) effective nanoparticulate recovery and (iii) limited adsorption and efficient desorption of undesired molecular impurities from within the adsorbent structure. Scouting experiments were completed using clean systems containing either pure BSAs or pure BSAp (see Chapter 3) but further adsorption experiments were indicated using a realistic complex feedstock to mimic the recovery of nanoparticle products from systems representative of industrial practices.

The adsorbents used in this study were selected as a consequence of their performance in the anion exchange recovery of soluble and particulate BSA. Ion exchange chromatography (IEC) is one of the most commonly used separation techniques (Bonnerjea *et al*, 1986) based upon the reversible adsorption of charged molecules to oppositely charged immobilised ligands (see Section 2.1.9). However, realistic complex feedstocks such as cell culture fluid and fermentation broths contain cells, cell debris and molecular impurities such as endotoxins , DNA and proteins, whose common indigenous negative charge means that a

Table 5.1 Summary of the selected adsorbent solid phases

ADSORBENT TYPE	ADSORBENT	PORE SIZE	MANUFACTURER
I	STREAMLINE (6% Agarose)	<0.2μm	Amersham Biosciences
II	PVA Mo	1μm	Swedish Construct
	PVA Zr	1μm	Swedish Construct
IV	2% ZsA	<0.4μm	Birmingham Construct

Table 5.1 represents the adsorbent solid phases included in the present study selected from the initial candidate adsorbent solid phases subsequent to physical and biochemical characterisation studies (Chapters 2 and 3). Remaining in the study was the Type I commercial adsorbent STREAMLINE alongside the macroporous Type II adsorbents manufactured by Igor Galaev (Lund University, Sweden) and the Birmingham pellicular construct (Type IV) manufactured by Yan Sun (Tianjin University, PR of China).

good separation of the desired product from the fluid or broth is difficult to achieve solely on charge differences. It was concluded that IEC would not generally be a suitable separation technique for the recovery of nanoparticulate products from such feedstocks and thus affinity capture of nanoparticles was considered as a suitable alternative.

Cibacron Blue 3GA is a monochlorotriazine textile dye (refer to Section 5.1.1) that has a reported affinity for human serum albumin (Leatherbarrow and Dean, 1980). Thus, this was selected as a readily available affinity model specifically employing HSA nanoparticles instead of BSA as previously studied (see Chapter 3).

The objective of the present study has been to investigate the recovery of nanoparticulate proteins that were included in the study as mimics for viruses and plasmid DNA. Much emphasis has also been placed on the requirement to separate such products from complex feedstocks and product components. Therefore to investigate this affinity model insect cell culture lysate was introduced as a test feedstock from which viral products would commonly be recovered such as baculovirus (refer forward to Section 5.1.3).

5.1.1 Cibacron Blue 3GA Pseudo Affinity Dye

In the present study Cibacron Blue 3GA, a monochlorotriazine textile dye (see Figure 5.1), was selected as a candidate affinity ligand recognised to exhibit general affinity interactions with a number of protein and enzyme groups (Table 5.2; Clonis and Lowe, 1980). The affinity of the dye for serum albumins, particularly human serum albumin (HSA) was exploited herein to investigate the performance of the selected adsorbent solid phases with both soluble and particulate forms of that protein (refer to Section 5.1.2). The binding interaction of HSA with Cibacron Blue 3GA has been considered in great depth. Studies by Leatherbarrow and Dean (1980) suggested that there are two types of dye-protein interactions

Figure 5.1 The principle structural elements of Cibacron Blue 3GA

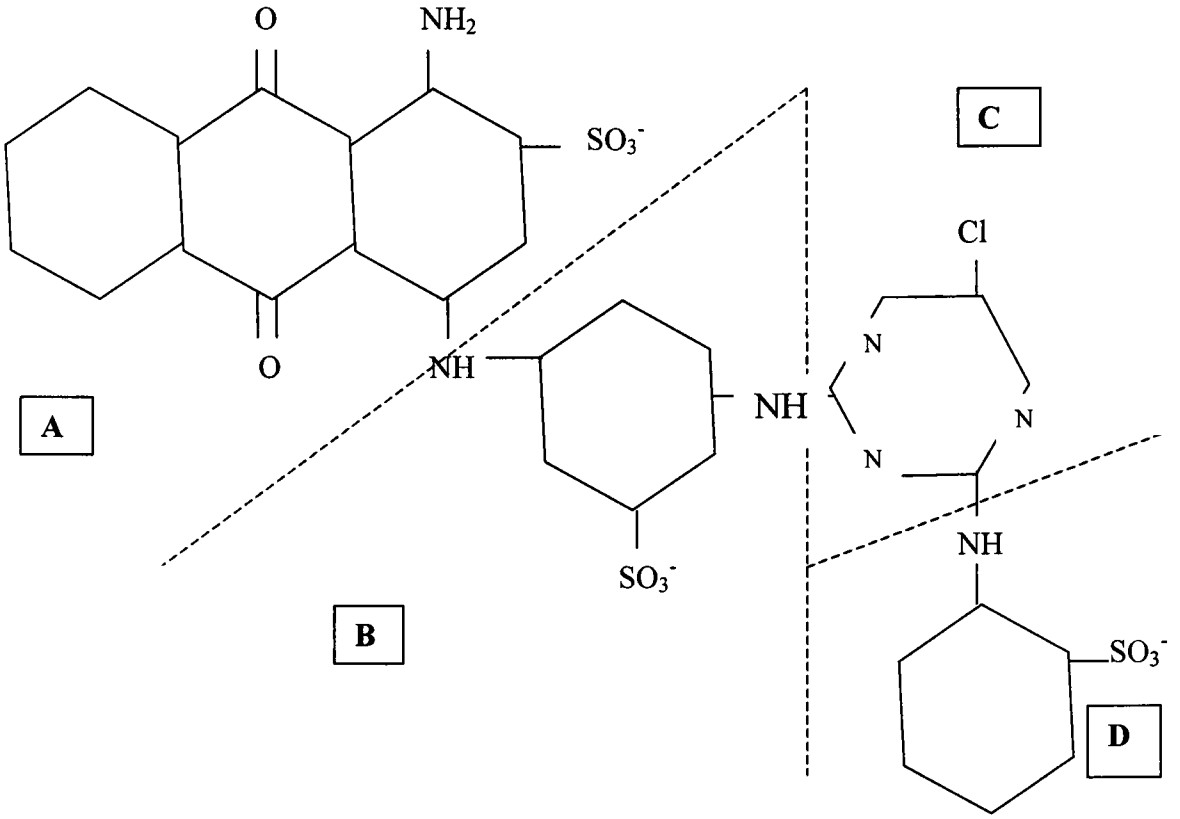

Figure 5.1 represents the structure of the triazine dye, Cibacron Blue 3GA where segment A represents the sulphonated anthraquinone and B represents the bridging diaminobenzene sulphonate. In addition, segment C is the reactive chlorotriazine functional group where nucleophilic substitution occurs with the hydroxide groups of a hydrophilic polysaccharide material. Finally, segment D represents the O-aminobenzene sulphonate ring.

Table 5.2 A selection of proteins and enzymes purified using Cibacron Blue 3GA

PROTEIN	SOURCE	REFERENCE
Alcohol dehydrogenase	Horse liver	Easterday and Easterday (1974)
	Yeast	Adinolfi and Hopkinson (1978)
Pyruvate kinase	Yeast	Kopperschlager *et al* (1968)
Albumin	Chicken egg	Dean and Watson (1979)
	Human serum	Young and Webb (1978)
	Bovine serum	Ticha *et al* (1978)
Interferon	Mammalian	Bollin *et al* (1978)
	Mouse	Boyer and Hsu (1993)

Table 5.2 represents a summary of proteins and enzymes that have been successfully purified using the triazine dye, Cibacron Blue 3GA. The dye is a pseudo affinity ligand that mimics the structure of enzyme substrates and can interact with the binding sites of structurally similar biomolecules.

that are related to the physiological function of HSA. The first interaction is via the hydrophobic fatty acid binding sites present on all albumins whilst the second is a more specific interaction with the commonly available billirubin binding site (see Section 3.2.3). Pannell *et al* (1974) and Beissner and Rudolph (1978) demonstrated further evidence of the specific binding mechanism of HSA. They discovered that the anthraquinone group of the Cibacron Blue 3GA dye is fundamental for the binding of HSA (refer to Figure 5.1). In addition, Leatherbarrow and Dean (1980) noted that Cibacron Blue 3GA and billirubin are structurally similar, since both molecules consist of planar aromatic ring systems and the position of the negatively charged groups can be superimposed. As a consequence of this specificity of HSA for Cibacron Blue 3GA this absolute-ligand interaction system was selected for the work presented herein.

5.1.2 Human Serum Albumin

Human serum albumin (HSA) is structurally similar to bovine serum albumin (see Section 3.1.3). The amino acid sequence is different (see Table 3.1), but both proteins contain the same number of lysine residues indicating that the behaviour of the proteins when conjugated to FITC or Rhodamine B isothiocyanate should be similar. HSA was selected for this study as a consequence of the affinity of the Cibacron Blue 3GA ligand for serum albumin and particularly human serum albumin.

5.1.3 IPL 41 Insect Cell Culture Medium

Subsequent to the selection of the affinity ligand and the protein of interest for this study, a feedstock system representative of insect cell culture was chosen. Like mammalian cell media, insect cell culture medium consists of numerous amino acids and sugars such as mono and disaccharides (see Appendix III) in addition to vitamins and sterols that cannot be

synthesised by insect cells. The representative feedstock, IPL-41 insect cell medium supplied by R. Jarman-Smith, (Animal Cell Technology Group, University of Birmingham), is a serum free medium supplemented with pluronic F-68, yeastolate and lipids (refer to the Appendix III). This resulted in fewer protein impurities within the system in comparison to serum containing media making it more suitable for Cibacron Blue affinity chromatography. This medium is used for the culture of a *Lepidopteran* cell line *sf-9* derived from the primary cell line *sf-21* isolated from *Spodoptera frugiperda* pupal ovaries (Vaughn *et al*, 1977).

Trschirley (1975) recognised that baculovirus infected Lepidoptera, and could be manipulated to infect insect cell cultures. Consequently, recombinant baculovirus infected cells are now commonly used for the high level expression of foreign genes for use in the biopharmaceutical industry (Kioukai *et al*, 1995). Consequently, the IPL-41 cell culture medium was thus selected as a representative complex feedstock for the recovery of nanoparticulate products

5.1.4 Rhodamine B Isothiocyanate

Laser scanning confocal microscopy (LSCM) was employed in this study to investigate the adsorption of fluorescently labelled HSAp. As a consequence of the spectrophotometric absorbance of Cibacron Blue 3GA dye, FITC (see Section 4.1.2.1) could not be employed because of interference. Thus, a probe that exploited the laser wavelength of 534nm was adopted in the form of Rhodamine B isothiocyanate, a commonly used fluorescent probe for protein and antibody conjugation. Rhodamine B isothiocyanate is characterised by a molecular weight of 536.1 and exhibits a characteristic wavelength of maximum absorption and emission of 510nm and 595nm respectively.

5.2 Materials and Methods

5.2.1 Chemicals

Cibacron Blue 3GA, Human Serum Albumin (Fraction V powder, 96% purity) and Rhodamine B Isothiocyanate were supplied by Sigma-Aldrich (Poole, Dorset, UK). All other chemicals and reagents were supplied at reagent grade unless otherwise stated by Sigma-Aldrich (Poole, Dorset, UK) or BDH (Poole, Dorset, UK).

5.2.2 Equipment

- Malvern Zetasizer 1000HS/IHPL, Malvern Instruments Ltd, Malvern, UK.
- Rotary blood mixer, Stuart Scientific Company Ltd, UK.
- Pharmacia LKB Ultrospec III spectrophotometer, Amersham Biosciences, Uppsala, Sweden.
- pH meter, Hanna Instruments, H19321, Microprocessor Bench pH meter.
- Millipore ultrafiltration unit, Millipore, Bedford, MA, USA.
- Pharmacia 1cm (id) chromatography column, Amersham Biosciences, Uppsala, Sweden.
- Peristaltic pump, model 101U (maximum output 15W). Watson-Marlow Company Ltd, Cornwall, UK.
- Water bath, Stuart Scientific Company Ltd, UK.
- Rotary mixing unit, Stuart Scientific Company Ltd, UK.
- Luminescence spectrometer LS50B, PERKIN-ELMER, High Wycombe, UK.
- Leiss 510 Laser Scanning Confocal Microscope, Zeiss Ltd, Stockport, UK.
- General laboratory glassware

5.2.3 Methods

The majority of methods employed in this chapter have been described in detail in the preceding Chapters 2, 3 and 4, and are crossreferenced accordingly. New methods are depicted below.

5.2.3.1 Preparation of Immobilised Cibacron Blue 3GA

Selected adsorbent solid phases were derivatised to impart pseudo-affinity functionality to the candidate ideal adsorbents. Cibacron Blue 3GA, a triazine dye, was immobilised onto the adsorbents using an adapted method first published by Dean and Watson (1979). Vacuum filtered adsorbent (25g) was suspended in 50ml of deionised water and 0.75g of Cibacron Blue 3GA was added and the mixture agitated for 15 minutes. Subsequent to the addition of the dye, 7.5g of NaCl was added and the mixture agitated for a further 30 minutes followed by the addition of 30ml of 1M $NaCO_3$. The mixture was transferred to a round-bottomed flask, attached to a rotary mixing unit and the flask was incubated in a water bath at 65°C for 24 hours under gentle agitation and semi-submersion. After incubation the solid phase was removed from the liquid phase and washed with alternate washes of hot and cold water to remove the unreacted dye. The remaining weakly bound dye was removed by specific displacement in a protein wash followed by a chaotropic elution step in a fixed bed contactor (Gibson, 1992). The adsorbent was suspended in Buffer A (10mM Tris-HCl, pH 7.5 with 0.01% Tween 20 and 0.02% sodium azide) and packed into a chromatography column. The column was loaded with 100ml of 1mg/ml bovine serum albumin at a flow rate of 1ml/min, and eluted with 100ml of 3M KSCN (in Buffer A) at 1ml/min. A final wash of Buffer A concluded the procedure and the adsorbents were stored at 4°C.

5.2.3.2 Estimation of the Immobilised Dye Concentration

The dye content of the adsorbent solid phases was estimated following a method proposed by Chambers (1977). The adsorbent particles were hydrolysed in the presence of a strong acid resulting in the release of the immobilised dye. The dye concentration was quantified spectrophotometrically against a previously prepared standard curve (see Appendix IV). Vacuum filtered adsorbent (0.5ml) was dispersed in 25ml of 6M HCl and agitated in a temperature controlled water bath at 95°C for 30 minutes. After hydrolysis the remaining solids were removed by centrifugation and 1ml of the supernatant was diluted to 200ml with deionised water. The absorbance of the supernatant at 595nm was recorded against a blank generated from a non-immobilised adsorbent sample treated in an equivalent manner. The dye concentration was estimated from the standard curve (see Appendix IV).

5.2.3.3 Total Protein Determination – Fluorescence Spectroscopy

The total protein concentration in adsorption/desorption experiments was determined using either the Bradford assay (see Section 3.2.6 and Appendix V) or a fluorescence assay exploiting the excitation and emission of fluorescein isothiocyanate (FITC) described in Section 4.2.3. The fluorescence from the probe was detected and the protein concentration determined using a luminescence spectrometer (LS50B, PERKIN-ELMER, UK). Fluorescence is a short-lived emission that usually occurs within 10^{-9} and 10^{-7} seconds of the samples being excited, and when the luminescence spectrometer is operating in the fluorescence mode two gating periods occur. In the first gating period (the point at which the device measures the fluorescence) the instrument integrates the excitation and emission signals. The second gating period occurs shortly before the next flash of fluorescence emission and integrates the signal detected by the device when no light is falling

on the detector. The second value obtained by the device is then subtracted as a blank from the first so that the corrected fluorescence is free from other signals detected by the device.

FITC was conjugated to HSAp primarily via the lysine residues on the protein surface using the method described in Section 4.2.3 to achieve a maximum load per mole of protein and enable nanoparticle detection at low concentrations (refer to Section 5.2.6.1; refer to Figure 5.2). It was expected that HSAp conjugated to FITC would behave differently to native HSAp. Lysine 220 is one of the amino acids present within the billirubin binding site. It is reported that the affinity interaction between Cibacron Blue 3GA, the affinity ligand employed in this study, and human serum albumin occurs at the billirubin binding site (Leatherbarrow and Dean, 1980). This is due to the structural similarities of billirubin and Cibacron Blue 3GA (Leatherbarrow and Dean, 1980). Consequently, a reduction in adsorption capacity of FITC conjugated HSAp in comparison to native HSAp was expected. It is also noteworthy that the pI of the protein may also change as the charge of the protein will alter as the lysine residues become utilised. To construct the fluorescence calibration curve (refer to Appendix VI) used in this study the protein concentration of the FITC conjugated nanoparticles was estimated using the Bradford assay (see Section 3.2.6). The HSAp samples were diluted by an appropriate amount and the fluorescence determined by excitation and emission of FITC at 488nm and 525nm respectively. The protein concentration was determined from the fluorescence calibration curve (refer to Appendix VI) and all the samples were analysed in duplicate.

Figure 5.2 Graph representing the fluorescence of FITC labelled HSAp at increasing concentrations of conjugated FITC

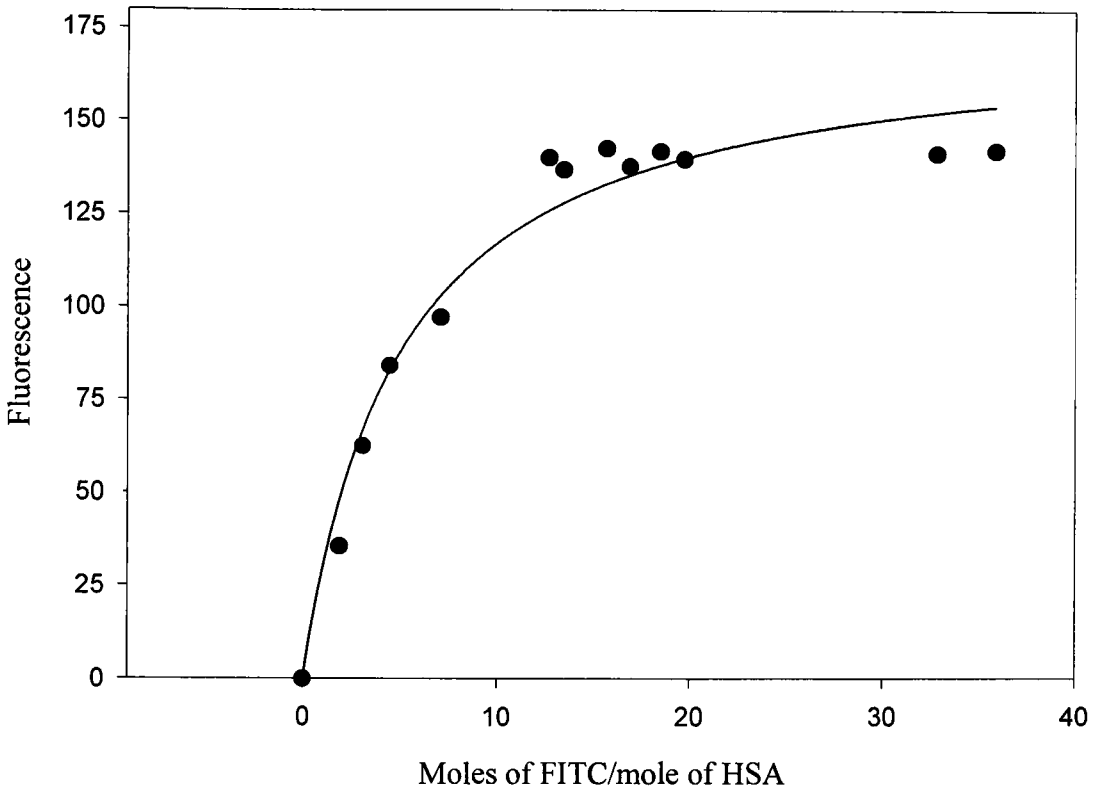

Figure 5.2 represents the fluorescence of FITC labelled HSAp with increasing concentrations of conjugated FITC. The molarity was determined following a method described in Section 3.2.6.1. FITC was loaded onto the HSAp at increasing concentrations and the fluorescence determined using a fluorimeter (PERKIN-ELMER, luminescence spectrometer). The measurement represents the fluorescence of the FITC (at a particular molar concentration) on 1 µg/ml of HSAp measured using the Bradford assay (see Section 3.2.6; refer to Appendix V).

5.2.3.4 Determination of the Maximum Fluorescein Isothiocyanate Concentration Loaded onto HSA Nanoparticles

FITC was conjugated to HSAp using the method described in Section 4.2.3, but varying the initial concentration of the FITC stock solution added to the HSAp during the conjugation step. FITC primarily conjugates to the lysine residues of protein molecules (see Table 3.1), and since HSA contains 59 lysine residues in total, this accounts for approximately 10% of the total protein molecule (see Table 3.1). Therefore it is assumed that once all the available lysine residues are exploited no further conjugation associated fluorescence will be detected.

The molar ratios of conjugated fluorescent probe to protein were determined using a method described by Kawamura (1977) exploiting the optical density of the FITC conjugated protein at 280nm and at 495nm using the following equation.

$$(3.14 \times OD_{495}) / OD_{280} - (0.30 \times OD_{495}) \qquad \text{Equation 5.1}$$

It is noteworthy that this method is only an approximation of the relative molar ratios as the optical density of HSAs at 280nm is different to the same concentration of HSAp. Amino acid analysis of HSAp (see Appendix VII) completed by Dr J. Fox, Alta Biosciences, University of Birmingham, indicated that at 220μg/ml measured at 280nm, the equivalent protein concentration estimated from amino acid analysis was 198μg/ml (see Appendix VII). Consequently the absorbance of HSAp at 280nm overestimates the protein concentration by approximately 10%.

For the purpose of HSAp detection and adsorption interference (refer forward to Table 5.5) the maximum fluorescence per mole of FITC was determined using Equation 5.1 to estimate the number of moles of FITC added at the conjugation step (see Section 4.2.3).

Figure 5.2 represents the determination of the maximum conjugated FITC loaded per mole of HSAp, where the amount of fluorescence detected reached a plateau. It is possible that further conjugation had occurred, but was not detected. In addition, at this plateau all the available lysine residues may have been exploited resulting in no further detectable FITC conjugation.

5.2.3.5 Preparation of the Insect Cell Culture Lysate

IPL-41 insect cell culture fluid, supplied by R. Jarman-Smith (Animal Cell Technology Group, University of Birmingham), was taken during the exponential growth phase of *sf-9* insect cells. Cells were seeded at a cell density of 0.2-0.4 x 10^6 cells/ml into a Techne flask containing IPL-41 medium supplemented with Pluronic 68, yeastolates and lipids. The cells were incubated at 27°C with agitation at 60rpm at pH 6.0-6.4. Once the cells had achieved a density of approximately 2 x 10^6 cells/ml the culture fluid was used as the representative complex feedstock in the study. The total protein concentration was estimated to be 1mg/ml using the Bradford assay attributed to the presence of growth factors and enzymes produced from the cells during the growth phase (see Section 3.2.6). Freeze-thawing the cell culture fluid three times lysed the cells within the medium to create a representative experimental feedstock for which the pH and conductivity was subsequently determined.

5.2.3.6 The Adsorptive Capture and Recovery of HAS Nanoparticles for the Selected Adsorbent Solid Phases

Preliminary batch binding studies employing BSAs and BSAp as representative contaminants, product components and nanoparticulate products respectively, were completed and described in Chapter 3. However these experiments exploited anion exchange

chromatography that has been considered to be unsuitable for the recovery of nanoparticulate products from complex feedstocks such as the insect cell lysate selected and included in the study (see Section 5.1). As a consequence, a pseudo-affinity dye ligand, Cibacron Blue 3GA was introduced into the study (see Section 5.1.1) and HSAp were fabricated as the test particulate adsorbate (see Section 5.1.2; Section 3.2.3).

Four different batch binding experiments were completed exploiting Cibacron Blue 3GA and HSAp. The initial experiment was a benchmark study performed as a comparison to the adsorption/desorption studies for BSAp to adsorbents derivatised with anion exchange chemistry (see Section 3.3.4). The studies in the previous chapters have been concerned with the performance of the solid phases for the efficient recovery of nanoparticulate products from clean systems. However, it is important to investigate the performance of the selected adsorbent solid phases in industrially realistic conditions and hence, experiments were completed exploiting particle numbers representing an average particle number from typical retrovirus or adenovirus titre (Hughes, 2001). Experiments were also completed with different nanoparticle concentrations in the presence or absence of cell culture lysate.

After the adsorbent was equilibrated in Buffer C the HSAp solution was added to 0.1ml of adsorbent and the system mixed rigorously for 2 hours at room temperature using a rotary mixer. Samples were taken at regular time intervals and the protein concentration was determined either by Bradford or fluorescence assays (see Section 3.2.6; 5.2.6). After the adsorption was completed at 120 minutes the adsorbents were washed in Buffer C (111mM sodium phosphate buffer, pH 6.4) to remove any unbound protein or cell debris from the system. The HSAp and intracellular proteins from the cell lysate were desorbed by suspending 0.1ml of protein loaded adsorbent in 1.5ml of 3M KSCN (in Buffer C). The system was mixed for 2 hours at room temperature using a rotary mixer and samples taken at

regular time intervals and assayed to determine the protein concentration using the Bradford and fluorescence assays.

It is well documented that Cibacron Blue 3GA has a tendency to leach from the adsorbent solid phases into the supernatant during the adsorption and desorption procedures (Stewart *et al*, 1990). Therefore when each binding experiment was completed blank samples containing equivalent volumes of adsorbent and buffer, (both Buffer C and 3M KSCN) were included to monitor dye leakage from the adsorbent solid phases.

5.3 Results and Discussion

5.3.1 Photon Correlation Spectroscopy Sizing of Human Serum Albumin Nanoparticles

Figure 5.3 represents the photon correlation spectroscopy sizing of human serum albumin nanoparticles showing an average particle size of 66nm with 89% of the particles within the size range of 50-80nm in diameter.

5.3.2 Determination of the Immobilised Dye Concentration

The concentration of Cibacron Blue 3GA dye immobilised to the adsorbent solid phases was determined using acid hydrolysis to cleave the dye from the adsorbent and a dye calibration curve (refer to Appendix IV). Table 5.3 represents the dye concentrations determined for each of the adsorbent solid phases, with STREAMLINE Blue exhibiting the highest dye content in contrast to much lower figures for PVA Mo Blue, PVA Zr Blue and 2% ZsA Blue. This was attributed to the increased internal surface area available for reaction for the STREAMLINE adsorbent particles in comparison to the other adsorbent solid phases included in the study. The Type II and Type IV adsorbent solid phases had limited internal surface area available for both ligand derivatisation and subsequent albumin adsorption due to the macroporous and pellicular structures respectively. Type II adsorbents were

characterised as assumed as having pore sizes greater than 0.6μm (refer to Figure 2.1). Therefore it can be concluded that the pore volume to adsorbent volume is greater for Type II adsorbents than for the Type I microporous adsorbent (see Figure 2.1). In addition, Type IV pellicular adsorbents are characterised by a solid core surrounded by a thin pellicle of porous material. It was demonstrated that the solid core comprised approximately 50% of the Type IV adsorbent used in this study (2% ZsA; see Section 4.3.1; Figure 4.14). Consequently it can be concluded that the surface are available for adsorption is much less than for STREAMLINE (Type I; see Figure 2.1). It could also be surmised that the PVA composite adsorbents contained less reactive hydroxyls that agarose resulting in lower concentrations of dye immobilised.

5.3.3 Preliminary Studies for the Affinity Capture and Recovery of HSA Nanoparticles

Preliminary studies for the affinity capture and recovery of 66nm HSA nanoparticles (see Section 5.3.1; Figure 5.3) exploiting the pseudo-affinity dye Cibacron Blue 3GA were completed. Figure 5.4 represents the adsorption profiles of the four selected adsorbent solid phases remaining in the study (STREAMLINE Blue, Type I; PVA Mo Blue and PVA Zr Blue, Type II; 2% ZsA Blue, Type IV). All of the adsorbents were characterised by an apparent slow adsorption rate suggesting nanoparticle penetration as was expected from the results presented in Chapter 4. Laser scanning confocal microscopy images (LSCM; see Figures 4.4, 4.9, and 4.12-4.14) suggested that 150nm BSAp (see Section 3.3.3) penetrated into the structure of each of these adsorbents and so it was therefore expected that 66nm HSAp would also penetrate into the adsorbent structures.

2% ZsA Blue was highlighted as having a superior adsorption capacity in comparison to the other adsorbents included in the study (see Table 5.4). This performance was

Figure 5.3 Size distribution of HSA nanoparticles

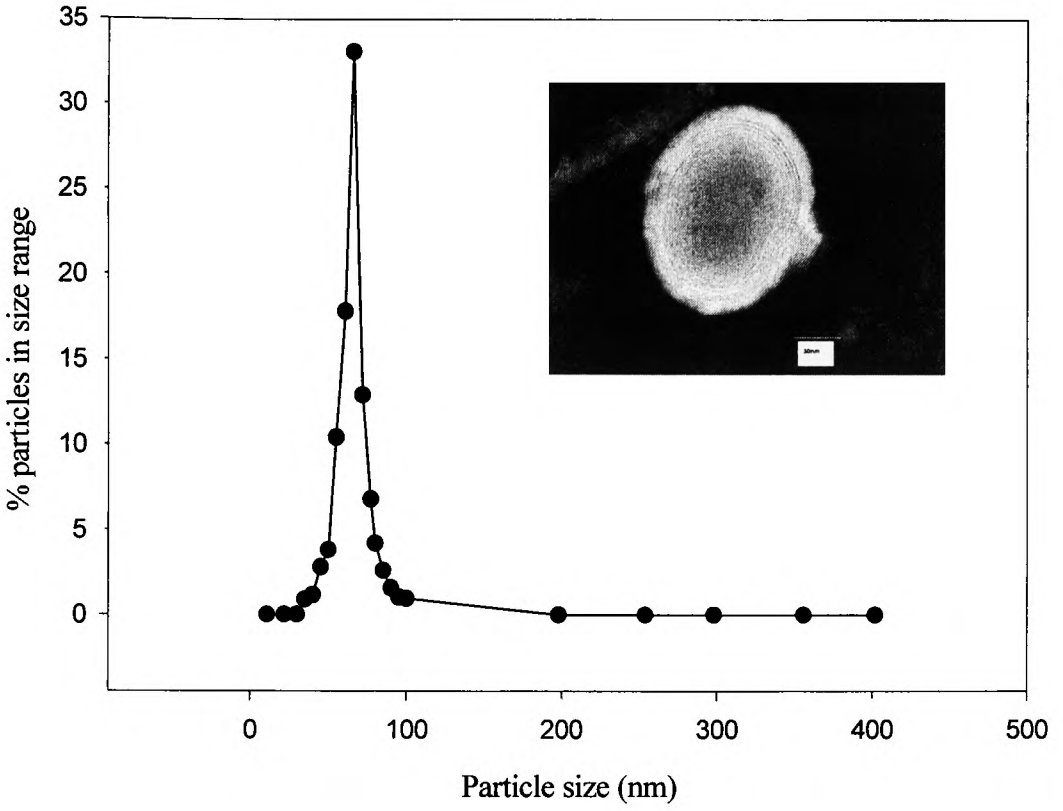

Figure 5.3 represents the size distribution of the fabricated HSA nanoparticles measured by photon correlation spectroscopy. The average particle size was determined as 66nm based on the Einstein-Diffusion Equation (see Section 3.1.2). In addition the nanoparticles were shown to be approximately spherical in nature by electron microscopy, and the size of the nanoparticle was also confirmed by this analysis.

Electron microscopy image (inset) represents a single HSA nanoparticle.

Table 5.3 Concentration of the Cibacron Blue 3GA dye immobilised to the adsorbent solid phases

ADSORBENT TYPE	ADSORBENT	DYE CONCENTRATION (μmol/ml settled adsorbent)
I	STREAMLINE Blue	3.9
II	PVA Mo Blue	0.068
	PVA Zr Blue	0.079
IV	2% ZsA Blue	0.01

Figure 5.3 represents the immobilised dye concentration of the adsorbent solid phases determined after acid hydrolysis to remove the dye from the adsorbent base (see Section 5.2.4; 5.2.5). The dye concentration was determined spectrophotometrically and calculated from the calibration curve (refer to Appendix IV) and converted into moles of dye immobilised per ml of settled adsorbent. The small ion capacities determined for the anion exchange derivatives of these base adsorbents are illustrated in Table 3.4.

Figure 5.4 Adsorption of HSA nanoparticles to the selected adsorbent solid phases

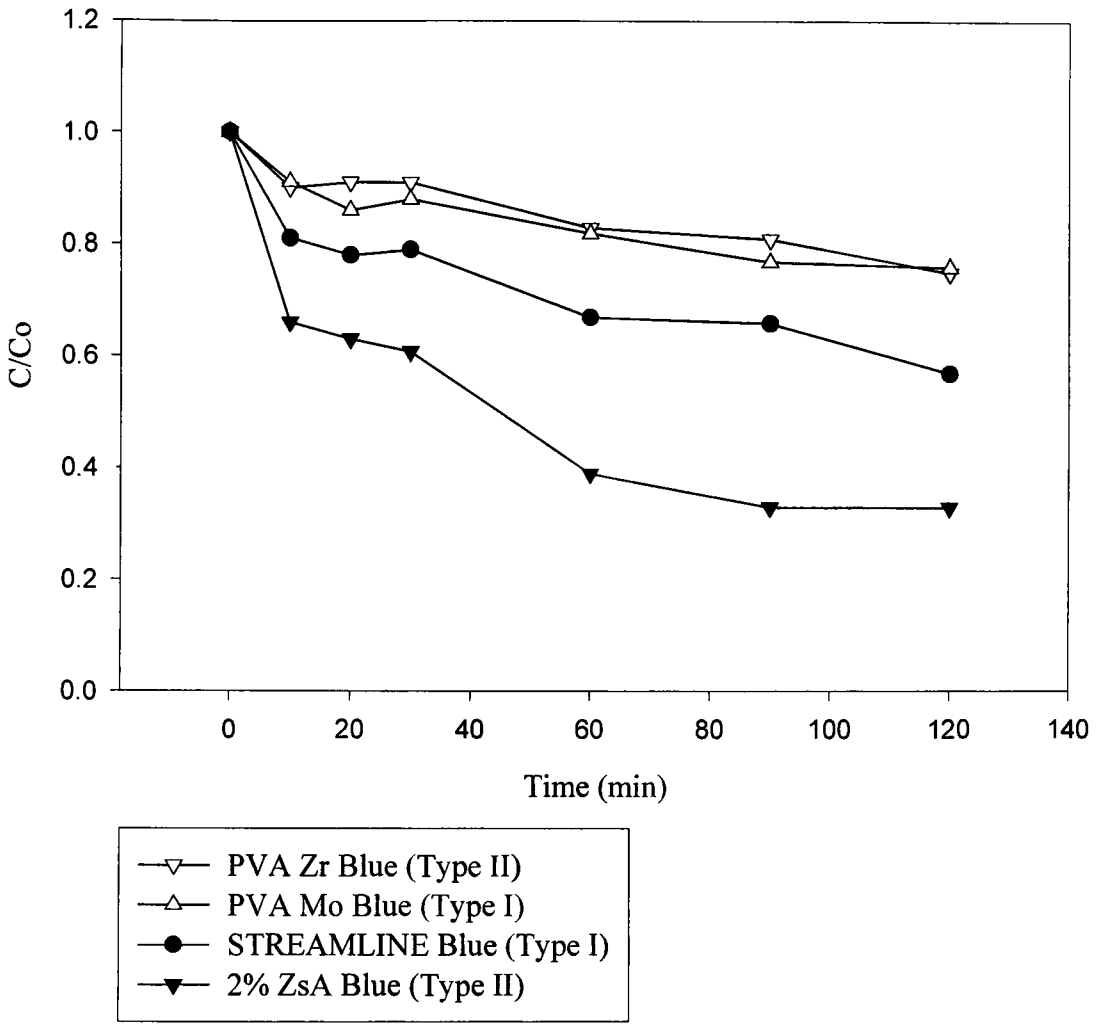

Figure 5.4 represents the binding of HSAp to adsorbents derivatised with Cibacron Blue 3GA dye. The adsorbents were washed before use in Buffer C then 0.1ml of adsorbent was added to 1.5ml of HSAp at a concentration of 220µg/ml suspended in Buffer C. The system was mixed at room temperature for 2 hours using a rotary mixer and samples were taken at regular time intervals and analysed in duplicate using the Bradford assay (see Section 3.2.6).

(Buffer C = 111mM sodium phosphate buffer, pH 6.4 with 0.02% sodium azide and 0.01% Tween 20).

Table 5.4 Summary of the adsorptive capacities and recoveries of HSAp for the selected adsorbent solid phases derivatised with Cibacron Blue 3GA

ADSORBENT TYPE	ADSORBENT	DYE CONCENTRATION (µmol/ml settled adsorbent)	HSAp CAPACITY (mg/ml adsorbent)	HSAp CAPACITY (particles/ml adsorbent)	% RECOVERY
I	STREAMLINE Blue (6%)	3.9	1.42	1.26×10^{13}	99.3
II	PVA Mo Blue	0.068	0.79	0.7×10^{13}	93.1
	PVA Zr Blue	0.079	0.83	0.73×10^{13}	70.8
IV	2% ZsA Blue	0.01	2.21	1.96×10^{13}	76.6

Table 5.4 represents a summary of the adsorption capacities and recoveries of HSAp for Cibacron Blue 3GA immobilised adsorbent solid phases. The adsorption capacities were calculated using difference analysis between the initial load and the end point of the experiment at 120 minutes. Adsorbent (0.1ml) was added to 1.5ml solution of HSAp at a concentration of 220µg/ml and the system mixed at room temperature for 120 minutes using a rotary mixing unit. After 120 minutes the adsorbents were washed in Buffer C to remove any unbound or loosely bound protein (5 x 1ml). The HSAp were eluted using 1.5ml of 3M KSCN added to 0.1ml of HSAp loaded adsorbent and mixed for 120 minutes at room temperature using a rotary mixer. The protein concentrations were determined using the Bradford assay and the recovery was expressed as a percentage of the total protein bound. The particle numbers were determined following the method described in Table 3.4 exploiting a particle diameter of 66nm.

(Buffer C = 111mM sodium phosphate buffer, pH 6.4 with 0.02% sodium azide and 0.01% Tween 20).

contradictory to what was expected based upon the dye content of the adsorbents (see Table 5.3) since 2% ZsA Blue exhibited the lowest dye concentration (0.01μmol dye/ml settled adsorbent). This data in addition to the LSCM images suggested that the ligand concentration could influence the adsorption of HSAp to the selected adsorbent solid phases. Figure 5.5 represents the LSCM profile of HSAp bound to 2% ZsA Blue at equilibrium (after 24 hours). The image demonstrates that 60% of the adsorbent radius (35μm) was exploited for adsorption with HSAp penetrating into the entire agarose layer available within the adsorbent structure. However, Figure 4.14 represents the LSCM image of BSAp bound to 2% ZsA DEAE at equilibrium (after 24 hours contact time). This image indicated that BSAp penetrated only into the initial 10.5μm of the adsorbent radius. This could be attributed to the different sizes of the nanoparticles as HSAp are significantly smaller than BSAp at 66nm in comparison to 150nm. However, the LSCM images of STREAMLINE and PVA Mo were similar for both the affinity (see Figures 5.6; 5.7) and anion exchange (see Figures 4.8; 4.12) form of the adsorbents suggesting that the size of nanoparticles does not influence the adsorption of HSAp into a 6% agarose material. It could therefore be surmised that the 2% agarose structure would enable easier penetration than a 6% agarose structure. Hence the results suggest that the high DEAE concentration of the anion exchange adsorbent (see Table 2.4) resulted in the pores becoming blocked near the surface preventing further penetration. With the 2% ZsA Blue adsorbent, the dye concentration is low that could enable the HSAp to travel further into the adsorbent structure unhindered.

A critical parameter to be considered is the recovery of nanoparticulate products once they have adsorbed to the adsorbent particles. HSAp bound under standardised conditions were recovered from the adsorbent solid phases using 3M KSCN in Buffer C, a chaotropic solution that is often used to strip residual material from an adsorbent as a prelude to the re-equilibration and re-use of the adsorbent solid phase (Bierau, 2001). Consequently, all of the

Figure 5.5 Laser scanning confocal microscopy image representing the adsorption of fluorescently labelled HSAp to 2% ZsA Blue

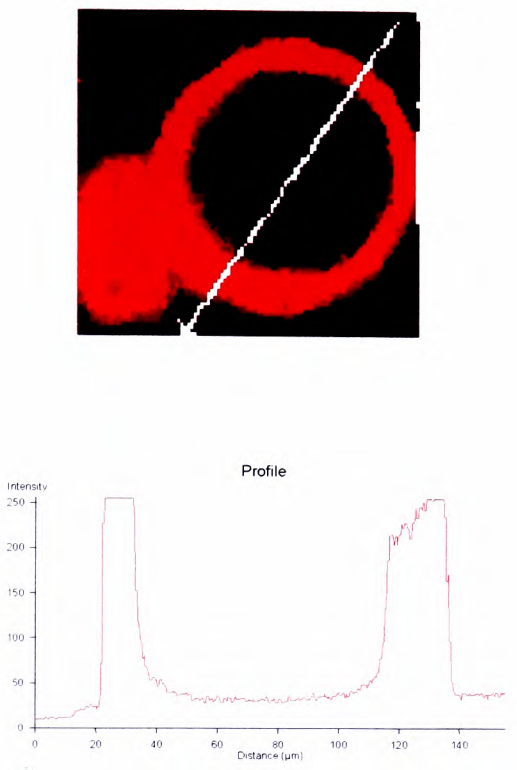

Figure 5.5 represents the laser scanning confocal microscopy image of fluorescently labelled HSAp after adsorption to 2% ZsA Blue. This image was the central optical slice produced using Rhodamine B isothiocyanate as the fluorescent label. This probe was conjugated to HSAp following the method described in Section 4.2.3 to enable the adsorption of HSAp to be imaged in the presence of the Cibacron Blue 3GA dye affinity ligand. HSAp (1.5ml) at a concentration of 220µg/ml were added to 0.1ml of adsorbent and mixed for 24 hours at room temperature. After the adsorption was stopped, the remaining Rhodamine-conjugated HSAp were removed from the system using washes of Buffer C (5 x 1ml washes). The adsorbent particles were imaged immediately using the laser scanning confocal microscopy. The profile represents the fluorescence detected along the length of the arrow on the image. (Buffer C = 111mM sodium phosphate buffer, pH 6.4 with 0.02% sodium azide and 0.01% Tween 20).

Figure 5.6 Laser scanning confocal microscopy image representing the adsorption of fluorescently labelled HSAp to STREAMLINE Blue

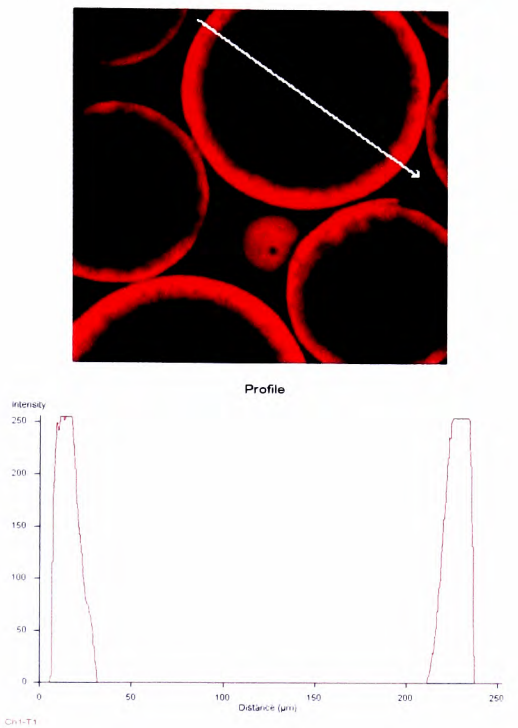

Figure 5.6 represents the laser scanning confocal microscopy image of Rhodamine B isothiocyanate labelled HSAp after adsorption to STREAMLINE Blue. HSAp (1.5ml) at a concentration of 220µg/ml were added to 0.1ml of equilibrated adsorbent and the samples mixed for 24 hours at room temperature, after which the excess unbound or loosely bound HSAp were removed using washes of Buffer C (5 x 1ml). The adsorbent particles were then imaged immediately using the laser scanning confocal microscope with the central optical slice shown. The profile is represented as the fluorescence detected along the length of the arrow depicted in the image. (Buffer C = 111mM sodium phosphate buffer, pH 6.4 with 0.02% sodium azide and 0.01% Tween 20).

Figure 5.7 Laser scanning confocal microscopy images representing the adsorption of fluorescently labelled HSAp to PVA Mo Blue and PVA Zr Blue

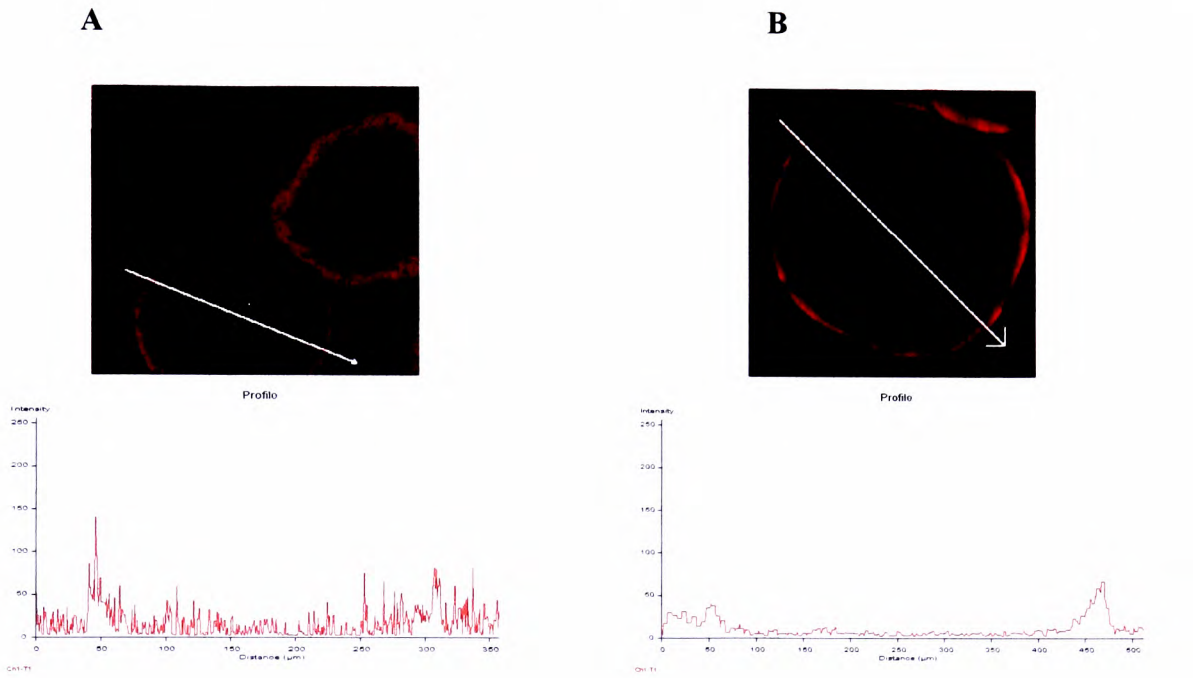

Figure 5.7 represents the laser scanning confocal microscopy images of Rhodamine B isothiocyanate labelled HSAp after adsorption to A) PVA Mo Blue and B) PVA Zr Blue. HSAp (1.5ml) at a concentration of 220µg/ml were added to 0.1ml of equilibrated adsorbent and the samples mixed for 24 hours at room temperature, after which the excess unbound or loosely bound HSAp were removed using washes of Buffer C (5 x 1ml). The adsorbent particles were then imaged immediately using the laser scanning confocal microscope with the central optical slice shown. (Buffer C = 111mM sodium phosphate buffer, pH 6.4 with 0.02% sodium azide and 0.01% Tween 20).

adsorbents included in the present study demonstrated an efficient recovery of HSAp (refer to Figure 5.8) where STREAMLINE Blue (Type I; Figure 2.1), PVA Mo Blue (Type II) and PVA Zr Blue (Type II) exhibited recoveries of greater than 90% (refer to Table 5.4). The poorest recovery of HSAp was demonstrated by 2% ZsA Blue (Type IV; see Figure 2.1) at 76.6% (see Table 5.4). This was attributed to the apparent depth of penetration of the nanoparticles to approximately 35μm as demonstrated by the laser scanning confocal microscopy image (see Figure 5.5). It was assumed that the depth of penetration resulted in a degree of nanoparticle entrapment within the adsorbent structure. In addition to the adsorption/desorption studies the leakage of Cibacron Blue 3GA dye from the adsorbent solid phases was also investigated. It was determined that if the adsorbents were extensively washed prior to use (i.e. 10 x adsorbent volume washes in the appropriate buffer) no dye leakage was detectable during the adsorption, washing or elution procedures.

5.3.4 The Affinity Capture and Recovery of Human Serum Albumin Nanoparticles Employing Industrially Realistic Particle Numbers

The aim of this chapter was to investigate the capture and recovery of nanoparticulate products from an industrially realistic system and hence it was important to investigate the recovery of nanoparticulate products from feedstocks characterised by suitable product concentrations. Therefore the adsorption of HSAp at a concentration of 1 x 10^8 particles/ml was investigated as a representative harvested virus feedstock (Hughes, 2001). The equivalent protein concentration of 84ng/ml was determined from the HSAp stock (220μg/ml) by Bradford assay prior to the required dilution of the supernatant. The Bradford assay cannot be used to detect protein concentrations of less than 1μg/ml (see Section 3.2.6) and hence a fluorescence assay exploiting FITC conjugated HSAp was employed to determine the nanoparticle concentration (see Section 5.2.6).

Figure 5.8 The recovery of HSA nanoparticles from the selected adsorbent solid phases

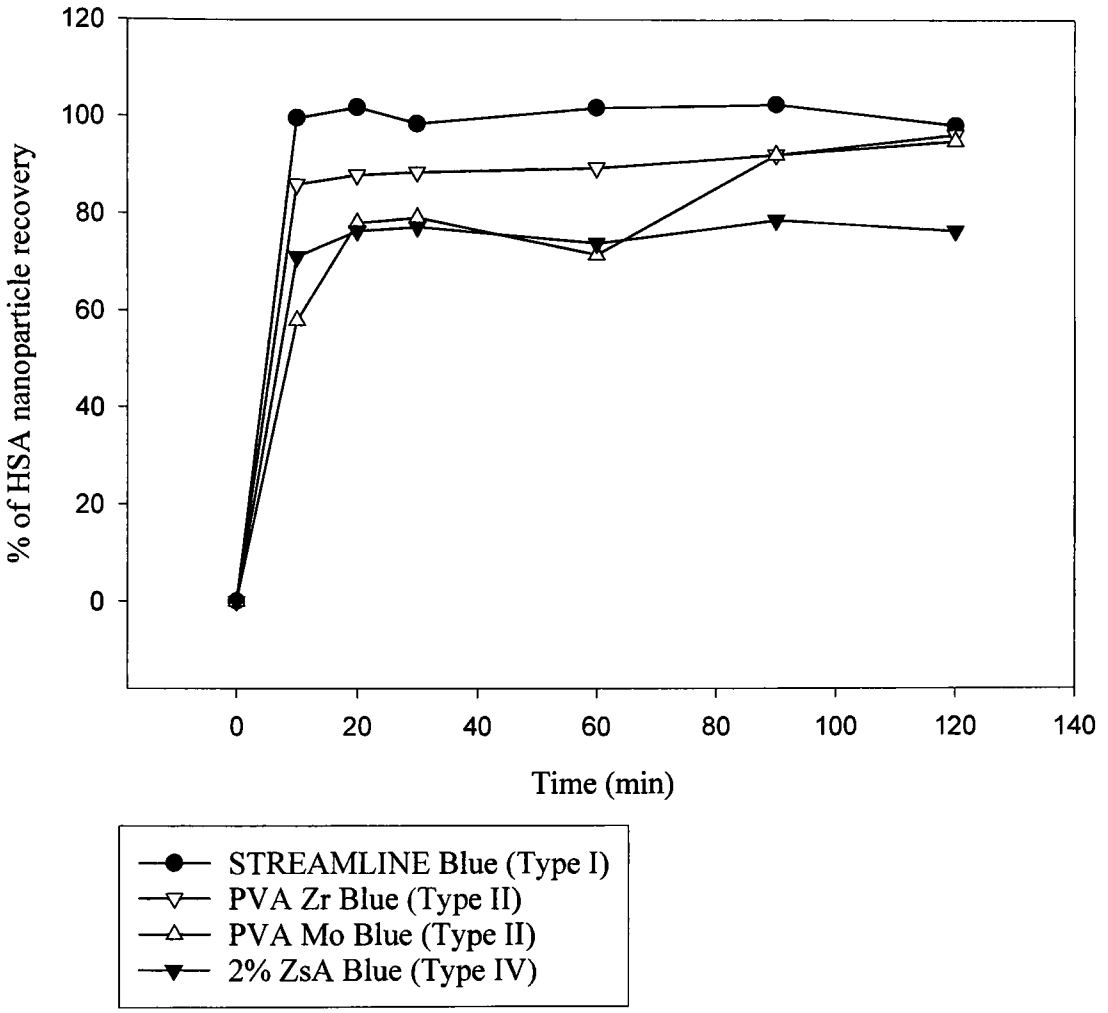

Figure 5.8 represents the recovery of HSA nanoparticles from adsorbents derivatised with Cibacron Blue 3GA. After adsorption the adsorbents were washed in Buffer C to remove all unbound HSA nanoparticles. Adsorbent (0.1ml) loaded with HSA nanoparticles was added to 1.5ml of 3M KSCN. This was mixed at room temperature on a rotary mixer for 2 hours and samples were taken at regular time intervals and analysed in duplicate using the Bradford assay. (Buffer C = 111mM sodium phosphate buffer, pH 6.4 with 0.02% sodium azide and 0.01% Tween 20).

The influence of the degree of FITC conjugation upon the adsorption of HSAp to Cibacron Blue 3GA solid phases was investigated with batch binding experiments completed for STREAMLINE Blue (the commercial benchmark adsorbent) and HSAp having different concentrations of conjugated FITC. The results from this study are expressed in Table 5.5 and it was concluded that as the concentration of FITC conjugated to the HSAp increased the adsorption capacity decreased and the recovery was maintained at approximately 100%. This observation could be attributed to several factors. FITC conjugates primarily to lysine residues (Pawley, 1995) and so it can be surmised that FITC will conjugate to lysine 220, an amino acid residue present in the billirubin binding site of HSA (Leatherbarrow and Dean, 1980; see Section 5.1.2). The affinity interaction between HSA and Cibacron Blue 3GA is thought to be due to the structural similarities of billirubin and the dye (see Section 5.1.1). Consequently any interruption of this interaction could result in lower adsorption capacities. In addition, there are negatively charged sulphate groups present on Cibacron Blue 3GA (see Figure 5.1) that could interact with positively charged amino acids present in HSA (see Table 3.1) including arginine, histidine and lysine (Leatherbarrow and Dean, 1980). Ideally an FITC concentration of less than 1 mole of FITC per mole of HSA would have been desirable for the study as the adsorptive capacity of STREAMLINE Blue was only reduced by approximately 7% at this concentration (see Table 5.5). However, due to the low concentration range of nanoparticles employed in these studies (see Section 5.2.8) the maximum FITC load of 12.7 moles of FITC per mole of protein was required for the adequate detection of the nanoparticles.

Figure 5.9 represents the adsorptive capture of FITC-HSAp at a concentration of 10^8 particles per milliliter of supernatant. All of the adsorbents remaining in the study (STREAMLINE Blue, Type I; PVA Mo Blue, Type II; PVA Zr Blue, Type II and 2% ZsA Figure 2.1) reached an adsorption equilibrium within 30 minutes and all Blue, Type IV; see

Table 5.5 Impact of the degree of FITC conjugation upon the adsorption of HSAp to STREAMLINE

MOLES OF FITC PER MOLE OF HSA	ADSORPTION CAPACITY (mg/ml adsorbent)	% RECOVERY IN 3M KSCN
0.0	1.45	100
1.89	1.32	100
3.06	1.30	102.3
4.45	1.02	108.7
7.08	0.92	101.7
12.49	0.67	102.9
12.7	0.66	102.2

Table 5.5 represents the effect of FITC on the adsorption of HSAp to STREAMLINE derivatised with Cibacron Blue 3GA. Subsequent to the conjugation of FITC to the HSAp the adsorption capacities were measured employing equivalent binding experiments as used in the previous batch binding studies (see Chapter 3). Pre-equilibrated adsorbent (0.1ml) was added to 1.5ml of FITC conjugated HSAp at a concentration of 220µg/ml. The samples were mixed at room temperature for 120 minutes using a rotary mixer. Samples were taken at regular time intervals and analysed in duplicate using the Bradford assay. The adsorbent was washed (5 x 1ml) in Buffer C (pH 6.4) then added to 1.5ml of KSCN (in Buffer C) and mixed at room temperature for120 minutes. Percentage recovery is expressed as a percentage of the bound protein recovered within 2 hours. (Buffer C = 111mM sodium phosphate buffer, pH 6.4 with 0.02% sodium azide and 0.01% Tween 20).

Figure 5.9 Adsorption of HSAp at a low initial nanoparticle concentration

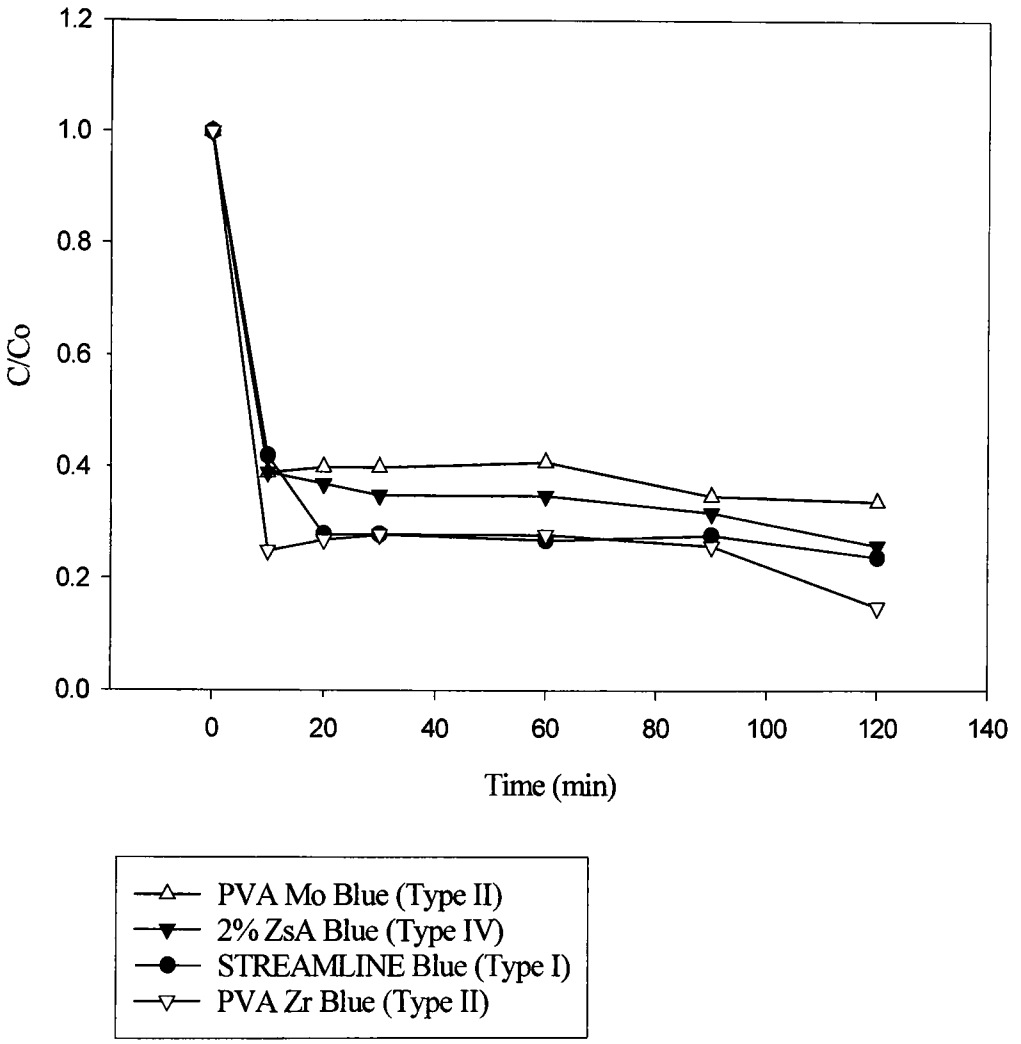

Figure 5.9 represents the binding of nanoparticles to adsorbents derivatised with Cibacron Blue 3GA. Nanoparticles were used at a low concentration (84ng/ml) to mimic a realistic viral titre of 10^8 particles/ml. To analyse the concentration of HSAp at this low concentration a fluorophore was attached to allow the concentration to be determined using fluorescence spectroscopy. The fluorophore used was fluoroscein isothiocyanate (FITC) and was immobilised via the lysine residues on the HSA protein. The fluorophore was added to a maximum fluorophore load of approximately 12.7moles of FITC per mole of protein (see Section 5.2.6.1) Adsorbent (0.4ml) was added to 6.0ml of HSA nanoparticles in Buffer C at a concentration of 84ng/ml. This was mixed at room temperature for 2 hours on a rotary mixer with samples taken at regular time intervals. The samples were analysed using a fluorescence assay.

(Buffer C = 111mM sodium phosphate buffer, pH 6.4 with 0.02% sodium azide and 0.01% Tween 20).

exhibited similar adsorption capacities (see Table 5.6). The rapid adsorption profiles were attributed to there being surface limited adsorption, due to the low nanoparticle concentration.

HSAp bound under standardised conditions were desorbed using 3M KSCN in Buffer C. The desorption profiles were unexpected as it was observed that there was no desorption of HSAp detected until 20 minutes after the initiation of the experiment (refer to Figure 5.10) This might be attributed to the nanoparticle concentration being too low to be detected by fluorescence microscopy (see Appendix VI). In addition, the recoveries were surprisingly low with 2% ZsA Blue exhibiting the highest recovery at 56.7% (see Table 5.6). These results suggested that the dye concentration on the adsorbent particles could influence the recovery of HSAp in 3M KSCN as 2% ZsA Blue had the lowest dye concentration of each of the adsorbents in the study (see Table 5.3). If there are fewer ligands available for binding then theoretically there should be fewer points of attachment. Hence, it should be easier to desorb the product as suggested for anion exchange groups (see Figure 3.7).

5.3.5 The Affinity Capture and Recovery of Human Serum Albumin Nanoparticles in the Presence of Insect Cell Culture Lysate

The preliminary affinity capture and recovery of HSAp exploiting the pseudo-affinity dye Cibacron Blue 3GA (see Section 5.3.3; 5.3.4) indicated that the affinity system could potentially be used to recover nanoparticulate products. One of the important factors associated with the recovery of nanoparticulate products such as retrovirus or adenovirus, is the recovery from complex feedstocks. Consequently, it was proposed that exploiting an affinity system for the fluidised bed adsorption of these products is a potentially suitable method for the downstream processing of nanoparticulate products. Fluidised Bed Adsorption Chromatography can be employed to circumvent problems associated with the

Table 5.6 Summary of the adsorptive capacities and recoveries of HSAp at a low initial concentration

ADSORBENT TYPE	ADSORBENT	HSAp CAPACITY (µg/ml adsorbent)	HSAp CAPACITY (particles/ml adsorbent)	% RECOVERY
I	STREAMLINE Blue	0.89	7.88×10^9	37.2
II	PVA Mo Blue	0.77	6.80×10^9	36.1
	PVA Zr Blue	0.99	8.76×10^9	42.9
IV	2% ZsA Blue	0.93	8.23×10^9	56.7

Table 5.6 represents the capacities and recoveries of HSAp of adsorbents derivatised with Cibacron Blue 3GA with a low initial nanoparticle concentration of 1 x10^8 particles/ml of supernatant having an equivalent protein concentration of 84ng/ml. Before use the adsorbents were washed in Buffer C to equilibrate the system, then 0.4ml of adsorbent was added to 6ml of HSAp containing supernatant (Buffer C = 111mM sodium phosphate buffer, pH 6.4 with 0.02% sodium azide and 0.01% Tween 20). The system was mixed for 120 minutes at room temperature using a rotary mixer with samples taken at regular time intervals and analysed using a fluorescence assay (see Section 5.2.6). The adsorptive capacities were determined by difference analysis and the recovery was expressed as a percentage of the HSAp bound during the adsorption procedure. The HSAp were recovered in 6ml of 3M KSCN added to 0.4ml of protein loaded adsorbent after 5 x 1ml washes with Buffer C, and mixed for 120 minutes at room temperature using a rotary mixer. Samples were taken at regular time intervals and assayed using a fluorescence assay (see Section 5.2.6).

Figure 5.10 Recovery of HSA nanoparticles

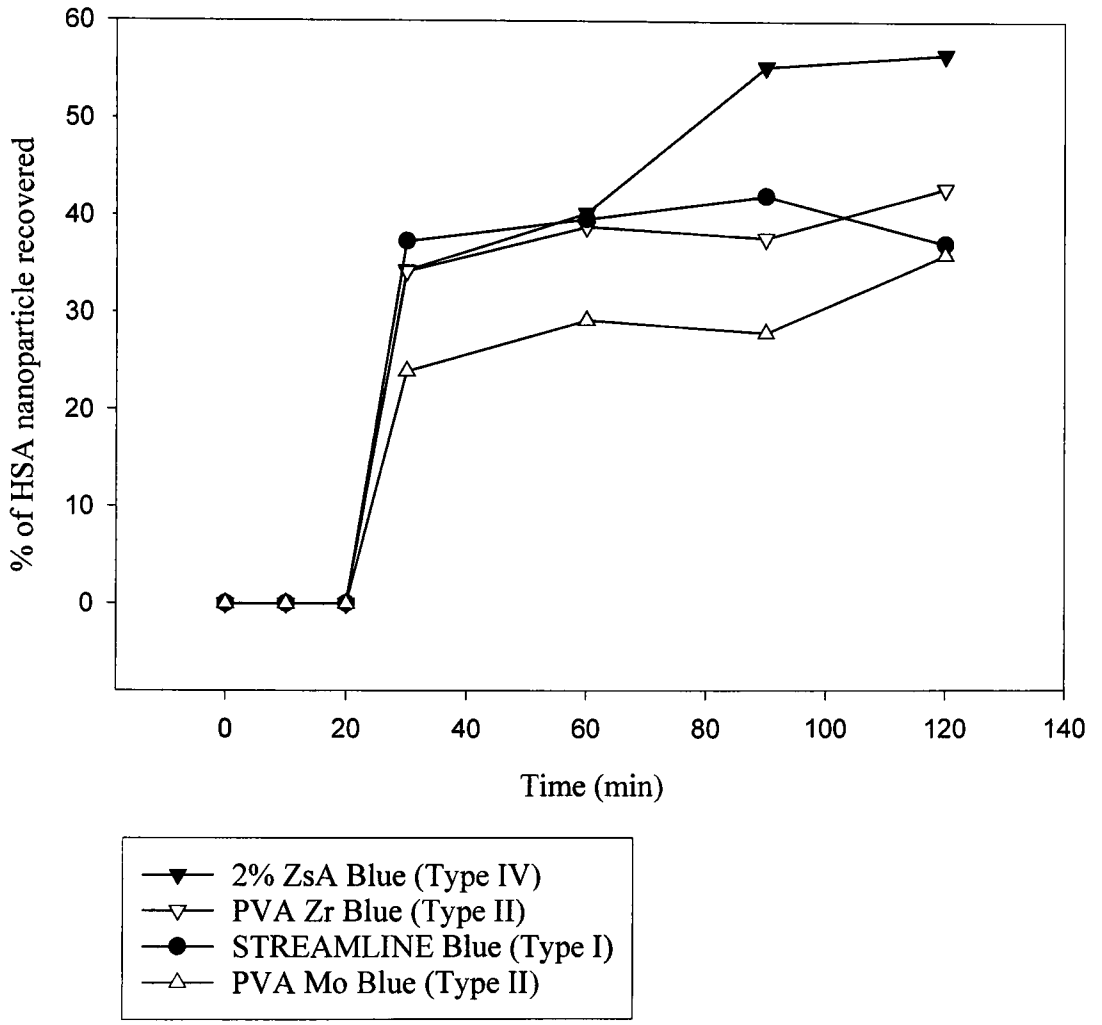

Figure 5.10 represents the recovery of FITC HSAp from adsorbents derivatised with Cibacron blue 3GA dye. After the adsorbents were loaded with HSAp they were washed in Buffer C (5 x 1ml) to remove unbound nanoparticles. Adsorbent (0.4ml) was added to 6.0ml of 3M KSCN and mixed at room temperature for 2 hours on a rotary mixer. Samples were taken at regular time intervals and analysed in duplicate using a fluorescence assay (see Section 5.2.6).

The percentage recovery represents the concentration of protein expressed as a percentage of the protein bound.

(Buffer C = 111mM sodium phosphate buffer, pH 6.4 with 0.02% sodium azide and 0.01% Tween 20).

chromatography of complex feedstocks (see Section 1.3; 1.4), whilst affinity chromatography can be exploited to attempt to separate the product from the feedstock components.

Proof of principle experiments were completed employing insect cell culture lysate (supplied by R. Jarman-Smith) as a representative feedstock (see Section 5.2.7) from which HSAp were recovered. HSAp were added to insect cell culture lysate to a final concentration of 10^8 particles/ml of supernatant. Figures 5.11 and 5.12 represent the adsorption profiles for FITC HSAp (measured employing fluorescence spectroscopy; see Section 5.2.6) and cell culture lysate components (measured employing the Bradford assay; see Section 3.2.6). The FITC HSAp load was exhausted (see Figure 5.11) which was attributed to the presence of feedstock components with which HSAp could associate including enzymes and growth factors produced by the cells during cell growth.

The profiles of cell lysate component adsorption were as expected subsequent to the studies completed for the adsorption of BSAs to the anion exchange derivatives of the adsorbents (see Chapter 3). The Type I microporous adsorbent, STREAMLINE Blue, exhibited a slow adsorption that did not reach completion within the experimental time (120 minutes; see Section 5.2.8). The adsorption onto the Type II macroporous adsorbents (PVA Mo Blue and PVA Zr Blue) and the Type IV pellicular adsorbent (2% ZsA Blue) was rapid which was attributed to the respective adsorbent structures.

2% ZsA Blue exhibited the lowest adsorption capacity of each of the adsorbents included in this study (see Table 5.7) that was attributed to either the low dye content of the adsorbent solid phase (see Table 5.3) or the limited surface area available for adsorption due to the pellicular structure of the adsorbent solid phase (see Section 1.5).

It is noteworthy that all of the adsorbents in the study demonstrated significant adsorption capacities for the insect cell culture lysate components. This suggests that this model affinity system (Cibacron Blue 3GA and human serum albumin) is not an ideal system

Figure 5.11 HSA nanoparticle adsorption at a low nanoparticle concentration

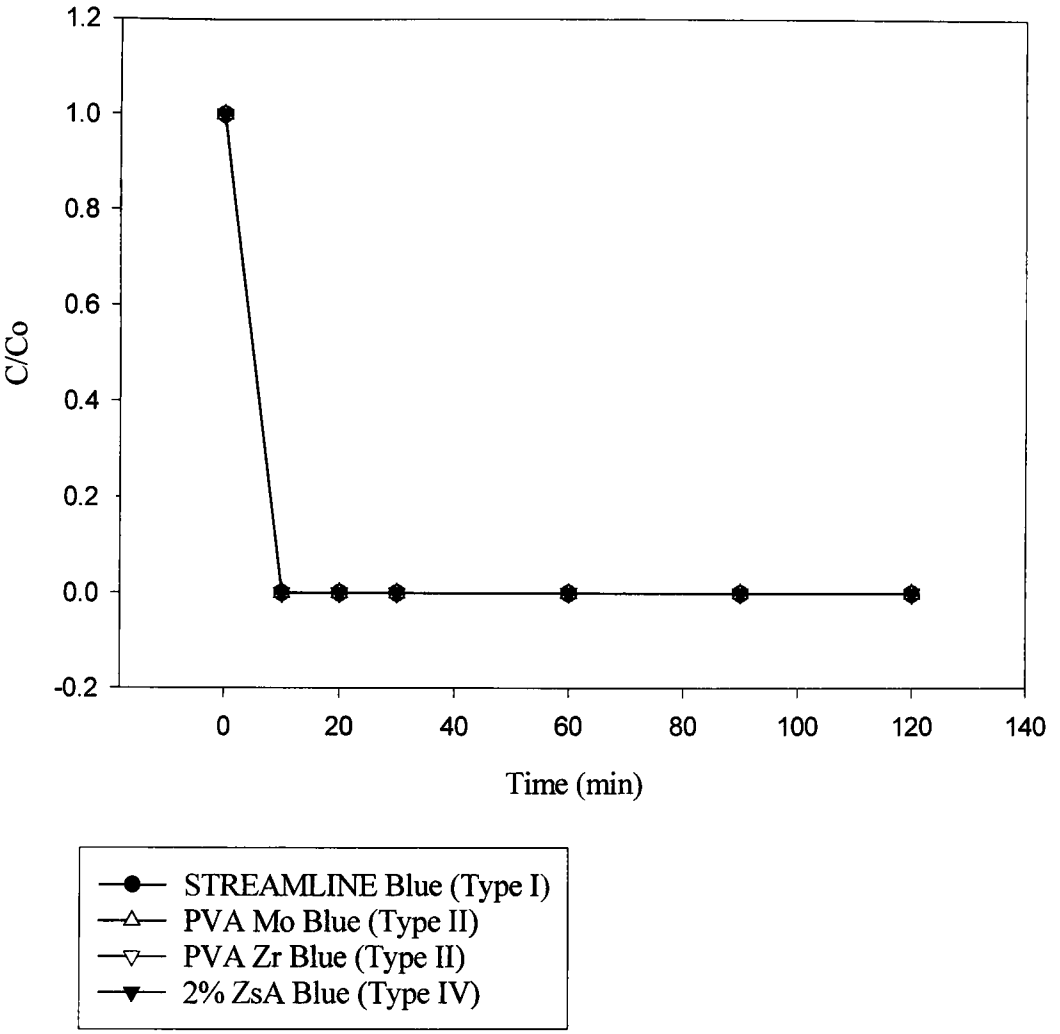

Figure 5.11 represents the adsorption of HSAp from cell lysate at a concentration of 10^8 particles/ml. Before use the adsorbents were washed in Buffer C to equilibrate the system. Adsorbent (0.4ml) was added to 6.0ml of cell lysate containing FITC conjugated nanoparticles. The system was mixed for 2 hours at room temperature using a rotary mixer. Samples (0.4ml) were taken at regular time intervals and analysed using a fluorescence assay.

The HSAp used in this study were estimated to contain 12.7 moles FITC per mole of protein. (Buffer C = 111mM sodium phosphate buffer, pH 6.4 with 0.02% sodium azide and 0.01% Tween 20).

Figure 5.12 The adsorption of insect cell culture lysate components to the selected adsorbent solid phases

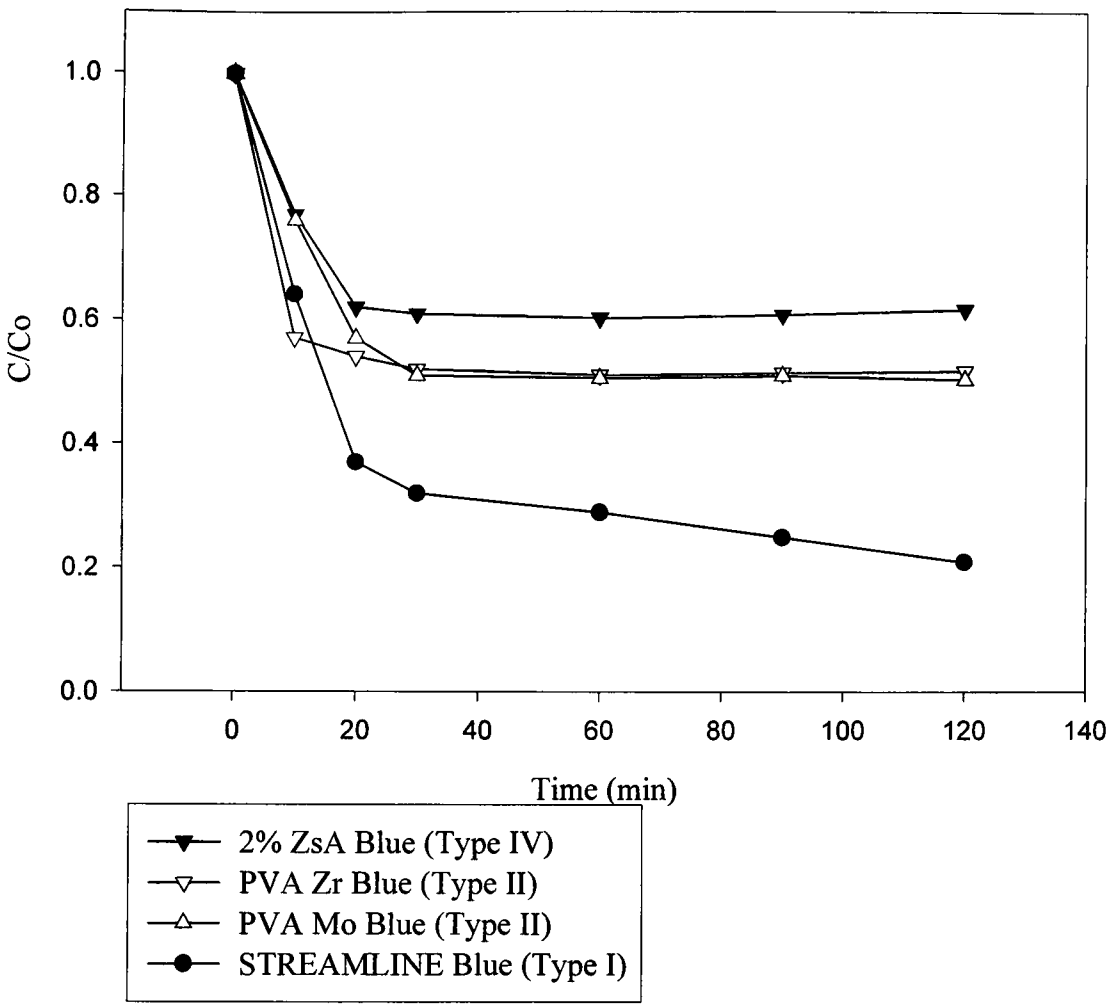

Figure 5.12 represents the adsorptive capture of insect cell culture lysate to the selected adsorbent solid phases immobilised with Cibacron Blue 3GA dye. The adsorbent (0.1ml) was washed in Buffer C prior to use to equilibrate the system, then 1.5ml of cell culture medium (containing lysed sf-9 cells) was added and mixed for 2 hours at room temperature using a rotary mixer. Samples were taken at regular time intervals and analysed in duplicate using the Bradford assay (see Section 3.2.6).

The initial Co concentration for the cell culture medium was measured at 1.05mg/ml using the Bradford assay (refer to Section 3.2.6). C/Co is measure of the protein concentration as a fraction of the initial protein concentration.

(Buffer C = 111mM sodium phosphate buffer, pH 6.4 with 0.02% sodium azide and 0.01% Tween 20).

Table 5.7 Summary of the adsorptive capacities of total protein and recoveries of insect cell culture lysate from the selected adsorbent solid phases

ADSORBENT TYPE	ADSORBENT	DYE CONCENTRATION (µmol dye/settled ml adsorbent)	TOTAL PROTEIN CAPACITY (mg/ml adsorbent)	% RECOVERY
I	STREAMLINE Blue	3.9	6.32	49.6
II	PVA Mo Blue	0.068	4.59	83.1
	PVA Zr Blue	0.079	4.46	77.9
IV	2% ZsA Blue	0.01	3.53	82.2

Table 5.7 represents the total protein capacities and recovery of the cell lysate components to adsorbents derivatised with Cibacron Blue 3GA dye (see Figure 5.13 and 5.15). Before use the adsorbent was extensively washed in Buffer C to equilibrate the system and 0.4ml of adsorbent was added to 6ml of cell lysate. The system was mixed for 120 minutes at room temperature using a rotary mixer with samples taken at regular time intervals and analysed using the Bradford assay and the capacities were determined by difference analysis. The recovery of HSAp in 6ml of 3M KSCN that was added to 0.4ml of protein loaded adsorbent is represented as the protein recovered expressed as a percentage of the protein adsorbed. (Buffer C = 111mM sodium phosphate buffer, pH 6.4 with 0.02% sodium azide and 0.01% Tween 20).

for the separation of nanoparticulate products from complex feedstocks. Ideally SDS PAGE analysis should have been completed to assess the adsorption and desorption and to determine product purity. However time constraints within the project did not allow for this.

Figures 5.13 and 5.14 represent the desorption profiles of HSAp and cell lysate components respectively. It is immediately apparent that the desorption of HSAp (measured by fluorescence spectroscopy; see Section 5.2.6) in the presence of cell culture lysate is very different to the desorption from a clean system (see Figure 5.10) as HSAp appeared to desorb within 10 minutes after the addition of 3M KSCN (see Figure 5.13). This could be attributed to the presence of the cell culture lysate components as the HSAp could have been bound less strongly to the Cibacron Blue 3GA ligand due to an increased number of interactions of the ligand with the cell culture lysate components (see Figure 5.11). In addition, the recovery of HSAp was greater in the presence of lysate components (see Figure 5.13; Table 5.8) than in clean systems (see Figure 5.10; Table 5.6). This may be attributed to both the presence of the lysate components and the dye concentration of the adsorbent solid phases. It was proposed that the recovery of HSAp from a clean system was low due to the increased number of potential ligand attachments per HSAp. Therefore, if the cell culture lysate components are interacting with the Cibacron Blue 3GA dye (as suggested in Figure 5.12) then fewer ligands will be available per HSAp. Thus reducing the affinity of the adsorbent for HSAp and increasing the recovery (see Figure 3.7).

The profiles for the recovery of cell culture lysate components (see Figure 5.14) were as expected based upon assumptions made about the adsorbents from previous studies (see Chapter 3). STREAMLINE Blue exhibited the poorest recovery at 49.6% that was attributed to the internal and external geometry of the adsorbent solid phase categorised as a microporous adsorbent (Type I) for the present study. It was expected that the small molecular weight components within the feedstock would diffuse into the microporous

Figure 5.13 Recovery of HSA nanoparticles

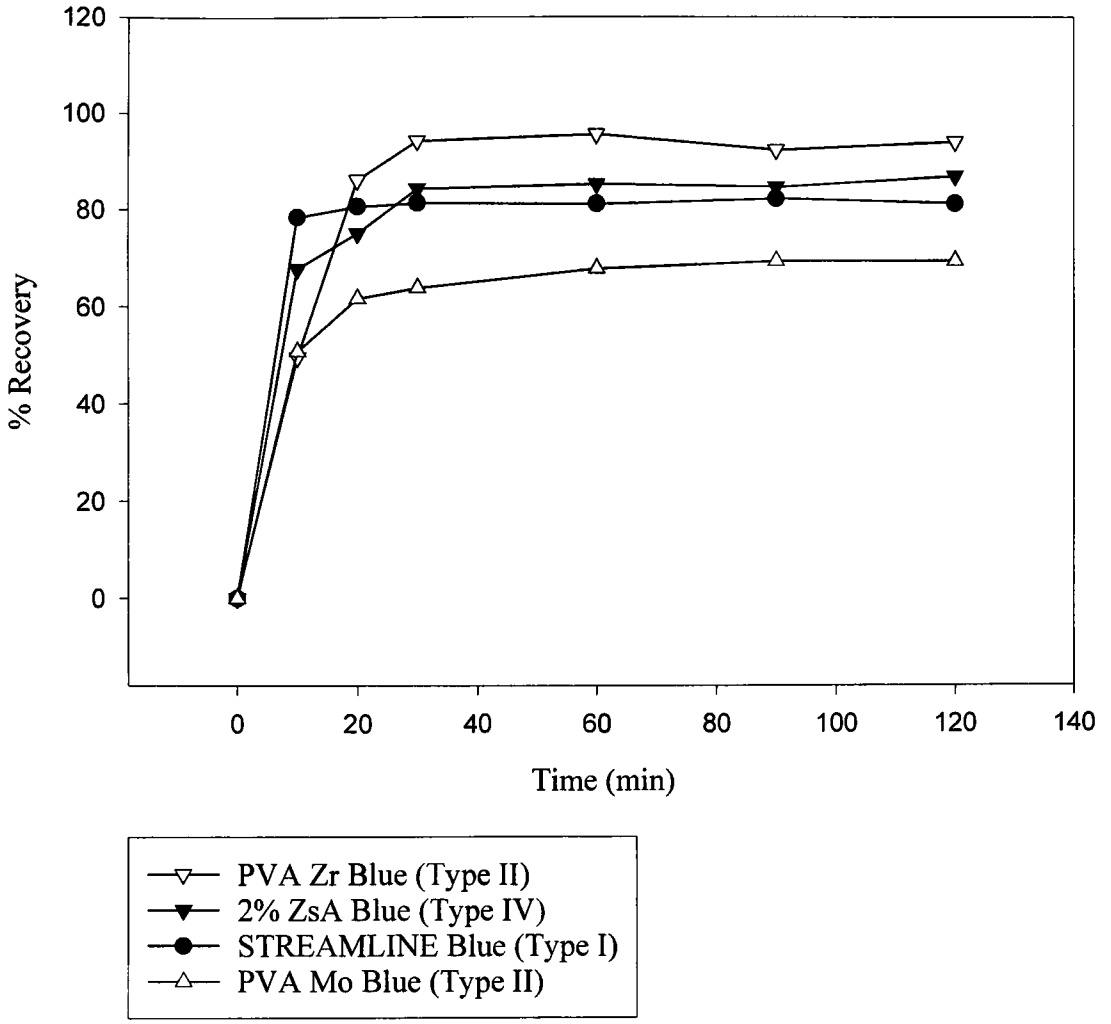

Figure 5.13 represents the recovery of FITC HSAp from adsorbents derivatised with Cibacron blue 3GA dye. After the adsorbents were loaded with nanoparticles recovered from cell culture lysate the adsorbents were washed in Buffer C to remove unbound protein from the system. Adsorbent (0.1ml) was added to 1.5ml of 3M KSCN and mixed for 2 hours at room temperature using a rotary mixer. Samples were taken at regular time intervals and analysed in duplicate using a fluorescence assay (see section 5.2.6).
(Buffer C = 111mM sodium phophate buffer, pH 6.4 with 0.02% sodium azide and 0.01% Tween 20).

Figure 5.14 The recovery of insect cell culture lysate components from the selected adsorbent solid phases

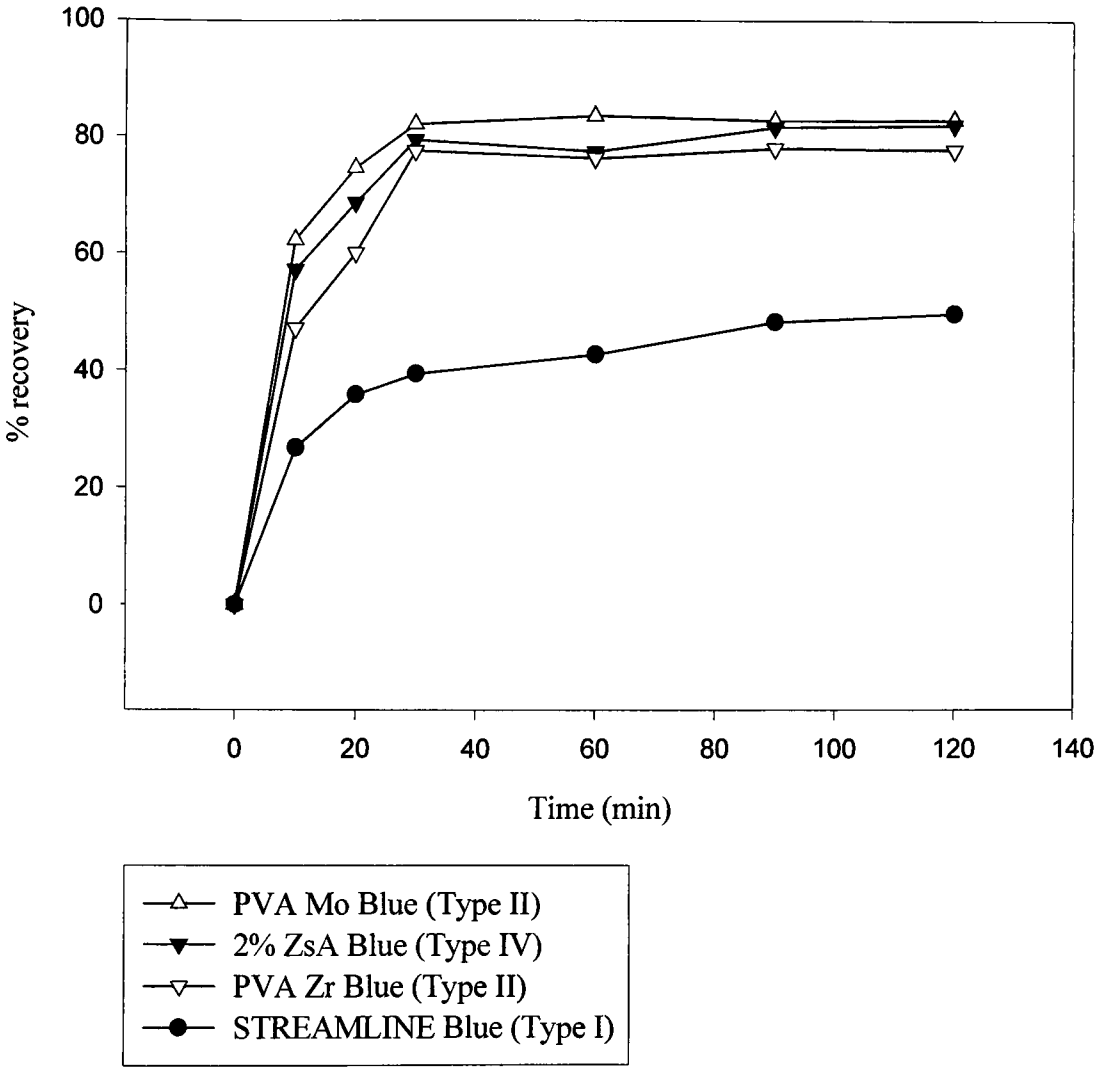

Figure 5.14 represents the recovery of insect cell culture lysate using 3M KSCN from the selected adsorbent solid phases immobilised with Cibacron Blue 3GA. The protein loaded adsorbent was washed in Buffer C (5 x 1ml) to remove any unbound cell culture lysate. The adsorbent (0.1ml) was added to 1.5ml of 3M KSCN and mixed for 2 hours at room temperature using a rotary mixer. Samples (0.1ml) were taken at regular time intervals and analysed in duplicate using the Bradford assay (see Section 3.2.6).

Table 5.8 Summary of the adsorptive capacities and recoveries of insect cell culture lysate containing HSAp from the selected adsorbent solid phases

ADSORBENT TYPE	ADSORBENT	DYE CONTENT (μmol/ml settled adsorbent)	HSAp CAPACITY (μg/ml adsorbent)	HSAp CAPACITY (particles/ml adsorbent)	% RECOVERY
I	STREAMLINE Blue	3.9	1.26	1.1×10^{11}	80.2
II	PVA Mo Blue	0.068	1.26	1.1×10^{11}	63.4
	PVA Zr Blue	0.079	1.26	1.1×10^{11}	91.3
IV	2% ZsA Blue	0.01	1.26	1.1×10^{11}	82.7

Table 5.8 represents the protein capacities and recoveries of the HSAp suspended in cell culture lysate to adsorbents derivatised with Cibacron Blue 3GA. Before use the adsorbents were extensively washed in Buffer C to equilibrate the system and 0.4ml was added to 6ml of cell culture lysate. The system was mixed for 2 hours at room temperature using a rotary mixer with samples taken at regular time intervals and analysed in duplicate using the fluorescence assay (see Section 5.2.6). HSAp were recovered in 6ml of KSCN added to 0.4ml of HSAp loaded adsorbent and mixed for 2 hours at room temperature. Samples were taken at regular time intervals and assayed in duplicate using the fluorescence assay. The % recovery was determined as a percentage of the total capacity. (Buffer C = 111mM sodium phophate buffer, pH 6.4 with 0.02% sodium azide and 0.01% Tween 20).

structure of the adsorbent as was indicated in Figure 5.12. It was therefore likely that poor recovery was due to the impurities being trapped within the adsorbent structure. For the remaining adsorbents the recoveries were greater than 77% that was again attributed to the respective adsorbent structures (see Table 5.7). The Type II macroporous adsorbents (PVA Mo Blue and PVA Zr Blue) were assumed to be characterised by large macropores (see Section 2.1.5) that would facilitate the diffusion of the impurities out of the adsorbent structure during the elution process. In addition, 2% ZsA Blue was a Type IV, pellicular adsorbent that had shorter diffusion distances over which the impurities were required to diffuse (see Figure 2.1).

5.3.6 General Conclusions

The aim of this chapter was to investigate the adsorption of HSAp exploiting industrially realistic particle numbers in a realistic complex feedstock (insect cell culture lysate) employing affinity chromatography. Initial experiments were completed with HSAp concentrations comparable to that for the BSAp batch binding experiments completed in Chapter 3. The results indicated HSAp capacities for Cibacron Blue 3GA derivatised adsorbents were similar to those achieved exploiting anion exchange chemistries for the adsorption of BSAp (see Table 3.4). In addition, the recovery of HSAp using 3M KSCN was adequate particularly for STREAMLINE Blue (Type I) and PVA Mo Blue (Type II) that exhibited recoveries greater than 90% (see Table 5.4). As a consequence of these results batch binding experiments were completed to assess the adsorption of HSAp at a concentration of 10^8 particles/ml to the Cibacron Blue 3GA derivatised adsorbents. All of the adsorbents included in the present study exhibited similar capacities due to the limited product available (see Table 5.6). However, the recovery of HSAp in 3M KSCN was poor at less than 50% for STREAMLINE Blue (Type I), PVA Mo Blue (Type II) and PVA Zr Blue

(Type II). 2% ZsA Blue demonstrated that highest recovery at 56% that was attributed to the low dye content of the adsorbent solid phase (see Table 5.3).

The recovery of HSAp was then further investigated exploiting an insect cell culture lysate as a representative complex feedstock. It was noted that the HSAp load was exhausted within 10 minutes and the recovery (in 3M KSCN) was better than that for HSAp desorbed in a clean system (compare Table 5.6 and Table 5.8). This was attributed to the presence of cell culture lysate components. The components of the lyaste are likely to include proteins such as enzymes and cell growth factors with which the FITC conjugated nanoparticles could electrostatically interact. Figures 5.13 and 5.15 indicate that there is a significant degree of adsorption of the cell lysate components, hence if the nanoparticles are interacting with these products then they could be removed from the sampling supernatant. Overall the results produced were similar to those for anion exchange chromatography. Therefore it was concluded that this particular affinity system would not be suitable for the recovery of nanoparticulate products from complex feedstocks. It is noteworthy that the FITC or Rhodamine B Isothiocyante conjugated HSAp are expected to behave differently to native HSAp due to the conjugation of the fluorescent probes to the lysine residues of human serum albumin. It was expected that the adsorption of HSAp would be influenced in addition to the likely occurence that the charge of the protein was altered as a consequence of the surface lysine residues (negatively charged residues) being the point of conjugation to the probe.

CHAPTER 6

CONCLUSIONS AND FURTHER WORK

6.1 Final Conclusions

The study presented here was concerned with investigating the effect of adsorbent design upon the separation of nanoparticulate products such as protein nanoparticles as representative viruses, plasmid DNA and drug delivery vehicles. Candidate adsorbent solid phases having discrete internal and external geometries were selected and characterised both physically and biochemically (see Table 2.1).

The current chromatographic processes for the purification of viruses and plasmid DNA employ materials and techniques primarily designed for the purification of smaller protein products. Product rich cell culture supernatants and cell lysates are currently clarified and concentrated by ultrafiltration/diafiltration and density gradient centrifugation techniques (Prazeres *et al*, 1999). The product is commonly recovered in a fixed bed chromatography step with adsorbent solid phases designed principally for the purification of proteins (Huyghe *et al*, 1995; Blanche *et al*, 2000). There are problems associated with such techniques for the recovery of these products, as due to process inefficiencies there is loss of product integrity, particularly with viruses and inherent handling losses. In addition, the adsorbent solid phases employed for the fixed bed recovery of the product are not optimally designed for such operations with nanoparticulate products resulting in product losses due to an inefficient system where product entrapment and co-purification of contaminants is likely.

A revised process method was proposed integrating the clarification, concentration and primary capture steps (see Figure 1.3). By employing fluidised bed adsorption chromatography the downstream processing steps are simplified. To increase the efficiency of this primary capture step both the adsorbent design and suitable ligands for nanoparticulate capture were considered.

6.1.1 Candidate Adsorbent Solid Phases

The experiments presented in Chapter 2 investigated the physical characteristics of adsorbent solid phases having different internal and external geometries designated Types I to IV (see Table 2.1 and Figure 2.1). Microporous adsorbents were designated as Type I adsorbent solid phases and were characterised by pore diameters of less than 0.2μm. Therefore the commercial benchmark adsorbent, STREAMLINE was designated as a Type I adsorbent. Type II adsorbent solid phases were classified as macroporous adsorbents having pore sizes greater than 0.6μm in diameter (see Figure 2.1). Type II adsorbents included in the present study were, POROS 50D, PVA, PVA TiO_2, PVA Mo, PVA Zr, Celbead (II) and Celbead Amino. These included both commercial and custom designed adsorbents (Swedish and Indian constructs). Two solid adsorbents were also included in the study and designated as Type III adsorbent solid phases, Toyopearl-HW40 and the Birmingham construct perfluorocarbon emulsion particles. The remaining adsorbent in the study, 2% ZsA (Birmingham construct) was designated as a Type IV pellicular adsorbent that comprised a dense solid zirconium silicate core surrounded by a 20μm porous skin of agarose having an assumed pore size of less than 0.4μm. The adsorbent solid phases were characterised in terms of size, shape, density and bed expansion characteristics to assess the suitability of these adsorbents for fluidised bed adsorption operations.

The physical characterisation studies (see Chapter 2) indicated that the candidate adsorbents were generally spherical in shape with the exception of the custom fabricated adsorbents Celbead (II) and Celbead Amino (Type II; see Figure 2.1; see Figures 2.8-2.18). The sizes of the adsorbent solid phases, determined using a Malvern Mastersizer (see Section 2.2.7.2; Malvern Instruments, UK) were varied (see Table 2.3). Perfluorocarbon emulsion particles were shown to have a particle size of 10μm whilst PVA Zr particles were 525μm in diameter (see Table 2.3). The measured densities of the adsorbents also varied with

perfluorocarbon emulsion particles having a density of 2.1g/ml in comparison to PVA at 1.12g/ml (see Table 2.4). Bed expansion characterisation studies indicated that all the fluidisable candidate adsorbent solid phases, with the exception of the perfluorocarbon emulsion, exhibited superior expansion characteristics in comparison to the commercial benchmark STREAMLINE (see Figure 2.20). POROS 50D and Toyopearl HW-40 were not included in the bed expansion studies due to their limited densities (see Table 2.4). The non-derivatised candidate adsorbents were immobilised with the anion exchange chemistry, diethylaminoethyl (DEAE), and the relative small ion capacities (SIC) were determined. SIC of the adsorbent solid phases varied depending upon the reactivity of the hydroxyls on the base material (agarose, cellulose or polyvinyl alcohol) and the surface area available for immobilisation (see Table 2.5).

Celbead Amino demonstrated a superior performance in comparison to the other adsorbent solid phases included in the study in terms of bed expansion characteristics (see Figure 2.20). All of the adsorbents included in the physical characterisation studies were further investigated by batch adsorption/desorption studies as described in Chapter 3.

6.1.2 Selection of Candidate Adsorbents Exploiting Synthetic Nanoparticles

Experiments summarised in Chapter 3 investigated the biochemical performance of the candidate adsorbent solid phases by investigating the adsorption/desorption characteristics of BSAs and BSAp exploiting anion exchange chromatography. BSAs was included in the present study to represent small molecular weight contaminants commonly found in cell culture lysates such as cells, cell debris and DNA and also as a model for the recovery of product from product components. A major problem associated with commercially realistic studies of virus or plasmid DNA recovery is the quantity of nanoparticulates required for representative studies. This problem was circumvented by

exploiting synthetic nanoparticles comprised of coacervated and crosslinked bovine or human serum albumin (see Section 3.1.1). The fabricated nanoparticles were sized using photon correlation spectroscopy (see Section 3.1.2). BSAp had an average particle size of 150nm in diameter (see Figure 3.4) whilst HSAp had an average particle size of 66nm in diameter (see Figure 5.3).

For the purpose of this study, STREAMLINE DEAE was selected as the benchmark adsorbent solid phase and the batch adsorption/desorption characteristics of each adsorbent BSAs and BSAp was investigated. The results indicated that the adsorbent design influenced the adsorption and recovery of both BSAs and BSAp. Rapid adsorption and desorption of BSAs was characteristic of the adsorbents perceived to have reduced diffusional limitations in comparison to STREAMLINE DEAE (see Figure 3.2). This included the macroporous (Type II) adsorbents where the convective pores were thought to facilitate the transport of large nanoparticulate products through the adsorbent particles to smaller diffusive pores contained within the adsorbent structure. The solid adsorbents had exclusive surface adsorption and so there were no diffusional limitations for BSAs adsorption. The surface area over which adsorption occurred was also thought to be reduced in the pellicular adsorbent (see Figure 3.2).

The relatively solid adsorbent Toyopearl HW-40 (Type III, see Figure 2.1) exhibited an unexpected desorption behaviour (see Figure 3.3). BSAs desorbed slowly suggesting that there were diffusional limitations due to BSAs penetration into the adsorbent structure. This was determined to be unlikely due to the limited pore size of Toyopearl HW-40 (see Table 2.1). Therefore it was assumed that the high small ion capacity (see Table 2.5) had a negative effect upon the desorption of BSAs. The effect of SIC on the adsorption and desorption of BSAs has not been fully investigated in this study. POROS 50D (Type II, see Figure 2.1) exhibited the highest BSAs capacity whilst the Type II, III and IV adsorbents all exhibited

adequate recoveries in comparison to STREAMLINE (see Table 3.4) attributed to the internal and external structures of the adsorbents. In contrast the Type II adsorbents Celbead (II) and Celbead Amino performed poorly in the adsorption and desorption studies respectively.

The adsorption and recovery of BSAp also appeared to be influenced by the design of the adsorbent solid phase. The results indicated two distinct adsorption profiles (see Figure 3.5) attributed to the pore structures of the adsorbents included in the study. The adsorbents with pore dimensions expected to exclude nanoparticles (Type III solid adsorbents) reached an equilibrium within 20 minutes attributed to exclusive surface binding. In contrast the adsorbent solid phases believed to possess larger pores (i.e. Type II macroporous adsorbents) reached equilibrium after an experimental time of 60 minutes indicating that BSAp had penetrated into the macroporous structure. Celbead Amino exhibited rapid BSAp adsorption that suggested that the adsorbent was not macroporous. The Type II adsorbents (with the exception of Celbead Amino) all exhibited diffusion limited adsorption that suggested that the macroporous classification was correct (see Figure 3.5). Desorption studies also confirmed that the small ion capacity (SIC) appeared to affect the recovery of BSAp. Both Type III adsorbents (Toyopearl HW-40 DEAE and perfluorocarbon emulsion DEAE) were characterised by slow desorption profiles (see Figure 3.6), which could only be attributed to the concentration of anion exchange groups available for adsorption since no penetration could have occurred.

Subsequent to the batch adsorption studies, the impact of small ion capacity on the recovery of BSAp was investigated exploiting the perfluorocarbon emulsion particles. This adsorbent was selected on the assumption of being solid in nature. Hence all the anion exchange groups immobilised onto the adsorbent would be present at the adsorbent surface and available for adsorption. Five perfluorocarbon emulsions were manufactured having

different SIC (see Section 3.2.8) and the adsorption and desorption of BSAp was studied. The results indicated that as the SIC decreased the binding capacities decreased and the recovery increased. It was therefore concluded that SIC influences the recovery of BSAp, but to optimise anion exchange adsorbents suitable for the recovery of nanoparticulate products requires further investigation.

The maximum binding capacities of BSAp to the selected adsorbent solid phases were determined using Langmuir assumptions. The results generated compared well with the theoretical linear isotherm (a reciprocal plot of the Langmuir isotherm) and thus it was concluded that the adsorption of BSAp to the selected adsorbent solid phases followed Langmuir assumptions (see Section 3.2.1). Subsequent to the studies presented in Chapter 3 POROS 50D, PVA DEAE, perfluorocarbon emulsion DEAE and Toyopearl DEAE were eliminated from further study, based upon conclusions about the physical and biochemical performance of the adsorbent solid phases.

6.1.3 Laser Scanning Confocal Microscopy as a Tool for Visualising Nanoparticulate and Soluble Protein Adsorption

Chapter 4 summarises experiments designed to visualise the adsorption of both BSAs and BSAp to the selected adsorbent solid phases. In Chapter 3 conclusions were made about the selected adsorbent solid phases based upon batch binding experimentation. This is an indirect method of assessing the performance of the adsorbent solid phases as the results only indicate how much protein (soluble or particulate) bound to the adsorbents and not how or where the protein was adsorbing. Therefore to obtain a realistic picture of the adsorptive capture laser scanning confocal microscopy (LSCM) was employed. Fluorescently labelled BSAs and BSAp were adsorbed to the selected adsorbents in an equivalent manner to the batch binding studies. The adsorbent particles were then visualised at equilibrium by LSCM.

All of the adsorbents included in the study (PVA TiO_2 DEAE, PVA Mo DEAE, PVA Zr DEAE, Celbead (II) DEAE, Celbead Amino, 2% ZsA DEAE and STREAMLINE DEAE) were characterised by adsorption in an outer layer of the adsorbent structure, whilst the inner part of the adsorbent remained unused. Celbead (II) DEAE was an exception to this observation where the pore structure can clearly be seen (see Figure 4.13).

The work completed in Chapters 3 and 4 indicated that anion exchange chromatography is not a suitable technique for the separation of nanoparticulate products from product components or complex feedstocks. All of the adsorbent solid phases included in the study exhibited high adsorption capacities for BSAs as well as BSAp. The anion exchange ligand, DEAE, attracts negatively charged biomolecules that complex biological feedstocks are likely to comprise.

6.1.4 The Recovery of Representative Nanoparticulates from a Representative Feedstock

Chapter 5 summarises experiments exploiting the model affinity system of Cibacron Blue 3GA and serum albumin. Nanoparticles fabricated from human serum albumin were recovered using the four remaining adsorbents (STREAMLINE, PVA Mo, PVA Zr and 2% ZsA) immobilized with the Cibacron Blue 3GA dye. HSAp were also recovered exploiting low nanoparticulate numbers representative of retroviral titres (Hughes, 2001) and in the presence or absence of cell culture lysate. The initial adsorption/desorption studies completed with HSAp indicated that this affinity model could be exploited for the recovery of nanoparticulate products. Therefore further studies were completed using an industrially realistic particle number of 10^8 particles/ml of supernatant. The results indicated that all of the adsorbents performed poorly under these conditions. However, to complete the study HSAp at low concentrations were recovered from an insect cell culture lysate, a

representative feedstock. In the presence of cell culture lysate the adsorption and recovery of HSAp with the Cibacron Blue 3GA ligand was improved with higher adsorption capacities and greater recoveries (see Table 5.6 and 5.7). This was attributed to the presence of the cell lysate components influencing the adsorption and desorption processes.

Based upon these results Cibacron Blue 3GA could be exploited for the recovery of nanoparticulate products. However, the adsorption/desorption of the cell culture lysate components was also investigated. The results indicated that there was a significant adsorption of the components on all of the adsorbent solid phases included in the present study. This was attributed to the negatively charged sulphate groups present within the structure of Cibacron Blue 3GA (see Figure 5.1) interacting with positively charged biomolecules. It was therefore concluded that Cibacron Blue 3GA would not be suitable for the capture and recovery of nanoparticulate products from complex biological feedstocks.

6.1.5 Concluding Remarks

Throughout the study the adsorbents demonstrating a poor performance either physically or biochemically, were removed from the study. The four adsorbents carried forward to the final study were considered to exhibit a superior performance for the recovery of nanoparticulate products. However, the study indicated that both the PVA Mo and PVA Zr (Swedish constructs) and 2% ZsA (Birmingham construct) could potentially be used for the recovery of nanoparticulate products demonstrating a better overall performance than the benchmark, STREAMLINE. In addition, it was also concluded in the study that anion exchange chromatography and dye affinity chromatography were not suitable methods for the recovery of such products due to the interactions of the ligands with the cell culture lysate components. It is also important to note that using such chemistries would not enable the particulate product to be separated from product components.

6.2 Further Work

Fluidised Bed Recovery of Nanoparticulate Products

The work completed in this study has highlighted that 2% ZsA, PVA Mo and PVA Zr demonstrated adequate recoveries of nanoparticulate mimics in comparison to the bench mark adsorbent STREAMLINE, based upon batch adsorption studies (see Chapters 3-5). Batch adsorption studies were adopted as scouting experiments to identify adsorbents that would be suitable for fluidised bed adsorption of nanoparticulates. Therefore the next obvious stage to this work would be to complete laboratory scale fluidised bed adsorption studies to assess the adsorbents further. This work would provide information concerning the dynamic binding capacities of the adsorbents as a function of the flow rate applied to the bed and hence indicate more accurately the potential performance of these adsorbents in a large scale fluidised bed process for the recovery of industrially relevant nanoparticulate products.

Recovery of Industrially Realistic Nanoparticulate Products

The work completed in this study has been concerned with the capture and recovery of nanoparticulate proteins exploited as naïve mimics for products such as retrovirus, adenovirus and plasmid DNA. Therefore proof of principle experiments are required employing such nanoparticulate products to investigate the effect of industrially relevant feedstocks on the recovery of nanoparticulates in relation to the adsorbent design.

Alternative Modes of Adsorption

The introduction of realistic products such as viruses will mean that alternative modes of capture should be considered. It was concluded that both anion exchange and dye affinity chromatography would not be suitable systems due to the significant degree of adsorption of soluble protein and cell culture lysate components. Other ligands that could be successfully

exploited for such applications include immobilised metal affinity chromatography (Porath *et al*, 1975). The principle of this technique is that amino acid residues such as histidine and also lysine and tryptophan to a degree can specifically interact through nonbonding lone-pair electron coordination with metal ions such as Cu (II), Ni (II) and Zn (II). In addition, for viral purification a histidine tag could be attached to the surface of the virus enabling purification of the product. Affinity systems could also be exploited, such as antigen-antibody interactions or interactions between molecules such as streptavidin and biotin.

Alternative Methods for the Recovery of Nanoparticulate Products

It is noteworthy that these ligands would be unlikely to separate the desired product from product components and therefore affinity chromatography techniques may not be suitable for the recovery of pure nanoparticulate products. Therefore other techniques should be considered for downstream processing of viruses and plasmid DNA. Gel filtration chromatography could potentially be used for the primary purification of large products from complex feedstock on the basis of size, however the viscosity of such feedstocks could be a limiting factor. Membrane separation techniques could also be considered as a suitable method for the purification of nanoparticulate products from complex feedstocks such that large pores within the membrane structures should enable the use of viscous, complex feedstocks, whilst the ligands attached to the membrane surface will capture the product. This is a technique that will be dependent on suitable ligands for separation and separating the product from product components may also be difficult.

Modification of Adsorbent Design to Improve Nanoparticulate Recovery

The results presented in this study highlighted that both pellicular (2% ZsA) and macroporous adsorbents (PVA Mo and PVA Zr) exhibited a superior performance to

conventional adsorbent solid phases. All of these adsorbents were prototypes hence there is much scope for the improvement of these adsorbents by altering the manufacturing process. Work has been completed on modifying the pellicular adsorbent 2% ZsA (Jahanshahi *et al*, manuscript submitted) to produce a robust adsorbent for direct product sequestration from cell disruptates. The results from this study and the work presented here indicated that the pellicular structure of the adsorbent resulted in potentially faster processing times and hence further work investigating the optimum pellicle depth for adequate recoveries of nanoparticulates whilst limiting processing times could be completed.

Recent work completed within the Biochemical Recovery Group, (Zhanren Zhang, personal communication) has been concerned with the production of adsorbents comprising a laminate coating of underivatised material. This work has potential applications for the recovery of nanoparticulate products as this laminate layer should enable the penetration of small products within the system, such as proteins and DNA whilst the larger desirable products will remain within the supernatant.

Appendix I Polyvinyl alcohol calibration curve

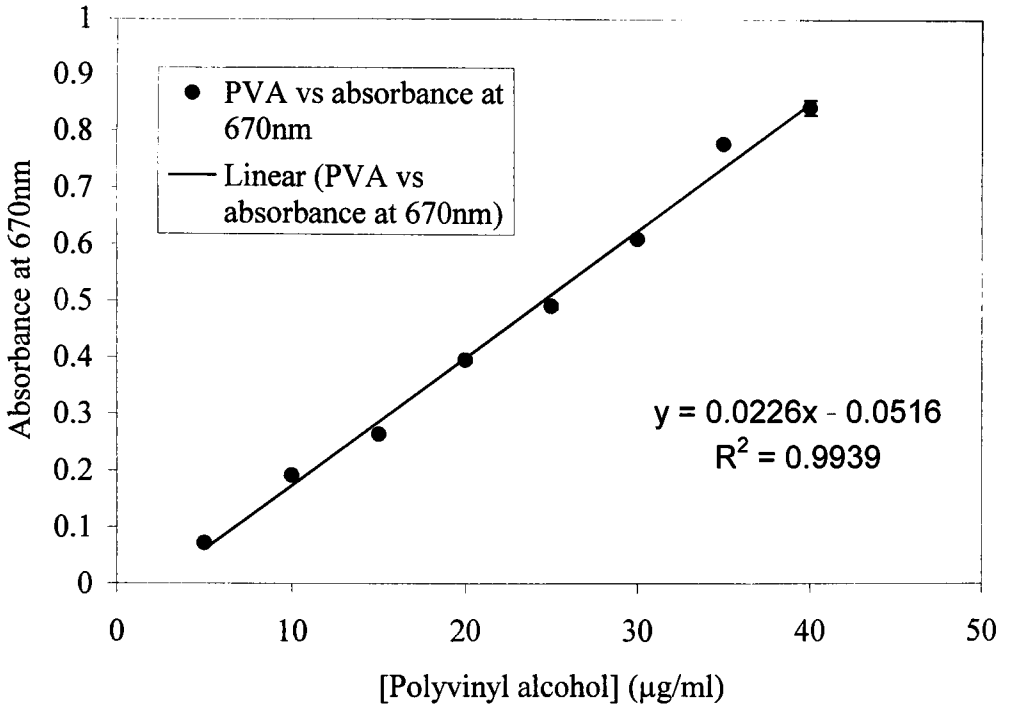

Appendix I represents a PVA calibration curve for determining the concentration of samples containing unknown quantities of PVA utilising the iodometric assay (see Section 2.2.3.1). PVA samples were prepared having different concentrations and were added to an iodine solution (see Section 2.2.3.1) in a 1:2 ratio. The samples were mixed and a green colour complex was formed which was measured spectrophotometrically at 670nm against a buffer blank of 10mM Tris-HCl buffer, pH 7.4 with 0.01% Tween 20 and 0.02% sodium azide).

Appendix II Bradford calibration curve for soluble BSA

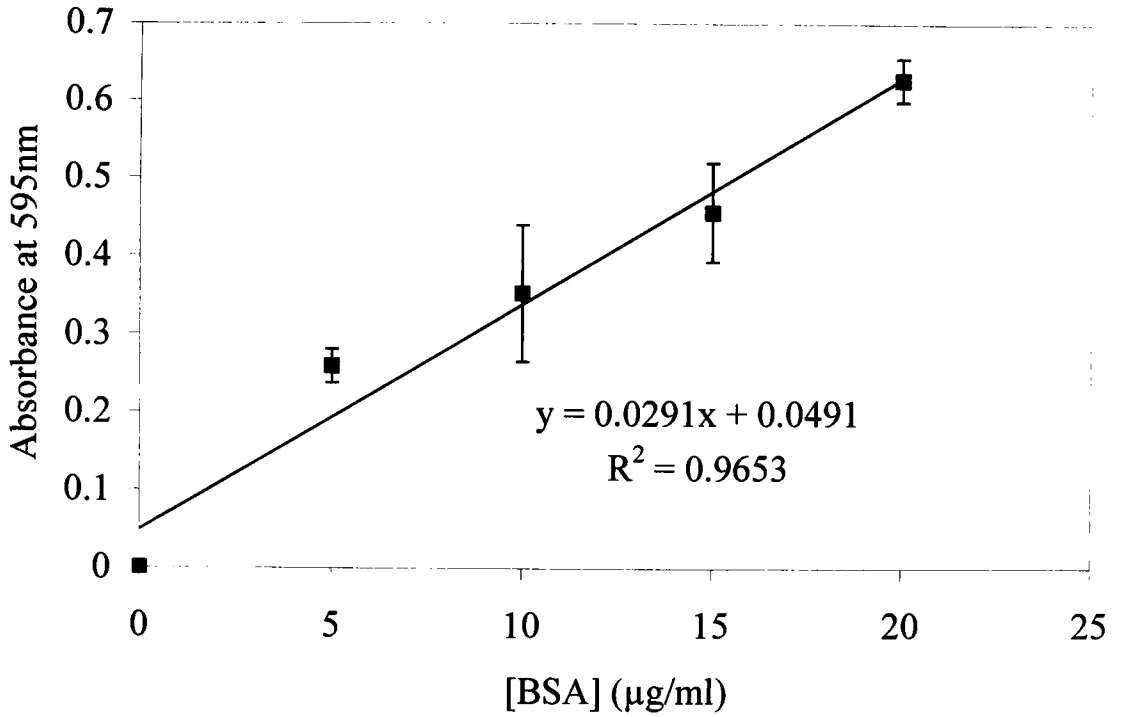

Appendix II represents the Bradford calibration curve for soluble BSA. Samples of the protein are prepared at concentrations between 5 and 50µg/ml from a 2mg/ml stock solution supplied by the manufacturer (PERBIO), in 10mM Tris-HCl, pH 7.4 with 0.02% Tween 20 and 0.01% sodium azide. An equal volume of Bradford assay reagent (see Section 3.2.6) is added to the sample, mixed and stored at room temperature for 5 minutes. The absorbance of the sample at 595nm is measured and plotted against the protein concentration to ascertain a calibration curve to determine unknown protein concentrations against a buffer blank.

Appendix III IPL-41 Insect cell culture medium components

COMPONENT	g/L
Inorganic Salts	
$CaCl_2 . H_2O$ (anhydrous)	0.5
$CoCl_2 . 6H_2O$	0.00005
$CuCl_2$ (anhydrous)	0.000158
$FeSO_4 . 7H_2O$	0.00055
$MgSO_4$ (anhydrous)	0.918
$MgCl_2 . 4H_2O$	0.00002
$(NH_4)_6Mo_7O_{25} . 4H_2O$	0.00004
KCl	1.2
$NaHCO_3$	0.35
NaH_2PO_4	1.009
$ZnCl_2$	0.00004
Amino Acids	
β-Alanine	0.3
L-Arginine.HCl	0.8
L-Aspartic Acid	1.3
L-Asparagine (anhydrous)	1.3
L-Cystine.2HCl	0.13
L-Glutamic Acid	1.5
L-Glutamine	1.0
Glycine	0.2
L-Histidine	0.2
Hydroxy-L-Proline	0.8
L-Isoleucine	0.75
L-Leucine	0.25
L-Lysine.HCl	0.7
L-Methionine	1.0
L-Phenylalanine	1.0
L-Proline	0.5
DL-Serine	0.4
L-Threonine	0.2
L-Tryptophan	0.1
L-Tyrosine.2Na	0.36
L-Valine	0.5

Appendix IV Cibacron Blue 3GA calibration curve

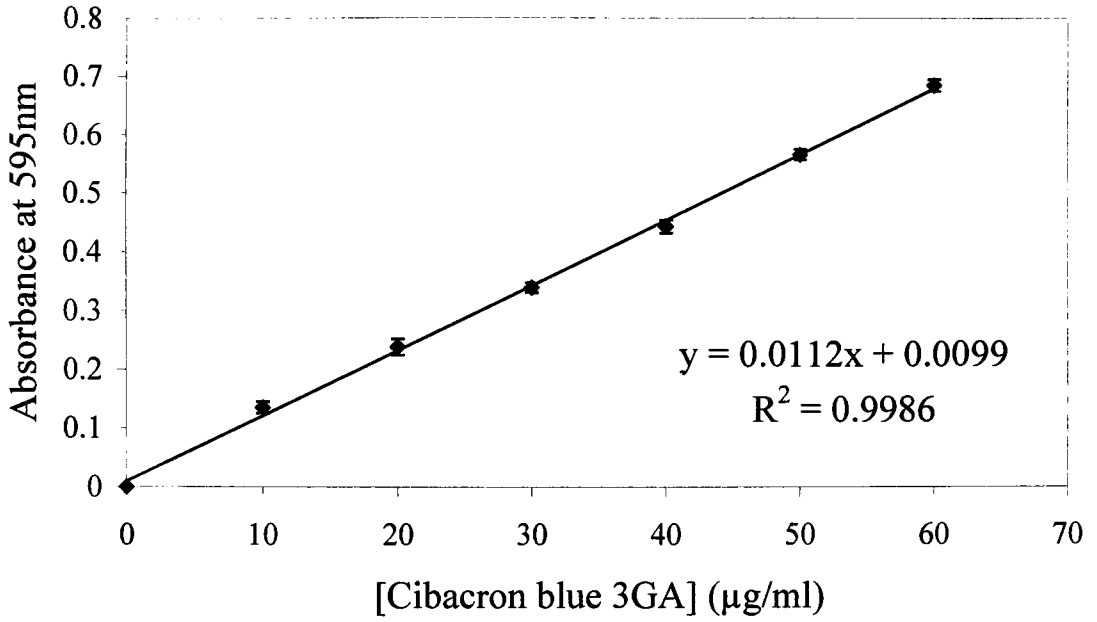

Appendix IV represents a Cibacron Blue 3GA calibration curve constructed by measuring the absorbance of the dye at 595nm at varying concentrations. By plotting the absorbance against dye concentration enabled a calibration curve to be constructed. Subsequent to the immobilisation of the dye to the adsorbent solid phases (see Section 5.2.4) the dye concentration was estimated after removal by acid hydrolysis using this calibration curve (see Section 5.2.5).

Appendix V Bradford calibration curve for soluble HSA

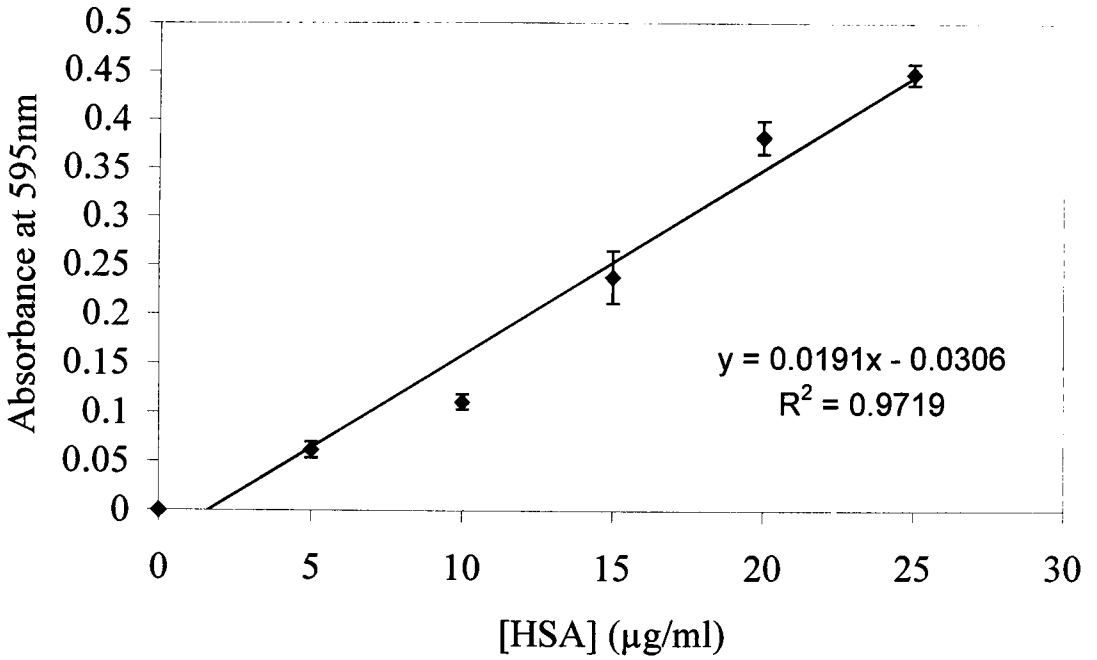

Appendix V represents the Bradford calibration curve for soluble HSA. Samples of the protein are prepared at concentrations between 5 and 25µg/ml from a 2mg/ml stock solution in Buffer C. An equal volume of Bradford assay reagent (see Section 3.2.6) is added to the sample, mixed and stored at room temperature for 5 minutes. The absorbance of the sample at 595nm is measured and plotted against the protein concentration to ascertain a calibration curve to determine unknown protein concentrations against a buffer blank of 10mM Tris-HCl, pH 7.4 with 0.01% Tween 20 and 0.02% sodium azide).

Appendix VI Fluorescence calibration curve

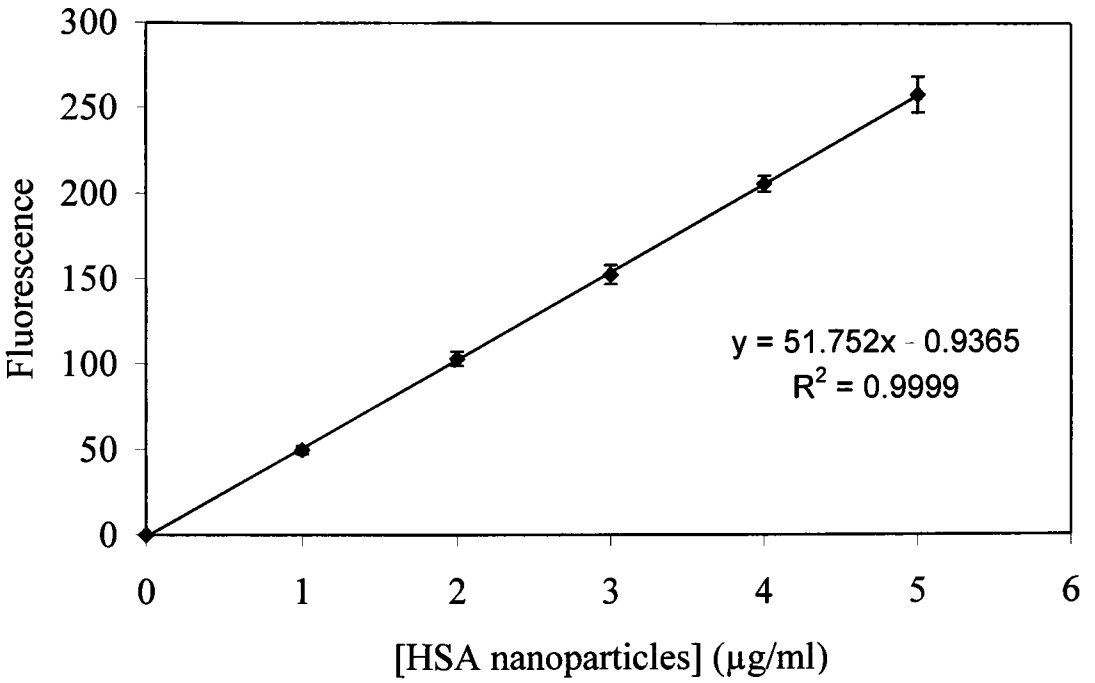

Appendix VI represents an example fluorescence calibration curve (see Section 5.2.6) determined from the fluorescence of samples, measured with a PERKIN-ELMER fluorimeter plotted against the protein concentration determined by the Bradford assay (see Section 3.2.6). The protein concentration of unknown samples was determined by relating the fluorescence detected to the protein concentration.

Appendix VII Amino acid analysis data

AMINO ACID	NMOLE/ML	µG/ML	MG/ML	G/100G
Cysteic acid	-	-	-	0.00
Aspartic acid	166.50	19	0.02	1.92
Threonine	108.53	11	0.01	1.10
Serine	97.60	9	0.01	0.85
Glutamic acid	182.54	24	0.02	2.36
Proline	78.00	8	0.01	0.76
Glycine	44.42	3	0.00	0.25
Alanine	180.30	13	0.01	1.28
Cystine	37.11	8	0.01	0.82
Valine	127.51	13	0.01	1.26
Methionine	14.48	2	0.00	0.34
Isoleucine	29.74	3	0.00	0.34
Leucine	204.23	23	0.02	2.31
Tyrosine	54.80	9	0.01	1.35
Phenylalanine	91.63	14	0.01	1.35
Histidine	74.33	10	0.01	1.02
Tryptophan		-		0.00
Lysine	150.42	19	0.02	1.93
Arginine	77.25	12	0.01	1.21
Totals	1,719.39	198	0.20	19.84

Dr J Fox, Alta Biosciences, University of Birmingham, completed the amino acid analysis after acid hydrolysis for 24 hours at 110°C. Asn and Gln are completely converted to Asp and Glu during the acid hydrolysis of the protein. The values for Thr and Ser have been corrected for hydrolysis losses of 5% and 10% respectively. Trp usually suffers complete loss during acid hydrolysis and is not normally quantified. In proteins Cys is usually observed as cystine. The recovery of Cys is variable when using standard hydrolysis conditions. The values have been rounded off.

REFERENCES

Adam and Holmes (1935) *Journal of the Society Chemical Industry*, **54**, 1

Adinolfi A and Hopkinson D.A (1978) Blue sepharose chromatography of human alcohol dehydrogenase: evidence for interlocus and interallelic differences in affinity characteristics, *Annals and Human Genetics*, **41**, 399-401

Adlercreutz P and Mattiasson B (1982) Oxygen supply to immobilized cells: oxygen supply by haemoglobin or emulsions of perfluorochemicals, *European Journal of Applied Microbiology and Biotechnology*, **16**, 165-170

Afeyan N.B and Fulton S.P (1991) Perfusion chromatography packing materials for proteins and peptides, *Journal of Chromatography*, **544**, 267-279

Afeyan N.B, Regnier F.E, Dean J and Robert C (1996) US Patent Application Number 5,552,041

Ahmed M and Pyle D.L (1999) Investigation of single protein adsorption on ion exchangers using confocal laser scanning microscopy, *Journal of Chemical Technology and Biotechnology*, **74**, 193-198

Aimer P, Howell J.A and Turner M (1989) Effect of concentration boundary layer development on the flux limitation in ultrafiltration, *Chemical Engineering Research Design*, **67**, 255-261

Amersham Biosciences (1997) Expanded Bed Adsorption: Principles and Methods. S-75182, Uppsala, Sweden

Amersham Biosciences (1997) Affinity Chromatography: Principles and Methods, S-75188, Uppsala, Sweden

Andreadis S.T, Roth C.M, LeDoux J.M, Morgan J.R and Yarmush M.L (1999) Large scale processing of recombinant retroviruses for gene therapy, *Biotechnology Progress*, **15**, 1-11

Anspach F.B, Curbelo D, Hartmann R, Garke G and Deckwer W-D (1999) Expanded bed chromatography in primary protein purification, *Journal of Chromatography A*, **865**, 129-144

Applied Biosystems Product Information: POROS 50D Perfusion Chromatography Media, Applied Biosystems, Framingham, MA, USA

Barnfield Frej A.K, Hjorth R and Hammarström A (1994) Pilot scale recovery of recombinant annexin V from unclarified *Eschericia c*oli homogenate using expanded bed adsorption, *Biotechnology and Bioengineering*, **44**, 922-929

Barnfield Frej A.K, Hammarström A, Jones I and Hjorth R (1997) Streamline expanded bed adsorption for the recovery of renatured human interleukin from *E.coli*, *Bioseparation*

Barthels C.R, Kleinmann G, Karzon N.J and Irish D.B (1958) A novel ion exchange method for the isolation of streptomycin, *Chemical Engineering Progress*, **54**, 49-52

Beissner R.S and Rudolph F.B (1978) Immobilised anthraquinone dyes for affinity chromatography, *Journal of Chromatography A*, **161**, 127-135

Belter P.A, Cunningham F.L and Chen J.W (1973) Development of a recovery process for novobiocin, *Biotechnology and Bioengineering*, **15**, 533-549

Bierau H, Zhang Z and Lyddiatt A (1999) Direct process integration of cell disruption and fluidised bed adsorption for the recovery of intracellular proteins, *Journal of Chemical Technology and Biotechnology*, **74**, 208-212

Bierau H (2001) Process integration of cell disruption and fluidised bed adsorption of microbial enzymes: Application to the retro-design of the purification of L-asparaginase, Ph.D thesis, University of Birmingham

Bierau H, Hinton R.J and Lyddiatt A (2001) Direct process integration of cell disruption and fluidised bed adsorption in the recovery of labile microbial enzymes, *Bioseparation*, **10**, 73-85

Bio-Rad Product Information, Running agarose gels, Bio-Rad, Hertfordshire, UK

Blackwell J and Marchessault R.H (1971) in: cellulose and cellulose derivatives, (eds. Bikales N and Segail L.E) Wiley-Interscience

Blanche F, Cameron B, Barbot A, Ferrero L, Guillemiu T, Guyot S, Somarriba S and Bison D (2000) Viral transfer technology, and improved anion exchange HPLC method for the detection and purification of adenoviral particles, *Gene Therapy*, **7**, 1055-1062

Bollin E, Vastola K, Oleszek D and Sulkowski E (1978) The interaction of mammalian interferons with immobilised Cibacron Blue F3GA: modulation in binding strength, *Preparative Biochemistry*, **8**, 259-274

Bonnerjea J, Hoare M and Dunnill P (1986) Protein purification: the right step at the right time, *Bio/technology*, **4**, 954-958

Boyer P.M and Hsu J.T (1993) Protein purification by dye-ligand chromatography, *Advances in Biochemical Engineering/ Biotechnology*, **49**, 1-45

Braas G, Searle P.F, Slater N and Lyddiatt A (1996) Strategies for the isolation and purification of retroviral vectors for gene therapy, *Bioseparation*, **5**, 211-228

Braas G, Walker S.G, Zhang Z and Lyddiatt A (2000) Recovery and manipulation of nanoparticulate bioproducts: relevance to the up-scaled manufacture of gene therapy vectors, *TransIChemE*, **78(C),** 11-18

Bradford M.M (1976) A rapid and sensitive method for the quantitation of microgram quantities of protein utilising the principle of protein-dye binding, *Analytical Biochemistry*, **72**, 248-254

Brown J.R (1977) Structure of bovine serum albumin, *Fed. Proc*, **34**, 591-566

Brunner K.H and Hemfort H (1988) Centrifugal separation in biotechnological processes. In: Mizrahi (ed) Advances in Biotechnological processes. Vol 8 Downstream processes; equipment and techniques, 33-49

Carlsson M, Gustafsson J, Hedman P, Pernemalm P and Lonngren J (1993) US Patent Application Number 07/956,776

Chambers G.K (1977) Determination of Cibacron Blue F3GA substitution in blue Sephadex and blue dextran Sepharose, *Analytical Biochemistry*, **83**, 551-556

Chang Y.K, McCreath G.E, Draeger N.M and Chase H.A (1993) Novel technologies for direct extraction of proteins, *TransIChemE*, **71** (B), 299-305

Chang Y.K and Chase H.A (1996) Development of operating conditions for protein purification using expanded bed techniques: Effect of degree of expansion on adsorption performance, *Biotechnology and Bioengineering*, **49**, 512-526

Chase H.A (1984) Prediction of the performance of preparative affinity chromatography, *Journal of Chromatography*, **297**, 179-202

Chase H.A (1994) Purification of proteins by adsorption chromatography in expanded beds, *Trends in Biotechnology*, **12**, 296-303

Chase H.A and Draeger N.M (1992) Expanded bed adsorption of proteins using ion-exchanger, *Separation Science and Technology*, **27** (4), 2021-2039

Clonis Y.D and Lowe C.R (1980) Triazine dyes, a new class of affinity labels for nucleotide dependant enzymes, *Biochemical Society*, **191**,247-251

Coester C, Kreuter J, Briesen H and Langer K (2000) Preparation of avidin labeled gelatin nanoparticles as carriers for biotinylated peptide nucleic acid, *International Journal of Pharmaceutics*, **196**, 147-149

Coffman J.L, Pierre G and Egisto B (1999) US Patent Application Number 5,906,747

Coomassie Protein Assay Reagent Kit Instructions, PERBIO, Cheshire, UK

Dasari G, Prince I and Hearn M.T.W (1993) High performance liquid chromatography of amino acids, peptides and proteins. CXXIV. Physical Characterisation of fluidized bed behaviour of chromatographic packing materials, *Journal of Chromatography*, **631**, 115-124

Datar R.V, Cartwright T and Rosen C.G (1993) Process economics of animal cell and bacterial fermentations: a case study analysis of tissue plasminigen activator, *Biotechnology*, **11**, 349-357

Davies M.J, Bruce I.HJ and Smethurst D.E (1994) Separation for Biotechnology 3 (Ed Pyle D.L) The Royal Society of Chemistry, Cambridge, 153

Dean P and Watson D (1979) Protein purification using immobilised triazine dyes, *Journal of Chromatography*, **165**, 301-319

Di Felice R (1995) Hydrodynamics of liquid fluidisation, *Chemical Engineering Science*, **50**, 1213-1245

Duckworth M and Yaphe W (1971) Preparation of agarose by fractionation from the spectrum of polysaccharides in agar, *Analytical Biochemistry*, **44**, 636-641

Durand J, Kojic L, Wang Y, Lee P, Cynader M.S and Gu Q (2000) Confocal imaging of N-methyl-d-aspartate receptors in living cortical neurons, *Neuroscience*, **97**, 11-12

Easterday R.L and Easterday I.M (1974) Affinity chromatography of kinases and dehydrogenases on Sephadex and Sepharose dye derivatives, *Advances in Experimental Medicine and Biology*, **42**, 123-133

Eggert M, Baltes T, Garret-Flaudy F, Freilag R (1998) Affinity precipitation – an alternative to fluidised bed adsorption?, *Journal of Chromatography A*, **827**, 269-280

Ergorov A.M, Vakhabbov A.K.H and Chernyak V.Y (1970) Isolation of agarose and granulation of agar and agarose gel, *Journal of Chromatography*, **46**, 143

Erickson J.C, Finch J.D and Greene D.C (1994) Direct capture of recombinant proteins from animal cell culture using a fluidised bed, Animal Cell Technology: Products for Today, Prospects for Tomorrow, 557-560, Butterworth and Heineman, Oxford

Ferreira, G.N.M, Cabral J.M.S and Prazeres D.M.F (1998) Purification of supercoiled plasmid DNA using chromatographic processes, *Journal of Molecular Recognition*, **11**, 250-251

Ferreira G.N.M, Monteiro G.A, Prazeres D.M.F and Cabral J.M.S (2000) Downstream processing of plasmid DNA for gene therapy and DNA vaccine applications, *Trends in Biotechnology*, **18**, 380-388

Finette G.M.S, Mao Q.M and Hearn M.T.W (1996) Studies on the expansion characteristics of fluidised beds with silica-based adsorbents used in protein purification, *Journal of Chromatography A,* **743**, 57-73

Fluorochem Product Information (1998) Perfluorodecalin, Fluorochem Limited, Derbyshire

Fulton S.P, Afeyan N.B, Gordon N.F and Regnier F.E (1991) Very high speed separation of proteins with a 20μm reversed phase sorbent, *Journal of Chromatography*, **547**, 452-456

Gallo J.M and Hassan E.E (1988) Receptor mediated magnetic carriers: basis for targeting, *Pharmaceutical Research*, **5**, 300-304

Garret-Flaudy F and Freitag R (2001) Use of the avidin (imino)biotin system as a general approach to affinity precipitation, *Biotechnology and Bioengineering*, **71**, 223-234

Garvey M.J, Tadros F and Vincent B (1974) A comparison of the volume occupied by macromolecules in the adsorbed state and in bulk solution. Adsorption of narrow molecular-

weight fractions of PVA at the polystyrene/water interface, *Journal of colloidal and Interface Science*, **49**, 57-68

Gibson N and Lyddiatt A (1990) Economic fabrication and utilisation of agar composites in bioselective recovery in fixed and fluidised beds, *Separations for Biotechnology* **2**, 152-161

Gibson N (1992) Liquid fluidised bed adsorption in protein recovery. Assembly and characterisation of dedicated solid phases, PhD Thesis, University of Birmingham

Gibson N and Lyddiatt A (1993) Cellulose composites in liquid fluidized bed adsorption and recovery of proteins: In, Cellulosics – materials for selective separations and other technologies (Eds) Kennedy J.F, Phillips G.O, Williams P.A, Ellis-Horwood, 55-62

Gilljam G, Siridewa K and Hammar L (1994) Purification of simian immunodeficiency virus, SIVMAC251, and its external envelope glycoprotein, GP148, *Journal of Chromatography A*, **675**, 89-100

Gilchrist G.R, Burns M.T and Lyddiatt A (1994) Solid phases for protein adsorption in liquid fluidised beds: In, Separations for Biotechnology 3, (ed) Pyle D.L, Royal Society of Chemistry, Cambridge, 186-192

Gilchrist G.R (1996) Direct fluidised bed adsorption of protein products from complex particulate feedstocks: Development of cellulose composites with selective binding properties, PhD Thesis, University of Birmingham

Gordon N.F, Moore C.M and Cooney C.L (1990) An overview of continuous protein purification processes, *Biotechnology Advances*, **8** (4), 741-762

Griessbach R (1939) *Ver. Duet. Chemiker, Beih*, **31**, 1-7

Gustavsson P.E, Axelsson A, Larsson P.O (1998) Direct measurements of convective fluid velocities in superporous agarose beads, *Journal of Chromatography A*, **795**, 199-210

Hamilton G.E, Morton P.H, Young T.W and Lyddiatt A (1999) Process intensification by direct product sequestration from batch fermentations: Application of a fluidised bed multi-bed external loop contactor, *Biotechnology and Bioengineering*, **64** (3), 310-321

Hansson M, Stahl S, Hjorth R, Uhlen M and Moks T (1994) Single Step recovery of a secreted recombinant protein by expanded bed adsorption, *Biotechnology*, **12**, 582-589

Haug A (1975) in: Chemistry of Algal Cell Wall Polysaccharides, MPT International Series in Biochemistry, vol 2, 348

Helfferich F (1962) Ion exchange, McGraw-Hill Book Company Inc

Herrman H and Hoenhal F.P (1964) Polyvinyl Alcohol, Academic Press

Hjerten S (1964) *Biochimica et Biophysica Acta*, **90**, 269

Hjorth R, Kampes S and Carlsson M (1995) Analysis of some operating parameters of novel adsorbents for recovery of proteins in expanded beds, *Bioseparation* **5**, 217-223

Hjorth R (1997) Expanded bed adsorption in industrial processing: Recent developments, *Trends in Biotechnology*, **15**, 230-235

Hubbuch J.J, Matthiesen D.B, Hobley T.J and Thomas, O.R.T (2001) High gradient magnetic separation versus expanded bed adsorption: a first principle comparison, *Bioseparation*, **10**, 99-112

Huddleston J.G, Viese A, Kohler K, Flanagan J.A, Enfors S.O and Lyddiatt A (1991) The molecular basis of partitioning in aqueous two-phase systems, *Trends in Biotechnology*, **9**, 381-388

Huddleston J.G, O'Brien S, Picard H and Lyddiatt A (1992) The recovery in aqueous two-phase systems of intracellular protein products from wet-milled brewers' yeast: In Solvent extractions in the process industries, (Eds) Logsdail D.H and Slater M.J, vol 2, 1048-1055, Elsevier Applied Science

Hughes C.P (2001) Design and evaluation of retroviral vectors for the immune gene therapy of acute myeloid leukaemia, Ph.D Thesis, King's College, London

Huyghe B.G, Lui X, Sutjipto S, Sugarman B.J, Hern M.T, Shepard M, Scandella C.J and Shabram P (1995) Purification of a type 5 recombinant adenovirus encoding human P35 by column chromatography, *Human Gene Therapy*, **6**, 1403-1416

Jiang W and Hearn M.T.W (1996) Protein interaction with immobilised metal ion affinity ligands under high ionic strength conditions, *Analytical Biochemistry*, **242**, 45-54

Josefson C.M, Johnston J.B and Trubey R (1984) Adsorption of organic compounds from water with porous poly(tetrafluoroethylene), *Analytical Chemistry*, **56**, 764-768

Kacar Y and Arica M.Y (2001) Procion green H-E4BD immobilised porous poly(hydroxyethylmethacrylate) ion exchange membrane: preparation and application to lysozyme adsorption, *Colloids and Surfaces B: Biointerfaces*, **22**, 227-236

Kahn D.W, Butler M.D, Cohen D.L, Gordon M, Kahn J.W and Winkler M.E (2000) Purification of plasmid DNA by tangential flow filtration, *Biotechnology and Bioengineering*, **69**, 101-106

Kasper C, Meringova L, Freitag R and Tennikova T (1998) Fast isolation of protein receptors from streptococci G by means of macroporous affinity discs, *Journal of Chromatography A*, **798**, 65-72

Kawamura A (1977) (ed) Fluorescent antibody techniques and their applications, 2nd Edition, University of Tokyo Press, Tokyo

Keese C.R and Giaever I (1983) Cell growth on liquid microcarriers, *Science*, **219**, 1448-1449

Kirkland J (1963) *Analytical Chemistry*, **35**, 2003

Kopperschlager G, Freyer R, Diezel W and Hofmann E (1968) Some kinetic and molecular properties of yeast phosphofructokinase, *FEBS Letters*, **1**, 137-141

Kopperschlager G, Bohme H.J and Hofamnn E (1982) Cibacron blue F3GA and related dyes as ligands in affinity chromatography, *Advances in Biochemical Engineering*, **25,** 101-138

Krassig H (1984) Structure and reactivity of cellulose fibres, *Papier*, **38**, 571-582

Kunii D and Levenspiel O (1991) Fluidisation Engineering, 2nd Edition

Kula M-R (1990) Trends and future prospects of aqueous two-phase extraction, *Bioseparation* **1**, 181-189

Lan J.W.C, Hamilton G.E and Lyddiatt A (1999) Physical and biochemical characterisation of a simple intermediate between fluidised and expanded bed contactors, *Bioseparation* **8**, 43-51

Lan Q, Bassi A.S, Zhu JX and Margaritis A (2001) A modified Langmuir model for the prediction of the effects of ionic strength on the equilibrium characteristics of protein adsorption onto ion exchange/ affinity adsorbents, *Chemical Engineering Journal,* **81**, 179-186

Langer K, Coester C, Weber C, Briesen H, Kreuter J (2000) Preparation of avidin labeled protein nanoparticles as carriers for biotinylated peptide nucleic acid, *European Journal of Pharmaceutics and Biopharmaceutics*, **49**, 303-307

Langmuir I (1916) *Journal of American Chemical Society*, **38**, 2221-2295

Leatherbarrow R.J and Dean D.G (1980) Studies on the mechanism of binding of serum albumins to immobilised Cibacron Blue F3GA, *Biochemical Journal*, **189**, 27-34

Leonard M, Farnier C and Dellacherie E (1995) Polyvinyl alcohol-coated macroporous polystyrene particles as stationary phases for the chromatography of proteins, *Journal of Chromatography*, **664**, 39-46

Levenspiel O (1972) Chemical Reaction Engineering, Wiley and Sons, New York

Levison P.R, Hopkins A.K, Hathi P, Badger S.E, Mann F, Dickson N and Purdom G (2000) Suspended bed chromatography, a new approach to downstream processing, *Journal of Chromatography A*, **890**, 45-51

Levy M.S, O'Kennedy R.D, Ayazi-Shamlou P and Dunnill P (2000) Biochemical engineering approaches to the challenges of producing pure plasmid DNA, *Trends in Biotechnology*, **18**, 296-305

Lihme A, Neilsen C.S, Thorkild C (1999) US Patent Application Number 5,866,006

Lihme A, Zafirakos E, Hansen M and Olander M (1999) Simplified and more robust EBA processes by elution in expanded bed mode, *Bioseparation* **8**, 93-97

Lin W, Coombes A.G.A, Davies M.C, Davis S.S and Illum L (1993) Preparation of sub 100nm human serum albumin nanospheres using a pH coacervation method, *Journal of Drug Targeting*, **1**, 237-243

Lin W, Coombes A.G.A, Garnett M.C, Davies M.C, Schacht E, Davis S.S and Illum L (1994) Preparation of sterically stabilized human serum albumin nanospheres using a novel dextranox-MPEG crosslinking agent, *Pharmaceutical Research*, **11**, 1588-1592

Linden T, Ljunglof A., Kula M-R and Thömmes J (1999) Visualising the component protein diffusion in porous adsorbents by confocal scanning laser microscopy, *Biotechnology and Bioengineering*, **65**, 622-630

Ljunglöf A and Hjorth R (1996) Confocal microscopy as a tool for studying protein adsorption to chromatographic matrices, *Journal of Chromatography A*, **746**, 75-83

Ljunglöf A and Thömmes J (1998) Visualising intraparticle protein transport in porous adsorbents by confocal microscopy, *Journal of Chromatography A*, **813**, 387-395

Ljunglöf A, Bergrall P, Bhikhabhai R and Hjorth R (1999) Direct visualisation of plasmid DNA in individual chromatography adsorbent particles by confocal scanning laser microscopy, *Journal of Chromatography A*, 844, 129-135

Ljunglöf A, Larsson M, Knuuttila K.G and Lindgren J (2000) Measurement of ligand distribution in individual adsorbent particles using confocal scanning laser microscopy and confocal micro-Raman spectroscopy, *Journal of Chromatography A*, **893**, 235-244

Lorens J.B, Sousa C, Bennett M.K, Molineaux S.M and Payan D.G (2001) The use of retroviruses as pharmaceutical tools for target discovery and validation in the field of functional genomics, *Current Opinion in Biotechnology*, **12**, 613-621

Lowe K.C (1987) Perfluorocarbons as oxygen transport fluids, *Comp. Biochem. Physiol*, **87A**, 839-843

Lundell M.J and Hirsh J (1994) A new visible light DNA fluorochrome for confocal microscopy, *BioTechniques*, **16**, 434-440

Lyddiatt A and O'Sullivan D.A (1998) Biochemical recovery and purification of gene therapy vectors, *Current Opinion in Biotechnology*, **9**, 177-185

Lyddiatt A (2002) Process chromatography: current constraints and future options for the adsorptive recovery of bioproducts, *Current Opinion in Biotechnology*, **13**, 95-103

Malvern Mastersizer Instruments Manual (1991) Malvern Instruments, Malvern, UK

Malvern Mastersizer Reference Manual (1991) Malvern Instruments, Malvern, UK

Marchessault R.H and Sarke A (1967) *Advances in Carbohydrate Chemistry*, **22**, 421

McCormick D.K (1993) Expanded bed adsorption – the first new unit operation in decades, *Biotechnology*, **11**, 1059-1060

McCreath G.E, Chase H.A, Purvis D.R and Lowe C.R (1992) Novel affinity separations based on perfluorocarbon emulsions. Use of a perfluorocarbon affinity emulsion for the purification of human serum albumin from blood plasma in a fluidised bed, *Journal of Chromatography*, **597**, 189-196

McCreath G.E, Chase H.A and Lowe C.R (1994) Novel affinity separations based on perfluorocarbon emulsions. Use of a perfluorocarbon affinity emulsion for the direct extraction of glucose-6-phosphate dehydrogenase from homogenised bakers yeast, *Journal of Chromatography A,* **659**, 275-287

McCreath G.E, Chase H.A and Owen R.O (1995) Expanded bed affinity chromatography of dehydrogenases from bakers yeast using dye-ligand perfluorocarbon supports, *Biotechnology and Bioengineering*, **48**, 341-354

McCreath G.E and Chase H.A (1996a) Affinity adsorption of *Saccharomyces cerevisiae* on Concavalin A perfluorocarbon emulsions, *Journal of Molecular Recognition*, **9**, 607-616

McCreath G.E and Chase H.A (1996b) Application of perfluorocarbon affinity emulsions for rapid isolation of *Staphylococcus aureus*, *Biotechnology Progress*, **12,** 77-83

Miyabe K and Guiochon G (2000) Kinetic study of the mass transfer of bovine serum albumin in anion exchange chromatography, *Journal of Chromatography A*, **866**, 147-171

Molday R.S and Mackenzie D (1982) Immunospecific ferromagnetic iron-dextran reagents for the labeling and magnetic separation of cells, *Journal of Immunological Methods*, **52**, 535-367

Morton P.H and Lyddiatt A (1992) Direct recovery of protein products from whole fermentation broths: a role for ion exchange adsorption in fluidized beds, In Ion exchange advances, (Ed) Slater M.J, 237-244, Elsevier Applied Science

Mullick A and Flickinger M.C (1999) Expanded bed adsorption of human serum albumin from very dense *Saccharomyces cerevisiae* suspensions on fluoride-modified zirconium, *Biotechnology and Bioengineering*, **65**, 282-290.

Nash D.C and Chase H.A (1997) Modifications of polystyrenic matrices for the purification of proteins III Effects of poly (vinyl alcohol) modification on the characteristics of protein adsorption on conventional and perfusion polystyrene matrices, *Journal of Chromatography A*, **776**, 65-73

Nguyen N and Tukey R.H (1997) Baculovirus directed expression of rabbit UDP glucuronosyltransferase in Spodoptera frugiperda cells, *Drug Metabolism and Diposition: The Biological Fate of Chemicals*, **25**, 745-749

O'Keeffe R.S, Johnston M.D and Slater N.K.H (1999) The affinity adsorptive recovery of an infectious herpes simplex virus vaccine, *Biotechnology and Bioengineering*, **62**, 537-545

Ondarza J and Hootman S.R (1997) Confocal microscopic analysis of intracellular pH regulation in isolated guinea pig pancreatic ducts, *The American Journal of Physiology*, **272**, G124-G134

O'Neil P.F and Balkovich E.S (1993) Virus harvesting and affinity based liquid chromatography- a method for virus concentration and purification, *Bio/Technology*, **11**, 173-178

Owen R.O, McCreath G.E and Chase H.A (1997) A new approach to continuous counter current protein chromatography: Direct purification of malate dehydrogenase from a *Saccharomyces cerevisiae* homogenate as a model system, *Biotechnology and Bioengineering*, **53**, 427-411

Pai A, Gondkar S, Sundaram S and Lali A (1999) Expanded bed adsorption on supermacroporous cross-linked cellulose matrix, *Bioseparation* **8**, 131-138

Pai A, Gondkar S and Lali A (2000) Enhanced performance of expanded bed chromatography on rigid superporous adsorbent matrix, *Journal of Chromatography A*, **867**, 113-130

Palsson E, Gustavsson P.E and Larsson P.O (2000) Pellicular expanded bed matrix suitable for high flow rates, *Journal of Chromatography* A, **878**, 4-52

Palsson E, Smeds A.L, Petersson A and Larsson P.O (1999) Faster isolation of recombinant factor VIII SQ with a superporous agarose matrix, *Journal of Chromatography A*, **840**, 39-50

Pannell R, Johnson D and Travis J (1974) Isolation and properties of human plasma alpha-1-proteinase inhibitor, *Biochemistry*, **13**, 5439-5445

Pawley J.B (ed) (1995) Handbook of biological confocal microscopy, 2nd Edition, Plenum Press

Peters T (1985) Serum albumin in advances in protein chemistry, Academic Press

Peterson E and Sober H (1956) Chromatography of proteins I: Cellulose ion exchange adsorbents, *Journal of Chromatography*, **78**, 751

Phillips A.W, Ball G.D, Fantes K.H, Finter N.B and Johnston M.D (1985) Experience in the cultivation of mammalian cells on the 8000 litre scale. In: Feder J and Tolbert W.R (eds) Large scale mammalian cell culture, 87-95, Academic Press

Porath J, Janson J.C and Laas T (1971) Agar derivatives for chromatography, electrophoresis and gel bound enzymes 1) Desulphated and reduced cross linked agar and agarose in spherical bead form, *Journal of Chromatography*, **60**, 167-177

Prazeres D.M.F, Schleup T and Cooney C (1998) Preparative purification of supercoiled plasmid DNA using anion-exchange, *Journal of Chromatography A*, **806**, 31-45

Prazeres D.M.F, Ferreira G.N.M, Monteiro G.A, Cooney C.L and Cabral J.M.S (1999) Large scale production of pharmaceutical grade plasmid DNA for gene therapy: problems and bottlenecks, *Trends in Biotechnology*, **17**, 169-174

Quinones-Garcia I, Rayner I, Levison P.R, Dickson N and Purdom G (2001) Performance comparisons of suspended bed and batch contactor chromatography, *Journal of Chromatography A*, **908**, 169-178

Richardson J.F and Zaki W.N (1954) Sedimentation and fluidisation Part 1, *TransIChemE*, **32**, s82-8100

Riggs J.L, Seimald R.J, Burckhalter J, Dawns C.M and Metcalf T.G (1958) Isothiocyanate compounds as fluorescent labeling agents for immune serum, *American Journal of Pathology*, **34**, 1081-1097

Righetti P.G and Caravaggio T (1976) Isoelectric points and molecular weights of proteins, *Journal of Chromatography*, **127**, 1-28

Robbins P.D and Wang D.I.C (1986) Dynamic batch adsorption chromatography for protein purification, *Abstracts of Papers of the American Chemical Society*, **192,** 7

Rodrigues A.E, Chenou C and Rendeules de la Vega M (1996) Protein separation by liquid chromatography using permeable POROS Q/M particles, *The Chemical Engineering Journal*, **61,** 191-201

Shabram P.W, Giroux D.D, Goudreau A.M, Gregory J.J, Horn M.T, Huyghe D.G, Lui X, Nannally M.H, Sugarman B.J and Sutjipto S (1997) Analytical anion exchange HPLC of recombinant type 5 adenoviral particles, *Human Gene Therapy*, **8**, 453-465

Sheppard C.J.R and Shotton D.M (1997) Confocal Laser Scanning Microscopy, BIOS Scientific Publishers

Sjoback R, Nygren J and Kubista M (1995) Absorption and fluorescence properties of fluorescein, *Spectrochimica Acta Part A: Molecular Spectroscopy*, **51**, L7-L212

Song L, Hennink E.J, Young I.T and Tanke H.J (1995) Photobleaching kinetics of fluorescein in quantitative fluorescence microcopy, *Biophysical Journal*, **68**, 2588-2600

Stewart D.J, Purvis D.R and Lowe C.R (1990) Affinity chromatography on novel perfluorocarbon supports. Immobilisation of CI reactive blue 2 on a polyvinyl alcohol coated perfluorocarbon support and its application in affinity chromatography, *Journal of Chromatography*, **510**, 177-187

Subramanian A, Von Cott K.E, Milbrath D.S and Velander W.H (1994) Role of local antibody density effects on immunoadsorbent efficiency, *Journal of Chromatography A*, **672**, 11-26

Sun Y, Pacek A.W, Nienow A.W and Lyddiatt A (2001) Fabrication and Characterisation of a novel pellicular adsorbent customized for the effective fluidized bed adsorption of protein products, *Biotechnology and Bioprocess Engineering*, **6**, 419-425

Taipa M.A, Kaul R.H, Mattiasson B and Cabral J.M.S (2000) Recovery of a monoclonal antibody from hybridoma culture supernatant by affinity precipitation with Eudragit S-100, *Bioseparation*, **9**, 291-298

Tennikov M.B, Gazdina N.V, Tennikova T.B and Svec F (1998) Effect of porous structure of macroporous polymer supports on resolution in high performance membrane chromatography of proteins, *Journal of Chromatography A*, **798**, 55-64

Thömmes J, Halfar M, Lenz S, Kula M.R (1995) Purification of monoclonal antibodies from whole hybridoma fermentation broth by fluidised bed adsorption, Biotechnology and Bioengineering, **43** (3), 205-211

Thömmes J (1997) Fluidised bed adsorption as a primary recovery step in protein purification, *In Advances in Biochemical Engineering*

Thwaites E, Burton S.C and Lyddiatt A (2002) Impact of the physical and topographical characteristics of adsorbent solid –phases upon the fluidised bed recovery of plasmid DNA from *Escherichia coli* lysates, *Journal of Chromatography A*, **943**, 77-90

Ticha M, Horejsi V and Barthova J (1978) Affinity electrophoresis of proteins interacting with blue dextran, *Biochimica et Biophysica Acta*, **534**, 58-63

Tooper E.B and Wirth L.F (1956) Ion exchange resins: in Ion Exchange Technology, ed. Nachod F.C and Sjchubert J, Academic Press

Tuncel A and Adil D (1993) Cibacron Blue F3GA attached monosize poly (vinyl alcohol) coated polystyrene microspheres for specific albumin adsorption, *Journal of Chromatography*, **634**, 161

Ujam L.B, Clemmitt R.H and Chase H.A (2000) Cell separation by EBA: use of ion exchange chromatography for the separation of *E.coli* and *S.cerevisiae*, *Bioprocess Engineering*, **23**, 245-250

Vaidya A.A, Lele B.S, Deshmukh M.V and Kulkarni M.G (2001) Design and evaluation of new ligands for lysozyme recovery by affinity thermoprecipitation, *Chemical Engineering Science*, **56**, 5681-5692

Varley D.L, Hitchcock A.G, Weiss A.M.E, Horler W.A, Cowell R, Peddie L, Sharpe G.S, Thatcher D.R and Hanak J (1999) Production of plasmid DNA for human gene therapy using modified alkaline lysis and expanded bed anion exchange chromatography, *Bioseparation*, **8**, 209-217

Vaughn J.L, Goodwin R.H, Tompkins G.J and McCawley P (1977) The establishment of two cell lines from the insect Spodoptera frugiperda (Lepidoptera; Noctuidae), *In Vitro*, **13**, 213-217

Walker S.G and Lyddiatt A (1996) Aqueous two phase partition of complex protein feedstocks derived from brain tissue homogenates, *Journal of Chromatography B*, **680**, 91-96

Walker S.G (1998) Application of aqueous two phase systems to the recovery of bioparticulates, PhD Thesis, University of Birmingham

Walker S.G and Lyddiatt A (1999) Processing of nanoparticulate products: application and optimization of aqueous two phase systems, *Journal of Chemical Technology and Biotechnology*, **74**, 250-255

Wheelwright S.M (1987) Designing downstream processes for large-scale protein purification, *Bio/Technology*, **5**, 789-793

Williams R.C, Vasta-Russell J.F, GlajchJ.L and Golebiowski K (1986) Separation of proteins on a polymeric fluorocarbon high performance liquid chromatography column packing, *Journal of Chromatography*, **371**, 63-70

Yang Y and Chase H.A (1994) Immobilisation of α-amylase on poly (vinyl alcohol) coated perfluorocarbon supports for use in enzyme reactors, *Biotechnology and Applied Biochemistry*, **28**, 145-154

Young J.L and Webb B.A (1978) Two methods for the separation of human alpha-fetoprotein and albumin. (A) Affinity chromatography using blue Sepharose CL-6B and (B) ampholyte displacement chromatography, *Analytical Biochemistry*, **88**, 619-623

Zhang L, Mizumoto K, Sato N, Kusumoto M, Niiyama H and Tanaka M (1999) Quantitative determination of apoptotic death in cultured human pancreatic cancer cells by propidium iodide and digitonon, *Cancer Letters*, **142**, 129-137

Zhang Z, Burton S.C, Williams S.L, Thwaites E and Lyddiatt A (2001) Design and assembly of solid-phases for the effective recovery of nanoparticulate bioproducts in fluidised bed contactors, *Bioseparation*, **10**, 113-132

Zurek C, Kubis E, Keup P, Harlen D, Thömmes J, Kula M-R, Halenberg C.P and Gellissen G (1996) Production of two aprotonin variants in *Hansensula polymorpha*, *Process Biochemistry*, **31**, 679-689